

3D Stiffness and Strength Degradation Models for Seismic
Progressive Collapse Analysis of Reinforced Concrete
Structures – Formulations and Implementations Framework

by

Silvena Stoeva Reshotkina

A thesis submitted to the Faculty of Graduate and Postdoctoral
Affairs in partial fulfillment of the requirements for the degree of

Doctor of Philosophy

in

Civil Engineering

Carleton University
Ottawa, Ontario

© 2015, Silvena Stoeva Reshotkina

Abstract

Realistic prediction of seismic progressive collapse behaviour is essential in vulnerability and performance assessment of reinforced concrete structures. In seismic events, structural components of typical buildings and bridges may be subjected to repeated cyclic load reversals and combined axial, flexure and shear effects, and are also expected to undergo inelastic deformations during the severe ground shaking of major earthquakes. As a result of accumulated damage during inelastic excursions, the seismic response of reinforced concrete members may exhibit stiffness degradation and strength deterioration. In the case of shear-critical columns in older deficient structures, severe degradations and pinching behaviour may be particularly pronounced in the cyclic response.

The principal objective of this research is to develop a comprehensive model for seismic response analysis of reinforced concrete structures subjected to multi-component seismic loading that captures the behaviour of members in new structures designed as ductile as well as non-ductile members in existing older deficient structures. The focus is on the formulation of a beam-column element using the concentrated plasticity approach and the development of a framework for the implementations of the new model using object oriented design concepts. The key modeling capabilities considered in this study include: capturing axial force-bending moment interactions; simulating post-yield hardening response; detecting brittle or limited ductility types of failure in shear; capturing degradation of shear strength in the plastic hinge zone with increased displacement ductility; simulating softening in the post-shear failure response; capturing stiffness

degradation and cyclic strength deterioration under repeated load reversals; tracking the progression and accumulation of damage and its effects on stiffness and strength degradation. Concentrated plasticity models are computationally more efficient than distributed plasticity fiber models and generally more practical for modeling complex phenomena like post-shear failure response since they require fewer parameters to capture the degrading behaviour under cyclic loading.

The element formulation employs yield surfaces and shear-failure surfaces as well as evolution models associated with the surfaces for the generalized plastic hinges at the element ends to model interactions among axial force, bending moments and shear forces in the inelastic response. The degradation of shear strength in the plastic hinge region with increasing flexural displacement ductility demand is captured by using ductility-related shear limit surface associated with the shear failure surface evolution model. The cyclic behaviour modeling is based on the incorporation of damage models in the beam-column element formulation to track the progression of damage and its effects on the gradual deterioration in stiffness and loss of strength. The quasi-elastic degraded cyclic response is controlled by cyclic models capturing the different degradation characteristics through interaction with damage models to consider the effects of accumulated damage. A consistent generalized approach for state determination is developed using event-based strategy, where an “event” occurs when the loading state of the element changes.

In the development of the object oriented implementation framework, the individual components of the proposed inelastic concentrated-plasticity model for capturing the

behaviour of ductile as well as non-ductile reinforced concrete members are identified and the functionalities of each component are defined. The following abstract base classes are established to describe the behaviour of individual components: beam-column element class, yield surface class, yield surface evolution class, shear failure surface class, shear failure surface evolution class, shear limit surface class, cyclic model class, cyclic control class, damage model class, damage progression class. The interface and the interactions between the abstract base classes are also established based on the required functionalities. The hierarchal structure of the proposed classes and the independent implementations for each of the main components of the formulations within a separate base class are designed to provide a comprehensive and flexible design that allows extensibility.

Dedicated to my husband

Acknowledgements

The author would like to express her sincere gratitude to her research supervisor, Professor David Lau for his guidance, support and helpful advice throughout the course of this research. Sincere appreciation is also extended to the members of the author's Ph.D. defense committee, Associate Professor Dan Palermo, Professor Fred Afagh, Assistant Professor Hassan Aoude, and Associate Professor Heng-Aik Khoo, for their insights and valuable suggestions.

Special thanks and appreciation go to the author's parents and sister for their constant encouragement and support. Finally, the author would like to thank her husband for his encouragement, patience and tremendous help.

The financial support to this research provided by the NSERC Canadian Seismic Research Network is also gratefully acknowledged.

Table of Contents

Abstract.....	ii
Acknowledgements	vi
Table of Contents	vii
List of Tables	xii
List of Figures.....	xiii
List of Appendices.....	xxi
List of Symbols	xxii
1 Chapter: Introduction	25
1.1 Background.....	25
1.2 Behaviour and Modeling of Reinforced Concrete Columns	26
1.2.1 Monotonic Behaviour.....	26
1.2.2 Cyclic Behaviour.....	29
1.2.3 Shear Critical Behaviour.....	34
1.2.4 Common Failure Modes of Reinforced Concrete Columns	36
1.3 Objectives and Scope	37
1.4 Thesis Outline.....	38
2 Chapter: Literature Review.....	46
2.1 Overview of Earlier Developments of Models for Nonlinear Response Analysis of Reinforced Concrete Structures.....	46
2.1.1 Earlier Developments in Concentrated Plasticity Models.....	47
2.1.2 Earlier Developments in Distributed Plasticity Models.....	51
2.2 Distributed Plasticity Models Incorporating Flexural and Shear Effects	57
2.3 Concentrated Plasticity Models Incorporating Flexural and Shear Effects	65

2.3.1	Concentrated Plasticity Models Based on Single-Component Hinges.....	68
2.3.1.1	Pincheira et al. (1999).....	69
2.3.1.2	Elwood (2002).....	73
2.3.1.3	Sezen and Chowdhury (2009)	81
2.3.1.4	Xu and Zhang (2011).....	88
2.3.2	Concentrated Plasticity Models Based on Generalized Hinges	95
2.3.2.1	Ricles et al. (1998).....	95
2.3.2.2	ElMandooh Galal (2002).....	103
2.3.2.3	Kaul (2004).....	111
2.4	Summary of Previous Research and Proposed Models	116
3	Chapter: Formulation of Beam-Column Element.....	159
3.1	Introduction	159
3.2	Updated Lagrangian Formulation.....	162
3.2.1	Formulation of Element Stiffness	163
3.2.2	Force Recovery	169
3.3	Inelastic Element Formulation.....	171
3.3.1	Axial Force-Bending Moment Interaction	171
3.3.1.1	Yield Surface Formulation	172
3.3.1.2	Yield Surface Evolution	176
3.3.1.2.1	Kinematic Control Surface Model.....	179
3.3.1.2.2	Updating the State of Evolution	184
3.3.1.3	Force Recovery.....	185
3.3.2	Axial Force-Shear Force Interaction.....	191
3.3.2.1	Shear Failure Surface Formulation.....	191
3.3.2.1.1	Shear Strength	193
3.3.2.2	Shear Failure Surface Evolution.....	196

3.3.2.2.1	Updating the State of Evolution	198
3.3.2.3	Force Recovery.....	199
3.3.3	Post-Yield Flexure-Shear Interaction.....	202
3.3.3.1	Shear Failure Modes and Criteria for Shear Failure.....	202
3.3.3.2	Shear Limit Surface Formulation	204
3.3.3.3	Shear Failure Surface Degradation.....	205
3.3.4	Element Tangent Stiffness	207
3.3.4.1	Element Tangent Stiffness for Plastic Hinge Model without Hardening	207
3.3.4.2	Element Tangent Stiffness for Hardening Model.....	210
3.3.4.3	Element Tangent Stiffness for Shear-Critical Column Model	212
3.3.4.3.1	Element Stiffness Including the Effects of Shear Deformations	212
3.3.4.3.2	Degradation of Element Tangent Stiffness.....	217
3.3.5	State Determination – Inelastic Response to Monotonic Loading.....	219
3.4	Quasi-Elastic Cyclic Formulation	228
3.4.1	Cyclic Stiffness Model.....	229
3.4.1.1	Event Based Formulation and State Determination	229
3.4.1.2	Stiffness Degradation	234
3.4.1.3	Biaxial Interaction Effects on Stiffness Degradation	236
3.4.2	Cyclic Pinching Model.....	237
3.4.2.1	Event Based Formulation and State Determination	237
3.4.2.2	Stiffness Degradation and Pinching	239
3.4.2.3	Biaxial Interaction Effects on Stiffness Degradation	240
3.4.3	Cyclic Strength Degradation Model.....	240
3.5	Damage Models.....	242
3.5.1	Overview of Damage Models for Reinforced Concrete Components and Structures	

3.5.2	Controlling Degrading Behaviour with Damage Models.....	247
3.6	Summary.....	249
4	Chapter: Implementation of Models in OpenSees Software Framework	319
4.1	Introduction	319
4.1.1	Object Oriented Programming Concepts	319
4.2	OpenSees Overview: Finite Element Classes for Structural Systems	324
4.2.1	Node, Element, Load and Constraint Classes	326
4.3	Object Oriented Design of New Models	328
4.3.1	Interface Design	329
4.3.2	Hierarchy Structure and Functionalities of New Classes	329
4.4	Implementation of New Models in OpenSees	336
4.4.1	Beam-Column Element Classes	336
4.4.1.1	Geometrically Nonlinear Elastic Element (ElasticGNL3D).....	337
4.4.1.2	Inelastic Elements (InelasticGNL3D)	338
4.4.1.2.1	Inelastic Element for Monotonic Response (InelasticMON3D).....	342
4.4.1.2.2	Inelastic Element for Cyclic Response (InelasticCYC3D).....	343
4.4.2	Yield Surface Classes.....	344
4.4.3	Shear Failure Surface Classes	347
4.4.4	Yield Surface Evolution Classes	348
4.4.5	Shear Failure Surface Evolution Classes	350
4.4.6	Plastic Stiffness Classes	352
4.4.7	Shear Limit Surface Classes.....	353
4.4.8	Cyclic Control and Cyclic Model Classes.....	354
4.4.9	Damage Model and Damage Progression Classes	360
4.5	Implementation Examples	361
4.5.1	Example on Cyclic Stiffness Model Event-Based Strategy	361

4.5.2	Examples with Cyclic Models	363
5	Chapter: Conclusions and Future Work	397
5.1	Summary.....	397
5.2	Conclusions	402
5.3	Recommendations for Future Work	403
Appendices.....		406
Appendix A : Element Class Details		406
A.1	Element Class UpdatedLagrangianBeamColumn3D	406
A.2	Element Class ElasticGNL3D.....	408
A.3	Element Class InelasticGNL3D	409
A.4	Element Class InelasticMON3D	411
A.5	Element Class InelasticCYC3D	412
References.....		413

List of Tables

Table 3-1 General state determination process for elements with yield surfaces and shear failure surfaces – Monotonic response	252
Table 3-2 Conditions for state determination – Monotonic response.....	253
Table 3-3 Path 1: from elastic (state 1) to flexural yielding (state 2). Conditions for state determination and transition between states	254
Table 3-4 Path 2: from elastic (state 1) to shear failure and post-shear failure degradation (state 3). Conditions for state determination and transition between states.....	256
Table 3-5 Conditions for maintaining / satisfying equilibrium - Case 1.1 to 1.5	258
Table 3-6 Conditions defining states in the cyclic stiffness model - positive excursions (deformations).....	263
Table 3-7 Conditions defining states in cyclic stiffness model - negative excursions (deformations).....	264
Table 3-8 State determination in cyclic stiffness model.....	265
Table 3-9 Cross-over event determination in cyclic stiffness model.....	267
Table 3-10 State determination in cyclic pinching model	268
Table 3-11 Cross-over event determination in cyclic pinching model.....	270
Table 4-1 Condition checks for loading state	365
Table 4-2 Cyclic response details	367

List of Figures

Figure 1-1 Hysteretic modeling types: (a) with no deterioration; (b) with cyclic strength degradation under repeated cycles; (c) with cyclic strength degradation under increasing displacement level; (d) with in-cycle strength degradation; (e) with stiffness degradation; (f) with pinching; (g) with combined cyclic strength and stiffness degradation; (h) with combined in-cycle strength and stiffness degradation.	40
Figure 1-2 Lateral load-top deflection hysteretic relationship in the direction of loading of test specimen U6 (Saatcioglu and Ozcebe 1989).....	41
Figure 1-3 Loss of lateral-load-carrying capacity of test specimen 4 (Sezen 2002)	42
Figure 1-4 Loss of axial-load-carrying capacity of test specimen 4 (Sezen 2002).....	43
Figure 1-5 Progressive flexure and shear damage in test specimen U3 (Saatcioglu and Ozcebe 1989)	44
Figure 1-6 Column failures from the 1999 Kocaeli, Turkey earthquake (Sezen 2002) ...	45
Figure 2-1 Concentrated plasticity models (Kaul 2004).....	119
Figure 2-2 Distributed plasticity models (Kaul 2004)	120
Figure 2-3 Schematic representation of nonlinear model (Pincheira et al. 1999)	121
Figure 2-4 Moment and rotation relation – hysteretic laws (Pincheira et al. 1999)	122
Figure 2-5 Shear force and displacement relation – hysteretic laws (Pincheira et al. 1999)	123
Figure 2-6 Free body diagram of column after shear failure (Elwood 2002).....	124
Figure 2-7 Shear failure defined by proposed drift capacity model (Elwood 2002)	125
Figure 2-8 Axial failure model (Elwood 2002)	126

Figure 2-9 Example of capabilities of Hysteretic uniaxial model (Elwood 2002)	127
Figure 2-10 Redefinition of backbone after failure is detected (Elwood 2002)	128
Figure 2-11 Shear spring in series model using Limit State uniaxial material model (Elwood 2002)	129
Figure 2-12 Rotational spring model (Elwood 2002).....	130
Figure 2-13 Axial spring in series model (Elwood 2002)	131
Figure 2-14 Hysteretic rules for lateral force-flexural displacement relationship (Sezen and Chowdhury 2009).....	132
Figure 2-15 Monotonic envelope for lateral force-shear displacement relationship (Sezen and Chowdhury 2009).....	133
Figure 2-16 Hysteretic rules for lateral force-shear displacement relationship (Sezen and Chowdhury 2009)	134
Figure 2-17 Schematic shear-flexural interaction model for columns (Xu and Zhang 2011).....	135
Figure 2-18 Illustration of the shear hysteretic model by Ozcebe and Saatcioglu (1989) (Xu and Zhang 2011).....	136
Figure 2-19 Hysteretic rules for the unloading stiffness (Xu and Zhang 2011).....	137
Figure 2-20 Examples of model defects in Ozcebe and Saatcioglu shear hysteretic model (a) nearly zero pinching stiffness and (b) negative hardening stiffness (Xu and Zhang 2011).....	138
Figure 2-21 Remedies for the defects in shear hysteretic model: (a) fix for nearly zero pinching stiffness and (b) fix for negative hardening (Xu and Zhang 2011).....	139
Figure 2-22 Rules for mapping between primary curves (Xu and Zhang 2010).....	140

Figure 2-23 Rules for mapping between unloading and reloading branches (Xu and Zhang 2010)	141
Figure 2-24 Model for degradation of concrete shear strength with flexural ductility proposed by Priestley et al. (1994) (Ricles et al. 1998)	142
Figure 2-25 Shear-Flexural Element (a) Component; (b) Flexural and Shear Subhinges (Ricles et al. 1998)	143
Figure 2-26 Schematics of (a) Yield Surfaces for Flexural Subhinges; (b) Shear Failure Isotropic Failure Surface (Ricles et al. 1998)	144
Figure 2-27 Degradation of Elastic Stiffness of (a) Shear Subhinge; (b) Effect on Element Shear Response (Ricles et al. 1998).....	145
Figure 2-28 (a) Element idealization (b) Plastic hinge idealization (ElMandooh Galal and Ghobarah 2003)	146
Figure 2-29 Yield surfaces for flexural subhinges (ElMandooh Galal and Ghobarah 2003)	147
Figure 2-30 Failure surface for shear subhinge (ElMandooh Galal and Ghobarah 2003)	148
Figure 2-31 Hysteretic model for flexural subhinge (ElMandooh Galal and Ghobarah 2003)	149
Figure 2-32 Combined flexure and shear response for columns (ElMandooh Galal 2002)	150
Figure 2-33 Shear force-deformation relationship for shear subhinge envelope (ElMandooh Galal and Ghobarah 2003).....	151
Figure 2-34 Axial force-moment interaction diagram (Kaul 2004).....	152

Figure 2-35 Idealization of the monotonic response (Kaul 2004)	153
Figure 2-36 Combined kinematic-isotropic hardening (Kaul 2004).....	154
Figure 2-37 Modes of shear failure (Kaul 2004)	155
Figure 2-38 Hysteretic/Cyclic pinching model for shear (Kaul 2004)	156
Figure 2-39 Full cycle pinching example (Kaul 2004).....	157
Figure 2-40 Half cycle pinching examples (Kaul 2004).....	158
Figure 3-1 Schematics of the element.....	271
Figure 3-2 Orientation of the element.....	272
Figure 3-3 Motion of a three-dimensional beam-column element	273
Figure 3-4 Cartesian degrees of freedom of the element in Deformed Configuration (1)	274
Figure 3-5 Force recovery – natural deformation approach: (a) Deformed Configuration (2); (b) Nodal displacements, projection in ${}^1x - {}^1y$ plane; (c) Rotations, projection in ${}^1x - {}^1y$ plane; (d) Nodal displacements, projection in ${}^1x - {}^1z$ plane; (e) Rotations, projection in ${}^1x - {}^1z$ plane	275
Figure 3-6 Yield surface model: (a) Force space; (b) Normalized force space	276
Figure 3-7 Examples of yield surface direction of evolution	277
Figure 3-8 Kinematic control surface	278
Figure 3-9 Translation in the kinematic control surface evolution model.....	279
Figure 3-10 Force-deformation response with kinematic hardening model.....	280
Figure 3-11 Kinematic control surface evolution model for cyclic loading: (a) $s_m g_m < 0$; (b) $s_m g_m > 0$	281

Figure 3-12 Relation of inelastic element response to plastic stiffness in kinematic control evolution model: (a) Relation between plastic stiffness and plastic deformations; (b) Force-deformation response.....	282
Figure 3-13 Incremental force: (a) Elastic-perfectly plastic material; (b) Elasto-plastic-strain hardening material.....	283
Figure 3-14 Directions of evolution: (a) Axial load is above the balanced failure point level (compression); (b) Axial load is below the balanced failure point level but above zero level (compression); (c) Axial load is below zero level (tension)	284
Figure 3-15 Centroidal direction of evolution with constant axial force: (a) Motion of the yield surface; (b) Change in elastic range during evolution	285
Figure 3-16 Mapping between subsequent surface (translated deformed) and initial yield surface	286
Figure 3-17 Inelastic force recovery example	287
Figure 3-18 Force recovery for the case of elastic-perfectly plastic materials	288
Figure 3-19 Force recovery for the case of hardening materials	289
Figure 3-20 Shear failure surface model: (a) Force space; (b) Normalized force space	290
Figure 3-21 Axial force-shear force interaction diagram: (a) Experimental (Vecchio and Collins 1986); (b) Model proposed by ElMandooh Galal and Ghobarah (2003).....	291
Figure 3-22 Degradation stiffness in post-shear failure force-deformation response.....	292
Figure 3-23 Non-uniform contraction evolution model.....	293
Figure 3-24 Mapping between subsequent surface (deformed) and initial shear failure surface	294
Figure 3-25 Force recovery to the shear failure surface	295

Figure 3-26 Shear failure modes.....	296
Figure 3-27 Model of a cantilever column	297
Figure 3-28 Post-yield degradation of the shear failure surface	298
Figure 3-29 State diagram for monotonic loading.....	299
Figure 3-30 Path 1: from elastic (state 1) to flexural yielding (state 2): (a) Force- deformation response for ductile behaviour; (b) Transition from state 1 to state 2; (c) Loading/Unloading criteria for state 2	300
Figure 3-31 Path 2: from elastic (state 1) to shear failure and post-shear failure degradation (state 3): (a) Transition from state 1 to state 3; (b) Loading / Unloading criteria for state 3	301
Figure 3-32 Path 3: from elastic (state 1) to flexural yielding (state 2) to shear failure and post-shear failure degradation (state 3); (a) Transition from state 2 to state 3; (b) Loading / Unloading criteria for state 3	302
Figure 3-33 Path 4: from elastic (state 1) to flexural yielding (state 2) to shear failure at degraded capacity and post-shear failure degradation (state 4).....	303
Figure 3-34 Path 5 (6): from shear failure and post-shear failure degradation (state 3 or 4) to residual shear capacity (state 5).....	304
Figure 3-35 Cyclic stiffness model – full cycle.....	305
Figure 3-36 Example of primary and follower half cycles.....	306
Figure 3-37 Cyclic stiffness model – response to primary half cycles in positive and negative excursions.....	307
Figure 3-38 Cyclic stiffness model – response to a primary half cycle and follower half cycles in positive excursions.....	308

Figure 3-39 State transition diagram in cyclic stiffness model: (a) positive excursions; (b) negative excursions	309
Figure 3-40 Cyclic pinching model – full cycle	310
Figure 3-41 Cyclic pinching model – response to primary half cycles in positive and negative excursions	311
Figure 3-42 Cyclic pinching model – response to a primary half cycle and follower half cycles in positive excursions.....	312
Figure 3-43 Cyclic pinching model – response to a primary half cycle and follower half cycles in positive and negative excursions	313
Figure 3-44 State transition diagram in cyclic pinching model: (a) positive excursions; (b) negative excursions	314
Figure 3-45 Cyclic strength degradation model – flexural response	315
Figure 3-46 Cyclic strength degradation model – shear response	316
Figure 3-47 Schematics of element – damage model interaction	317
Figure 3-48 Interaction with damage model at element component level.....	318
Figure 4-1 Conceptual module layout of OpenSees software framework. Reproduced from Fenves et al. (2004)	369
Figure 4-2 Main high-level abstractions in OpenSees software framework. Reproduced from Fenves et al. (2004)	370
Figure 4-3 Main classes of a finite element model	371
Figure 4-4 Beam-column element class hierarchy.....	372
Figure 4-5 Element ElasticGNL3D collaboration diagram	373
Figure 4-6 Element InelasticMON3D collaboration diagram	374

Figure 4-7 Element InelasticCYC3D collaboration diagram.....	375
Figure 4-8 Yield surface class hierarchy	376
Figure 4-9 Shear failure surface class hierarchy.....	377
Figure 4-10 Yield surface evolution class hierarchy	378
Figure 4-11 PlasticHardening3D collaboration diagram	379
Figure 4-12 Shear failure surface evolution class hierarchy.....	380
Figure 4-13 SFS_NonUniform3D collaboration diagram	381
Figure 4-14 Plastic flexural stiffness class hierarchy	382
Figure 4-15 Degrading shear stiffness class hierarchy	383
Figure 4-16 Shear limit surface class hierarchy.....	384
Figure 4-17 Cyclic control class hierarchy	385
Figure 4-18 CyclicControl3D collaboration diagram	386
Figure 4-19 Cyclic stiffness class hierarchy	387
Figure 4-20 Cyclic pinching class hierarchy	388
Figure 4-21 Cyclic strength degradation class hierarchy.....	389
Figure 4-22 Biaxial effects on stiffness class hierarchy	390
Figure 4-23 Damage model class hierarchy. Reproduced from Altoontash (2004)	391
Figure 4-24 Damage progression class hierarchy.....	392
Figure 4-25 Cyclic response example.....	393
Figure 4-26 Example of reinforced concrete column subjected to cyclic loading	394
Figure 4-27 Example 1 cyclic response: lateral load - displacement at top of column ..	395
Figure 4-28 Example 2 cyclic response: lateral load-displacement at top of column	396

List of Appendices

Appendix A : Element Class Details	406
A.1 Element Class UpdatedLagrangianBeamColumn3D	406
A.2 Element Class ElasticGNL3D	408
A.3 Element Class InelasticGNL3D	409
A.4 Element Class InelasticMON3D	411
A.5 Element Class InelasticCYC3D	412

List of Symbols

A	Cross-section area
A_s	Equivalent shear area
dF	Force increment
dF_{trial}	Trial incremental force
dF^*	Force component for inelastic hardening
$d\Delta$	Incremental displacement
$d\Delta_e$	Elastic component of the incremental displacement
$d\Delta_n$	Incremental natural displacement
$d\Delta_p$	Plastic component of the incremental displacement
DI	Diagonal contraction factor matrix for yield surface evolution
DI_s	Diagonal contraction factor matrix for shear failure surface evolution
E	Modulus of elasticity
g	Gradient at the point on the yield surface
G	Shear modulus
I	Moment of inertia
K_C	Complete element stiffness matrix
K_{deg}	Degradation stiffness
K_e	Element elastic stiffness matrix
K_g	Geometric stiffness matrix
K_p	Plastic stiffness matrix

K_{p0}	Initial plastic stiffness matrix
K_r	Plastic reduction matrix
K_s	Shear stiffness
K_t	Tangent stiffness matrix
L	Element length
M_y	Applied moment about y – axis
M_z	Applied moment about z – axis
$M_{yn,p}$	Moment strength about y – axis at load P
$M_{zn,p}$	Moment strength about z – axis at load P
M_{ynb}	Moment strength about y – axis at balanced point
M_{znb}	Moment strength about z – axis at balanced point
P	Axial force in the element
P_{bn}	Balanced axial load
P_{cn}	Axial compressive strength
P_{tn}	Tensile strength
T	Translation vector for yield surface evolution
u_n	Natural axial deformation
V	Shear force
V_n	Nominal shear capacity
V_u	Shear force in the member at shear failure
Δ_a	Drift at axial failure
Δ_f	Flexural deformation
Δ_s	Drift at shear failure

Δ_{sh}	Shear deformation
λ	Magnitude of plastic deformation
ϑ	Poisson's ratio
θ_{nx}	Natural rotation about x – axis
θ_{ny1}	Natural rotation about y – axis at element end 1
θ_{ny2}	Natural rotation about y – axis at element end 2
θ_{nz1}	Natural rotation about z – axis at element end 1
θ_{nz2}	Natural rotation about z – axis at element end 2
$\theta_{rbm,y}$	Rigid-body rotation about y – axis
$\theta_{rbm,z}$	Rigid-body rotation about z – axis
ρ''	Transverse reinforcement ratio
Φ	Yield surface function
Φ_s	Shear failure surface function

1 Chapter: Introduction

1.1 Background

Structural components of typical buildings and bridges are expected to undergo inelastic deformations during the severe ground shaking of major earthquakes. For structures designed according to capacity design principles, plastic hinges are expected to form at designated structural members specifically designed as ductile components to dissipate seismic energy through inelastic deformations. However, older structures were typically not designed following the ductile approach. For example, reinforced concrete structures designed prior to the 1970s are deficient in their seismic resistance due to inadequate detailing, such as inadequate development length and insufficient and widely spaced transverse reinforcement. Experimental research and post-earthquake reconnaissance have demonstrated that deficient reinforced concrete components are vulnerable to shear or shear-flexure failure during earthquakes.

In seismic events, reinforced concrete members may be subjected to repeated cyclic load reversals and combined axial, flexure and shear effects. The seismic response of reinforced concrete members may exhibit stiffness degradation and strength deterioration as a result of accumulated damage during inelastic excursions. Shear-critical reinforced concrete columns may suffer severe degradations and exhibit pinching behaviour.

In order to be able to more realistically assess the seismic behaviour and performance of reinforced concrete structural systems, accurate and computationally efficient numerical

models that capture the behaviour of members designed as ductile as well as non-ductile members are needed. Research is required to develop practical analytical models that capture the full interaction of axial, flexure and shear effects and the effects of accumulation and progression of damage on the response of reinforced concrete members under multi-component seismic loading, which comprises biaxial cyclic loading with variable axial load effects. This is essential not only to achieve more resilient design of new structures but also to devise reliable and efficient retrofit and rehabilitation strategies for old deficient structures to intervene the formation seismic progressive collapse mechanism.

1.2 Behaviour and Modeling of Reinforced Concrete Columns

This section describes the main aspects of the behaviour of reinforced concrete columns, broadly divided into monotonic and cyclic behaviour, and summarizes the common modeling approaches developed for nonlinear response analysis with focus on beam-column models.

1.2.1 Monotonic Behaviour

Response characteristics of reinforced concrete structural members, including the effective elastic stiffness, nominal strength, post-yield hardening, etc. are dependent on a number of parameters such as reinforcing steel distribution, confinement provided to concrete by transverse reinforcing bars and axial load levels.

Reinforced concrete members tend to show high initial flexural stiffness prior to cracking of the concrete but due to the low tension capacity of concrete, increased flexure causes tension cracks which reduce the cross-section stiffness to the cracked stiffness. Upon further increase of the flexure, the reinforcing steel yields which leads to significant decrease in the member stiffness. The distribution of tension cracks depends on the moment gradient and in frames subjected to lateral loads, these cracks are mostly located at the member ends where the maximum moments occur. When reinforced concrete beam-column members are modeled by line elements, a common approach is to use equivalent effective stiffness to approximate the uncracked/cracked stiffness of the member up to yielding. The effective stiffness of a reinforced concrete member also depends on the axial load level, since compression tends to delay cracking, and tension tends to accelerate it.

The initiation of yielding in the reinforcing steel also depends on the axial load level, which can be captured by using an axial force-moment (P-M) interaction diagram. The balanced point in the P-M interaction diagram represents the case where the concrete starts to crush in compression as the outermost steel rebars begin to yield in tension. The axial load level also affects the post-yield flexural behaviour of reinforced concrete members. At lower axial load, post-yield flexural behaviour is dominated by the tensile reinforcing steel and shows hardening. The rate of hardening gradually reduces as the response approaches the ultimate strength, reached when the concrete in compression crushes. At higher axial load, reinforced concrete members exhibit less post-yield hardening followed by pronounced softening response due to concrete crushing and rebar

buckling. The post-yield flexural behaviour also depends on the confinement of concrete. For example, in members where sufficient and closely spaced transverse reinforcement provide effective confinement, the concrete strength and ductility are significantly higher than for unconfined reinforced concrete members. Idealized models describing the constitutive relation for confined concrete have been developed by Kent and Park (1971), Park et al. (1982) (modified Kent and Park model), Sheikh and Uzumeri (1982), Mander et al. (1988), Saatcioglu and Razvi (1992), among others. Concrete material models, together with models describing the constitutive relation for reinforcing steel, can be used for moment-curvature analysis of a reinforced concrete cross-section to obtain the effective stiffness, moment at yield at certain axial load level, curvature capacity, etc. In reinforced concrete frame members, when the moment at a member end exceeds the yield moment, the end plastifies and a plastic hinge of a finite length forms. The plastic rotation capacity of a frame member depends on the ultimate curvature at the member end and the plastic hinge length. Several semi-empirical formula have been proposed for estimation of plastic hinge length, including those proposed by Corley (1966), Mattock (1967), Sawyer (1964), Priestley et al. (1996).

Inelastic flexural response of reinforced concrete members can be modeled by using elastic frame elements with nonlinear rotational springs at the ends. The rotational spring models describe the moment-rotation relation based on reasonable assumptions but tend to oversimplify the complex reinforced concrete behaviour, in particular the interactions of axial load and bending moments. Inelastic flexural response can also be modeled using generalized plastic hinge formulation based on stress resultant plasticity concepts. In the latter approach, the interaction of axial load and bi-directional bending moments is

captured by multi-axial yield surface and post-yield flexural behaviour is modeled by the evolution of the yield surface. Since maximum moments, and therefore yielding and inelastic deformations, in frame members typically occur at the member ends, inelastic analysis can be performed by using yield surfaces modeled as concentrated plastic hinges at the element ends. To more accurately capture the spread of plasticity along the element length, distributed plasticity models can be used where the formulation includes several integration points along the element length. Another approach which captures the axial force-moment interaction effects on the inelastic flexural response of reinforced concrete members is based on fiber models using constitutive relations of concrete and steel material models. The yield-surface approach and the fiber-section approach can be used in either concentrated plasticity models or distributed plasticity models. A detailed review of models for nonlinear response analysis of reinforced concrete structures is presented in Chapter 2.

1.2.2 Cyclic Behaviour

In major earthquakes, reinforced concrete members may be subjected to severe cyclic loadings. During inelastic excursions of repeated reversed cycles, members accrue damage which causes degradation in stiffness and loss of strength, and may eventually lead to collapse. To quantify the seismic damage to individual structural components or the global structure, several damage indices have been proposed, including Park and Ang (1985), Kratzig et al. (1989), Kunnath et al. (1992), Mehanny and Deierlein (2001). Local damage indices for individual elements may be based on a combination of force, displacement, plastic deformations and dissipated hysteretic energy.

Damage indices can also be used to degrade constitutive stiffness and strength parameters of the element during the course of analysis. Calibration of the damage models with experimental data is usually required. In the yield-surface approach based on stress and strain resultants, only a few parameters control the cyclic response of the reinforced concrete component, whereas in the fiber model approach the cyclic response is affected by the combined response of many fiber models each with specific material properties, and damage models need to be incorporated at material level, for which experimental data may not be readily available.

Under cyclic loading, several aspects of the reinforced concrete member behaviour need to be modeled in addition to those discussed in Section 1.2.1. Figure 1-1 shows hysteretic modeling types describing different characteristics of the cyclic behaviour of reinforced concrete members, including strength deterioration, stiffness degradation and pinching behaviour.

Two types of strength degradation can be distinguished as cyclic strength degradation and in-cycle strength degradation (FEMA P-440A). Strength degradation, also referred to as strength deterioration, is evidenced by the reduction in lateral strength of the member, ΔF . Structural components may experience cyclic strength degradation upon reversals of the loading or during subsequent loading cycles. The level of inelastic displacement may be maintained at the same inelastic displacement in subsequent loading cycles, as shown in Figure 1-1(b) or increased during each subsequent cycle, as shown in Figure 1-1(c). In-

cycle strength degradation, shown in Figure 1-1(d), is characterized by loss of the lateral strength upon increasing the inelastic displacement within the same cycle. It is manifested by the negative post-yield stiffness, $k_{p,deg}$. As emphasized in FEMA P-440A, it is important to make a distinction between cyclic and in-cycle strength degradation since the latter may lead to lateral dynamic instability of a structural system.

Stiffness degradation is characterized by a reduction in the slope of the force-deformation hysteresis curve, $k_{e,deg}$, during unloading and reloading, as shown in Figure 1-1(e). The elastic stiffness degrades progressively with increasing peak deformation and the number of deformation cycles with excursions in the inelastic range of the member. Peak-oriented reloading stiffness has been found to match relatively closely the reinforced concrete member response observed in experiments.

Pinching behaviour is manifested by significant reduction in stiffness during reloading after unloading, followed by partial recovery of stiffness after displacement is reversed, as shown in Figure 1-1 (f). Pinching behaviour is commonly associated with opening of cracks when displacement is imposed in one direction. Upon closing of cracks the stiffness is partially recovered when displacement is reversed in the opposite direction. Pinching behaviour may also be associated with bond slip.

Figure 1-1(g) shows combined cyclic strength degradation with stiffness degradation, and Figure 1-1(h) shows combined in-cycle strength degradation with stiffness degradation, which may be observed in the seismic response of reinforced concrete members.

One of the major factors affecting the cyclic behaviour of reinforced concrete members is the reinforcement detailing. The cyclic response of members designed and detailed to develop desirable ductile flexural yielding prior to shear failure or anchorage and lap splice failures is, generally, characterized by stable hysteretic loops. Typically, such components exhibit small stiffness degradation, have considerable energy absorption capacity and are capable of sustaining large inelastic deformations prior to experiencing strength degradation caused by concrete crushing or rebar buckling/ fracture. Many older deficient reinforced concrete structures, however, have reinforcement that does not provide sufficient confinement to the concrete. As demonstrated in experimental studies (Ghee et al. 1989, Saatcioglu and Ozcebe 1989, Watanabe and Ichinose 1992, Wong et al. 1993, Priestley et al. 1994), under cyclic loading such components may suffer severe stiffness and strength degradation, with low ductility capacity and possible shear failure under combined axial-flexure-shear effects. Shear-critical reinforced concrete components may also demonstrate significant pinching behaviour as more damage is accumulated.

As noted previously, a common approach for nonlinear response analysis of reinforced concrete structures is to model structural components using elastic frame elements with concentrated nonlinear rotational springs at the ends. A hysteretic moment-rotation relation describes the entire cyclic response of the nonlinear spring. The monotonic moment-rotation curve envelops the cyclic response and hysteretic rules define the stiffness in the unloading and reloading states. In this approach, by using a pre-defined

"back-bone" curve to enforce the relation between a singular force quantity and its deformation component, the inelastic response (yielding) is not clearly separated from the degraded elastic cyclic response.

In models based on generalized plastic hinge formulation, the inelastic response is modeled using yield surface and evolution models, and the degraded elastic hysteretic response is captured by cyclic models. In the models with rotational springs described previously, relation between a singular force quantity and its corresponding deformation component is enforced, whereas the yield surface models are defined for multiple components in force space and cyclic models for each of these components can be incorporated in the formulation. Separate hysteretic models can be defined to capture the different characteristics of the cyclic response of reinforced concrete members described above.

As mentioned previously, damage models can be incorporated in the element formulation to degrade the stiffness and strength properties of the element during analysis. Models using this approach are capable of more realistically capturing the effects of accumulation and progression of damage on the degradations of structural components compared to models using initially predefined degradation parameters for the entire analysis. It has also been observed in experimental studies that damage accumulated in cyclic excursions in one direction affects not only stiffness and strength parameters of a component in the direction of loading but also the behaviour in other out-of-plane directions. To consider

these interaction effects on stiffness and strength degradation, multi-component damage models that capture hysteretic damage in multi-directions are needed.

Models with rotational springs and models with yield surfaces are primarily suitable to capture the inelastic flexural response of reinforced concrete components. Behaviour of shear critical columns and aspects of modeling shear failure are discussed in the next section.

1.2.3 Shear Critical Behaviour

Shear critical behaviour is observed in reinforced concrete columns with inadequate seismic detailing mainly in old structures constructed prior to the 1970s. Such columns may fail in shear prior to yielding in flexure. Shear failure may also occur if shear demand exceeds shear capacity of the member at relatively low ductility level. Shear failure is also observed under large lateral drifts after flexural yielding due to weakening of the shear resisting mechanism in the plastic hinge region (Ghee et al. 1989, Wong et al. 1993, Priestley et al. 1994, Sezen 2002). Models describing the relation of shear strength degradation with displacement ductility have been proposed by Aschheim and Moehle (1992), Priestley et al. (1994), Sezen and Moehle (2004), among others. As observed in experimental studies of columns with high shear, shear cracks develop and propagate rapidly as the member is subjected to lateral displacements, after which axial load carrying capacity also degrades with increasing displacements. Elwood (2002) proposed empirical relations for drift ratios at shear failure and drift ratio at axial failure of shear-damaged columns.

Shear failure can be captured based on strength criteria in the case where shear capacity of the member is lower than the shear demand and brittle shear failure occurs prior to yielding, and in the case where shear capacity of the member is comparable with the flexure capacity and shear failure occurs at low ductility levels. Strength criteria can be incorporated in reinforced concrete frame element models as nonlinear shear springs at the ends of the element. Similarly to the nonlinear rotational spring models, a hysteretic shear force-deformation relation describes the inelastic and cyclic response of the shear spring. To account for the interaction of axial load and bi-directional shear forces, multi-axial shear failure surfaces can be used in the element formulation. In the latter approach, the post-shear failure behaviour characterized by severe strength degradation can be modeled by the evolution of the shear failure surface.

To capture shear failure in the case where shear capacity is higher than the shear demand but degrades under increasing inelastic displacements, a displacement ductility based criteria are needed in addition to the strength based criteria. Models describing the relation of shear strength degradation and displacement ductility can be included in the evolution of the shear failure surface to capture the effects of inelastic flexure-shear interaction.

Frame element models for reinforced concrete members incorporating flexure and shear effects based on the distributed plasticity and the concentrated plasticity approach are reviewed in Section 2.2 and Section 2.3, respectively.

1.2.4 Common Failure Modes of Reinforced Concrete Columns

As demonstrated in experimental studies and observed in post-earthquake reconnaissance, the common failure modes of reinforced concrete columns can be summarized as follows: ductile governed by flexural plastic hinging, moderately ductile with shear failure resulting from exceedance of degraded shear capacity in the flexural plastic hinge zone, limited ductile with shear failure resulting from exceedance of shear capacity after yielding at relatively low ductility levels, and brittle failure governed by shear failure as the initiating failure mechanism.

The ductile failure mode is a desired failure mode that can be controlled by specifically designing and detailing the reinforced concrete component to form flexural plastic hinges at designated locations and dissipate seismic energy through inelastic deformations. The flexural cyclic response of reinforced concrete columns designed and detailed following the ductile approach is characterized by stable hysteretic loops. Figure 1-2 shows the lateral load-top deflection relationship of a reinforced concrete column designed and detailed as ductile obtained in the experimental study conducted by Saatcioglu and Ozcebe (1989).

Failure modes of reinforced concrete columns governed by brittle shear failure and flexure-shear interaction leading to shear failure have to be prevented because they may cause undesired collapse mechanism. Experimental research has been conducted on flexure-shear types of column failure by Ghee et al. (1989), Saatcioglu and Ozcebe

(1989), Wong et al. (1993), Priestley et al. (1994), Elwood (2002), Sezen (2002), Sezen and Moehle (2006), among others. It has been demonstrated that shear cracks develop and propagate rapidly in reinforced concrete columns with high shear stress subjected to lateral displacements. It has also been observed that axial load carrying capacity in shear-damaged columns degrades with increasing lateral displacements. Axial failure occurs when the shear-damaged column can no longer sustain axial loads. Figures 1-3 to 1-6 show examples of column failures from experimental studies and observed earthquake damage. Behaviour governed by brittle shear failure is observed when the reinforced concrete column fails in shear prior to yielding in flexure, which is sudden in nature. Limited ductile behaviour with shear failure is observed when the shear demands exceeds the shear capacity after flexural yielding and hardening at relatively low displacement ductility level. Moderately ductile behaviour with shear failure of reinforced concrete columns is observed under large lateral drifts after flexural yielding due to deterioration of the shear strength in the flexural plastic hinge region.

1.3 Objectives and Scope

The objective of this research is to develop the formulation of a comprehensive 3D beam-column model for seismic response analysis of reinforced concrete structures subjected to multi-component seismic loading, including biaxial load reversals and variable axial load, and to propose the framework for the implementations of the new model using object oriented design concepts. The present research is aimed at deriving a unified and consistent new model capable of capturing the entire range of nonlinear behaviour of reinforced concrete frame members, from ductile to brittle, and in between, which can

arise from the interaction between axial, shear and flexure effects, and their evolution during the progression and accumulation of damage. The proposed model is aimed at capturing the post-peak degradation behaviour of members in reinforced concrete frame structures, which would lead to more accurate account for the progression of damage and the redistribution of load in the global structure, and realistic prediction of the failure mechanism in the seismic progressive collapse analysis.

This research is focused on the development of the beam-column element formulation based on concentrated plasticity approach and the framework for the implementation of new models employing object oriented design to facilitate extensibility and flexibility. The full implementation of the derived models and more extensive verification studies on nonlinear response analysis of reinforced concrete frame structures are recommended as future research.

1.4 Thesis Outline

Chapter 1 presents an introduction on the background of seismic progressive collapse analysis and a discussion on the main aspects of the monotonic and cyclic behaviour of reinforced concrete columns. Shear-critical behaviour observed in reinforced concrete columns in older deficient structures with inadequate seismic detailing and the common failure modes of reinforced concrete columns are also discussed. The objectives and scope of this research are presented.

Chapter 2 presents a review of existing analytical models for nonlinear seismic response analysis of reinforced concrete structures. Concentrated and distributed plasticity models

incorporating flexural and shear effects are carefully reviewed. Advantages and the limitations of the existing models are discussed.

Chapter 3 provides the mathematical background to the formulation of the proposed beam-column model for seismic progressive collapse analysis of reinforced concrete structures. The concentrated plasticity-based formulation for inelastic modeling incorporating yield surface, shear failure surface, shear limit surface and evolution models is explained. The cyclic model formulation that captures stiffness degradation, strength deterioration and pinching, and incorporates the effects of progression of damage on the post-peak cyclic behaviour is also explained.

Chapter 4 describes the framework for the implementations of the proposed model using object oriented design. The abstract base classes established to describe the behaviour of the individual components of the proposed model and the interface for the interaction between the base classes are also presented. Some column verification examples are also included in this chapter.

Chapter 5 presents conclusions and summarizes the main aspects of this research. Recommendations are suggested for future research to incorporate full implementation of the developed models and conduct more extensive verification examples of frame structures.

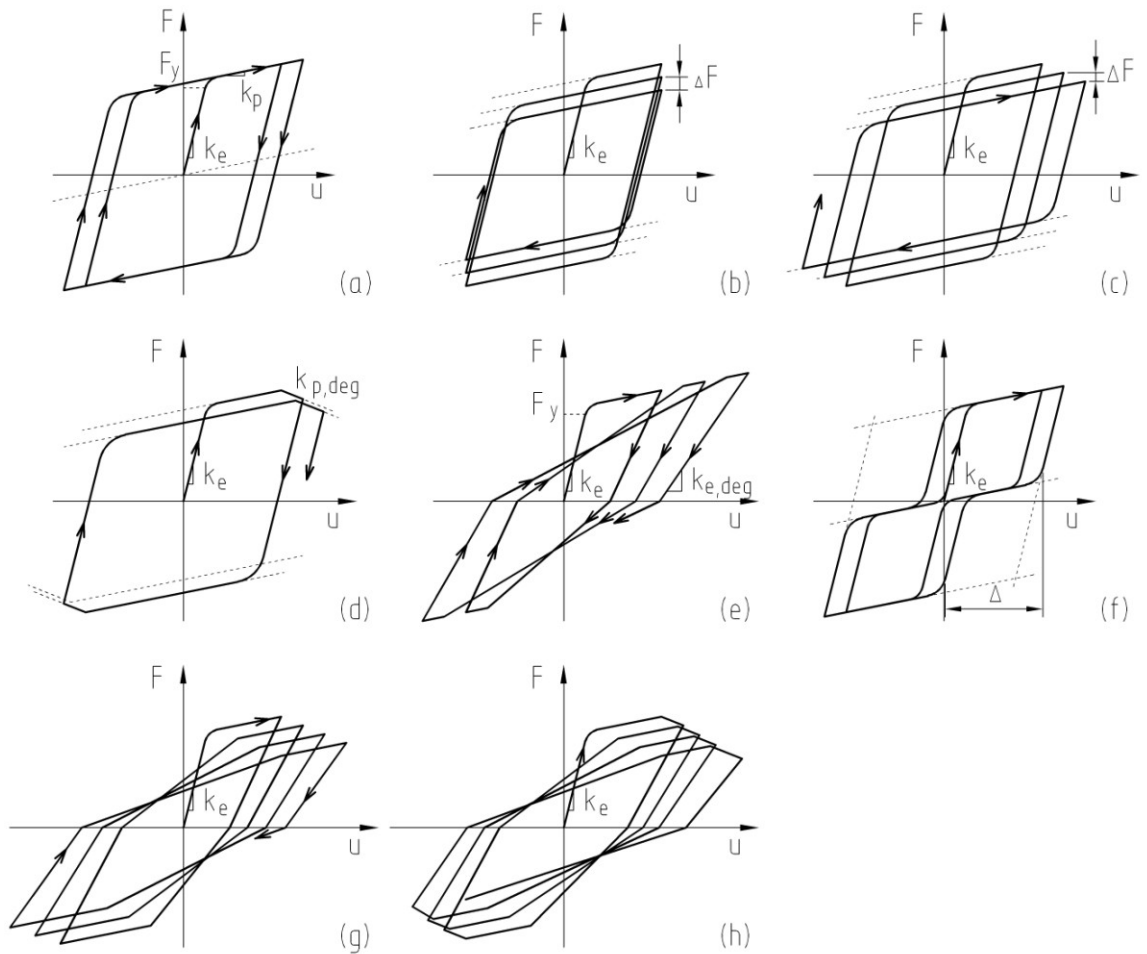


Figure 1-1 Hysteretic modeling types: (a) with no deterioration; (b) with cyclic strength degradation under repeated cycles; (c) with cyclic strength degradation under increasing displacement level; (d) with in-cycle strength degradation; (e) with stiffness degradation; (f) with pinching; (g) with combined cyclic strength and stiffness degradation; (h) with combined in-cycle strength and stiffness degradation.

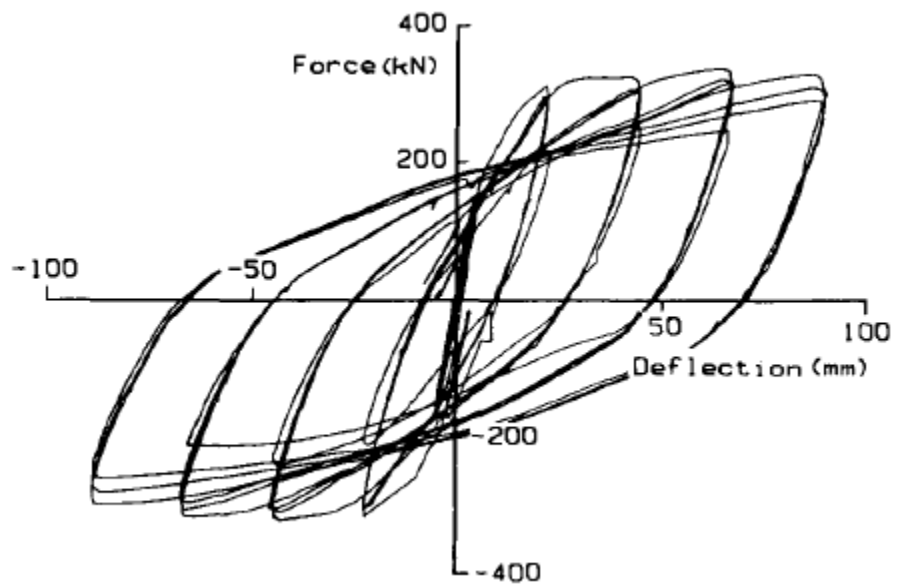


Figure 1-2 Lateral load-top deflection hysteretic relationship in the direction of loading of test specimen U6 (Saatcioglu and Ozcebe 1989)



Figure 1-3 Loss of lateral-load-carrying capacity of test specimen 4 (Sezen 2002)



Figure 1-4 Loss of axial-load-carrying capacity of test specimen 4 (Sezen 2002)

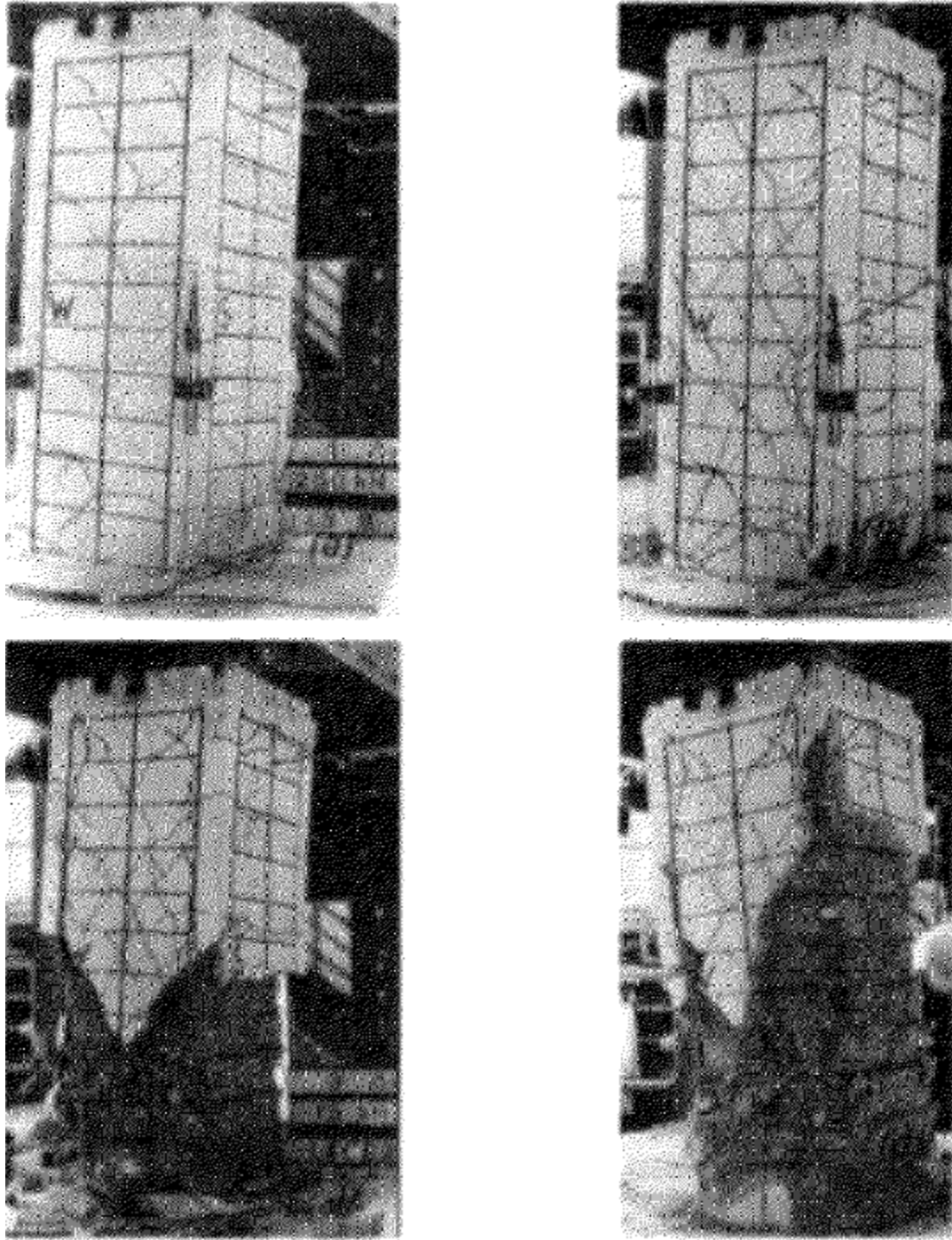


Figure 1-5 Progressive flexure and shear damage in test specimen U3 (Saatcioglu and Ozcebe 1989)



Figure 1-6 Column failures from the 1999 Kocaeli, Turkey earthquake (Sezen 2002)

2 Chapter: Literature Review

2.1 Overview of Earlier Developments of Models for Nonlinear Response Analysis of Reinforced Concrete Structures

Comprehensive reviews of earlier developments in modeling and analysis of the nonlinear seismic response of reinforced concrete structures are presented in Filippou and Issa (1988), Taucer et al. (1991), Filippou et al. (1992), Spacone et al. (1996), among others.

Authors have proposed different classifications for nonlinear models but the common of these classifications is that they are primarily based on the level of accuracy and refinement of the models. As summarized by Taucer et al. (1991) and Spacone et al. (1996), the models for nonlinear response analysis of reinforced concrete structures can be divided into three main categories depending on the level of complexity as follows: global models which represent the structure by only a few selected degrees of freedom; discrete finite element models which capture the hysteretic behaviour of reinforced concrete members; and microscopic finite element models primarily used to study different physical nonlinearities by discretizing members and joints into a large number of finite elements. Generally, discrete finite element models are considered the most suitable for conducting nonlinear seismic response analysis of large scale structures since they allow more insight into the seismic response of structural members as well as the entire structure compared to the global models, and are computationally more efficient compared to the microscopic finite element models.

Here, a brief summary of the earlier developments in discrete finite elements for modeling the inelastic response of reinforced concrete components is first presented in order to outline the framework for the more recent developments that incorporate the modeling of more complex hysteretic behaviour such as the effects of shear failure and post-shear failure behaviour.

Depending on the basic assumptions for the location and distribution of the plastic zones, the discrete finite elements, also referred to as frame elements, can be categorized as concentrated plasticity and distributed plasticity models.

2.1.1 Earlier Developments in Concentrated Plasticity Models

It is generally observed that under seismic excitations the inelastic behaviour of reinforced concrete frames is concentrated at the ends of girders and columns where maximum moments occur. As noted by Taucer et al. (1991), and Spacone et al. (1996), among others, considering the general observations for the locations of the inelastic deformations in reinforced concrete components, an early modeling approach is based on concentrated plasticity models using nonlinear rotational springs to represent the inelastic behaviour.

Some of the first nonlinear frame models are the models proposed by Clough et al. (1965), Clough and Johnston (1966) and Giberson (1967). The Clough model allows for a bilinear elastic-strain hardening moment-rotation relation and consists of two

components in parallel. One of the components is an elastic-perfectly plastic element with nonlinear springs at the ends where the inelastic deformations are concentrated, and the other component is a linear elastic element to represent strain-hardening. Takizawa (1976) has modified the Clough model to account for the cracking of concrete by using a multilinear moment-rotation relation. A limitation of the parallel component elements is the difficulty in accounting for stiffness degradation of reinforced concrete components under reversed cyclic loading. The series model formally introduced by Giberson (1967), also known as the one-component model, consists of a linear elastic element and two nonlinear rotational springs attached at the element ends where all inelastic deformations are concentrated, as shown in Figure 2-1(a). This model overcomes the limitation of the Clough model in modeling stiffness degradation by allowing for more complex hysteretic laws to describe the moment-rotation relations of the nonlinear springs.

The first hysteretic law describing the flexural behaviour of reinforced concrete components under cyclic load reversals was proposed by Clough et al. (1965). Takeda et al. (1970) proposed a more refined hysteretic model for the cyclic stiffness degradation in flexure and is still widely used in many beam-column models. One of the first qualitative models describing the shear force-shear deformation hysteretic relation for reinforced concrete components was proposed by Celebi and Penzien (1973). Based on experimental observations, Ozcebe and Saatcioglu (1989), among other researchers, proposed a hysteretic shear force-deformation model that describes the stiffness degradation and pinching behaviour.

As summarized by Spacone et al. (1996), some of the earlier models for nonlinear seismic response analysis of reinforced concrete components also included modeling of the pinching behaviour (Banon et al. 1981, Brancaleoni et al. 1983), and fixed-end rotations for modeling bar pull-out (Otani 1974, Otani et al. 1985, Filippou and Issa 1988).

Even though the effects of axial load on the flexural capacity have been recognized by some researchers (e.g. Kanaan and Powell 1973), the axial force-bending moment interaction is typically ignored in the earlier models that are based on nonlinear rotational single-degree-of-freedom springs.

An approach based on the principles of the theory of plasticity has been used by many researchers to include the axial load effects in concentrated plasticity models. In this approach, the axial force-bending moment interaction is described by means of a yield surface for the stress resultants and a flow rule for the direction and relative magnitude of strain resultants, i.e. hinge rotations and axial extensions. Figure 2-1(b) shows the schematics of a concentrated plasticity model based on a yield surface formulation. Multilinear constitutive relations representing concrete cracking, reinforcing steel yielding and strain hardening as well as stiffness degradation are modeled by using multiple yield and subsequent loading surfaces with associated hardening rules for the nonlinear hinges. Takayanagi and Schnobrich (1979) were some of the first researchers to account for the axial force-bending moment interaction effects in their study on seismic response of coupled shear wall systems. Takizawa and Ayoama (1976) introduced a

concentrated plasticity model including stiffness degradation for biaxial bending conditions based on two interaction surfaces in moment space representing cracking and yielding. Chen and Powell (1982) developed generalized plastic hinge concepts to incorporate axial-moment interaction and stiffness degradation for three-dimensional beam-column elements under biaxial bending based on multi-axial yield surfaces.

A different approach to incorporate axial force-bending moment interaction in concentrated plasticity elements is based on using a set of zero-length springs to represent concrete and reinforcing steel. These models are also referred to as multi-spring hinge models. Lai et al. (1984) proposed a model that consists of a linear elastic element with one inelastic element at each end. Each inelastic element comprises four effective steel springs and five effective concrete springs describing the constitutive material relations for steel and concrete, respectively. Saiidi et al. (1986) refined the nine-spring hinge model proposed by Lai et al. (1984) by considering four composite springs at each corner of the section and one concrete spring at the centre effective only in compression. Jiang and Saiidi (1990) further improved the computational efficiency and numerical stability of the model by using only four composite springs for the inelastic hinge.

The nonlinear frame models based on the concentrated plastic hinge concepts are a simplification of the actual behaviour of reinforced concrete members which is characterized by the gradual spread of inelastic deformations along the member as a function of the loading history. The element formulations of the concentrated plasticity models are based on plasticity relationships between the member end forces and the

member end deformations, and therefore these relationships require calibrations based on expected axial load and moment gradient along the member. The main advantage of concentrated plasticity models is their relative simplicity and computational efficiency.

2.1.2 Earlier Developments in Distributed Plasticity Models

The frame elements based on the distributed plasticity approach provide a more accurate description of the inelastic behaviour of reinforced concrete members. The formulations of distributed plasticity models allow plastic hinges to form at any integration point of the finite element model. The response of the entire element is obtained by numerical integration of the section response at the predefined integration points. The number of integration points and their location depend on the numerical integration method. The nonlinear behaviour at a cross section can be described by constitutive relations using either a stress-resultant plasticity-based approach or a fiber discretization approach.

As summarized in the early literature surveys conducted by Filippou and Issa (1988), Taucer et al. (1991), Spacone et al. (1996), some of the first distributed plasticity models for beams are the models proposed by Soleimani et al. (1979) and Meyer et al. (1983). The axial force-bending moment interaction is neglected in the earlier models. Roufaiel and Meyer (1987) extended the model proposed by Meyer et al. (1983) to include the effects of shear and axial forces on the flexural hysteretic behaviour based on a set of empirical rules. Darvall and Mendis (1985) proposed a similar but simpler model in which the end inelastic deformations follow a trilinear moment-curvature relation.

Keshavarzian and Schnobrich (1985) extended the model proposed by Soleimani et al. (1979) to account for axial force-bending moment interaction.

Takayanagi and Schnobrich (1979) proposed a beam-column element subdivided into a finite number of longitudinal subelements, each represented by a nonlinear rotational spring. This model was used in their study on seismic response analysis of coupled shear walls to account for the variation of axial load. As noted by Taucer et al. (1991), although the inelastic deformations are essentially concentrated in the end springs, this model belongs to the group of distributed plasticity models because it accounts for inelastic deformations along the length of the element.

Emori and Schnobrich (1981) studied the nonlinear response of a plane frame combined with a shear wall using different beam-column models. In one of the models, the element is composed of a series of nonlinear rotational springs similar to the model used by Takayanagi and Schnobrich (1979). Another is the layer model in which inelastic deformations are allowed to occur over a finite length at the ends of the element. Axial force-bending moment interaction is accounted for in the layer model.

Filippou and Issa (1988) also proposed a beam-column element subdivided into subelements in series by a different approach. A separate subelement is used to describe the effect of flexure, shear and bond-slip. The complex hysteretic behaviour of the reinforced concrete member is modeled through the interaction and combination of the different subelements. Following a similar approach, D'Ambrisi and Filippou (1999)

proposed a frame element for modeling the cyclic response of reinforced concrete elements including also the effects of shear sliding in the critical regions and the shear distortion along the element based on a phenomenological shear force-shear distortion relationship.

The distributed plasticity elements are formulated using either the standard displacement-based (stiffness) approach or the flexibility-based approach. An overview of the displacement-based and the flexibility-based element formulations is presented by Taucer et al. (1991).

The early distributed plasticity elements proposed by Kang and Scordelis (1977), Hellesland and Scordelis (1981), Mari and Scordelis (1984) among others, are formulated with the classical stiffness method using cubic Hermitian polynomials to approximate the deformations along the element. The limitations of displacement-based elements stem from the assumption of cubic interpolation functions which result in a linear curvature distribution along the element. However, the curvature distribution is highly nonlinear in the inelastic region and this may cause numerical instability problems. The problems may be alleviated by using a very fine discretization in the inelastic region but at increased computational efforts.

Menegotto and Pinto (1977) proposed a formulation based on interpolation of both section deformation and section flexibilities and include axial force-bending moment

interaction. Mahasuverachai and Powell (1982) proposed flexibility-dependent shape functions for inelastic pipe elements that are continuously updated during the analysis.

As discussed by Taucer et al. (1991) and Spacone et al. (1996), the more recent developments in distributed plasticity models follow a trend toward flexibility-based element formulations and discretization of the section into fibers. A distributed plasticity model based on a fiber section approach is schematically shown in Figure 2-2(a). Among the earlier flexibility-based fiber elements are those proposed by Kaba and Mahin (1984), Zeris and Mahin (1988, 1991). The flexibility-based element formulations used in these models allow more accurate description of the force distribution within the element. The formulations are based on the assumption for the force interpolation functions that the bending moment distribution along the element is linear and the axial force distribution is constant. Independent from the state of the element, the force interpolation functions strictly satisfy the equilibrium, and thus overcome some of the limitations of displacement-based elements. A challenge for the flexibility-based elements is their implementation into existing finite element programs based on the direct stiffness method. Ciampi and Carlesimo (1986) proposed a consistent state determination procedure for flexibility-based elements. The method originally proposed by Ciampi and Carlesimo (1986) is refined by Taucer et al. (1991) and Spacone et al. (1996) and applied to the formulation of fiber beam-column elements.

Neuenhofer and Filippou (1997) have also discussed in details the advantages of flexibility-based beam-column elements over displacement-based elements. The main

advantage is that fewer flexibility-based elements are required to represent the nonlinear behaviour of a frame member, and thus keeping the number of degrees of freedom in a structural model to a minimum.

As mentioned before, the nonlinear section response in distributed plasticity elements can be described using the stress-resultant plasticity-based approach. Figure 2-2(b) shows the schematics of a distributed plasticity model based on a yield surface formulation. El-Tawil and Deierlein (1996) have implemented yield-surface models to describe the section force-deformation behaviour at integration points in a beam-column element developed for analysis of reinforced concrete and composite members. As summarized by Mehanny (1999), the approach used by El-Tawil and Deierlein (1996) follows the work of Dafalias and Popov (1977), Orbison (1982), Hilmy (1984) and Zhao (1993).

The fiber approach for describing the nonlinear section response is based on discretization of the cross-section into individual fibers representing longitudinal reinforcing steel, confined concrete area, and unconfined concrete cover. Each fiber is associated with the uniaxial constitutive relation of an appropriate material model. At section level, the nonlinear response under axial force and bending moment is derived by integrating the fiber stresses over the cross-section and the axial force-bending moment interaction is thus accounted for. The element response is derived by integrating the section response along the element length.

Fiber models are also used for moment-curvature analysis of reinforced concrete sections. Properties such as yield moment and curvature, ultimate moment and curvature ductility capacity can be obtained from moment-curvature analysis. These properties are required to determine the monotonic moment-rotation relationship, yield surface, plastic rotation capacity, effective cracked stiffness, etc., which are used in models based on the stress-resultant plasticity-based formulation.

In summary, numerous beam-column elements based on the concentrated- and distributed-plasticity concepts have been developed in earlier studies; however, the focus is mainly on modeling the ductile response of reinforced concrete members governed by flexural yielding.

As described previously, reinforced concrete columns in existing older structures may not, however, have the lateral strength or displacement ductility to develop flexural yielding and withstand the strength and ductility demands imposed during major earthquakes. As observed in major earthquakes and demonstrated in experimental studies on cyclic behaviour of reinforced concrete structural components (Sezen 2002, Elwood and Moehle 2003), reinforced concrete columns with insufficient or poorly detailed transverse reinforcement may exhibit a brittle shear failure or a ductile shear failure in the flexural plastic hinge zone. The post-shear failure behaviour of columns subjected to cyclic loadings is characterized by severe strength and stiffness degradation and increased pinching.

Recent efforts have been undertaken in the development of models for the nonlinear response of reinforced concrete members susceptible to nonductile and ductile shear failure under the combined action of axial force, shear and bending moments. A review of the developments of beam-column elements incorporating the effects of shear failure and post-shear failure behaviour is presented in the next section.

2.2 Distributed Plasticity Models Incorporating Flexural and Shear Effects

A state-of-the-art review of recent developments in distributed plasticity models incorporating flexural and shear behaviour based on the fiber approach is presented in Ceresa et al. (2007). As summarized by Ceresa et al. (2007), existing fiber beam-column models can be divided into two main groups depending on the approach for modeling the shear effects. Models in the first group are based on superimposing independent models for flexural and shear mechanisms and using strut-and-tie method to derive the shear contribution. Models in the second group use formulations based on different constitutive relations to describe the flexural and shear behaviour, such as microplane theory (Petrangeli et al. 1999), smeared crack theory (Vecchio and Collins 1986, Bentz 2000, Remino 2004, Bairan 2005), and damage mechanics (Kotronis and Mazars 2005, Mazars et al. 2006).

The element formulations in earlier fiber models are typically based on the Euler-Bernoulli beam theory and neglect shear effects. In many of the recent studies, the Timoshenko beam theory is introduced into the fiber approach to account for shear effects.

As summarized by Ceresa et al. (2007), among the models based on strut-and-tie method for considering the shear contribution and superposition of flexural and shear models are the models proposed by Guedes et al. (1994), Ranzo and Petrangeli (1998), Shirai et al. (2001), Martinelli (2008).

Guedes et al. (1994) proposed a displacement-based frame element for modeling the nonlinear response of shear-dominated reinforced concrete members using the Timoshenko beam theory. The nonlinear section response under axial force and bending moments is derived based on the fiber approach. The shear resistance is considered based on a strut-and-tie model but contributions from arch action, aggregate interlock and compressive concrete are not included.

Martinelli et al. (2008) proposed another displacement-based element based on the Timoshenko beam theory. The developed finite element is based on the model proposed by Garstka (1993), in which a fiber model for deformations due to flexural and axial forces is coupled with a truss model for the shear effects. In the model proposed by Martinelli et al. (2008), the shear-flexure is assumed to take place in limited zones at the ends of the element. Different contributions to shear resistance such as arch action, truss mechanism, aggregate interlock and compressive concrete are accounted for in the model.

Ranzo and Petrangeli (1998) proposed a two-dimensional flexibility-based element for nonlinear response analysis of reinforced concrete structures including shear effects. At section level, the flexural response is derived based on the fiber approach while the shear response is described by an empirical shear force-shear distortion hysteretic model. The shear strength is considered as the sum of different components, concrete contribution and truss mechanism formed by the transverse reinforcement, as proposed by Priestley et al. (1994). The flexural and shear mechanisms are coupled by a damage criterion at section level following the model proposed by Priestley et al. (1994) for degradation of concrete shear strength with flexural ductility. The element state determination follows the iterative procedure proposed by Petrangeli and Ciampi (1997).

Marini and Spacone (2006) proposed a flexibility-based fiber element based on the Timoshenko beam theory that accounts for shear effects. The formulation of the two-dimensional element follows the flexibility approach presented in Spacone et al. (1996). The section response to axial and bending effects is described based on the fiber approach. The shear response is described by a phenomenological shear force-shear deformation relationship, similarly to the approach used in Martino et al. (2000). The proposed shear constitutive law accounts for the increase in shear capacity due to axial compression. Damage effects due to cracking are also considered in the model. Shear deformations are uncoupled from axial and bending effects in the section stiffness, but shear and bending forces become coupled at the element level by imposing equilibrium along the element. It is highlighted that section constitutive laws that exhibit softening

such as the shear model proposed by Marini and Spacone (2006) may cause localization and non-uniqueness of the solution as discussed in Coleman and Spacone (2006).

Generally, in fiber beam-column models based on superposition of flexure and shear models, a shear model acts in series with the fiber section, but the response of the shear model is uncoupled from the flexural or axial deformations at section level, thus full coupling of axial, shear and flexure effects is not accounted for. To overcome this limitation, models based on fiber constitutive relations that incorporate the shear effects have been proposed as summarized next.

Petrangeli et al. (1999) proposed a flexibility-based fiber beam-column element for modeling the shear behaviour and its interaction with axial force and bending moments in reinforced concrete members. As a fiber element, this model shares various features of previous fiber models such as those proposed by Kaba and Mahin (1984), Mari and Scordelis (1984), Zeris and Mahin (1988). The element state determination is based on the iterative solution procedure presented in Petrangeli and Ciampi (1997). The shear mechanism is modeled at fiber level by introducing biaxial constitutive relations for concrete based on the microplane approach (Bazant and Oh 1985, Bazant and Prat 1988, Bazant and Ozbolt 1990, Ozbolt and Bazant 1992). The shear deformations are determined by imposing equilibrium between the concrete and transverse reinforcement. By using biaxial constitutive relations, the formulations of this model describe the softening behaviour of reinforced concrete members under monotonic and cyclic loading in a more robust and consistent way, without the need for superposition of separate

flexure and shear models as in the truss and strut-and-tie approaches. On the other hand, this model is computationally more demanding compared to the models based on truss analogies and it has some difficulties in directly accounting for the different mechanisms that contribute to shear resistance. As reported by Petrangeli et al. (1999), the model tends to underestimate the shear capacity in regions where the contribution to shear resistance from direct strut action is more significant since the local effects due to supporting and loading details are not accounted for in the formulations.

As summarized by Ceresa et al. (2007), fiber models for reinforced concrete incorporating shear effects based on the smeared crack approach have been proposed by Vecchio and Collins (1988), Bentz (2000), Remino (2004), Bairan (2005).

The smeared crack approach for modeling cracked concrete was introduced by Rashid (1968). In this approach, the cracked concrete is represented as an elastic orthotropic material with reduced modulus of elasticity in the direction normal to the crack plane and the cracked concrete behaviour is described by an average stress-strain relationship. The smeared crack approach describes the cracked concrete response in a more global sense compared to the discrete crack model originally developed by Ngo and Scordelis (1967). The discrete crack approach is based on a predefined crack pattern while in the smeared crack approach cracking is modeled as an averaged distributed effect with directionality.

Following the smeared crack concepts, Mitchell and Collins (1974) proposed the diagonal compression field theory based on the assumption that concrete carries no

tension after cracking and shear is carried by a field of diagonal compression. The formulations are based on equilibrium, compatibility and constitutive relationships in terms of average strains and stresses. Reinforcing steel is assumed to be smeared throughout the element and perfectly bonded to concrete. Vecchio and Collins (1986) proposed the modified compression field theory (MCFT), a modification of the diagonal compression field theory, in which the tension stiffening effect in concrete is considered by imposing average tensile stress across the crack. In this approach, iterative procedure for finding the stress and strain distribution is required, and the shear strain profile is determined from equilibrium of two adjacent sections. The method has been shown to be capable of predicting the response of reinforced concrete to in-plane shear, flexural and axial stresses. A limitation is that only monotonic load is considered in the formulation. Vecchio and Collins (1988) applied the MCFT for modeling the response of reinforced concrete beams subjected to shear. Since the analytical model based on the MCFT requires considerable computational effort, Vecchio and Collins (1988) proposed two alternative approximate solutions by using a predefined parabolic shear strain or constant shear flow distribution.

Vecchio (1999), and Palermo and Vecchio (2002) proposed modifications and extensions to the MCFT to model the response of reinforced concrete panels and shear walls under cyclic loading. The method has also been used in studies conducted on concrete frames and beam-column joints to some success. It has been observed in applications of the MCFT that the method does not capture very well the response of beams with little or no transverse reinforcement. To overcome this limitation, Vecchio (2000) proposed a new

conceptual model, called disturbed stress field model, to describe the behaviour of cracked reinforced concrete.

Bentz (2000) proposed a fiber model for predicting the load-deformation response of reinforced concrete sections subjected to shear, axial forces and bending moments based on the MCFT (Vecchio and Collins 1986). The model is implemented in a computer program called Response-2000. The applications of this model capture the cases of monotonic in-plane bending, shear and axial loading.

Remino (2004) proposed an implementation of the smeared crack approach into a fiber beam-column element based on the Timoshenko beam theory. The flexibility-based formulation of the two-dimensional element follows the method proposed by Spacone et al. (1996). The constitutive relations describing the fiber response are based on the Rose-Shing model (Rose 2001) which follows the concepts of the MCFT with modifications in terms of material constitutive relations, aggregate interlock law and crack kinematics. The interaction between axial force, shear and flexure is thus accounted for at fiber level. The model has been verified only for the static monotonic response of reinforced concrete piers. As reported by Remino (2004), numerical difficulties have been encountered in cyclic analysis due to the use of the Rose-Shing model to describe the cyclic response of the fibers as well as the adopted incremental-iterative solution procedure.

Mullapudi et al. (2010) proposed an implementation of the softened membrane model into a fiber beam-column element based on the Timoshenko beam theory. The softened membrane model (Zhu and Hsu 2002) belongs to the family of smeared crack models. As summarized by Mullapudi et al. (2010), the development of the softened membrane model is a progression of the work by Belarbi and Hsu (1995), Pang and Hsu (1995, 1996), Hsu and Zhang (1996), Zhang and Hsu (1998), Zhu et al. (2001). In this approach, the biaxial state of stress of cracked concrete in the directions of orthotropy is considered and the Poisson's effect is included. The softened membrane model has been shown to be capable of predicting the pre-peak as well as the post-peak response of cracked concrete. By using biaxial constitutive relations for describing the fiber response, the interaction between axial, flexural and shear responses is accounted for at fiber level. The flexibility-based formulation of the element follows the methods proposed by Spacone et al. (1996), Neuenhofer and Filippou (1997), Ayoub and Filippou (2000). The model has been verified using experimental data from shake table tests of reinforced concrete columns.

Mazars et al. (2006) proposed a displacement-based fiber beam-column element based on the Timoshenko beam theory and constitutive relations to account for the shear response of reinforced concrete components. For concrete, uniaxial constitutive law is used based on the model proposed by La Borderie (1991) and the principles of damage mechanics and plasticity. The model is suitable for describing cyclic loadings considering damage by using damage coefficients for tension and compression, and including crack closure and permanent effects. However, the assumption of uniaxial constitutive relations and

linear shear stresses results in limitations in the accurate representing of the anisotropic response of reinforced concrete sections due to shear cracking.

Ceresa et al. (2009) developed a fiber beam-column element based on the Timoshenko beam theory and biaxial constitutive relations for modeling the shear response and the shear-flexure interaction in reinforced concrete members. The two-dimensional element is formulated according to the displacement-based approach. The shear mechanism is modeled at fiber level using biaxial constitutive relations for cracked reinforced concrete based on the cyclic formulations of the MCFT (Vecchio 1999, Palermo and Vecchio 2003). The interaction between axial, flexural and shear responses is accounted for at fiber level. The model has been verified using experimental data from cyclic tests of reinforced concrete short piers and walls. As reported by Ceresa et al. (2009), numerical difficulties have been encountered mainly due to the limitations of the employed constitutive models and further improvements in the modeling of the post-peak behaviour are needed.

2.3 Concentrated Plasticity Models Incorporating Flexural and Shear Effects

A review of recent developments in concentrated plasticity models incorporating the flexural and shear behaviour of reinforced concrete members is presented in this section. In the concentrated plasticity approach, the inelastic flexure and shear responses of a reinforced concrete column are modeled by the nonlinear hinges at the ends of the element. In some of the models, the element formulations are based on single-component hinges while in others, on multi-component hinges. The models are characterized by

different levels of complexity and refinement. The effects of axial load on the flexural and shear behaviour are accounted for in some of the models.

The models based on single-component hinges generally consist of an elastic element and single-degree-of-freedom springs attached at the ends of the elastic element. A nonlinear rotational spring is used to model the moment-rotation relationship based on a hysteretic model. Several hysteretic models for the flexural behaviour have been developed, with Takeda et al. (1970) being one of the more popular. A nonlinear shear spring is used to model the shear force-shear deformation relationship based on a hysteretic shear model. The model proposed by Ozcebe and Saatcioglu (1989) is considered to be the pioneering work in the hysteretic shear models for reinforced concrete members. In general, the hysteretic models are based on a predefined backbone curve and a set of hysteretic rules, which control the unloading, reloading and pinching behavior. The backbone curve is commonly derived from the monotonic response, which can be obtained from experimental data or section analysis, and is used as an envelope for the cyclic response. In this approach, there is no clear distinction between the inelastic response and the degraded elastic cyclic response. In single-component hinges, the relation between a singular force action and its deformation component is enforced, thus force interaction is not readily taken into account. Special techniques need to be employed for considering the effects of interaction between axial force, moment and shear force as discussed later.

Among the concentrated plasticity models capturing shear effects based on single-component hinge approach are the models proposed by Pincheira et al. (1999), Lee and

Elnashai (2001, 2002), Elwood and Moehle (2004), Sezen and Chowdhury (2009), Xu and Zhang (2010).

The models with multi-component hinges, also referred to as generalized plastic hinge models, are commonly based on stress resultant plasticity concepts. In structural analysis, the plasticity concepts are applied based on multi-axial yield functions defined in terms of forces and plastic flow criteria given by evolution rules for inelastic hardening/softening response. For flexural response, a yield function defined in terms of axial force and moments can be used which allows modeling the inelastic axial force-moment interaction. Yielding occurs when the force state of a member reaches the yield surface, and the response to continued loading is governed by the evolution of the yield surface. Hardening response is generally modeled by using a kinematic rule, an isotropic rule or a combination of the two. The kinematic rule results in translation of the yield surface in force space without changes in size or shape, while the isotropic rule results in uniform expansion of the yield surface. To model the shear failure and the post-shear failure behavior, a shear failure surface can be used. To consider the effects of variable axial load on the shear behaviour, the shear failure surface can be defined in terms of axial force and shear forces. Shear failure occurs when the shear force state of a member reaches the shear failure surface. The post-shear failure response to continued loading characterized by softening or strength degradation can be modeled by using a contraction rule that results in shrinking of the shear failure surface.

After yielding and/or failing in shear, the element accumulates damage and the element stiffness degrades. Upon unloading, the force point is inside the yield surface and/or the shear failure surface and the degraded elastic response is independent from the formulation of the yield surface and/or shear failure surface. The degraded elastic behaviour of the element under cyclic loading is modeled by using cyclic models that capture degradation in elastic unloading/reloading stiffness and pinching of the hysteretic loops. Inherent feature of the generalized-hinge approach is that the inelastic response is modeled separately from the degraded elastic response. As noted above, no clear distinction between the inelastic response and the cyclic response is made in the models based on single-component hinges.

Among the generalized plastic hinge models capturing the behaviour of nonductile reinforced concrete columns are the models proposed by Yang (1994), Ricles et al. (1998), Abou-Elfath et al. (1998), ElMandooh Galal and Ghobarah (2003), Kaul (2004). Mostafaei and Kabeyasawa (2007) also proposed a model based on springs in series for capturing the flexure and shear behaviour of reinforced concrete columns by a different approach. Fiber hinge model is used to capture the axial-flexure behaviour and the constitutive relationship for the shear spring is based on the MCFT (Vecchio and Collins, 1986).

2.3.1 Concentrated Plasticity Models Based on Single-Component Hinges

In this section, some of the concentrated plasticity models incorporating flexural and shear effects based on single-component hinges are reviewed.

2.3.1.1 Pincheira et al. (1999)

Formulations:

Pincheira et al. (1999) proposed a concentrated plasticity model for the cyclic response of nonductile reinforced concrete columns by incorporating the shear effects. The approach is an extension of the two-dimensional single-component model originally developed for flexural behaviour by Giberson (1969). As summarized by Pincheria et al. (1999), earlier efforts to develop models representing the nonductile response of older reinforced concrete columns focus on anchorage and lap splice failures of the longitudinal reinforcement (Jordan 1990, Pincheira and Jirsa 1992, Kurama et al. 1996) and do not include the nonlinear shear response or do not capture the interactions with the shear effects (Pincheira and Jirsa 1992). The main characteristics of the model proposed by Pincheira et al. (1999) include capturing of flexural or shear failures under monotonic and cyclic loading.

The element consists of an elastic interior, two rotational springs at each end and a shear spring at midpoint, as schematically shown in Figure 2-3. The element stiffness is derived based on the flexibility approach by adding the flexibility matrices of the elastic subelement, the rotational springs and the shear spring and including both flexural and shear deformations.

The hysteretic law describing the flexural response is based on the model proposed by Takeda et al. (1970) with modifications to include strength degradation due to anchorage

or splice failures (Pincheira et al. 1992), and to include flexural cracking, as shown in Figure 2-4. The multilinear backbone curve incorporates segments for elastic behaviour prior to flexural cracking, reduced stiffness following flexural cracking and prior to yielding, post-yield hardening and a post-peak negative slope that continues until the member response reaches the residual moment capacity. Anchorage slip, lap-splice slip, section degradation and buckling of longitudinal reinforcement between ties are considered in defining the flexural backbone curve by introducing a segment with negative slope to represent the in-cycle flexural strength degradation with increasing rotation amplitudes. The unloading stiffness is assumed to degrade based on maximum rotation amplitude and empirical degradation parameters. The reloading stiffness is assumed to be peak-oriented.

The shear response model used in the element formulation is developed by Dotiwala (1996), and Pincheira and Dotiwala (1996). The multilinear shear force-deformation backbone curve and hysteretic rules are as shown in Figure 2-5. The backbone curve for the shear response is obtained up to the maximum strength by using the modified compression field theory (MCFT) (Vecchio and Collins, 1986), which requires iterative and computationally intensive procedure. Even though valid strictly for monotonic loading behaviour, the MCFT has been chosen since it provides a general approach for calculating the shear response of reinforced concrete members considering the effects of flexure and axial load. The backbone curve incorporates a segment for elastic behaviour prior to shear cracking. After the onset of shear cracking, the shear force-deformation relation follows reduced shear stiffness until reaching the maximum shear capacity. The

post-peak shear response is modeled by a negative slope until reaching the residual shear capacity. The cyclic shear response is based on the concepts of stiffness degradation proposed by Chen and Powell (1982) and Ricles et al. (1991) with modifications to include pinching of the hysteresis loops and cyclic strength degradation, as shown in Figure 2-5. Degradation in unloading stiffness is considered based on maximum plastic shear deformation attained in the current inelastic excursion and empirical degradation parameters. The reloading stiffness is assumed to degrade based on the plastic deformation attained during the inelastic excursion in the opposite direction and empirical degradation parameters, and thus cyclic strength degradation is accounted for in the formulation. The amount of pinching is assumed to depend on the reloading stiffness and an empirical controlling parameter.

Analysis results using the beam-column element developed for modeling the response of nonductile reinforced concrete columns have been compared with experimental data from cyclic lateral load tests with either no axial load or constant axial load. As noted by Pincheira et al. (1999), the comparison of the cyclic response with experimental results showed that good correlation of the post-shear failure behaviour was in many cases not possible due to uncertainty associated with the cyclic degradation parameters.

Summary of Findings and Discussion:

The beam-column element has been incorporated in the DRAIN-2D analysis program (Kannan and Powell, 1973; Pincheira and Jirsa, 1992). The existing solution algorithm of DRAIN-2D could not handle negative stiffness. As reported by Pincheira et al. (1999),

numerical difficulties were encountered when the response is on the descending branch, and necessitated revisions of the solution strategy to find an approximate solution. On the post-peak negative slope for any of the nonlinear springs, a small but positive arbitrary slope is used resulting in a force unbalance which is applied to the model in the next time step. The procedure may require considerable computational effort and the model may not adequately capture the dynamic characteristics of a softening structure.

The proposed model is capable of capturing the overall strength and stiffness degradation properties of older reinforced concrete columns exhibiting a shear dominated behaviour with essentially no flexural ductility. However, experimental research studies have shown that shear strength of columns degrades in the flexural plastic hinge zone with increasing displacement ductility demand (Aschheim and Moehle 1992, Wong et al. 1993, Priestley et al. 1994). In this model degradation in shear strength and stiffness is initiated after the member response reaches the peak of the backbone curve defined for the shear spring. If the estimated shear strength is higher than the flexural yield strength, and given limited post-yield hardening in the flexural response, shear degradation will not be initiated in the model. In order to capture shear failure and post-shear failure behaviour after the column develops flexural yielding and exhibits some displacement ductility, shear failure determination should be based on both force and deformation considerations. To overcome this limitation, models developed in more recent research (Elwood 2002, Kaul 2004, Sezen and Chowdhury 2009) incorporate force-based and displacement ductility-based criteria to determine shear failure.

2.3.1.2 Elwood (2002)

Formulations:

Elwood (2002) proposed a different approach to capture shear and axial failures in shear-critical reinforced concrete columns based on drift capacity models. As summarized by Elwood (2002), existing models for predicting the degradation of shear strength of columns with increasing flexural displacement ductility, such as the models proposed by Watanabe and Ichinose (1992), Aschheim and Moehle (1992), Priestley et al. (1994), Sezen (2002), are not adequate for predicting the drift ratio at shear failure.

Elwood (2002, 2004) has developed an empirical model to estimate the drift at shear failure of reinforced concrete columns experiencing flexural yielding before shear failure and a shear-friction model that relates the axial capacity of the column to the drift ratio after shear failure. The proposed drift capacity models are incorporated in a nonlinear uniaxial constitutive model to initiate strength degradation in an analytical model of a reinforced concrete member and capture the shear and axial load failures.

Based on evaluation of results from an experimental database of shear-critical columns, the following empirical equation has been proposed to estimate the drift ratio at shear failure:

$$\frac{\Delta_s}{L} = \frac{3}{100} + 4\rho'' - \frac{1}{500} \frac{v}{\sqrt{f'_c}} - \frac{1}{40} \frac{P}{A_g f'_c} \geq \frac{1}{100} \text{ (psi units)} \quad (2.1)$$

where Δ_s/L is the drift ratio at shear failure, ρ'' is the transverse reinforcement ratio, v is the nominal shear stress, f'_c is the concrete compressive strength, P is axial load at time of shear failure for variable axial load tests, and A_g is the gross cross-sectional area. After shear failure, the axial load supported by the column is assumed to be determined based on the shear-friction mechanism. The free-body diagram of a shear damaged column is shown in Figure 2-6. Based on the shear-friction concepts and on observations from experimental tests, the following empirical equation has been developed to estimate the drift ratio at axial failure of a shear-damaged column:

$$\left(\frac{\Delta}{L}\right)_{axial} = \frac{4}{100} \frac{1 + (\tan\theta)^2}{\tan\theta + P \left(\frac{s}{A_{st}f_{yt}d_c \tan\theta} \right)} \quad (2.2)$$

where $(\Delta/L)_{axial}$ is the drift ratio at axial failure, d_c is the depth of the column core from centre line to centre line of the ties, s is the spacing of the transverse reinforcement, A_{st} and f_{yt} are the area and yield strength of the transverse reinforcement, P is the axial load on the column, and θ is the critical crack angle from the horizontal and is assumed to be 65° in the derivation of the model.

Limit state curve based on the empirical drift capacity model is used to detect the onset of shear failure in the model as defined by the intersection point of the load-deformation curve of the column and the limit state curve, as shown in Figure 2-7. Similarly, limit state curve based on the shear-friction model is used to determine when axial failure occurs, as shown in Figure 2-8. As noted by Elwood (2002), according to this model,

columns with a low axial load or drift demand are not expected to experience axial failure.

The limit state curves are incorporated into an existing hysteretic model similar to that developed by Filippou and Spacone (1996). The force-deformation relation of the hysteretic model shown in Figure 2-9 includes strength degradation, stiffness degradation and pinching. At detection of failure, the backbone curve for force-deformation relationship of the hysteretic model is redefined to initiate strength degradation, as illustrated in Figure 2-10. As noted by Elwood (2002), the point of failure might not lie on the pre-defined force-deformation relation of the hysteretic model, as shown in Figure 2-10(b), since the limit curve can be defined as uncoupled from the backbone curve and exceedance of the limit curve is checked after each converged step. Therefore it is recommended to use small load steps to accurately determine when the limit curve is exceeded.

The limit state model, which is the hysteretic model extended to include a limit state curve, is used in beam-column elements to model shear and axial load failure and strength degradation in shear-critical reinforced concrete columns as described next.

The shear spring in series model consists of a beam-column element connected in series with a shear spring, as shown in Figure 2-11. In this model the limit state model is used to describe the shear force-shear deformation relationship of the shear spring. The incorporated limit state curve is defined based on the shear force and the total

displacement to ensure that shear failure is based on the sum of the flexural and shear deformations. It is assumed that the flexural deformations modeled by the beam-column element include also the contribution from anchorage bar slip. When the beam-column response intersects the limit curve, shear failure is detected and the backbone curve of the shear spring is redefined to initiate strength degradation, as illustrated in Figure 2-11. Considering experimental results showing that shear deformations increase significantly after shear failure (Sezen 2002), the force-deformation relationship of the shear spring is assumed to follow a negative slope upon additional lateral displacement demand while the beam-column element is assumed to unload allowing a small reduction in flexural deformations.

Based on observations from experimental tests (Nakamura and Yoshimura 2002), the slope of strength degradation of the total response of the beam-column is assumed to be linear from the point of shear failure to the point of axial failure and can be estimated as follows:

$$K_{deg}^t = \frac{V_u}{(\Delta_a - \Delta_s)} \quad (2.3)$$

where V_u is the ultimate shear capacity of the column, Δ_s is the corresponding drift at shear failure, and Δ_a is the drift at axial failure for the axial load at the time of shear failure.

Thus, following the flexibility approach the degrading slope of the shear spring is determined as follows:

$$K_{deg} = \left(\frac{1}{K_{deg}^t} - \frac{1}{K_{unload}} \right)^{-1} \quad (2.4)$$

where the unloading stiffness of the beam-column, K_{unload} , must be provided before the analysis.

As reported by Elwood (2002), numerical problems are encountered when the beam-column response has a negative slope after shear failure is detected due to the lack of unique solution for an increase in the total displacement. Therefore, it is recommended that the beam-column response maintain a positive slope.

The rotational spring model consists of a linear elastic element connected with rotational springs at each end, as shown in Figure 2-12. The limit state model is used to define the moment-rotation relationship for a rotational spring. The rotational springs are incorporated in the beam-column element such that the beam-column displacement is equal to the sum of the flexural and shear deformations. The deformation due to bar slip is accounted for in the model by assuming an initial slope in the backbone curve of the rotational spring. As in the shear spring in series model described previously, the limit state curve used to determine the onset of shear failure is defined based on the column shear and the total displacement. When the beam-column response reaches the limit curve, the backbone curve of the rotational spring is redefined to initiate strength

degradation, as illustrated in Figure 2-12. As pointed out by Elwood (2002), the rotational spring model has improved numerical stability compared with the springs in series model, however, all nonlinearities due to flexural and shear deformations are lumped in the rotational springs and are not determined separately.

The axial spring in series model extends the shear spring in series model to capture axial load failure of a shear-damaged column by adding an axial failure spring connected in series, as shown in Figure 2-13. The limit curve defining the relationship between the axial load and total lateral drift for the axial failure spring is based on the shear-friction mechanism that assumes shear failure has already occurred. Thus, post-processing is required to confirm that shear failure occurred before axial failure. After axial failure is detected, the backbone curve of the axial spring is redefined to initiate loss of axial load capacity, as illustrated in Figure 2-13. Based on experimental results suggesting that an increase in lateral shear deformations may lead to an increase in axial deformations, and loss of axial load (Elwood 2002, Lynn 2001, Sezen 2002), shear-axial coupling after the onset of axial failure is considered in this model by forcing the axial spring response to follow the axial limit curve upon additional lateral displacement demand.

Summary of Findings and Discussion:

The proposed drift capacity models are incorporated in a nonlinear uniaxial constitutive model implemented in the OpenSees structural analysis platform (McKenna et al. 2004) and can be used with a beam-column element to model shear and axial load failure and strength degradation of existing reinforced concrete columns.

In models that have previously been proposed for modeling shear failure and post-shear failure behaviour of nonductile reinforced concrete columns, such as the model developed by Pincheira et al. (1999), shear failure is detected only when the shear in the column exceeds the shear capacity of the shear spring. By using the drift capacity model developed by Elwood (2002) to detect shear failure and initiate strength degradation based on the drift ratio of the column, the model allows flexural yielding before shear failure, and thus overcomes the limitations in the previous models that fail to capture shear-flexure failure mode.

As discussed by Elwood (2002), existing shear-strength models, such as the models by Priestley et al. (1994) and Sezen (2002), developed to represent the degradation of shear strength with increasing inelastic displacements are more appropriate for estimating the column capacity for conventional strength-based design and may not adequately predict the drift ratio at shear failure after flexural yielding due to sensitivity to variations in the shear strength and flexural strength. Considering the deficiencies in existing shear-strength models, Elwood (2002) has developed an empirical drift capacity model to provide a more reliable estimate of the drift at shear failure of existing reinforced concrete columns. The proposed empirical drift capacity models are less sensitive to variability in the shear capacity or the shear demand after yielding in flexure compared with the shear-strength model developed by Sezen (2002) due to the relatively steep slope of the relationship between shear stress and drift ratio at shear failure.

The drift capacity model proposed by Elwood (2002) has also been used in a beam-column model developed by Kaul (2004) as discussed later.

To model the deterioration in axial load capacity of a shear-damaged column which may result in loss of ability to support gravity loads, Elwood (2002) has proposed a modified shear-friction model that relates the axial load capacity to the drift ratio of a column and developed an equation for estimating the drift ratio at axial failure. There are certain limitations in the axial failure model. The shear-friction mechanism assumes that the full yield capacity of the transverse reinforcement can be attained and maintained after shear failure. In older reinforced concrete columns, sufficient anchorage of the transverse reinforcement may not be provided, thus reduction of the contribution of transverse reinforcement should be considered in the model. Furthermore, the shear-friction model is based on the assumption that the shear failure plane is continuous and distinct. However, the complex behaviour of a column suffered failure in shear may lead to different mechanisms for supporting axial load such as partial bearing support and discontinuous shear plane which cannot be captured by this model. The axial failure model has been derived based on limited available experimental data comprising only 12 columns subjected to unidirectional lateral loading.

The focus of this research is to capture shear and axial failure and model the strength degradation behaviour of existing reinforced concrete columns subjected to seismic loading. The proposed drift capacity models for determining the onset of shear and axial failure are incorporated into existing hysteretic model which considers stiffness

degradation, strength deterioration and pinching behaviour. The effects of accumulation of damage on the degrading behaviour of reinforced concrete columns under cyclic loadings have not been investigated.

2.3.1.3 Sezen and Chowdhury (2009)

Formulations:

Sezen and Chowdhury (2009) have developed a springs in series macromodel incorporating the effects of shear and axial load failure to simulate the cyclic response of older reinforced concrete columns. The total lateral response is modeled by combining the flexural, longitudinal bar slip and shear deformation responses, each of which is modeled by a spring. It is assumed that each spring is subjected to the same level of lateral force. For each spring, a force-deformation relation based on the monotonic response is defined, and is assumed to be an envelope for the corresponding cyclic response. For the pre-peak response, it is assumed that the deformations of each component are simply added to predict the total response. However, modeling of the post-peak response requires evaluation of the column behaviour based on a classification proposed by Setzler and Sezen (2008). According to this classification, five categories of column behaviour can be identified considering the potential for flexural, shear, or axial load failure.

The flexure response of a reinforced concrete column is modeled by using a primary curve and a hysteretic model based on the model developed by Takeda et al. (1970). The primary curve is based on the monotonic lateral force-flexural displacement relation. The

monotonic flexural response is obtained by using moment-curvature analysis and calculating the flexural displacements. The flexural displacements are calculated by integrating the curvature distribution along the length of the column prior to yielding and by using a plastic hinge model after yielding. Post-peak strength degradation is considered by including a linear descending branch in the monotonic flexural response curve. The original Takeda model has been modified by replacing the trilinear primary curve with the monotonic envelope described above. The hysteretic rules of the Takeda model have also been modified to account for further stiffness degradation due to increased damage at large deformations. The slope of the reloading branch is decreased with increasing maximum deformation and the slope of the unloading branch is increased as a function of the previous maximum deformation, as shown in Figure 2-14. The proposed slope of the unloading branch is obtained as the unloading slope proposed originally by Takeda et al. (1970) multiplied by a factor of 1.7 as follows:

$$k_1 \text{ or } k_2 = 1.7k_0 \left(\frac{D_y}{D} \right)^{0.4} \quad (2.5)$$

where k_1 and k_2 are the slopes of the unloading branches, k_0 is the slope of the line connecting the cracking point and yield point, D is the maximum deflection attained in the direction of the loading, and D_y is the yield deflection.

The longitudinal bar slip contribution to the total lateral response is modeled by a rotational spring at each end of the column macromodel. The formulation of the rotational spring incorporates a primary curve and hysteretic rules. The primary curve defining the monotonic lateral force-slip displacement relation is based on the monotonic

bar slip model developed by Sezen and Moehle (2003) and Sezen and Setzler (2008). In this model, it is assumed that slip occurs in bars under tension only, and that the rotation is about the neutral axis. The slip rotation is calculated as:

$$\theta_s = \frac{slip}{d - c} \quad (2.6)$$

where slip is the extension of the outermost tension bar from the column end, and d and c are the distances from the extreme compression fiber to the centroid of the tension steel and the neutral axis, respectively. The contributions from the elastic and the inelastic portions of the development length of the bar are considered in determining the slip deformation in Equation (2.6). The lateral displacement component due to slip deformations is obtained as the product of the slip rotation and the column length. Strength degradation is considered by including a descending branch in the monotonic envelope after the peak strength is reached.

The hysteretic rules for the longitudinal bar slip response model are based on the hysteretic model developed by Saatcioglu et al. (1992). To increase the computational efficiency of the macromodel, the hysteretic rules used in the proposed slip model are simplified compared to those in the original model by Saatcioglu et al. The slope of the unloading branch is assumed to be linear, and the slopes of the unloading and reloading branches are changed only when the lateral force becomes zero. Thus, the hysteretic slip model is similar to the hysteretic flexural model shown in Figure 2-14.

The shear response of a reinforced concrete column is modeled by a shear spring incorporating a primary curve defining the monotonic lateral force-shear displacement and a hysteretic model. The primary curve up to the maximum shear strength is obtained by using the computer program Response-2000 (Bentz 2000) based on the MCFT (Vecchio and Collins 1986). The MCFT incorporated into Response-2000 is a force-based approach which stops when the maximum strength is reached. After the maximum shear strength is reached, the monotonic shear response is defined by a piecewise linear model, as shown in Figure 2-15. The model proposed by Gerin and Adebar (2004) is modified and used to determine the shear displacement at the onset of shear strength degradation:

$$\Delta_{v,u} = \left(4 - 12 \frac{(V_n/bd)}{f'_c} \right) \gamma_n L \quad (2.7)$$

where γ_n is the uniform shear strain equal to $\Delta_{v,n}/L$, where $\Delta_{v,n}$ is the shear displacement corresponding to the peak strength V_n , calculated from MCFT; b and d are the width and effective depth of the cross section, respectively; f'_c is the concrete compressive strength; and L is the column length.

The shear displacement at axial load failure is given by:

$$\Delta_{v,f} = \Delta_{ALF} - \Delta_{f,f} - \Delta_{s,f} \geq \Delta_{v,n} \quad (2.8)$$

where Δ_{ALF} is the total displacement capacity of the column at loss of axial load carrying capacity; $\Delta_{f,f}$ is the final or maximum flexural displacement; and $\Delta_{s,f}$ is the final slip displacement. The total drift at axial load failure is calculated from the axial capacity model proposed by Elwood (2002) given by Equation (2.2).

The hysteretic rules for the shear response model are based on the model proposed by Ozcebe and Saatcioglu (1989). The original Ozcebe and Saatcioglu model considers strength deterioration, pinching and stiffness degradation but is suitable primarily for modeling columns designed to yield in flexure prior to shear failure. The proposed model shown in Figure 2-16 incorporates modifications to better simulate stiffness degradation and capture the response of columns failing in shear prior to flexural yielding or after flexural yielding with exhibiting limited displacement ductility. In the proposed model, the reloading branch is aiming toward the peak displacement and load reached before unloading in the previous cycle. The revised and reduced unloading branch is given by:

$$k_2 \text{ or } k'_2 = 0.2k_y \left(1 - 0.07 \frac{\Delta}{\Delta_y} \right) \quad (2.9)$$

where Δ is the maximum displacement reached during the previous cycle before unloading, Δ_y is the deflection at yielding, and k_y is the slope at yielding.

The total lateral response of a reinforced concrete column is modeled by combining the responses of the flexure, longitudinal bar slip and shear models incorporated in the macromodel. To obtain the monotonic pre-peak response, it is assumed that the deformation components are simply added. The coupling of the flexure, slip and shear responses in the monotonic post-peak response requires evaluation of the column behaviour to determine the type of failure mode based on the classification proposed by Setzler and Sezen (2008). In this classification, five categories are identified based on comparing the shear strength, the yield strength and the flexural strength of a column to

determine whether the column behaviour is governed by shear, flexure or the interaction between shear and flexure. For each category, different rules for combining the monotonic post-peak flexure, slip and shear responses are established. To obtain the hysteretic response of the column macromodel up to the peak strength and during unloading and reloading, it is assumed that the three deformation components can be added. The post-peak hysteretic response of the column macromodel is assumed to be bound by the total monotonic response calculated according to the rules of the column classification.

The proposed macromodel for predicting the cyclic response of reinforced concrete columns has been verified using experimental data from the column tests conducted by Saatcioglu and Ozcebe (1989) and Sezen and Moehle (2006). As noted by Sezen and Chowdhury (2009), these are the only available large-scale reinforced concrete column tests where the relations between the cyclic lateral load and flexure, bar slip and shear displacements are reported separately.

Summary of Findings and Discussion:

Sezen and Chowdhury (2009) have developed a macromodel for predicting the cyclic response of existing reinforced concrete columns by coupling the flexural, bar slip and shear deformation responses. As experimental studies suggest (Saatcioglu and Ozcebe 1989, Sezen and Moehle 2006), each of the three deformation components may have significant contribution to the total lateral response of the member. In previous research the bar slip deformation component is either ignored or included in the flexure routine

(Pincheira et al. 1999). Thus, the motivation for this research is to investigate the interaction and combination of these deformation components, including the effects of strength and stiffness degradation, and verify each response component using experimental data.

The proposed hysteretic models are based on existing hysteretic models for cyclic flexure, reinforcement slip and shear response developed in previous research (Takeda et al. 1970, Alsiwat and Saatcioglu 1992, Saatcioglu et al. 1992, Ozcebe and Saatcioglu 1989). The proposed modifications are intended to better simulate the behaviour of columns failing in shear before yielding or after flexural yielding with exhibiting limited displacement ductility. In-cycle strength deterioration is considered in each of the proposed response models by including a descending branch in the monotonic envelopes after the peak strength is reached. Stiffness degradation is also considered in each of the hysteretic models by using peak-oriented reloading slope and by reducing the slope of the unloading branch with increasing maximum displacements. Pinching behaviour is accounted for in the shear hysteretic model. The formulation of the cyclic degradation, however, has limitations since it is based entirely on previous maximum deformations. Depending on the details the model may not capture strength degradation during subsequent cycles maintained at the same inelastic displacement.

The effects of shear and axial load failure are accounted for in the macromodel by incorporating a shear model with degradation related to the drift and by aggregating the flexure, bar slip and shear responses to obtain the total lateral response after identifying

the failure mode. The onset of shear failure and the slope of shear degradation in the shear response model are determined using the drift capacity models developed by Gerin and Adebar (2004) and Elwood (2002). The evaluation of the potential failure mode is based on comparing the column shear and flexural strengths according to the classification proposed by Setzler and Sezen (2008). Thus, the prediction of shear failure and the ensuing strength degradation is based on both force and displacement ductility criteria. However, the classification proposed by Setzler and Sezen (2008) is not intended for finite element analysis which limits the implementations and applications of the model.

2.3.1.4 Xu and Zhang (2011)

Formulations:

Xu and Zhang (2011) have developed a hysteretic model to account for the shear and flexure interaction effects on the seismic response of reinforced concrete columns. The hysteretic model consists of a flexure and a shear spring connected to each end of a column, as shown in Figure 2-17. The column is assumed to be divided into two cantilever columns at the inflection point and modeled by two rigid elements. The primary curves and the hysteretic rules defined for the flexure and shear springs consider strength deterioration, pinching behaviour and stiffness degradation due to the interaction between the axial load, shear force and bending moment.

The total primary curve for the hysteretic model is derived based on the MCFT (Vecchio and Collins 1986) considering the coupling between axial load, shear force and bending

moment at section level. In this research, the total primary curve up to the maximum strength is obtained using the computer program Response-2000 (Bentz 2000) in which the MCFT is incorporated. The total primary curve is broken into flexural and shear primary curves by separating the contributions to the column displacement from shear and flexure deformations. The shear and flexure deformations are obtained by integrating the shear strain and the curvature, respectively, in each section along the length of the column. After the maximum strength, the yield platform and the descending branch of the primary curves are defined based on empirical relationships proposed by Sezen (2008). The flexural primary curve defined as the moment-rotation relationship and the shear primary curve defined as the shear force-shear displacement relationship are used as envelopes for the hysteretic responses of the flexure and the shear curves, respectively.

The hysteretic models for the flexure and shear cyclic responses are based on the model proposed by Ozcebe and Saatcioglu (1989) combined with the model by Takeda et al. (1970). The original model developed by Ozcebe and Saatcioglu (1989) is illustrated in Figure 2-18. Modifications have been made to extend the Ozcebe and Saatcioglu model for the flexural response and to improve the numerical stability for finite element analysis applications.

The modified degrading unloading stiffness in the proposed shear hysteretic model is given by:

$$k_{uld1} = k_2 1.4 e^{-0.35(\Delta/\Delta_y)^{0.01}} (1 - 0.02 \Delta/\Delta_y)^{3.5} \quad (2.10)$$

$$k_{uld2} = 0.6 k_2 1.3 e^{-0.35(\Delta/\Delta_y)^{0.01}} (1 - 0.02 \Delta/\Delta_y)^{5.5} \quad (2.11)$$

where Δ_y is the deflection at yield, and Δ is the deflection where unloading starts, both in the quadrant where the current unloading is taking place; k_2 is the slope of line connecting the yield point in the same quadrant to the cracking point in the opposite direction, shown in Figure 2-19. The unloading stiffness in the shear response follows the slope given by k_{uld1} from the point of unloading to the level corresponding to the cracking point, and the slope given by k_{uld2} from the cracking point level to the zero force level, as shown in Figure 2-19.

The degrading unloading stiffness in the proposed flexure hysteretic model is also based on the Ozcebe and Saatcioglu shear model and is given by:

$$k_{uld1} = k_2 1.2 e^{-0.125(\theta/\theta_y)^{0.25}} (1 - 0.016 \theta/\theta_y)^{3.5} \quad (2.12)$$

$$k_{uld2} = 0.7 k_2 1.2 e^{-0.125(\theta/\theta_{\Delta y})^{0.35}} (1 - 0.020 \theta/\theta_y)^{4.5} \quad (2.13)$$

where θ_y is the rotation at yield, and θ is the rotation where unloading starts. Similarly to the shear hysteretic model, the unloading stiffness in the flexure response follows the slope given by k_{uld1} from the point of unloading to the level corresponding to the cracking point, and the slope given by k_{uld2} from the cracking point level to the zero force level, as shown in Figure 2-19.

Pinching behaviour is not included in the flexure hysteretic model. The pinching stiffness in the original Ozcebe and Saatcioglu shear model is replaced by the slope k_p used for reloading in the opposite direction given by:

$$k_p = 0.56k_2 1.2e^{-0.125(\theta/\theta_y)^{0.35}} (1 - 0.020 \theta/\theta_y)^{3.5} \quad (2.14)$$

In the shear hysteretic model, the rules controlling the pinching stiffness in the original Ozcebe and Saatcioglu model have been modified to avoid problems such as nearly zero pinching stiffness and negative hardening stiffness when the previous peak is below the shear force level at cracking, as illustrated in Figure 2-20. In the revised shear hysteretic model, the reloading stiffness aims toward the last peak that is larger than the shear force level at cracking, as shown in Figure 2-21.

Cyclic strength degradation is accounted for in the shear hysteretic models based on the model by Ozcebe and Saatcioglu. The reloading stiffness aims toward a ‘hardening reference point’ whose shear force, V'_m , is a fraction of the shear force on the primary curve, V_m , corresponding to the maximum displacement, Δ_m , as shown in Figure 2-18.

The shear at the ‘hardening reference point’ is given by:

$$V'_m = V_m e^{\left[-0.014n \sqrt{\Delta_m/\Delta_y} - 0.010\sqrt{n}(\Delta_m/\Delta_y)\right]} \quad (2.15)$$

where n is the number of cycles in one direction within its maximum displacement range, $\Delta_m \pm \Delta_{cr}$.

In the flexure hysteretic model, cyclic strength degradation is considered in a similar way. The moment at the ‘hardening reference point’ is given by:

$$M'_m = M_m e^{\left[-0.002n \sqrt{\theta_m/\theta\Delta_y} - 0.010\sqrt{n}(\theta_m/\theta_y)\right]} \quad (2.16)$$

where n is the number of cycles in one direction within its maximum rotation range, $\theta_m \pm \theta_{cr}$, and M_m is the bending moment on the flexural primary curve corresponding to θ_m .

The hysteretic model described above considers the coupling of shear and flexure behaviour and is developed for modeling the response of reinforced concrete columns subjected to cyclic lateral loading and constant axial load. This hysteretic model is extended by Xu and Zhang (2010) to include the effects of variable axial load by introducing the concept of normalization of primary curves based on technique called “shifting of primary curves” (Saatcioglu et al. 1983). In this approach, the family of primary curves for a reinforced concrete column at axial load levels within the range of -5% to 40% of the column ultimate axial load capacity is generated from relationships to the primary curve corresponding to 5% axial load, which is used as the reference primary curve in the model. It is assumed that the primary curves under variable axial load can be parameterized in terms of the cracking point, the yield displacement, the yielding load and the ultimate capacity, as illustrated in Figure 2-22. It is assumed that the yield displacement remains unchanged for different level of axial load and that the ultimate lateral load capacity corresponds to a displacement ductility level of 2.0. For the descending branch in the primary curves at displacement ductilities larger than 2.0, it is assumed that the lateral load ratio is constant and equal to that at ultimate lateral load capacity.

To establish loading/unloading criteria considering the effects of variable axial load, rules for mapping between the unloading and reloading branches of primary curves at different axial load level are proposed, as illustrated in Figure 2-23. It is assumed that the ratio of the current lateral load on the unloading/reloading branch, V_{eff} , and the lateral load on the primary curve, V_m , corresponding to the maximum experienced lateral displacement, Δ_{max} , is constant for a fixed displacement ductility level and is defined as a stress level index expressed as:

$$\text{Stress Level Index} = \frac{V_{eff}}{V_m} \quad (2.17)$$

The stress level index is assumed to be independent of axial load. To determine the loading state at the current time step when both the axial load and the lateral deflection vary, a two-stage loading approach is adopted based on the assumption above. First, the lateral deflection is kept constant and the effective lateral load is varied for the given stress level index to determine the level of axial load. Second, the axial load level is kept constant and the shear and flexure hysteretic models are used to model the cyclic response.

The proposed hysteretic model has been verified using experimental data for flexure-dominated and shear-dominated columns.

Summary of Findings and Discussion:

The proposed model has been implemented as a user element in the commercial finite element analysis software ABAQUS and can be used to model the nonlinear response of

reinforced concrete columns under combined action of shear, bending moment and variable axial load. The primary curves for the flexure and shear springs are defined considering the coupling between axial load, shear force and bending moment. The model has been shown to predict well the behaviour of flexure-dominated and shear-dominated columns. However, shear-to-total displacement ratio is assumed to be constant and thus degradation of shear strength with increasing displacement ductility is not accounted for in the model, which is important for detecting shear failure after flexural yielding.

The proposed hysteretic rules governing the cyclic response of the flexure and shear springs are based on existing hysteretic models (Ozcebe and Saatcioglu 1989, Takeda et al. 1970). The proposed modifications are aimed at improving the numerical stability for finite element analysis and extending the application of the Ozcebe and Saatcioglu (1989) for modeling flexural hysteretic response. The proposed hysteretic models can capture stiffness degradation, pinching behaviour and cyclic strength degradation including loss of strength in subsequent cycles at the same ductility level.

In most of the previous models based on single-component springs to model flexure and shear behaviour, the effects of variation of axial load on the moment capacity and the shear capacity are not considered. Xu and Zhang (2010) proposed a technique based on normalization of the primary curves to account for the effects of variable axial load.

The total displacement is determined based on the shear and flexure deformation components but deformations associated with bond slip and longitudinal reinforcement development are not included in the formulation.

2.3.2 Concentrated Plasticity Models Based on Generalized Hinges

In most of the concentrated plasticity models based on the single-component hinge approach that have been reviewed in the previous section, the axial force-moment interaction is not considered, resulting in important limitations. As described in ElMandooh Galal (2003) and Kaul (2004), the effects of variable axial load on the flexural and shear capacity, the hardening rate, plastic rotation capacity, etc. can be significant. In addition, single-component hinge models are more suitable for modeling the planar behaviour of reinforced concrete components since interaction effects due to bidirectional loading are ignored.

To overcome some of the limitations in the single-component hinge models, recent studies have employed yield-surface and evolution models approach to account for the force interaction in the case of multiaxial loading (Ricles et al. 1998, ElMandooh Galal 2003, Kaul 2004). These models are reviewed next.

2.3.2.1 Ricles et al. (1998)

Formulations:

Ricles et al. (1998) present a stress resultant lumped-plasticity formulation to model the response of nonductile reinforced concrete columns subjected to biaxial cyclic loading.

The element formulation accounts for inelastic response including yielding, hardening and softening, and degraded elastic response incorporating the effects of shear failure and post-shear failure behaviour. The beam-column element consists of a linear elastic beam placed in series with zero-length nonlinear hinges at each end of the element. Each hinge consists of a series of three flexural subhinges and one shear subhinge, as shown in Figure 2-25. Inelastic flexural and shear deformations develop only in the flexural and shear subhinges. The inelastic behaviour is modeled by using yield surfaces and shear failure surfaces for the flexural and shear subhinges, respectively, and evolution rules that define how the subsequent loading surfaces evolve during the plastic flow.

A yield surface is defined for each flexural subhinge, as shown in Figure 2-26(a). Yielding in a flexural subhinge occurs when the force point of the subhinge's action reaches the yield surface. The post-yield force interaction and strain hardening behaviour in flexure are controlled by kinematic hardening rules resulting in translation of a yield surface. The relationships between actions and deformations of a yielding flexural subhinge are derived based on Mroz's theory (Mroz 1969), and used to determine the tangent flexibility matrix of the flexural subhinge. The force-deformation relationships of the three initially rigid-plastic consecutive flexural subhinges combine with that of the elastic beam resulting in a multilinear moment-rotation relationship for the entire element, as illustrated in Figure 2-26(a). The three consecutive flexural subhinges are used to model the inelastic flexural behaviour of a reinforced concrete member characterized by concrete cracking, yielding of the longitudinal reinforcement, and

attaining the ultimate capacity. The yield function of a flexural subhinge is assumed to be an elliptical function of the two bending moments given by:

$$\phi(S, \alpha) = \left(\frac{M_y - \alpha_y}{M_{yy}} \right)^2 + \left(\frac{M_z - \alpha_z}{M_{zy}} \right)^2 \quad (2.18)$$

where M_y , M_z , M_{yy} , M_{zy} , α_y and α_z are the moments acting on the subhinge, the flexural yield capacities of a subhinge, and the coordinates that define the position of the centre of the subhinge's yield surface in biaxial flexural space with respect to the element's local y – and z –axes.

The tangent flexibility matrix of a yielded flexure subhinge relates the subhinge force increment to the plastic deformation increment. The tangent flexibility matrix used here is similar to that derived in Chen and Powell (1982) and is given as:

$$[F_{pf,i}] = \frac{\{n\}\{n\}^T}{\{n\}^T [K_{pfi}] \{n\}} \quad (2.19)$$

where $\{n\}$ is the outward normal vector to the yield surface at the action point, and $[K_{pfi}]$ is the diagonal plastic stiffness matrix from the individual flexural action-deformation relationships.

A shear failure surface is defined for each shear subhinge, as shown in Figure 2-26(b). Shear failure occurs in a shear subhinge when the shear force point reaches the shear failure surface. Upon detection of shear failure at a shear subhinge, the shear subhinge develops flexibility and shear capacity deteriorates with further shear deformation. The post-shear failure inelastic behaviour is controlled by an isotropic contraction rule

resulting in uniform shrinking of the shear failure surface toward the yield surface defined by the yield strength of the transverse reinforcement. The rate of isotropic contraction depends on the shear force increment and the shape of the subsequent shear-force interaction surface is determined by a linear interpolation between the original shear failure surface and the transverse reinforcement yield surface. Contraction of the shear failure surface is also considered by applying displacement ductility-related criteria. The element's flexural displacement ductility demand imposed about each axis is monitored and the shear capacity is updated based on the model for degradation of concrete shear strength developed by Priestley et al. (1994) shown in Figure 2-24. The shear failure function of a shear subhinge is assumed to be an elliptical function in biaxial shear force space given by:

$$F(V_y, V_z, V_y^c, V_z^c) = \left(\frac{V_y}{V_y^c}\right)^2 + \left(\frac{V_z}{V_z^c}\right)^2 \quad (2.20)$$

where V_y , V_z , V_y^c and V_z^c are the applied shear forces and the shear capacities of a shear subhinge with respect to the y – and z –axes. The initial shear capacity is based on the equation for prediction of shear strength proposed by Priestley et al. (1994).

The shear subhinge flexibility matrix is related to the rate of contraction of the shear failure surface and is given as:

$$[F_{pv}] = \begin{bmatrix} \frac{1}{k_{vy}} & 0 \\ 0 & \frac{1}{k_{vz}} \end{bmatrix} \quad (2.21)$$

where k_{vy} and k_{vz} are the plastic shear subhinge stiffness defining the shear unloading rate about the y – and z – axes, respectively.

The flexibility matrices of the flexural and shear subhinges are summed to obtain a hinge's flexibility matrix at ends I and J of the element, as follows:

$$[F_p^I] = \sum_{i=1}^3 [F_{pf,i}^I] + [F_{pv}^I] \quad (2.22a)$$

$$[F_p^J] = \sum_{i=1}^3 [F_{pf,i}^J] + [F_{pv}^J] \quad (2.22b)$$

The shear and flexural components of the subhinges' deformations are considered in determining the total deformation of a hinge as proposed by Yang (1994). The flexibility matrix for the entire element is obtained by combining the tangent flexibility matrices of the hinges at each end and the flexibility matrix of the elastic element. The tangent stiffness of the element is obtained by inverting the flexibility matrix. A limiting value of the plastic shear subhinge stiffness is used to ensure that the element tangent flexibility is non-singular as proposed by Yang (1994). Thus, the element maintains an increase in shear deformation associated with degradation in shear strength.

Degradation in elastic stiffness in the hysteretic response of reinforced concrete members under cyclic loading is considered in the element formulation by assigning a finite value for the elastic flexibility to the initially rigid-plastic subhinges that have accumulated plastic deformations.

The modeling of degradation in elastic stiffness in the flexural subhinges follows the method proposed by Chen and Powell (1982). Stiffness degradation is assumed to be in inverse proportion to the largest previous hinge deformation. Unloading and reloading stiffnesses of a flexural subhinge depend on the previous maximum positive and negative hinge deformations and are controlled by empirical degradation coefficients.

After shear failure occurs in a shear subhinge, the opening of shear cracks is idealized as plastic shear deformations in the model. In the event of unloading, the elastic unloading stiffness of a shear subhinge is defined as:

$$K_s = \frac{V_r}{\beta_3 \Delta_{cr}} \quad (2.23)$$

where β_3 is a parameter having a constant value between 0 and 1.0; and V_r and Δ_{cr} are the shear force and plastic shear deformation (crack opening), respectively, when elastic unloading occurs in the shear subhinge. Upon complete unloading, the flexibility of the shear subhinge is assumed to be infinite leading to zero hinge stiffness until the shear crack width based on accumulated plastic shear deformation closes under reversed loading, as illustrated in Figure 2-27(a). The shear force-deformation relationship of the element subjected to a full loading cycle is shown in Figure 2-27(b), where upon the closure of the shear crack under reversed loading, the reloading elastic stiffness is assumed to be aiming toward the point of previous maximum deformation.

The beam-column element developed for modeling the response of shear-critical reinforced concrete columns has been verified by comparing the analytical results with

experimental data from biaxial cyclic lateral load tests with either no axial load or constant axial load.

Summary of Findings and Discussion:

The concentrated-plasticity beam-column element is capable of capturing stiffness and strength degradation and pinching behaviour which are characteristics of shear-critical reinforced concrete members' response to cyclic loading.

The yield surface of the flexural subhinges is defined as a function of the two bending moments, and thus the interaction between axial load and bending moments is not considered in the formulation, which limits the use of the model in conditions of variable axial load common for seismic loading.

In-cycle strength degradation is modeled by using isotropic contraction rule resulting in a negative slope in the shear subhinge force-deformation relationship after shear failure. By using isotropic contraction rule to define the evolution of the shear failure surface, coupling in shear strength degradation between the two lateral directions is considered. However, it might be appropriate to consider non-uniform contraction rule by employing some damage index to account for the accumulation of damage in each lateral direction.

In the study conducted by Ricles et al. (1998), the shear-strength model developed by Priestley et al. (1994) is incorporated in the beam-column element to initiate degradation of shear strength. The Priestley model provides a relationship between the shear strength

and the displacement ductility, hence, the beam-column model accounts for the shear-flexure interaction effects in the plastic hinge zone and allows for flexural yielding before shear failure of the member. However, some deficiencies in using shear-strength models for predicting the displacement at shear failure of reinforced concrete columns are discussed by Sezen (2002). As pointed out by Sezen, a relatively small variation in the shear strength model or in the shear demand results in a relatively large change in the estimated displacement at shear failure. An alternative approach for predicting the drift ratio at which shear failure occurs is proposed by Elwood (2002) as discussed in the previous section.

Cyclic strength degradation in reversed loading at the same displacement level is accounted for by considering kinematic hardening behaviour with elastic stiffness degradation in the flexure subhinge formulation. Degradation in stiffness is considered in the hysteretic models of the flexural and shear subhinges, however, the coupling effects in stiffness degradation between the two lateral directions under biaxial cyclic loading are not addressed. Furthermore, the degradation in elastic unloading and reloading stiffnesses of the flexural subhinges and the degradation in elastic unloading stiffness of the shear subhinge are entirely based on peak deformations and constant empirical parameters. The incorporation of damage models may be appropriate to account for the effects of accumulation of damage on the stiffness degradation. The total displacement is determined based on the shear and flexure deformation components but deformations associated with bond slip and longitudinal reinforcement development are not included in the formulation.

2.3.2.2 ElMandooh Galal (2002)

Formulations:

ElMandooh Galal (2002) and ElMandooh Galal and Ghobarah (2003) have developed a beam-column element for modeling the flexural and shear behaviour of reinforced concrete columns subjected to biaxial cyclic loading and variable axial load. The element formulation considers strength deterioration, stiffness degradation and pinching behaviour. The concentrated-plasticity beam-column element consists of an elastic element with plastic hinges at each end. Each plastic hinge consists of a series of three flexural subhinges and one shear subhinge. The nonlinear beam-column element and details of the plastic hinge are shown in Figure 2-28. The inelastic deformations are concentrated in the flexural and shear subhinges. The inelastic flexural and shear behaviour are modeled by using yield surfaces and failure surfaces in the formulation of the flexural and shear subhinges, respectively. The plastic flow and the associated evolution of the subsequent loading surfaces are controlled by evolution models defined for the flexural and shear subhinges. Stiffness degradation behaviour is considered in the model when reversed loading is applied assuming that stiffness degrades independently for each moment or force component for each subhinge.

The three flexural subhinges placed in a series in a plastic hinge are used to represent the stages in the inelastic flexural behaviour of a reinforced concrete member characterized by concrete cracking, yielding of the longitudinal reinforcement, and attaining the ultimate capacity. The interaction between the four actions at a flexural subhinge, i.e. axial force, bending moments and torsional moment, is modeled by using a four-

dimensional yield surface. A two-dimensional interaction surface is illustrated in Figure 2-29 instead of the four-dimensional relationship for the purpose of clarity. Yielding in a flexural subhinge occurs when the force point of the subhinge's actions reaches the yield surface. A quadratic function is assumed to represent the yield surface given by:

$$\Phi_{mi}(S_m, \alpha_i) = \left(\frac{M_y - \alpha_{iM_y}}{M_{iy}}\right)^2 + \left(\frac{M_z - \alpha_{iM_z}}{M_{iz}}\right)^2 + \left(\frac{M_x - \alpha_{iM_x}}{M_{ix}}\right)^2 + \left(\frac{F_x - \alpha_{iF_x}}{F_{ix}}\right)^2 \leq 1 \quad (2.24)$$

where α_i is the current position of the yield surface for the flexural forces, F_x , M_y , M_z and M_x , at hinge i . After initial yielding at a “cracking” flexural subhinge, the strain hardening behaviour in flexure is controlled by kinematic hardening rules resulting in translation of the yield surface till it reaches the next yield surface. Then both yield surfaces translate in the force space till reaching the outermost yield surface. The relationships between actions and deformations of a yielding flexural subhinge prior to reaching the outermost yield surface are derived based on Mroz's theory (Mroz 1969). Upon reaching the outermost yield surface, the translation of the three yield surfaces follows the Ziegler's hardening rule (Ziegler 1959).

A shear failure surface is defined for the shear subhinge in a plastic hinge, as shown in Figure 2-30. Shear failure occurs when the force point of shear subhinge's actions reaches the shear failure surface. The interaction between the axial load and the shear forces is considered in the formulation of the shear failure surface. The failure surface is expressed by a quadratic function given as follows:

$$\Phi_s(S_s, F_x) = \left(\frac{V_y}{V_y^f} \right)^2 + \left(\frac{V_z}{V_z^f} \right)^2 + \left(\frac{F_x - F_{av}}{F_{ult} - F_{av}} \right)^2 \leq 1 \quad (2.25)$$

where F_{ult} is the element axial compressive capacity, T_{ult} is the element tensile capacity, and $F_{av} = (|F_{ult}| + |T_{ult}|)/2$ is the average axial force. The shear capacities, V_y^f and V_z^f , are based on the equation proposed by Priestley et al. (1994).

The post-shear failure behaviour characterized by softening is modeled by using an isotropic contraction rule forcing the shear surface to shrink toward a residual shear surface defined based on the contribution to shear strength by the transverse reinforcement. The rate of isotropic contraction depends on the plastic stiffness for the shear subhinge along the y and z axes.

The flexure and shear subhinges in the plastic hinges at each end of the element are assumed to be initially rigid, thus the initial stiffness is the stiffness of the interior elastic element. After yielding, the flexure subhinges are assumed to develop flexibility. Upon load reversals, the flexibility of a flexure subhinge is divided into elastic flexibility, $[F_{sem}^I]$, and plastic flexibility, $[F_{spm}^I]$. After shear failure, the shear subhinge is also assumed to develop flexibility, $[F_{sps}^I]$. The shear force flexibility matrix used for the descending branch is similar to that proposed by Ricles et al. (1998):

$$[F_{sps}] = \begin{bmatrix} 1 & 0 \\ K_{vy} & \\ 0 & 1 \\ & K_{vz} \end{bmatrix} \quad (2.26)$$

where K_{vy} and K_{vz} represent plastic stiffness for shear subhinge in the y – and z –axis, respectively.

The tangent flexibility matrices, $[F_p^I]$ and $[F_p^J]$, at each end are determined by summation of the flexibilities of the subhinges as follows:

$$[F_p^I] = \sum_{i=1}^3 ([F_{sem,i}^I] + [F_{spm,i}^I]) + [F_{sps}^I] \quad (2.27a)$$

$$[F_p^J] = \sum_{i=1}^3 ([F_{sem,i}^J] + [F_{spm,i}^J]) + [F_{sps}^J] \quad (2.27b)$$

The flexibility matrix for the entire element is obtained by adding the tangent flexibility matrices of the hinges at each end and the flexibility matrix of the elastic element. The tangent stiffness of the element is obtained by inverting the flexibility matrix.

Including elastic and plastic flexure subhinge flexibilities represents elastic stiffness degradation with reduced overall element stiffness when the element is subjected to repeated reversed cyclic loading. The plastic flexibility matrix of a yielded flexure subhinge is derived following the approach by Chen and Powell (1982):

$$[F_{spm,i}] = \frac{\{n\}\{n\}^T}{\{n\}^T [K_{spm,i}] \{n\}} \quad (2.28)$$

where $\{n\}$ is the outward normal vector to the yield surface at the action point, and $[K_{spm,i}]$ is the diagonal plastic stiffness matrix from the individual flexural action-deformation relationships.

The elastic flexibility of a flexure subhinge is assumed to be inversely proportional to the previous hinge secant stiffness, K_s , and is given by:

$$[F_{sem,i}] = \alpha_m \left(\frac{d_i^p}{\sum_{i=1}^3 d_i^p} \right) \frac{1}{K_s} \quad (2.29)$$

where K_s is the secant stiffness of the previous cycle and α_m is an arbitrary degradation coefficient in the range from 0 to 1. The parameters, d_i^p , are depicted in Figure 2-31. Thus, stiffness degradation and cyclic strength deterioration in repeated cycles at the same ductility level are accounted for in the moment-rotation response of a flexural subhinge component, as shown in Figure 2-31.

Degradation in elastic shear stiffness and pinching behaviour are considered in the shear force-deformation hysteretic relationship, as shown in Figure 2-33. Upon load reversal in the post-peak shear response, the stiffness of the shear subhinge reduces when the shear force reaches zero. The flexibility matrix of the shear subhinge during pinching is defined as:

$$[F_{sps}] = \alpha_p [F_s] = \alpha_p \frac{1}{GA'L} \begin{bmatrix} 1 & 1 \\ 1 & 1 \end{bmatrix} \quad (2.30)$$

where α_p is an arbitrary degradation coefficient in the range from 0 to 1, $[F_s]$ is the initial shear flexibility matrix, GA' is the effective shear rigidity, and L is the element length.

Following a complete loading cycle, shear stiffness degradation is introduced by using a reduced elastic shear stiffness given by:

$$F_s = \alpha_s \frac{1}{K_s} \quad (2.31)$$

where α_s is an arbitrary degradation coefficient ranging from 0 to 1 and K_s is the secant stiffness, as shown in Figure 2-31.

Event-based solving technique is used for state determination at the element level. Event factors are defined for the flexure and shear subhinges to cause the occurrence of events such as reaching a yield surface, change in stiffness and shear failure.

To define the moment-rotation relationship used in the analytical model, the contributions from flexural, bond slip and shear deformations are considered as follows:

$$\theta_{tot} = \theta_f + \theta_s + \gamma_v \quad (2.32)$$

where θ_f is the rotation due to flexure, θ_s is the rotation due to reinforcement bond slip, and γ_v is the rotation due to shear.

The rotation component due to flexure, θ_f , is calculated by integrating the curvature along the length of the column and using the plastic hinge model. The contribution to the total rotation from the lumped rotation near the fixation point due to reinforcement bond slip is calculated as:

$$\theta_s = \frac{\delta_s}{d - c} \quad (2.33)$$

where d is the depth to the tensile reinforcement, c is the depth of the compressions zone, and δ_s is the slip, which is determined based on the model developed by Alsiwat and Saatcioglu (1992).

The shear deformations are calculated using the equation for shear stiffness proposed by Park and Paulay (1975).

The following approach is adopted to determine the post-peak negative stiffness in case of shear failure in the analytical model. The post-peak shear stiffness is assumed to degrade based on the loss of strength and the yield displacement. In this approach, the negative stiffness for the cases of moderate ductility behaviour with shear failure and limited ductility with brittle shear failure are defined as:

$$K_{vy} = -\frac{V_y^i - V_y^r}{2\Delta_y} \text{ for moderate ductility} \quad (2.34a)$$

$$K_{vy} = -\frac{V_y^i - V_y^r}{\Delta_y} \text{ for limited ductility} \quad (2.34b)$$

where V_y^i and V_y^r are the initial shear capacity and the residual shear strength in y direction, as shown in Figure 2-32.

The beam-column element developed for modeling the biaxial flexural and shear responses of reinforced concrete columns has been verified by using experimental data for different loading conditions including biaxial cycling loading and variable axial load.

Summary of Findings and Discussion:

The beam-column element based on lumped-plasticity modeling is capable of capturing the stiffness and strength degradation and pinching behaviour of reinforced concrete columns subjected to bidirectional cyclic loading and variable axial load.

The yield surface for a flexural subhinge is defined as a function of the axial load, the two bending moments and the torsional moment. Thus, the effects of variable axial load on the lateral moment capacity are accounted for by using the interaction surface. Similarly, the shear failure surface is defined as a function of the shear forces and the axial load, thus accounting for the interaction effects on the shear capacity.

The effects of axial load variation on the element stiffness are also included in the formulation by considering the following. The plastic flexibility of a yielded flexure subhinge depends on the normal vector to the yield surface, which depends on the current force state governed by the interaction surface. The plastic flexibility of a flexural subhinge is used in the determination of the element's total flexibility and stiffness matrices.

In-cycle strength degradation upon the detection of shear failure is modeled by using isotropic contraction rule resulting in a negative slope in the shear subhinge force-deformation relationship. The negative stiffness is controlled by input parameters based on evaluation considering the potential for shear failure or shear-flexure failure.

A limitation in this model is that interaction between moment and shear is not included in the formulation of the beam-column element. Ductile behaviour governed by flexural yielding and limited ductility behaviour governed by brittle shear failure can be captured by the model. However, modeling of moderate ductility behaviour with shear failure due to degradation in shear strength with increasing ductility requires additional considerations and evaluations of the potential failure mode prior to analysis.

Degradation in stiffness is considered based on the assumption that it is independent for each moment or force component. However, ignoring coupling in stiffness degradation between the two lateral directions may not adequately predict the biaxial cyclic response of reinforced concrete members under various loading conditions. Furthermore, degradation in unloading and reloading stiffness and cyclic strength deterioration are considered based on peak deformations and constant empirical degradation coefficient. The incorporation of damage models may be appropriate to account for the effects of accumulation and progression of damage on the response of the column.

2.3.2.3 Kaul (2004)

Formulations:

Kaul (2004) has developed a beam-column element for modeling of strength and stiffness degradation of older, shear-critical reinforced concrete columns. The element formulation accounts for large deformations, inelastic response including yielding, hardening and softening, and degraded elastic response. Large deformation effects are incorporated in

the formulation by employing an updated Lagrangian approach and a force recovery technique, which distinguishes rigid body deformations from natural element deformations. The inelastic behaviour is modeled using a yield surface and evolution models that specify how the yield surface is modified during the plastic flow. The formulation of the yield surface models extends the work by El-Tawil and Deierlein (1998). The yield surface is assumed to be a continuous, convex function of axial force and bending moment. The initiation of yielding in the element occurs when the force point reaches the yield surface, and the maximum level of hardening is determined by the nominal surface, as shown in Figure 2-34. The model accounts for in-cycle strength degradation by allowing a negative stiffness segment in the monotonic flexural response of the reinforced concrete element, as illustrated in Figure 2-35. The post-yield force interaction and the hardening and softening behaviour are controlled by evolution rules based on combined kinematic translation and non-uniform expansion and contraction of the yield surface, as shown in Figure 2-36. The combined kinematic and isotropic response is considered in the formulation by separating the kinematic and the isotropic plastic stiffnesses. The kinematic plastic stiffness varies as a function of the surface translation, and primarily affects the hardening response. The isotropic plastic stiffness varies as a function of cumulative plastic deformations or a damage index based on plastic displacement component and is used primarily to control the softening behaviour. The decrease in the hardening rate with cumulative plastic strains is accounted for in the evolution models by using a degrading coefficient to control the rate of changing the plastic stiffness relating the incremental force with the incremental plastic deformation.

The nonlinear hysteretic response of a reinforced concrete element subjected to inelastic cyclic excursions is modeled by using cyclic stiffness models. These cyclic models are used to control the relationship between the element shear force and the rotation at each end of the element during the degraded elastic response. Unloading stiffness is degraded by using a damage factor based on cumulative plastic rotations while the reloading stiffness is a weighted function of unloading stiffness and the stiffness required for a peak-oriented response. Event-based formulation is used to determine the loading/unloading state of the element.

Shear failure and post-shear failure behaviour including shear-axial response interaction are incorporated in the model for shear-critical reinforced concrete columns. Force-based and displacement ductility-based criteria are used to determine the shear failure mode. Three conditions of shear failure are considered in the formulation. For columns with low shear capacity, brittle failure occurs when the shear capacity is exceeded prior to flexural yielding, as shown in Figure 2-37, case 1. For columns with comparable shear and moment capacity, failure occurs when the shear capacity is exceeded after yielding and hardening in moment, as shown in Figure 2-37, case 2. For columns with initial shear capacity sufficiently higher than the shear demand, shear-flexure failure is considered as the shear strength degrades with increasing displacement ductility, as shown in Figure 2-37, case 3. The equations for calculating drift ratios at shear failure and at axial failure proposed by Elwood (2002) are used to determine the shear critical response. Considering that in the conducted tests the peak shear in the columns is between 1.0 and

0.7 of V_n with maximum drift ratio less than 0.06, an equation to determine the initiation of shear failure is developed as follows:

$$\frac{V}{V_n} = \frac{1}{\alpha} \ln \left(a_0 \frac{\Delta}{L} + b_0 \right) + c_0 \quad (2.35)$$

where, α is a constant that controls the curvature of the curve, a_0 and b_0 are drift ratios at shear failure corresponding to $V/V_n = 1.0$ and $V/V_n = 0.7$, respectively, and are derived from Equation (2.1) proposed by Elwood (2002). The parameters α and c_0 are calculated such that $V/V_n = 0.5$ at $\Delta/L = 0.1$.

Under the assumption that the force point unloads from the yield surface after shear failure the post-shear failure behaviour of the element is incorporated in the cyclic models of the element formulation. Similar concepts are used by Elwood (2002). The elastic element stiffness is derived based on the flexibility approach to include the shear components of the deformation. The negative shear stiffness causes the element to soften in shear and unload in moment, as the imposed drift reaches the drift at axial failure. A hysteretic model shown in Figure 2-38 is developed to model the pinching response of an element after shear failure based on the assumption that pinching deformation is a function of the peak shear deformations. The hysteretic rules consider full cycles and half cycles of loading, as shown in Figures 2-38 and 2-40.

The beam-column element developed for modeling shear-critical reinforced concrete columns has been verified by comparing the analytical results with experimental data from tests conducted by Elwood (2002) and Sezen (2002).

Summary of Findings and Discussion:

The proposed models have been implemented in the software framework system OpenSees (McKenna et al. 2004) by using object-oriented programming concepts with focus on extensibility and flexibility which is a significant advantage.

The concentrated-plasticity beam-column element is capable of capturing stiffness and strength degradation and pinching behaviour which are characteristics of shear-critical reinforced concrete members' response to cyclic loading. A limitation in the formulation is that cyclic strength degradation is entirely based on the peak plastic deformations and the direction of evolution. Depending on the evolution model, cyclic strength degradation may not be captured by this model in the case of subsequent loading cycles with multiple excursions to the same inelastic displacement. The yield surface is defined in terms of axial force and bending moment and thus, the effects of variable axial load on the lateral moment capacity are accounted for. Decreasing hardening rate with accumulation of plastic deformations is also considered in the formulation of the combined hardening rule. The yield surface and the evolution rules are developed only for modeling the planar behaviour of reinforced concrete structural members. Hence, biaxial moment interaction is not considered in the model. To extend the formulation of the beam-column element for modeling three-dimensional behaviour, the coupling effects in stiffness and strength

degradation between the two lateral directions are issues that need to be addressed. Deformations associated with bond slip and longitudinal reinforcement development are not included in the formulation and the effects of these deformations on the stiffness and ductility limits of reinforced concrete columns subjected to combined axial load, bending and shear still need to be investigated.

2.4 Summary of Previous Research and Proposed Models

In recent studies, both concentrated and distributed plasticity models have been developed for seismic response analysis of reinforced concrete structures incorporating flexure and shear effects. The section behaviour of a reinforced concrete member is described by stress resultant plasticity-based models in some of the existing models, and by fiber models in others. Generally, the concentrated plasticity models are computationally more efficient than the distributed plasticity fiber models, and also more practical for modeling complex phenomena like post-shear failure response considering that they require fewer parameters to capture the degrading behaviour under cyclic loading.

Existing concentrated plasticity models incorporating flexure and shear effects have been carefully reviewed in this chapter. Each of the reviewed models provides valuable insights on the simulations of the cyclic response of older shear-critical reinforced concrete column members. However, further developments of consistent, computationally efficient models that capture accurately the three-dimensional behaviour

of reinforced concrete components and implementations of the models in finite element analysis platforms are still needed in this research area.

This research is focused on the development of a comprehensive 3D model for seismic response analysis of reinforced concrete frame structures subjected to multi-component seismic loading which comprises biaxial cyclic loading with variable axial load effects. As summarized in Chapter 1, the nonlinear behaviour of reinforced concrete frame members may be: ductile governed by flexural plastic hinging, moderately ductile with shear failure resulting from exceedance of degraded shear capacity in the flexural plastic hinge zone, limited ductile with shear failure resulting from exceedance of shear capacity after yielding at relatively low ductility levels, and brittle governed by shear failure as the initiating failure mechanism. The new model proposed in this research is capable of covering the entire range of behaviour from ductile to brittle and in between which can arise from interaction between the axial, shear and moment capacities and their evolution during the progression of damage in inelastic load reversals. The proposed model is especially suitable for analysis of progressive collapse behaviour of reinforced concrete structures by considering the effects of accumulation of damage on stiffness and strength degradation of structural components beyond the peak response.

From the performed literature review it is evident that existing degradation models are mostly suitable for analysis of two-dimensional behaviour of reinforced concrete components or do not capture the full interaction of axial, flexure and shear effects or the effects of accumulation of damage on the three-dimensional behaviour. The proposed

model is unique in considering the full axial-flexure-shear interaction effects and the effects of progression of damage on the post-peak stiffness and strength degradation of components subjected to biaxial reversed cyclic loading with variable axial load in a consistent and comprehensive manner.

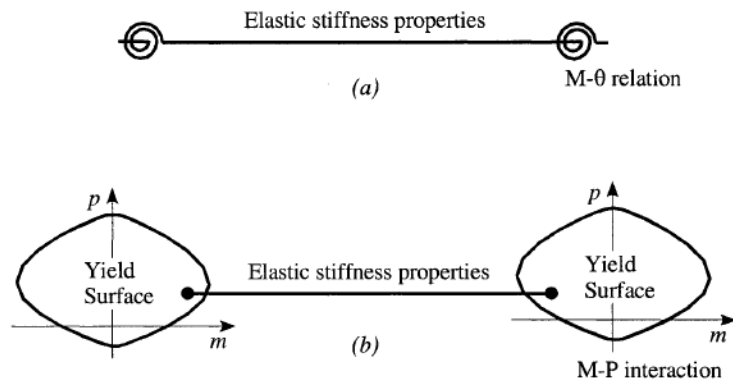


Figure 2-1 Concentrated plasticity models (Kaul 2004)

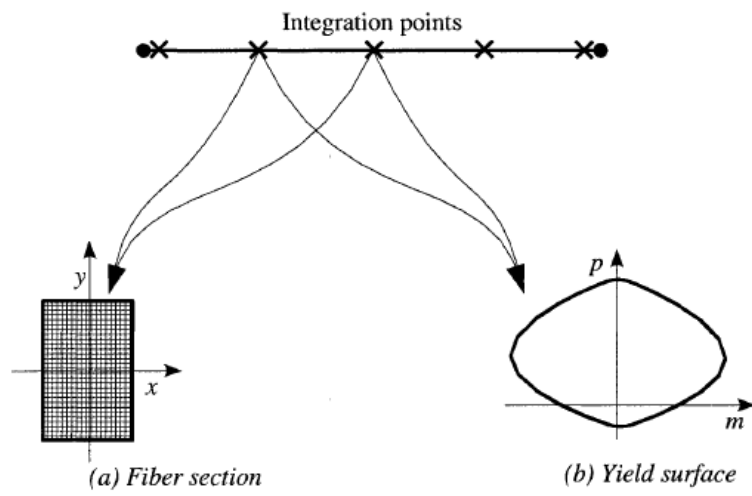


Figure 2-2 Distributed plasticity models (Kaul 2004)

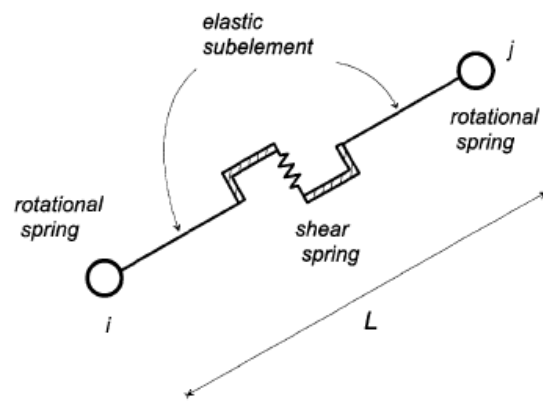


Figure 2-3 Schematic representation of nonlinear model (Pincheira et al. 1999)

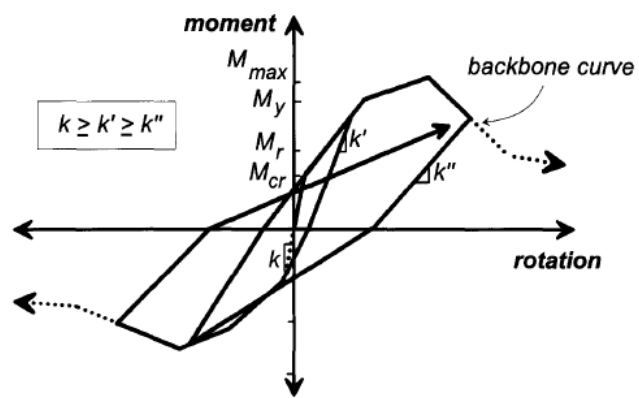


Figure 2-4 Moment and rotation relation – hysteretic laws (Pincheira et al. 1999)

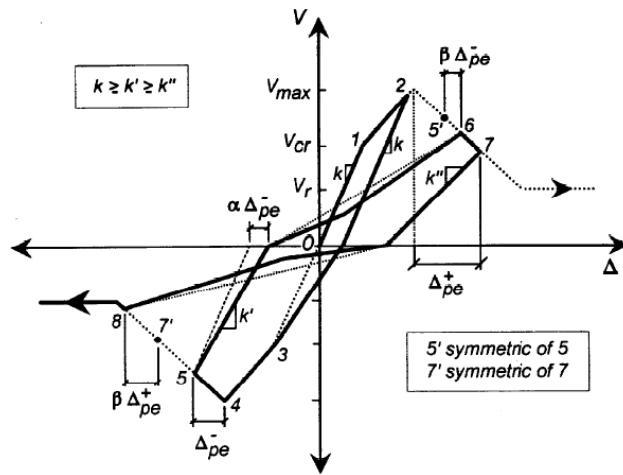


Figure 2-5 Shear force and displacement relation – hysteretic laws (Pincheira et al. 1999)

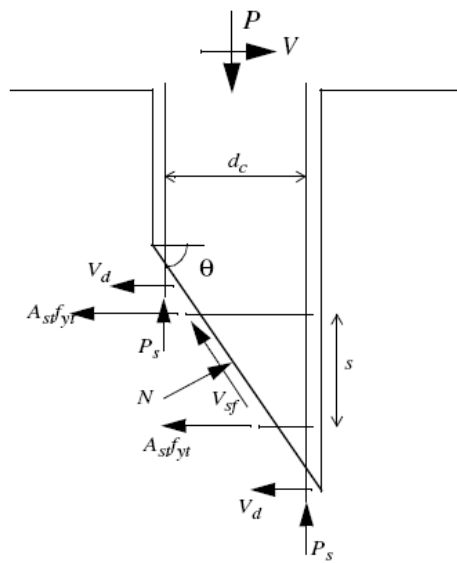


Figure 2-6 Free body diagram of column after shear failure (Elwood 2002)

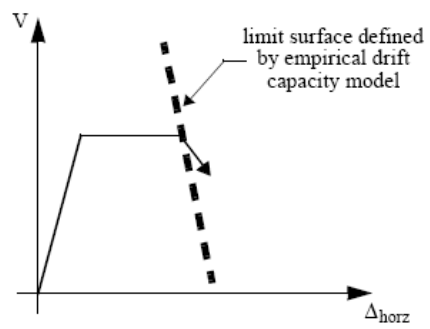


Figure 2-7 Shear failure defined by proposed drift capacity model (Elwood 2002)

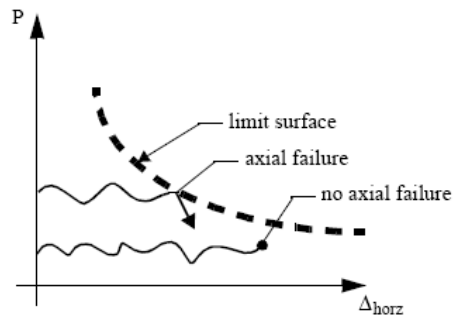


Figure 2-8 Axial failure model (Elwood 2002)

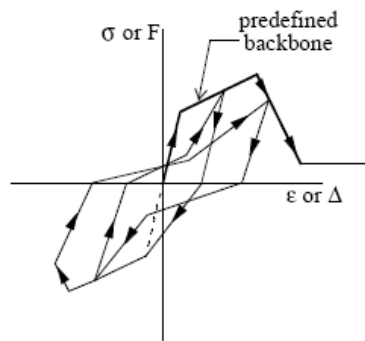


Figure 2-9 Example of capabilities of Hysteretic uniaxial model (Elwood 2002)

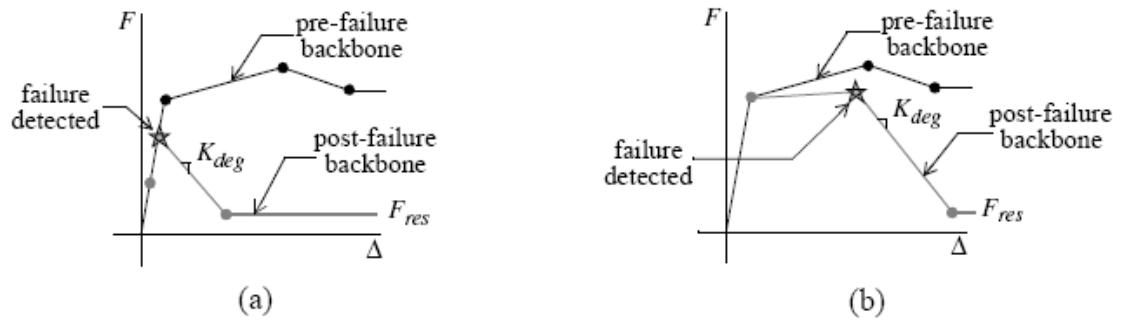


Figure 2-10 Redefinition of backbone after failure is detected (Elwood 2002)

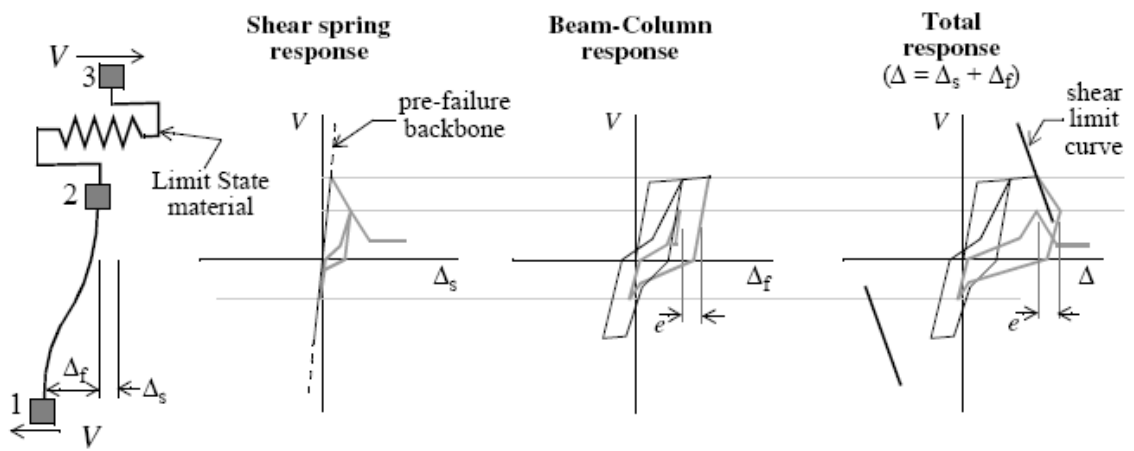


Figure 2-11 Shear spring in series model using Limit State uniaxial material model (Elwood 2002)

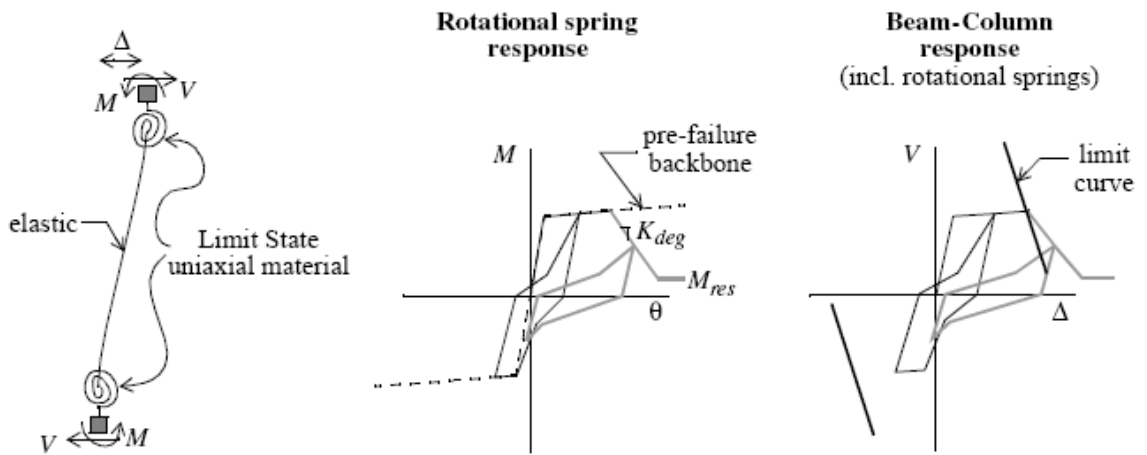


Figure 2-12 Rotational spring model (Elwood 2002)

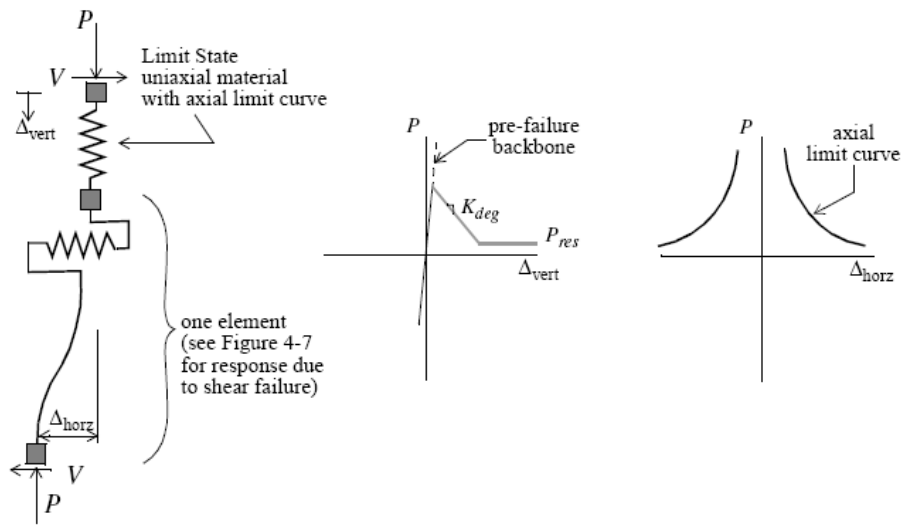


Figure 2-13 Axial spring in series model (Elwood 2002)

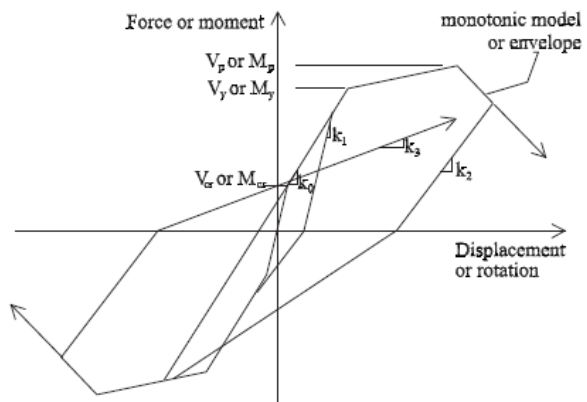


Figure 2-14 Hysteretic rules for lateral force-flexural displacement relationship (Sezen and Chowdhury 2009)

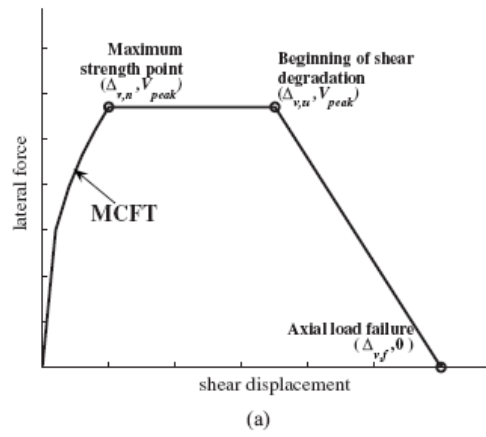


Figure 2-15 Monotonic envelope for lateral force-shear displacement relationship (Sezen and Chowdhury 2009)

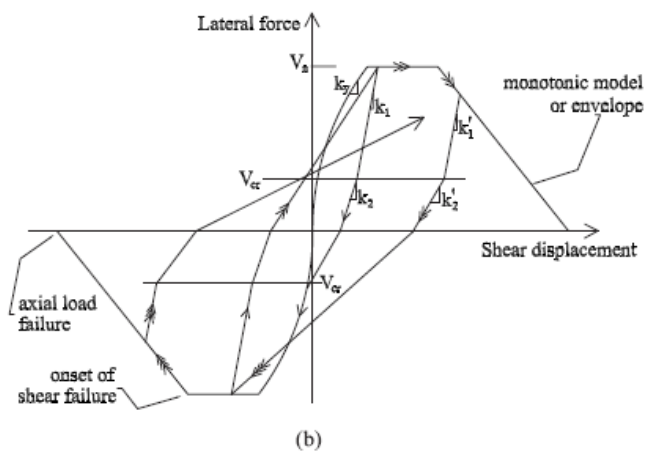


Figure 2-16 Hysteretic rules for lateral force-shear displacement relationship (Sezen and Chowdhury 2009)

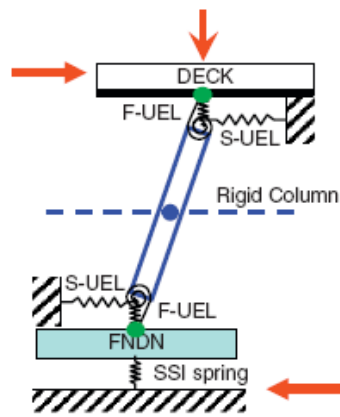


Figure 2-17 Schematic shear-flexural interaction model for columns (Xu and Zhang 2011)

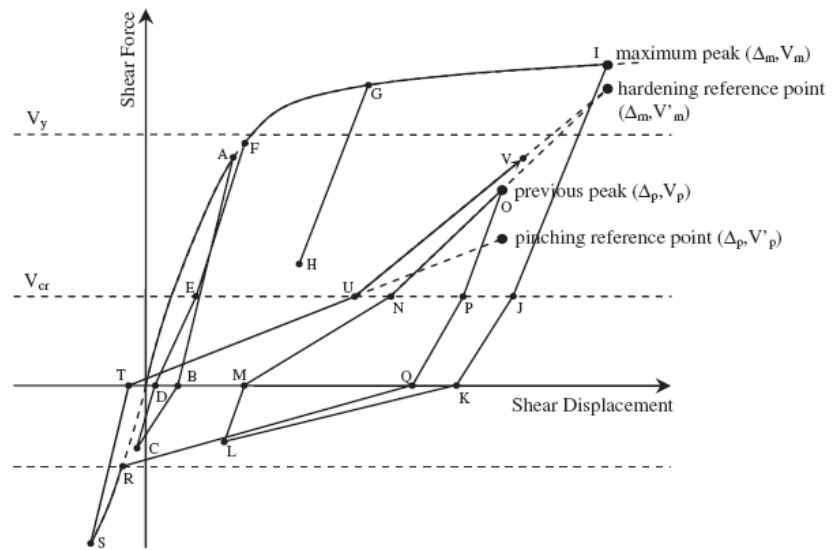


Figure 2-18 Illustration of the shear hysteretic model by Ozcebe and Saatcioglu (1989) (Xu and Zhang 2011)

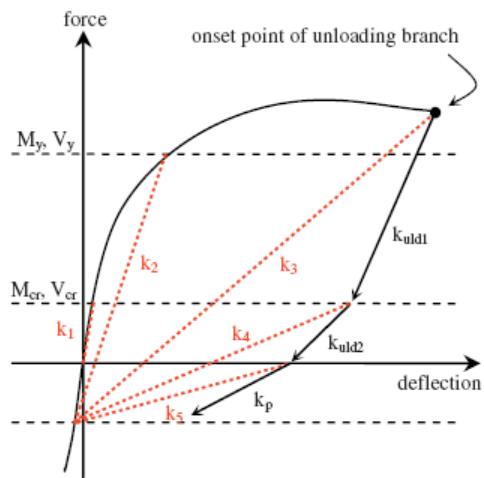


Figure 2-19 Hysteretic rules for the unloading stiffness (Xu and Zhang 2011)

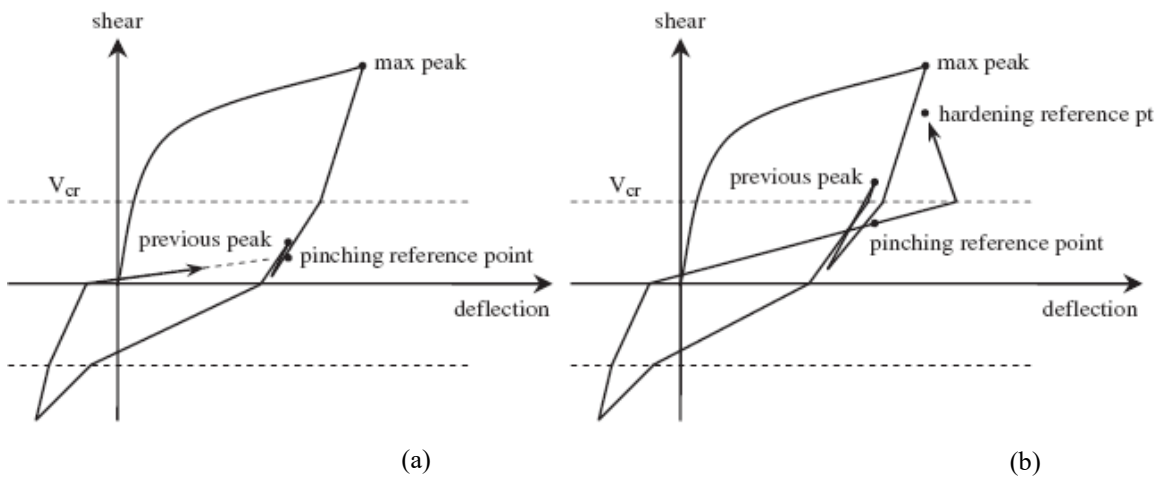


Figure 2-20 Examples of model defects in Ozcebe and Saatcioglu shear hysteretic model (a) nearly zero pinching stiffness and (b) negative hardening stiffness (Xu and Zhang 2011)

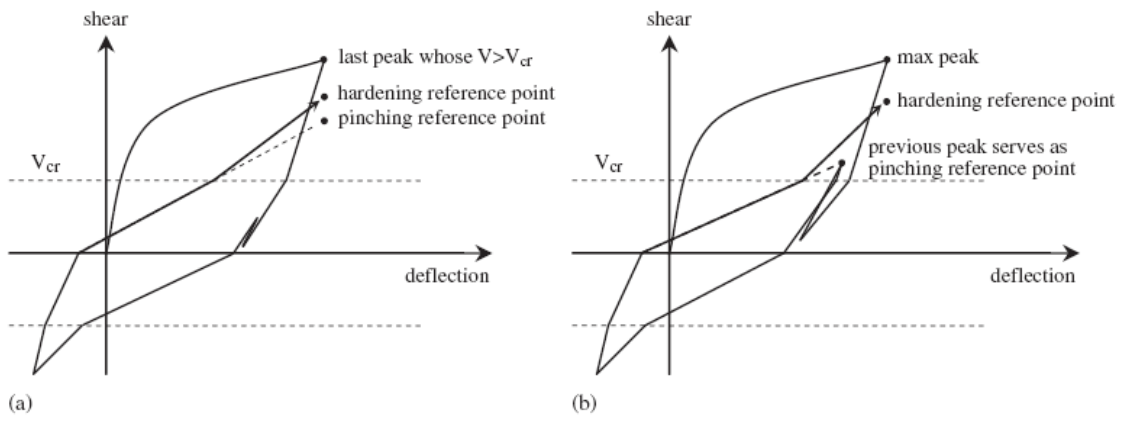


Figure 2-21 Remedies for the defects in shear hysteretic model: (a) fix for nearly zero pinching stiffness and (b) fix for negative hardening (Xu and Zhang 2011)

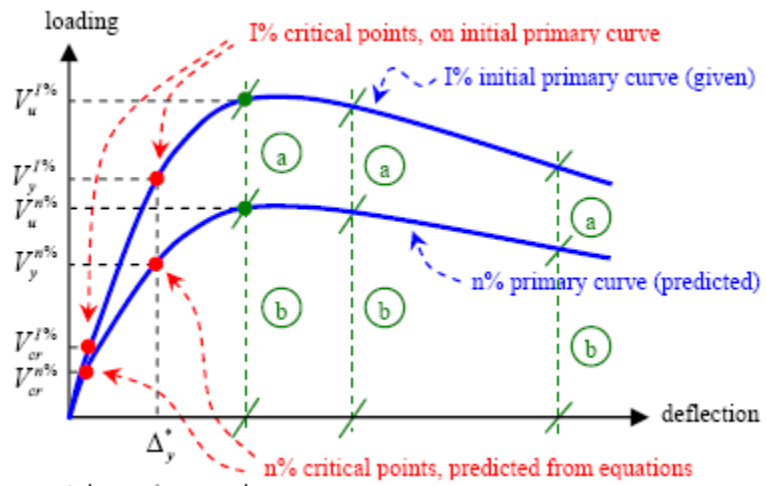


Figure 2-22 Rules for mapping between primary curves (Xu and Zhang 2010)

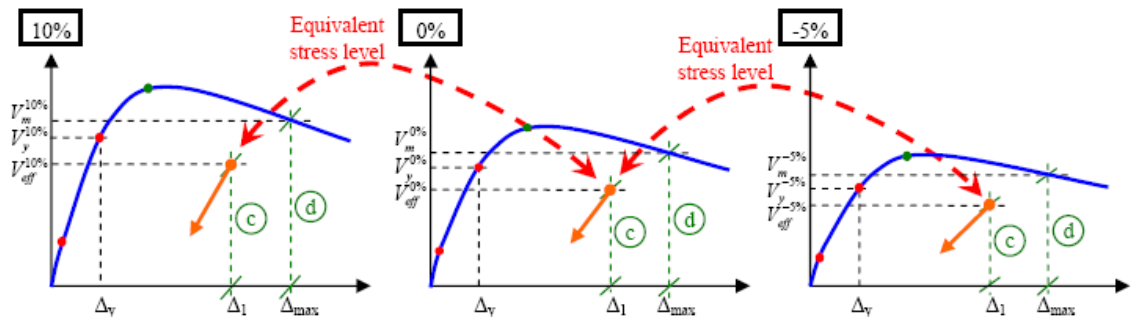


Figure 2-23 Rules for mapping between unloading and reloading branches (Xu and Zhang 2010)

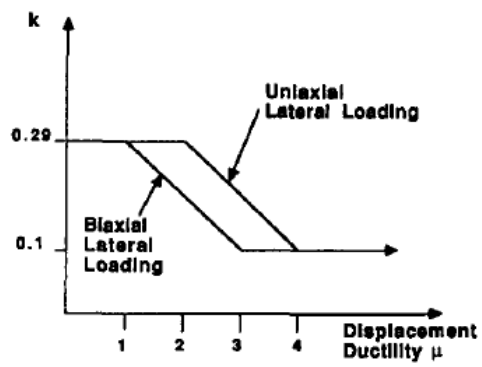


Figure 2-24 Model for degradation of concrete shear strength with flexural ductility proposed by Priestley et al. (1994) (Ricles et al. 1998)

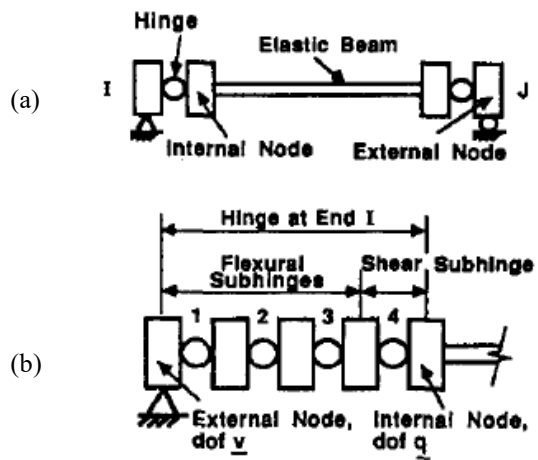


Figure 2-25 Shear-Flexural Element (a) Component; (b) Flexural and Shear Subhinges (Ricles et al. 1998)

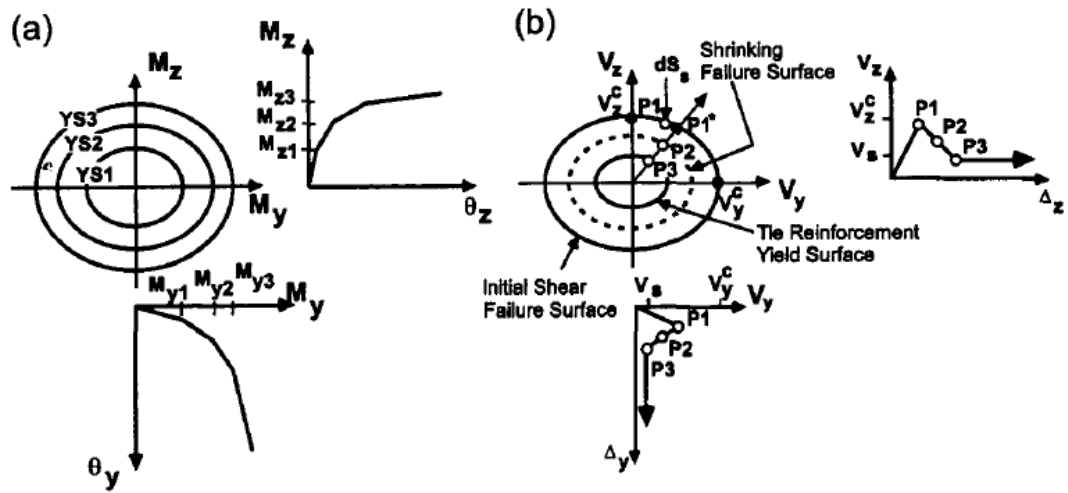


Figure 2-26 Schematics of (a) Yield Surfaces for Flexural Subhinges; (b) Shear Failure Isotropic Failure Surface (Ricles et al. 1998)

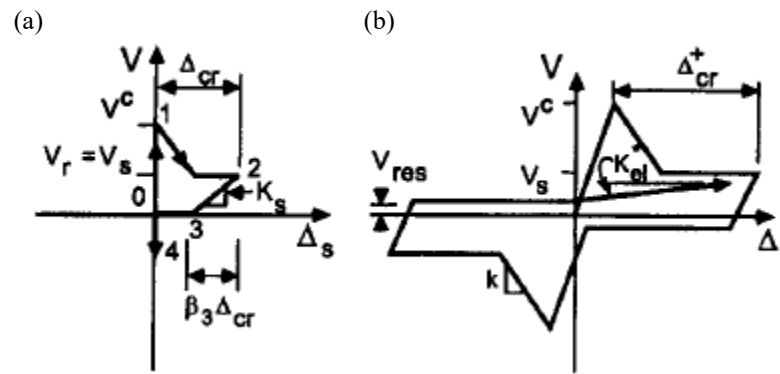


Figure 2-27 Degradation of Elastic Stiffness of (a) Shear Subhinge; (b) Effect on Element Shear Response (Ricles et al. 1998)

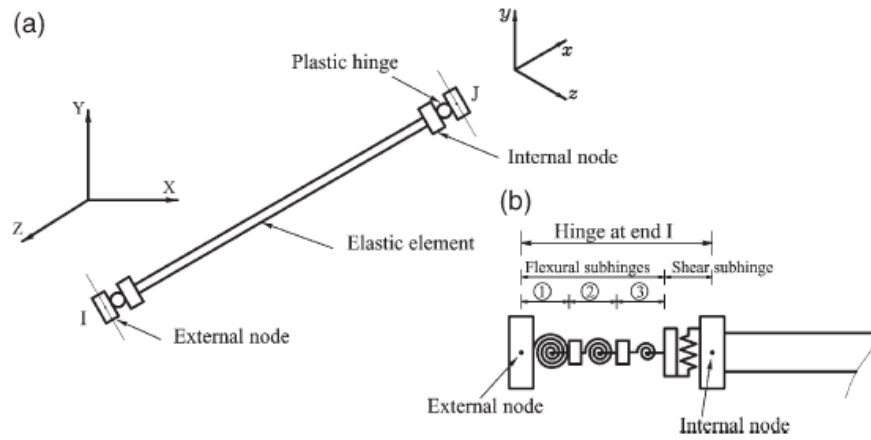


Figure 2-28 (a) Element idealization (b) Plastic hinge idealization (ElMandooh Galal and Ghobarah 2003)

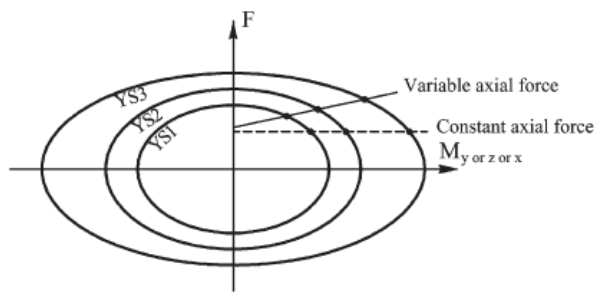


Figure 2-29 Yield surfaces for flexural subhinges (ElMandooh Galal and Ghobarah 2003)

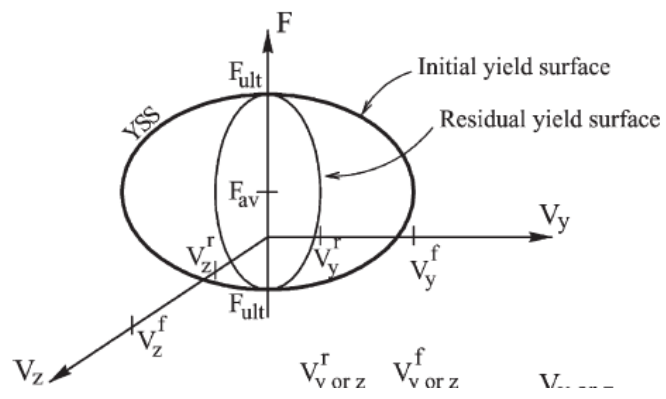


Figure 2-30 Failure surface for shear subhinge (ElMandooh Galal and Ghobarah 2003)

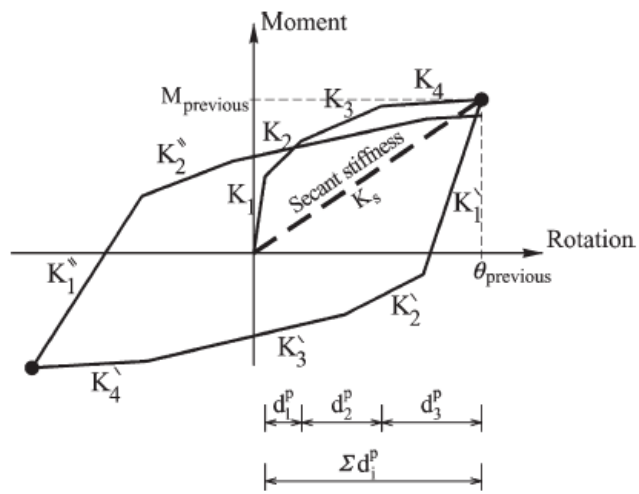


Figure 2-31 Hysteretic model for flexural subhinge (ElMandooh Galal and Ghobarah 2003)

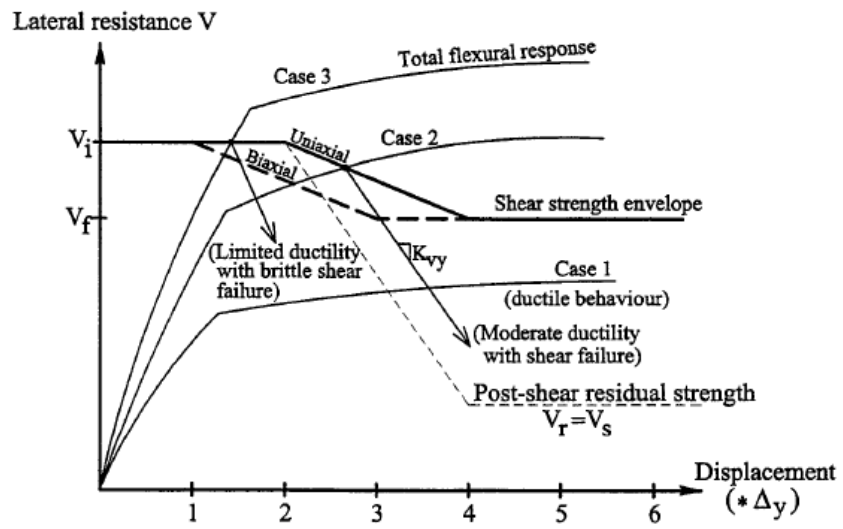


Figure 2-32 Combined flexure and shear response for columns (ElMandooh Galal 2002)

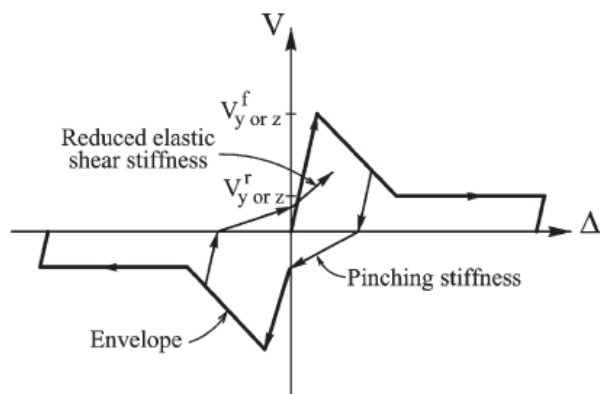


Figure 2-33 Shear force-deformation relationship for shear subhinge envelope (ElMandooh Galal and Ghojarah 2003)

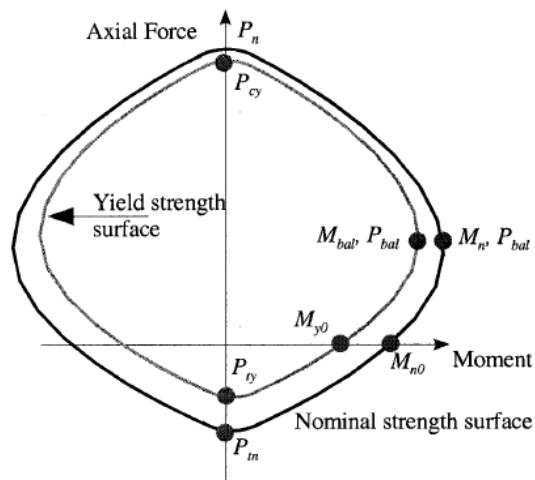


Figure 2-34 Axial force-moment interaction diagram (Kaul 2004)

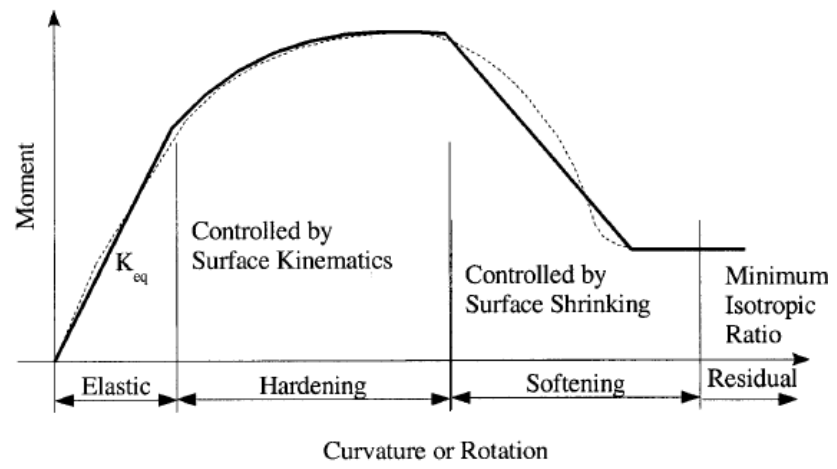


Figure 2-35 Idealization of the monotonic response (Kaul 2004)

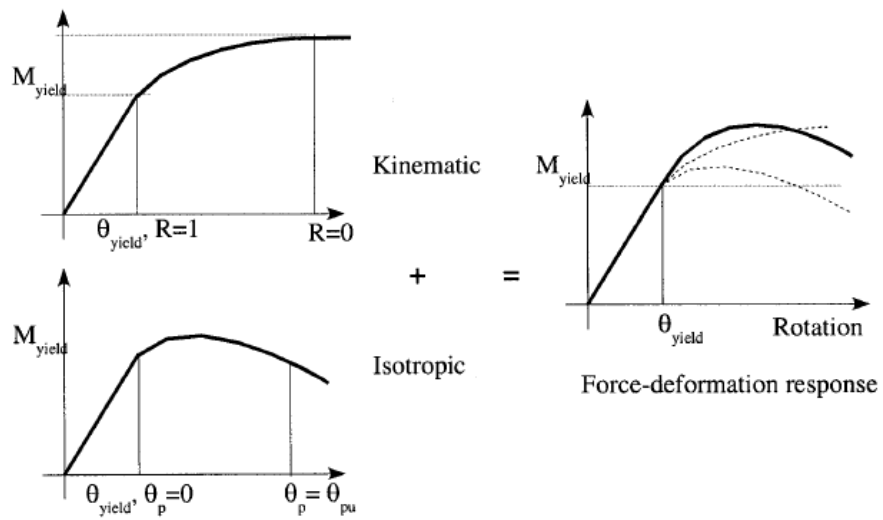


Figure 2-36 Combined kinematic-isotropic hardening (Kaul 2004)

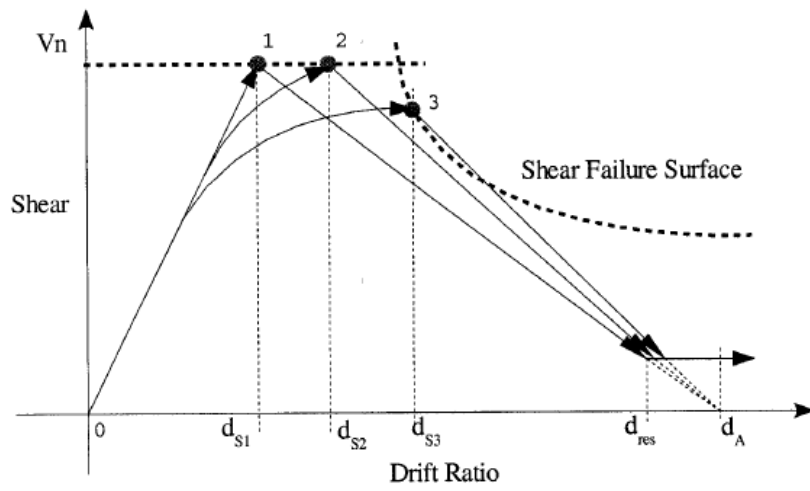


Figure 2-37 Modes of shear failure (Kaul 2004)

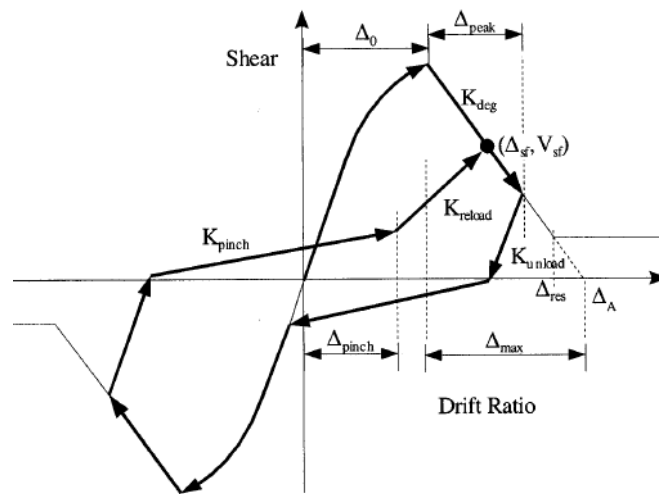


Figure 2-38 Hysteretic/Cyclic pinching model for shear (Kaul 2004)

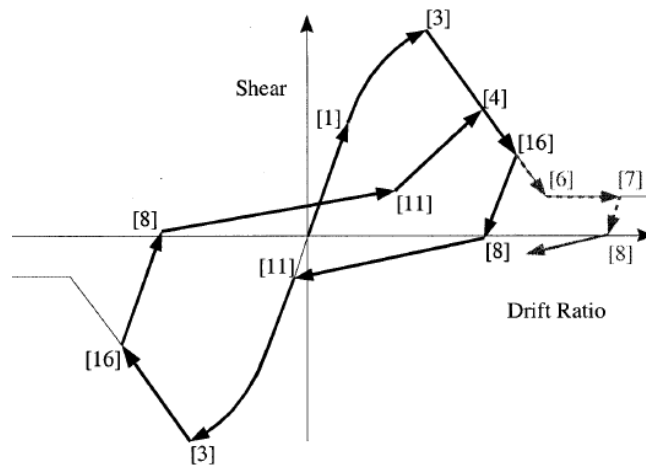


Figure 2-39 Full cycle pinching example (Kaul 2004)

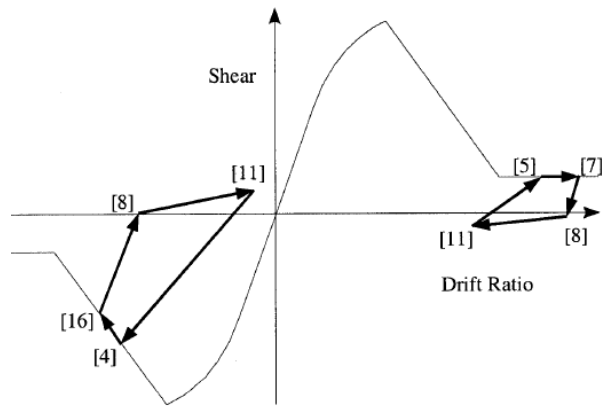


Figure 2-40 Half cycle pinching examples (Kaul 2004)

3 Chapter: Formulation of Beam-Column Element

3.1 Introduction

Realistic prediction of seismic progressive collapse behaviour is essential in vulnerability and performance assessment of reinforced concrete structures. The proposed model described herein is an important tool for accurate capturing of the degradation behaviour of reinforced concrete components and the damage characteristics of global structures from initiation and progression of failure till ultimate collapse during major earthquakes. Numerical simulation models capable of accurate capturing of damage and degradation response characteristics would lead to more resilient earthquake design of new structures as well as more efficient retrofit and rehabilitation strategies for existing older deficient structures.

As described in Section 1.2, the response of reinforced concrete components depends on various parameters such as reinforcement steel distribution, confinement provided to the concrete by reinforcing bar ties, axial load levels, amplitudes of inelastic cyclic excursions and number of repeated reversed loading cycles. The initiation of yielding and the post-yield response of reinforced concrete components are sensitive to axial load levels. Damage accumulated during inelastic cyclic excursions, including concrete cracking and loss of bond in the rebars, affects the stiffness and strength degradations in structural components. Older reinforced concrete columns, where sufficient confinement to the concrete is not provided, may suffer severe stiffness and strength degradations and be susceptible to shear failure. Degradation in shear strength of reinforced concrete

members with insufficient transverse reinforcement is also affected by inelastic flexure-shear interaction.

This chapter describes the underlying formulations of the analysis model developed for capturing the behaviour of reinforced concrete members designed as ductile as well as non-ductile shear-critical column members in existing older structures. The element formulation is based on the concentrated plasticity approach and the inelastic behaviour modeling is based on stress-resultant plasticity concepts using force interaction surfaces and evolution models. As discussed in Chapter 2, compared to distributed plasticity models based on fiber section approach, concentrated plasticity models based on stress-resultant plasticity concepts are computationally more efficient and more suitable for capturing nonlinear degradation response through calibration using component tests data on phenomenological force-deformation relations and hysteretic curves.

The formulation consists of beam-column element with zero-length generalized plastic hinges concentrated at the ends of the element, as shown in Figure 3-1. The element between the hinges is elastic. Each hinge has three deformations, an axial deformation and rotations about the local element axes. The contributions from shear deformations in the hinge are added to the rotations due to flexure. Each hinge is modeled as two subhinges in series, one for the flexural behaviour and one for the shear behaviour. Yield surface is defined to model the interaction between axial force and biaxial bending moments. Post-yield force interaction and inelastic hardening in flexure is captured by the yield-surface evolution models. Shear failure is captured by shear failure surface

defined in terms of axial force and shear forces. Post-shear failure softening behaviour is captured by shear-failure surface evolution models. The rate of hardening and softening is controlled by separate plastic material models. Deterioration of shear strength in the plastic hinge zone with increasing flexural displacement ductility demand is accounted for by using ductility-related shear limit surface. Force recovery procedures for the inelastic behaviour are also described.

The approach used in the cyclic behaviour modeling is based on the incorporation of damage models in the beam-column element formulation to track the evolution of damage and its effects on the gradual deterioration in stiffness and loss of strength. Upon unloading and subsequent reloading after yielding in flexure and/or failure in shear, the quasi-elastic response is controlled by cyclic models capturing the deterioration and pinching characteristics of the hysteretic behaviour. Degradation in elastic unloading stiffness is achieved using damage models based on maximum inelastic deformations and dissipated hysteretic energy. Reloading stiffness is formulated based on pinching and peak-oriented hysteretic models. The formulation of the cyclic models is based on an event-to-event strategy, assuming that an “event” for a cyclic model occurs when the loading state of the element changes.

As described earlier, accumulated damage in cyclic excursions in one direction affects not only stiffness and strength parameters of a component in the direction of loading but also the behaviour in other out-of-plane directions. The cyclic models proposed by Kaul (2004) for 2D cases are extended to capture full 3D behaviour under general cyclic

loading by considering biaxial interaction effects on stiffness and strength degradation based on multi-component damage models capturing hysteretic damage in multi-directions.

Strength degradation under repeated cyclic load reversals is also considered. A cyclic strength degradation model is proposed, which controls the contraction of the yield surface and/or shear failure surface at the end of each half cycle by using cumulative damage indices based on the total hysteretic energy dissipated by the structural member.

The proposed beam-column element is suitable to model nonlinear hysteretic behaviour of reinforced concrete columns under general 3D loading conditions, i.e. biaxial reversed cyclic loading with variable axial load, by considering full nonlinear axial-flexure-shear interaction and damage accumulation effects on the degradation behaviour of structural components.

3.2 Updated Lagrangian Formulation

In this study, the updated Lagrangian formulation (Bathe 1996) is implemented assuming large displacements and large rotations but small strains. There are two types of Lagrangian formulations – Total Lagrangian (TL) and Updated Lagrangian (UL). TL is based on a fixed frame of reference, while UL is based on a reference system that is updated as the element deforms. The 2D UL formulations used in Kaul (2004) are extended in the present study to 3D beam-column elements. Implementing the UL formulation for structural analysis requires linearization of the tangent stiffness and an

accurate force-recovery algorithm. The formulation of the element stiffness and the force recovery technique for elastic elements based on the natural approach (Conci and Gattass 1990, McGuire et al. 2000) are described in this section. Incorporation of large deformation capabilities for inelastic elements is described in the subsequent sections.

3.2.1 Formulation of Element Stiffness

The elastic stiffness matrix for three-dimensional frame elements in terms of the degrees of freedom, $\{u_1 \ v_1 \ w_1 \ \theta_{x1} \ \theta_{y1} \ \theta_{z1} \ u_2 \ v_2 \ w_2 \ \theta_{x2} \ \theta_{y2} \ \theta_{z2}\}$, and the section properties of the member, $\vartheta, E, I, A, G = E/2(1 + \vartheta)$, is:

$$[K_e] = \begin{bmatrix} \frac{EA}{L} & 0 & 0 & 0 & 0 & 0 & -\frac{EA}{L} & 0 & 0 & 0 & 0 & 0 \\ 0 & \frac{12EI_z}{L^3} & 0 & 0 & 0 & \frac{6EI_z}{L^2} & 0 & -\frac{12EI_z}{L^3} & 0 & 0 & 0 & \frac{6EI_z}{L^2} \\ 0 & 0 & \frac{12EI_y}{L^3} & 0 & -\frac{6EI_y}{L^2} & 0 & 0 & 0 & -\frac{12EI_y}{L^3} & 0 & -\frac{6EI_y}{L^2} & 0 \\ 0 & 0 & 0 & \frac{EJ}{2(1+\vartheta)L} & 0 & 0 & 0 & 0 & 0 & -\frac{EJ}{2(1+\vartheta)L} & 0 & 0 \\ 0 & 0 & -\frac{6EI_y}{L^2} & 0 & \frac{4EI_y}{L} & 0 & 0 & 0 & \frac{6EI_y}{L^2} & 0 & \frac{2EI_y}{L} & 0 \\ 0 & \frac{6EI_z}{L^2} & 0 & 0 & 0 & \frac{4EI_z}{L} & 0 & -\frac{6EI_z}{L^2} & 0 & 0 & 0 & \frac{2EI_z}{L} \\ -\frac{EA}{L} & 0 & 0 & 0 & 0 & 0 & \frac{EA}{L} & 0 & 0 & 0 & 0 & 0 \\ 0 & -\frac{12EI_z}{L^3} & 0 & 0 & 0 & -\frac{6EI_z}{L^2} & 0 & \frac{12EI_z}{L^3} & 0 & 0 & 0 & -\frac{6EI_z}{L^2} \\ 0 & 0 & -\frac{12EI_y}{L^3} & 0 & \frac{6EI_y}{L^2} & 0 & 0 & 0 & \frac{12EI_y}{L^3} & 0 & \frac{6EI_y}{L^2} & 0 \\ 0 & 0 & 0 & -\frac{EJ}{2(1+\vartheta)L} & 0 & 0 & 0 & 0 & 0 & \frac{EJ}{2(1+\vartheta)L} & 0 & 0 \\ 0 & 0 & -\frac{6EI_y}{L^2} & 0 & \frac{2EI_y}{L} & 0 & 0 & 0 & \frac{6EI_y}{L^2} & 0 & \frac{4EI_y}{L} & 0 \\ 0 & \frac{6EI_z}{L^2} & 0 & 0 & 0 & \frac{2EI_z}{L} & 0 & -\frac{6EI_z}{L^2} & 0 & 0 & 0 & \frac{4EI_z}{L} \end{bmatrix} \quad (3.1)$$

The geometric stiffness matrix for three-dimensional frame elements derived by McGuire et al. (2000) is used in the formulation. $[K_g]$ in terms of the degrees of freedom $\{u_1 \ v_1 \ w_1 \ \theta_{x1} \ \theta_{y1} \ \theta_{z1} \ u_2 \ v_2 \ w_2 \ \theta_{x2} \ \theta_{y2} \ \theta_{z2}\}^T$, is:

$$[K_g] = \begin{bmatrix} \frac{P}{L} & 0 & 0 & 0 & 0 & 0 & 0 & -\frac{P}{L} & 0 & 0 & 0 & 0 & 0 \\ 0 & \frac{6P}{5L} & 0 & 0 & 0 & \frac{P}{10} & 0 & -\frac{6P}{5L} & 0 & 0 & 0 & \frac{P}{10} & 0 \\ 0 & 0 & \frac{6P}{5L} & 0 & -\frac{P}{10} & 0 & 0 & 0 & -\frac{6P}{5L} & 0 & -\frac{P}{10} & 0 & 0 \\ 0 & 0 & 0 & \frac{PI_\rho}{LA} & 0 & 0 & 0 & 0 & 0 & -\frac{PI_\rho}{LA} & 0 & 0 & 0 \\ 0 & 0 & -\frac{P}{10} & 0 & \frac{2PL}{15} & 0 & 0 & 0 & \frac{P}{10} & 0 & -\frac{PL}{30} & 0 & 0 \\ 0 & \frac{P}{10} & 0 & 0 & 0 & \frac{2PL}{15} & 0 & -\frac{P}{10} & 0 & 0 & 0 & 0 & -\frac{PL}{30} \\ -\frac{P}{L} & 0 & 0 & 0 & 0 & 0 & \frac{P}{L} & 0 & 0 & 0 & 0 & 0 & 0 \\ 0 & -\frac{6P}{5L} & 0 & 0 & 0 & -\frac{P}{10} & 0 & \frac{6P}{5L} & 0 & 0 & 0 & 0 & -\frac{P}{10} \\ 0 & 0 & -\frac{6P}{5L} & 0 & \frac{P}{10} & 0 & 0 & 0 & \frac{6P}{5L} & 0 & \frac{P}{10} & 0 & 0 \\ 0 & 0 & 0 & -\frac{PI_\rho}{LA} & 0 & 0 & 0 & 0 & 0 & \frac{PI_\rho}{LA} & 0 & 0 & 0 \\ 0 & 0 & -\frac{P}{10} & 0 & -\frac{PL}{30} & 0 & 0 & 0 & \frac{P}{10} & 0 & \frac{2PL}{15} & 0 & 0 \\ 0 & \frac{P}{10} & 0 & 0 & 0 & -\frac{PL}{30} & 0 & -\frac{P}{10} & 0 & 0 & 0 & 0 & \frac{2PL}{15} \end{bmatrix} \quad (3.2)$$

As explained in McGuire et al. (2000), the above geometric stiffness matrix contains a second order term corresponding to every first order term in the elastic stiffness matrix of the element given in Equation (3.1). The interaction of axial force and St. Venant torsion as well as the geometric interaction of axial force and bending in the principal directions (i.e. flexural buckling modes considered) are considered in the formulation. The shear forces are determined from the bending moments carried by the member. Hence, the interactions between the axial force, bending moments and shear forces are considered in the formulation of the new 3D beam-column element.

The derivation of the geometric stiffness matrix presented in McGuire et al. (2000) is based on the principle of virtual work. Figure 3-2 shows the orientation of the element in the global XYZ coordinate system. Figure 3-3 shows the previous converged state of the element denoted by the left superscript 1 and the next deformed state denoted by the left superscript 2. The element force in state 2 is,

$$\{ {}^2F \} = \{ {}^1F \} + \{ \delta F \} \quad (3.3)$$

Applying the principle of virtual work to the deformed state,

$$\bar{\delta}W = \bar{\delta}W_{external} + \bar{\delta}W_{internal} = 0 \quad (3.4)$$

$$\bar{\delta}W_{external} = \{ \bar{\delta}\Delta \}^T [\{ {}^1F \} + \{ \delta F \}] \quad (3.5)$$

where, $\{ \bar{\delta}\Delta \}$ are the virtual displacements.

The derivations of the virtual internal work, $\bar{\delta}W_{internal}$, for combined bending and axial force and combined torsion and axial force are provided in McGuire et al. (2000).

The shape functions used to describe the virtual work integrals in terms of nodal displacements assume linear expressions for axial and torsional effects and cubic polynomials for flexural effects.

The shape functions for the axial effects are as follows:

$$\begin{aligned}
N_{u1} &= \left(1 - \frac{x}{L}\right) \\
N_{u2} &= \left(\frac{x}{L}\right)
\end{aligned}
\tag{3.6}$$

The shape functions for the flexural effects are as follows:

$$\begin{aligned}
N_{v1} &= 1 - 3\left(\frac{x}{L}\right)^2 + 2\left(\frac{x}{L}\right)^3 \\
N_{v2} &= 3\left(\frac{x}{L}\right)^2 - 2\left(\frac{x}{L}\right)^3 \\
N_{\theta z1} &= x\left(1 - \frac{x}{L}\right)^2 \\
N_{\theta z2} &= x\left[\left(\frac{x}{L}\right)^2 - \frac{x}{L}\right] \\
N_{w1} &= 1 - 3\left(\frac{x}{L}\right)^2 + 2\left(\frac{x}{L}\right)^3 \\
N_{w2} &= 3\left(\frac{x}{L}\right)^2 - 2\left(\frac{x}{L}\right)^3 \\
N_{\theta y1} &= -x\left(1 - \frac{x}{L}\right)^2 \\
N_{\theta y2} &= x\left[\frac{x}{L} - \left(\frac{x}{L}\right)^2\right]
\end{aligned}
\tag{3.7}$$

The shape functions for the torsional effects are as follows:

$$\begin{aligned}
N_{\theta x1} &= \left(1 - \frac{x}{L}\right) \\
N_{\theta x2} &= \left(\frac{x}{L}\right)
\end{aligned}
\tag{3.8}$$

The right subscripts 1 and 2 correspond to the nodes 1 and 2 of the element, as shown in Figure 3-4. In terms of nodal displacements,

$$\{u_1 \ v_1 \ w_1 \ \theta_{x1} \ \theta_{y1} \ \theta_{z1} \ u_2 \ v_2 \ w_2 \ \theta_{x2} \ \theta_{y2} \ \theta_{z2}\}^T,$$

$$u = [N_{u1} \ 0 \ 0 \ 0 \ 0 \ 0 \ N_{u2} \ 0 \ 0 \ 0 \ 0 \ 0]$$

$$\{u_1 \ v_1 \ w_1 \ \theta_{x1} \ \theta_{y1} \ \theta_{z1} \ u_2 \ v_2 \ w_2 \ \theta_{x2} \ \theta_{y2} \ \theta_{z2}\}^T$$

$$v = [0 \ N_{v1} \ 0 \ 0 \ 0 \ N_{\theta z1} \ 0 \ N_{v2} \ 0 \ 0 \ 0 \ N_{\theta z2}]$$

$$\{u_1 \ v_1 \ w_1 \ \theta_{x1} \ \theta_{y1} \ \theta_{z1} \ u_2 \ v_2 \ w_2 \ \theta_{x2} \ \theta_{y2} \ \theta_{z2}\}^T$$

(3.9)

$$w = [0 \ 0 \ N_{w1} \ 0 \ N_{\theta y1} \ 0 \ 0 \ 0 \ N_{w2} \ 0 \ N_{\theta y2} \ 0]$$

$$\{u_1 \ v_1 \ w_1 \ \theta_{x1} \ \theta_{y1} \ \theta_{z1} \ u_2 \ v_2 \ w_2 \ \theta_{x2} \ \theta_{y2} \ \theta_{z2}\}^T$$

$$\theta_x = [0 \ 0 \ 0 \ N_{\theta x1} \ 0 \ 0 \ 0 \ 0 \ 0 \ N_{\theta x2} \ 0 \ 0]$$

$$\{u_1 \ v_1 \ w_1 \ \theta_{x1} \ \theta_{y1} \ \theta_{z1} \ u_2 \ v_2 \ w_2 \ \theta_{x2} \ \theta_{y2} \ \theta_{z2}\}^T$$

The geometric stiffness matrix for two-dimensional frame elements for combined bending and axial force in terms of the degrees of freedom,

$\{u_1 \ v_1 \ \theta_{z1} \ u_2 \ v_2 \ \theta_{z2}\}^T$, is:

$$[K_{g,bending}] = \begin{bmatrix} \frac{P}{L} & 0 & 0 & -\frac{P}{L} & 0 & 0 \\ 0 & \frac{6P}{5L} & \frac{P}{10} & 0 & -\frac{6P}{5L} & \frac{P}{10} \\ 0 & \frac{P}{10} & \frac{2PL}{15} & 0 & -\frac{P}{10} & -\frac{PL}{30} \\ -\frac{P}{L} & 0 & 0 & \frac{P}{L} & 0 & 0 \\ 0 & -\frac{6P}{5L} & -\frac{P}{10} & 0 & \frac{6P}{5L} & -\frac{P}{10} \\ 0 & \frac{P}{10} & -\frac{PL}{30} & 0 & -\frac{P}{10} & \frac{2PL}{15} \end{bmatrix} \quad (3.10)$$

The geometric stiffness matrix for frame elements for combined torsion and axial force in terms of the degrees of freedom, $\{\theta_{x1} \quad \theta_{x2}\}^T$, is:

$$[K_{g,torsion}] = \begin{bmatrix} \frac{PI_\rho}{LA} & -\frac{PI_\rho}{LA} \\ -\frac{PI_\rho}{LA} & \frac{PI_\rho}{LA} \end{bmatrix} \quad (3.11)$$

The geometric stiffness matrix for three-dimensional frame elements given in Equation (3.2) is obtained by adding the terms of the geometric stiffness matrices for bending in the $x - y$ plane, in the $x - z$ plane, as well as the effects of St. Venan torsion-axial force interaction.

The complete element stiffness, $[K_C]$ including the geometric nonlinear effects is:

$$[K_C] = [K_e] + [K_g] \quad (3.12)$$

where $[K_e]$ is the elastic stiffness of the element. For elastic static analysis, the use of the geometric stiffness may not be critical, however, for dynamic analysis problems, ignoring the geometric stiffness can cause convergence problems.

3.2.2 Force Recovery

The force recovery approach is based on separating the rigid body motion from the total displacements. In this approach, the natural displacement increments, $\{d\Delta_n\}$, are calculated from the displacement increments transformed to the last converged state.

Consider the motion of a beam-column element in a stationary Cartesian coordinate system, as shown in Figure 3-3. Configuration (0) represents the initial undeformed state. Configuration (1) is the current deformed and known equilibrium state. Configuration (2) is the neighbouring deformed equilibrium state, which has to be found. Since configuration (1) is the last converged state, the local coordinate system (1x 1y 1z) is used as the reference system for the next step to find deformed configuration (2), as shown in Figure 3-4.

The natural axial deformation as well as the natural rotations and the rigid body rotations are illustrated in Figure 3-5(a) to (e).

The natural axial deformation, u_n , can be expressed as:

$$u_n = {}^2L - L = \sqrt{(L + u_2 - u_1)^2 + (v_2 - v_1)^2 + (w_2 - w_1)^2} - L \quad (3.13)$$

Equation (3.13) can be simplified as follows:

$$\begin{aligned} (u_n)^2 + 2Lu_n + L^2 \\ = L^2 + 2L(u_2 - u_1) + (u_2 - u_1)^2 + (v_2 - v_1)^2 + (w_2 - w_1)^2 \end{aligned} \quad (3.14)$$

Neglecting the higher order term $(u_n)^2$ as it is sufficiently small compared to u_n , then:

$$u_n \approx (u_2 - u_1) + \frac{1}{2} \left[\frac{(u_2 - u_1)^2}{L} + \frac{(v_2 - v_1)^2}{L} + \frac{(w_2 - w_1)^2}{L} \right] \quad (3.15)$$

The rigid body rotations about y – and z –axis, respectively, are:

$$\begin{aligned} \theta_{rbm,y} &= -\tan^{-1} \frac{(w_2 - w_1)}{(L + u_2 - u_1)} \\ \theta_{rbm,z} &= \tan^{-1} \frac{(v_2 - v_1)}{(L + u_2 - u_1)} \end{aligned} \quad (3.16)$$

The natural rotations are:

$$\begin{aligned} \theta_{nx} &= \theta_{x2} - \theta_{x1} \\ \theta_{ny1} &= \theta_{y1} - \theta_{rbm,y} \\ \theta_{ny2} &= \theta_{y2} - \theta_{rbm,y} \\ \theta_{nz1} &= \theta_{z1} - \theta_{rbm,z} \\ \theta_{nz2} &= \theta_{z2} - \theta_{rbm,z} \end{aligned} \quad (3.17)$$

where:

θ_{nx} is the natural rotation about x – axis

θ_{ny1} is the natural rotation about y – axis at element end 1

θ_{ny2} is the natural rotation about y – axis at element end 2

θ_{nz1} is the natural rotation about z – axis at element end 1

θ_{nz2} is the natural rotation about z – axis at element end 2

The incremental natural displacement vector, $\{d\Delta_n\}$, can be represented as:

$$\{d\Delta_n\} = \{0 \ 0 \ 0 \ 0 \ \theta_{ny1} \ \theta_{nz1} \ u_n \ \theta_{nx} \ 0 \ 0 \ \theta_{ny2} \ \theta_{nz2}\}^T \quad (3.18)$$

The force increment can be expressed as:

$$\{dF\} = [K_e + K_g]\{d\Delta_n\} \quad (3.19)$$

The total element force in the converged configuration (2) is given as:

$$\{^2F\} = \{^1F\} + \{dF\} = \{^1F\} + [K_e + K_g]\{d\Delta_n\} \quad (3.20)$$

3.3 Inelastic Element Formulation

For stress resultant frame analysis, plasticity theory is extended by using stress resultant interaction surfaces to describe the interactions between member forces, such as axial force, shear forces and bending moments. Under seismic loading, maximum moments typically occur at the member ends of frame elements and inelastic deformations are expected to concentrate at the ends of the elements. Thus, inelastic behaviour can be modeled by using fixed-length generalized plastic hinges at element ends.

3.3.1 Axial Force-Bending Moment Interaction

3.3.1.1 Yield Surface Formulation

Yielding occurs when the force state of a member reaches the yield surface. The yield surface for the flexural subhinge is defined in terms of axial force and bending moments, as shown in Figure 3-6. The yield surface is assumed to be a continuous, convex, rate independent function of axial force and bending moments on a cross-section of the member, and can be represented as follows:

$$\Phi(p, m_y, m_z) = 1 \quad (3.21)$$

where p , m_y and m_z are normalized axial force and bending moments about y , and z – axis, respectively. For reinforced concrete sections, the axial force and moments are normalized by the axial load and the moments at the balanced failure point, P_{bn} , $M_{y nb}$ and $M_{z nb}$, respectively.

The shape of the yield surface depends on the section and material characteristics. For example, reinforced concrete sections with symmetric steel distribution will be symmetric along the moment axes but offset with respect to the axial force axis. Similarly, reinforced concrete sections with non-uniform steel distribution will be unsymmetric along the moment and axial force axes.

The yield surface developed herein follows a form similar to that proposed by El-Tawil (1996) for biaxial bending of symmetric reinforced concrete sections. The surface is described by two equations, one above the balanced point and another below the balanced

point. As proposed by El-Tawil (1996), the biaxial bending interaction curve at an axial load level P , can be described by the relation:

$$\left(\frac{M_z}{M_{zn,p}}\right)^n + \left(\frac{M_y}{M_{yn,p}}\right)^n = 1.0 \quad (3.22)$$

where, n is the interaction exponent. Above the balanced point:

$$\begin{aligned} M_{zn,p} &= M_{znb}(1 - (\delta P/\Delta P)^{cz}) \\ M_{yn,p} &= M_{ynb}(1 - (\delta P/\Delta P)^{cy}) \end{aligned} \quad (3.23)$$

And, below the balanced point:

$$\begin{aligned} M_{zn,p} &= M_{znb}(1 - (\delta P/\Delta P)^{tz}) \\ M_{yn,p} &= M_{ynb}(1 - (\delta P/\Delta P)^{ty}) \end{aligned} \quad (3.24)$$

where:

$$\delta P = (P - P_{bn}) \quad \text{if } P \geq P_{bn} \quad (3.25a)$$

$$= (P_{bn} - P) \quad \text{if } P < P_{bn} \quad (3.25b)$$

$$\Delta P = (P_{cn} - P_{bn}) \quad \text{if } P \geq P_{bn} \quad (3.26a)$$

$$= (P_{bn} - P_{tn}) \quad \text{if } P < P_{bn} \quad (3.26b)$$

P is the applied axial load (positive in compression, negative in tension)

P_{cn} is the axial compressive strength

P_{tn} is the tensile strength

P_{bn} is the balanced axial load

M_z is the applied moment about z – axis

M_y	is the applied moment about y – axis
$M_{zn,p}$	is the moment strength about z – axis at load P
$M_{yn,p}$	is the moment strength about y – axis at load P
M_{znb}	is the moment strength about z – axis at balanced point
M_{ynb}	is the moment strength about y – axis at balanced point
c_z, c_y	is the exponents above the balanced point (compression)
t_z, t_y	is the exponents below the balanced point (tension)

The strength characteristics of the cross section of the member, P_{cn} , P_{tn} , P_{bn} , M_{znb} , M_{ynb} , may be determined from a fiber analysis. The parameters, c_z, c_y, t_z, t_y and n , which control the shape of the yield surface can be obtained using a fiber analysis through trial and error and curve fitting. For bi-symmetric reinforced concrete cross sections, these parameters are calibrated (El-Tawil 1996) as follows:

$$c_z = c_y = 1.6$$

$$t_z = t_y = 1.9$$

$$n = 1.5 + 0.5(\delta P / \Delta P) \quad \text{for } P \geq P_{bn}$$

$$n = 1.5 + (\delta P / \Delta P)^2 \quad \text{for } P < P_{bn}$$

By substituting Equation (3.23) in (3.22),

$$\left(\frac{M_z}{M_{znb} (1 - (\delta P / \Delta P))^{c_z}} \right)^n + \left(\frac{M_y}{M_{ynb} (1 - (\delta P / \Delta P))^{c_y}} \right)^n = 1.0 \quad (3.27)$$

By substituting Equations (3.25a) and (3.26a) in (3.25), and normalizing by the axial load and moment strength at and above the balanced point:

$$\left(\frac{M_z/M_{znb}}{\left(1 - \left(\frac{P/P_{bn}-1}{P_{cn}/P_{bn}-1}\right)^{cz}\right)} \right)^n + \left(\frac{M_y/M_{ynb}}{\left(1 - \left(\frac{P/P_{bn}-1}{P_{cn}/P_{bn}-1}\right)^{cy}\right)} \right)^n = 1.0 \quad (3.28)$$

$$\text{Let } m_z = M_z/M_{znb}, m_y = M_y/M_{ynb}, p = P/P_{bn}$$

The yield function in terms of normalized force components is expressed as follows:

$$\Phi(p, m_y, m_z) = \left(\frac{m_z}{\left(1 - \frac{p-1}{\frac{P_{cn}}{P_{bn}}-1}\right)^{cz}} \right)^n + \left(\frac{m_y}{\left(1 - \frac{p-1}{\frac{P_{cn}}{P_{bn}}-1}\right)^{cy}} \right)^n = 1.0 \quad (3.29)$$

And the exponent, n , in terms of normalized axial load,

$$n = 1.5 + 0.5 \left(\frac{p-1}{\frac{P_{cn}}{P_{bn}}-1} \right) \quad (3.30)$$

Similarly, below the balanced point the yield function,

$$\left(\frac{M_z/M_{znb}}{\left(1 - \left(\frac{1-P/P_{bn}}{1-P_{tn}/P_{bn}}\right)^{tz}\right)} \right)^n + \left(\frac{M_y/M_{ynb}}{\left(1 - \left(\frac{1-P/P_{bn}}{1-P_{tn}/P_{bn}}\right)^{ty}\right)} \right)^n = 1.0 \quad (3.31)$$

And the yield function in terms of normalized force components is,

$$\Phi(p, m_y, m_z) = \left(\frac{m_z}{\left(1 - \frac{1-p}{1 - \frac{P_{tn}}{P_{bn}}}\right)^{tz}} \right)^n + \left(\frac{m_y}{\left(1 - \frac{1-p}{1 - \frac{P_{tn}}{P_{bn}}}\right)^{ty}} \right)^n = 1.0 \quad (3.32)$$

And the exponent, n, in terms of normalized axial load,

$$n = 1.5 + \left(\frac{1-p}{1 - \frac{P_{tn}}{P_{bn}}} \right)^2 \quad (3.33)$$

3.3.1.2 Yield Surface Evolution

An evolution rule determines how the yield surface evolves in force space, which results in hardening/softening in force-deformation response. Hardening response is generally modeled by using a kinematic rule, an isotropic rule or a combination of the two. The kinematic rule results in translation of the yield surface in force space without change in size or shape, while the isotropic rule results in uniform expansion of the yield surface. For most structural materials, kinematic hardening rule more accurately describes the physical behaviour under cyclic loading by accounting for the Bauschinger effect. However, a combination of kinematic and isotropic rules is necessary to model the softening response.

In the proposed formulation, a combination of kinematic hardening rule and non-uniform contraction rule is considered. The evolution model developed by Kaul (2004) for yield

surfaces in terms of axial force and bending moment for modeling planar behaviour is modified and extended to yield surfaces defined in terms of axial force and biaxial bending moments to model 3D behavior by considering the effects of accumulated damage in inelastic excursions in one direction on the behaviour in other out-of-plane directions.

Irrespective of the evolution rule, surface evolution depends on two parameters, the magnitude of evolution, and the direction of evolution. The magnitude of evolution is governed by the plastic stiffness, $[K_p]$, a 3x3 diagonal matrix which contains terms for the axial force, $(K_{p,P})$, and for the bending moments, (K_{p,M_y}) and (K_{p,M_z}) .

For isotropic hardening/softening, the surface expands/contracts uniformly in all directions. In the case of non-uniform expansion/contraction rule, the surface can expand/contract differently in each direction, e.g. positive and negative directions along the axial force axis and the bending moment axes (y and z axes), which results in changes in both size and shape of the yield surface.

For kinematic hardening, the direction of surface translation is specified by the evolution direction. Summary of the main kinematic rules for surface translation can be found in El-Tawil (1996), Chen and Han (2007). In case of Prager's hardening rule with associated flow (normality) rule, motion of the yield surface is in direction parallel to the normal vector at the current force point location. Ziegler's hardening rule (1959) suggests that the surface motion is directed along a unit vector connecting the surface centre to the

current force state. For bi-symmetric, non-offset surfaces, the centre of the yield surface is clearly defined. However, for surfaces representative of typical reinforced concrete sections, the centre cannot be easily defined. For example, it could be the centroid (corresponding to the axial load level at the balanced point) or the origin. Mroz's rule (1969) suggests that motion of the yield surface is directed along the force increment, dF . Also, it is feasible for the surface to translate along force components, generally moment axis which results in constant- P translation. Examples of evolution directions, normal (direction of translation is normal to the yield surface at the force point), radial (the yield surface moves radially along the direction joining the force point with the surface origin), centroidal (the surface moves along the direction joining the force point with the surface centroid corresponding to the balanced point), and constant- P , are illustrated in Figure 3-7.

The proposed evolution model is based on a combination of a kinematic rule and a non-uniform contraction rule. The kinematic rule in the evolution model is used to model the hardening response in flexure. This model is based on the kinematic control surface model developed by Kaul (2004) for yield surfaces in terms of axial force and bending moment for modeling planar behaviour. In the present study, Kaul's kinematic control surface model is extended to yield surfaces in terms of axial force and biaxial bending moments for modeling 3D behaviour. Within the same cycle, the evolution model proposed in this study uses only the kinematic hardening rule to control the evolution of the yield surface. Magnitude of kinematic plastic stiffness and direction of translation are discussed in the section that follows.

The non-uniform contraction rule in the proposed evolution model is used to model the strength degradation under repeated cyclic load reversals. At the end of each half cycle, i.e. at the zero force point or when the force switches direction, the yield surface is contracted using damage indices based on plastic deformations and hysteretic energy. The non-uniform contraction rule is discussed in details in Section 3.4.3.

3.3.1.2.1 Kinematic Control Surface Model

In this model, the yield surface translation is limited by an inner kinematic control surface that has the same shape as the initial yield surface but smaller size than the yield surface, as shown in Figure 3-8. The size of the inner kinematic control surface can be determined based on the difference of the ultimate moment capacity and the moment at yield. The translation of the centroid of the yield surface cannot exceed beyond the inner kinematic control surface, unless a residual hardening rate is specified. The kinematic plastic stiffness is proportional to the drift (dR) of the yield surface centroid from the inner control surface, as shown in Figure 3-9, in a P – M plane for the purpose of clarity, where M is the resultant bending moment. The plastic stiffness can also be described as inversely proportional to the back-stress, which is defined as the distance from the current position of the yield surface centroid to its original position. The plastic stiffness components for the axial force, $(K_{p,P})$, and for the bending moments, (K_{p,M_y}) and (K_{p,M_z}) , are not constant in the post-yield response; they are reduced as the member accumulates damage due to large inelastic deformations and repeated load reversals. The plastic stiffness components, (K_{p,F_i}) , start from a high initial stiffness, (K_{p0,F_i}) , and

asymptotically reduce to zero, as the centroid of the yield surface approaches the inner kinematic control surface. The yield surface translates rapidly when the centroid is in proximity of its initial location and slows down as the centroid approaches the control surface. This results in gradual reduction of the amount of hardening in the force-deformation response, as shown in Figure 3-10.

The kinematic plastic stiffness varies as a function of the drift of the centroid from the kinematic control surface, dR , and affects the hardening response. Given the back-stress unit vector, $\{s\} = \{s_p \quad s_{my} \quad s_{mz}\}^T$, oriented from the centre of the yield surface, o , to the centre of the control surface, a , (Figure 3-9), plastic stiffness can be calibrated to the drift of the yield surface centre to the control surface centre. Initially for the untranslated state of yield surface, the drift $dR = 1$ and the plastic stiffness $[K_p] = [K_{p0}]$. As the yield surface centroid, o , approaches the control surface, the drift, dR , approaches zero and the plastic stiffness, $[K_p]$, also approaches zero using an exponential relation with the drift. The centroid point, o , follows the yield surface evolution, which is confined within the control surface.

As the yield surface centroid translates under cyclic loading, two cases are possible: either the components of the back-stress vector, $\{s\}$, are along the vector components of the surface gradient, $\{g\}$, at the force point, or opposite. Of particular interest are the moment components, since moments can change more dramatically compared to axial forces in a beam-column element. If $\{s\}\{g\}^T < 0$, as in the case of inelastic excursion in one direction, then $[K_p]$ can be calibrated with dR , (Figure 3-11a). However, in the

beginning of the inelastic excursion in the opposite direction, the moment component of the back-stress vector are along the moment component of the surface gradient, $\{s\}\{g\}^T > 0$, and the drift point o lies on path $(b - c)$ from the previous excursion (Figure 3-11b). The drift point o is measured with respect to the surface along point c . To determine the value of dR in this case, a point on the future path $(c - d)$ is needed. Since the future path $(c - d)$ is unknown, an approximation can be made by using another reference point, o' , which is at $p = s_p, m_y = 0, m_z = 0$. This point always lies at or in between the history path $(b - c)$ and the future path $(c - d)$ of point o for centroidal or constant- P evolution. The value of dR can be computed by:

$$\begin{aligned} s_m \cdot g_m < 0, \quad dR &= \text{drift}(o) \\ s_m \cdot g_m > 0, \quad dR &= 2\text{drift}(o') - \text{drift}(o) \end{aligned} \tag{3.34}$$

If the yield surface centroid, point o , moves outside the control surface, in the case when residual hardening rate is specified, the sign of $\text{drift}(o)$ changes and the same equation holds.

The above formulation forces the response to be perfectly plastic when point o reaches the control surface. It is possible to specify some residual hardening instead of $[K_p] = 0$ when point o reaches the control surface, in which case the yield surface centroid can translate beyond the limits of the control surface with $[K_p] = [K_{p,\text{residual}}]$.

The advantage of using an inner kinematic control surface to control the translation of the yield surface compared to other approaches such as bounding surface (El-Tawil 1996) and multiple yield surfaces (Chen and Powell 1982, Ricles et al. 1998, ElMandooh Galal

2002) is that the problem with overlapping of surfaces is avoided and the need for adopting special techniques when the limits of translation have been reached is eliminated.

As mentioned previously, one of the parameters that describe the surface evolution is the magnitude of evolution. To determine the magnitude of evolution in the kinematic control surface model, the plastic stiffness, $[K_p]$, is required. Constant values of the components of the plastic stiffness, (K_{p,F_i}) , imply that the element shows continuous hardening response at a constant rate (post-yield response follows a straight line). The physical behaviour of reinforced concrete members, however, is characterized by initially higher rate of hardening which is then gradually reduced due to concrete crushing and/or bar buckling. In the proposed evolution model, plastic-hardening material models are used to control the rate of hardening. Plastic-hardening material models provide a relationship between the plastic stiffness for each force component of the yield surface and the corresponding plastic deformation components, as shown in Figure 3-12. In the kinematic control surface model, the plastic stiffness, $[K_p]$, is defined as a nonlinear function of dR to achieve the decreasing rate of hardening,

$$[K_p] = [K_{p0}](1 - \exp(-DI \cdot dR)) \quad (3.35)$$

where $[K_{p0}]$ is the initial plastic stiffness, and DI is a damage index.

The incremental force, $\{dF\}$, can be represented as a sum of a component tangential to the yield surface, $\{dF_t\}$, and a component for inelastic hardening due to $[K_p]$, $\{dF^*\}$, as

shown in Figure 3-13b. Thus, a target point can be determined based on $\{dF^*\}$ to which the surface translates. The procedure for calculating the force component $\{dF^*\}$ is given in Section 3.3.4.

Different types of direction of evolution are explored for the kinematic control surface model such as normal, centroidal, radial and constant-P evolution, as shown in Figure 3-14. The difference in the evolution directions varies depending on the force point location and the shape of the surface. The normal and the centroidal directions of evolution have similar direction components regardless of the location of the force point on the surface. Radial direction of evolution can have opposite direction component from the normal and centroidal evolution, for example, when the force point is located between the balanced failure point level and the zero axial load level. The constant-P evolution, i.e. the translation of the yield surface is restrained to be parallel to the M –axis, results in greater drift of the yield surface than the other evolution types, especially when the force point is located away from the balanced failure point level.

As discussed in Kaul (2004), another aspect of cyclic response of reinforced concrete members is the change in the extent of the elastic range, which increases in the first few cycles and then remains relatively constant for a non-softening behaviour. This increase is modeled well by using normal and centroidal direction of evolution. A case of centroidal direction of evolution with constant axial load is shown in Figure 3-15. As the yield surfaces translate away from its initial position, the centroidal direction gradually

aligns with the direction parallel to the M –axis, which eventually leads to constant- P translation and constant elastic range.

3.3.1.2.2 Updating the State of Evolution

The formulation of the evolution model based on a kinematic hardening rule and non-uniform contraction rule is based on maintaining two states – the initial state of the yield surface and the current translated deformed state of the subsequent surface. The updating of the state of evolution is achieved by using mapping between the state of the initial yield surface, represented by superscript 0, and the current state, represented by superscript 1, as shown in Figure 3-16. The surfaces shown in Figure 3-16 are drawn in $p - m$ plane for clarity, where m is the normalized resultant moment, however, the formulations are valid for 3D case. A translation vector, $\{T\}$, of size 3×1 , accounts for the motion of the yield surface in force space. A contraction factor matrix, $[DI]$, of size 3×3 , represents the contraction of the yield surface along each force axis. The matrix $[DI]$ is equal to the identity matrix for the initial state of the yield surface or in case of kinematic hardening only.

At any trial step i , a force state on the subsequent yield surface, $\{F_i^1\}$, can be mapped to a corresponding force state on the initial yield surface, $\{F_i^0\}$, so that iterations can be performed using the original yield surface functions. The force vector $\{F_i^1\}$ can be expressed as:

$$\{F_i^1\} = [DI_i]\{F_i^0\} + \{T_i\} \quad (3.36)$$

And the inverse relationship is simply:

$$\{F_i^0\} = [DI_i]^{-1}(\{F_i^1\} - \{T_i\}) \quad (3.37)$$

The contraction factor matrix $[DI_i]$ is a diagonal matrix and its components are $[DI_{p,i}]$, $[DI_{m_y,i}]$, $[DI_{m_z,i}]$. The component for axial load, $[DI_{p,i}]$, can be either $[DI_{p_c,i}]$ or $[DI_{p_t,i}]$ depending on whether P is compression or tension. The component for moment about y –axis, $[DI_{m_y,i}]$, can be either $[DI_{m_y^+,i}]$ or $[DI_{m_y^-,i}]$ depending on whether M_y is positive or negative. Analogically, the component for moment about z –axis, $[DI_{m_z,i}]$, can be either $[DI_{m_z^+,i}]$ or $[DI_{m_z^-,i}]$ depending on whether M_z is positive or negative. The terms of $[DI_i]$ are determined based on damage indices, as explained in details in Section 3.4.3.

Thus, the state of the subsequent yield surface during the evolution is maintained by the translation vector, $\{T\}$, and the diagonal contraction factor matrix, $[DI]$. The advantage of using the mapping technique is that the force vector corresponding to the current state is updated depending on the translation and contraction of the subsequent surface, while the equations and parameters used for deriving the yield surface function remain unchanged. Thus, the extensibility of the formulations is facilitated for defining different yield surface functions.

3.3.1.3 Force Recovery

For an element with yield surfaces describing the yielding and the post-yield force

interaction at the ends, the assumption is that the force moves along the yield surface. Due to the convexity of the yield surface and also depending on the size of the load increment, there may be situations when this requirement is violated and force recovery procedures are needed to return the force point on the yield surface. These cases are summarized as follows:

- When plastic hinge occurs within a load increment
- When plastic hinge exists at the beginning of an increment
- When plastic hinge unloads elastically during a load increment
- When unloaded plastic hinge is formed again during subsequent reloading

Force recovery procedures are described first for the case of elastic-perfectly plastic materials, and then for the case of hardening materials.

For the elastic-perfectly plastic case, an element is considered in a particular stage of the global analysis, as shown in Figure 3-17. The steps of the force recovery procedure are shown in Figure 3-18. At load step i , both ends are elastic, and f_i represents the force point location. In the load increment from step i to step $i + 1$, end 1 continues to load elastically, while end 2 plastifies.

The trial incremental forces are determined as:

$$\{dF_{trial}\} = [K_e]\{d\Delta\} \quad (3.38)$$

For a linear elastic case, as is the case for end 1, the trial forces remain the final forces for that step. For end 2, if $\{dF_{trial}\}$ results in a force point f_{i+1}^1 that lies outside the yield

surface, the incremental step needs to be divided. The force point is first returned to the yield surface, f_{i+1}^2 , along the direction of the force increment at a fraction τ of the current load increment. The fraction τ represents the elastic portion of the step and can be determined iteratively using the yield surface equation and applying the regula falsi technique for proper conversion (McGuire et al. 2000). The resultant force increment from step i to step $i + 1$ is divided into two internal steps, from f_i to f_{i+1}^2 and from f_{i+1}^2 to f_{i+1}^3 . The forces $\{F_{i+1}^2\}$ and $\{F_{i+1}^{1-2}\}$ corresponding to these force point locations can be calculated as:

$$\{F_{i+1}^2\} = \{F_i\} + \tau\{dF_{trial}\} \quad (3.39)$$

and

$$\{F_{i+1}^{1-2}\} = (1 - \tau)\{dF_{trial}\} \quad (3.40)$$

where $\{F_{i+1}^{1-2}\}$ is the inelastic portion of the trial force.

The magnitude of plastic deformation $\{\lambda\}$ can be calculated by:

$$\{\lambda\} = [[G]^T [K_e] [G]]^{-1} [G]^T \{F_{i+1}^{1-2}\} \quad (3.41)$$

where $[G]$ is the gradient matrix at the point on the surface.

The force at the end of the step $\{F_{i+1}^{2-3}\}$ corresponding to force point f_{i+1}^3 is given as:

$$\{F_{i+1}^{2-3}\} = \{F_{i+1}^2\} + \left\{ \{F_{i+1}^{1-2}\} - [K_e] \{d\Delta_p\} \right\} \quad (3.42)$$

The use of a plastic reduction matrix, as described in Section 3.3.4.1, causes the element forces at the plastified end to move tangent to the yield surface. Due to the convexity of the yield surface, the force point drifts away from the surface during continued plastic

action. Therefore, the force point needs to be moved back onto the yield surface. There are different methods to contain the drift. Normal return is the shortest distance of a force point to the surface, however locating the normal on the surface is an expensive iterative task. Radial return or centroidal return can also be used because of its simplicity (Bathe, 1996).

In this formulation, centroidal return is used to contain the tangential drift of the force point to the surface. Thus, the force at the end of the step is $\{F_{i+1}^{3-4}\}$ corresponding to point f_{i+1}^4 located on the yield surface.

For unsymmetric surfaces and depending on the load/boundary conditions, there may be an axial force imbalance between the two ends of the element at the end of this step. In such case, the axial force at the two ends can be averaged and the force point for the plastified end 2 is moved back onto the yield surface using constant – P return. When the moments and the axial forces are balanced, the shear force, V , is updated by using the equilibrium relation:

$$V = (M_1 + M_2)/L \quad (3.43)$$

If the element continues to load from step $i + 1$ to step $i + 2$, the entire step is inelastic for the plastified end 2. Equation (3.42) can be used to determine the final force at the end of the step, and centroidal return is applied to contain the drift of the force point from the yield surface.

Computationally, it is convenient to assume an allowable tolerance for exceeding the boundaries of the yield surface, typically 2% - 5% of the yield surface size. The approach for calculating the error and ensuring that the updated force point lies within the specified tolerance zone follows that described in Chen and Powell (1982).

For the case of hardening materials, the same element is considered, as shown in Figure 3-17. Under the kinematic hardening rule, the yield surface translates in force space due to the plastic stiffness component, $[K_p]$, as described in Section 3.3.1.2. The presence of the plastic stiffness component implies that the force increment will not be tangential to the yield surface, as illustrated in Figure 3-13. The new location of the yield surface is determined based on the inelastic hardening portion of the force increment, $\{dF^*\} = [K_p]\{d\Delta_p\}$.

Similarly to the example on force recovery for elastic-perfectly plastic material, at load step i , both end 1 and 2 are elastic. In the load increment from step i to step $i + 1$, under the trial force increment $\{dF_{trial}\}$ end 1 continues to load elastically, while the force point at end 2 moves outside the yield surface initiating yielding and hardening, as shown in Figure 3-19. To compute the final forces at end 2, the load step needs to be divided internally into elastic and inelastic portion. Similarly to the case without hardening, the inelastic portion of the force increment is:

$$\{F_{i+1}^{1-2}\} = (1 - \tau)\{dF_{trial}\} \quad (3.44)$$

The magnitude of plastic deformation $\{\lambda\}$ can be calculated by:

$$\{\lambda\} = \left[[G]^T [K_e + K_p] [G] \right]^{-1} [G]^T \{F_{i+1}^{1-2}\} \quad (3.45)$$

The resultant force increment from step i to step $i + 1$ is based on dividing into two internal steps, from f_i to f_{i+1}^2 and from f_{i+1}^2 to f_{i+1}^3 , as shown in Figure 3-19.

The force at the end of the step corresponding to point f_{i+1}^3 is given as:

$$\{F_{i+1}^{2-3}\} = \{F_{i+1}^2\} + \left\{ \{F_{i+1}^{1-2}\} - [K_e][G]\{\lambda\} \right\} \quad (3.46)$$

As described in Section 3.3.1.2, the resultant force increment due to hardening, $\{dF^*\}$, is outside the yield surface, and the surface translates such that the point corresponding to $\{dF^*\}$ is on the updated surface. Generally, the force corresponding to point f_{i+1}^3 is not on the updated surface and centroidal return is used to control the drift. Thus, the force at the end of the step is $\{F_{i+1}^{3-4}\}$ corresponding to point f_{i+1}^4 located on the yield surface.

The resulting imbalance in axial load between ends 1 and 2 can be averaged and updated for each end. The force point for the plastified end 2 is set back to the surface using constant $-P$ return. The shear force, V , is updated by using the equilibrium relation given in Equation (3.43).

The above force recovery procedure assumes that the element is geometrically linear. To include geometric nonlinear effects, the geometric stiffness matrix is added to the

element elastic stiffness matrix, $[K_e + K_g]$, and $\{dF_{\text{trial}}\}$ is determined based on the force recovery techniques described in the section on large deformations.

In addition to reaching the yield surface or moving outwards to the translated state of the surface during inelastic hardening, change in subsequent loading may cause the plastic hinge to unload elastically. In this event, the entire load increment is repeated using the elastic properties.

3.3.2 Axial Force-Shear Force Interaction

3.3.2.1 Shear Failure Surface Formulation

Shear failure is detected when the shear force state of a member reaches the shear failure surface. The shear failure surface for the shear subhinge is defined in terms of axial force and shear forces, as shown in Figure 3-20. Similarly to the yield surface, the shear failure surface is assumed to be a continuous, convex function of axial force and shear forces on a cross-section, and can be defined as:

$$\Phi_s(p, v_y, v_z) = 1 \quad (3.47)$$

where p , v_y and v_z are normalized axial force and shear forces in y , and z – axis, respectively. For reinforced concrete sections, the axial force and shear forces are normalized by the axial load and the shear forces at the balanced failure point, P_{bn} , V_{ynb} and V_{znb} , respectively.

The shape of the yield surface depends on the section and material characteristics. For example, reinforced concrete sections with symmetric steel distribution will be symmetric along the shear force axes but offset with respect to the axial force axis. Similarly, reinforced concrete sections with non-uniform steel distribution will be unsymmetric along the shear force and axial force axes.

Based on the experimental tests and the theoretical verifications of Vecchio and Collins (1986), ElMandooh Galal (2002) proposed a simplified ellipsoidal shear strength-axial strength interaction diagram, as shown in Figure 3-21.

The shear failure surface developed herein follows a form similar to that proposed by ElMandooh Galal (2002) for biaxial shear of symmetric reinforced concrete sections.

$$\Phi_s(P, V_y, V_z) = \left(\frac{V_y}{V_{ynb}} \right)^2 + \left(\frac{V_z}{V_{znb}} \right)^2 + \left(\frac{P - P_{bn}}{P_{cn} - P_{bn}} \right)^2 = 1.0 \quad (3.48)$$

where:

P_{cn} is the axial compressive strength

P_{tn} is the tensile strength

$P_{bn} = (|P_{cn}| + |P_{tn}|)/2$; axial load at balanced failure point (average axial force)

V_{ynb}, V_{znb} is the lateral shear strength in y and z directions at balanced failure point (average axial force)

$$\text{Let } v_z = V_z/V_{znb}, v_y = V_y/V_{ynb}, p = P/P_{bn}$$

Then the shear failure surface function in terms of normalized force components is,

$$\Phi_s(p, v_y, v_z) = (v_y)^2 + (v_z)^2 + \left(\frac{p-1}{P_{cn}/P_{bn} - 1} \right)^2 = 1.0 \quad (3.49)$$

The shear forces, V_y and V_z , are calculated using Equation (3.43) for y and z directions, respectively.

Another option that is also considered for the shear failure surface function is to follow the same form as the yield surface function described in Section 3.3.1.1. If the normalized bending moments are replaced with normalized shear forces in Equation (3.29), the shear failure surface function above the balanced failure point becomes:

$$\Phi_s(p, v_y, v_z) = \left(\frac{v_z}{\left(1 - \frac{p-1}{\frac{P_{cn}}{P_{bn}} - 1} \right) cz} \right)^n + \left(\frac{v_y}{\left(1 - \frac{p-1}{\frac{P_{cn}}{P_{bn}} - 1} \right) cy} \right)^n = 1.0 \quad (3.50)$$

Similarly, below the balanced failure point the shear failure surface function is,

$$\Phi_s(p, v_y, vm_z) = \left(\frac{v_z}{\left(1 - \frac{1-p}{1 - \frac{P_{tn}}{P_{bn}}} \right) tz} \right)^n + \left(\frac{v_y}{\left(1 - \frac{1-p}{1 - \frac{P_{tn}}{P_{bn}}} \right) ty} \right)^n = 1.0 \quad (3.51)$$

3.3.2.1.1 Shear Strength

The total shear strength of reinforced concrete elements is due to the contributions from the concrete, steel truss and axial force mechanisms. The shear strength of a reinforced

concrete member used in the formulation of the shear failure surface can be determined by using existing shear strength prediction models such as those proposed by Priestley et al. (1994) and Sezen and Moehle (2004).

The design equation for the prediction of nominal shear capacity proposed by Priestley et al. (1994) is as follows:

$$V_n = V_c + V_s + V_p \quad (3.52)$$

where V_c , V_s and V_p are the contributions to shear strength capacity of the member from concrete, a truss mechanism, and an arch mechanism associated with axial load, respectively.

The concrete contribution is given by:

$$V_c = k\sqrt{f'_c}A_e \text{ (MPa)} \quad (3.53)$$

where the effective shear area is taken as $A_e = 0.8A_g$, and the parameter k depends on the member displacement ductility level.

The contribution of transverse reinforcement to shear strength is based on a truss mechanism using a 30° degree angle between the compression diagonals and the column longitudinal axis. For rectangular columns, the truss-mechanism component is given by:

$$V_s = \frac{A_v f_{yh} D'}{s} \cot 30^\circ \quad (3.54)$$

where D' is the distance between centres of the perimeter hoop measured parallel to the applied shear.

The enhancement to shear strength due to the arch-mechanism is given by:

$$V_p = \frac{h - c}{2a} P \quad (3.55)$$

where c is the depth of the compression zone, and a is the shear span, i.e. distance from section with maximum moment to point of inflection.

Similar to other shear strength prediction models (Aschheim and Moehle 1992, Priestley et al. 1994), the model proposed by Sezen and Moehle (2004) relates the column shear strength to the displacement ductility demand. The shear strength is expressed as the summation of strength contributions from the concrete and the reinforcement through a 45° truss model as follows:

$$V_n = V_c + V_s = k \frac{A_v f_y d}{s} + k \left(\frac{0.5 \sqrt{f'_c}}{a/d} \sqrt{1 + \frac{P}{0.5 \sqrt{f'_c} A_g}} \right) 0.8 A_g \text{ (MPa)} \quad (3.56)$$

where a/d is the aspect ratio of the column and k is a ductility-related factor similar to that used by Priestley et al. (1994). The factor k is defined equal to 1.0 for displacement ductility less than 2, equal to 0.7 for displacement ductility exceeding 6, and varies linearly for intermediate displacement ductility. The axial load effects are accounted for in the concrete component of the shear strength.

3.3.2.2 Shear Failure Surface Evolution

Similarly to the yield surface formulation, an evolution model is defined for the shear failure surface to describe how the surface evolves in force space after detection of shear failure. The post-shear failure response to continued loading, i.e. increasing inelastic deformations, is characterized by softening or in-cycle strength degradation. The softening behaviour can be modeled by using a contraction rule that results in shrinking of the shear failure surface.

In the proposed evolution model, a non-uniform contraction rule is considered so that the surface can contract differently in each direction, e.g. positive and negative directions along the axial force axis and the shear force axes (y and z axes), which results in change in both size and shape of the surface. The evolution of the shear failure surface depends on two parameters, the magnitude of evolution, and the direction of evolution.

The magnitude of evolution is determined as a function of the degradation stiffness, $[K_{deg}]$. As reported by Elwood (2002), once the column fails in shear, a linear degradation stiffness can be used based on experimental observations that at the time of axial failure, the shear capacity of the column degrades to approximately zero (Nakamura and Yoshimura 2002). Thus, the slope of degradation, K_{deg} , is given by:

$$K_{deg} = \frac{V_u}{(\Delta_a - \Delta_s)} \quad (3.57)$$

where V_u is the shear force in the member at shear failure, Δ_s is the corresponding drift at shear failure, and Δ_a is the drift at axial failure, as illustrated in Figure 3-22.

The determination of the drift at shear failure is described in Section 3.3.3.

After shear failure, the axial load supported by the column can be assumed to be determined based on the shear-friction mechanism. Based on the shear-friction concepts and on observations from experimental tests, Elwood (2002) proposed the following empirical equation to estimate the drift ratio at axial failure of a shear-damaged column:

$$\left(\frac{\Delta}{L}\right)_{axial} = \frac{4}{100} \frac{1 + (\tan\theta)^2}{\tan\theta + P \left(\frac{s}{A_{st}f_{yt}d_c \tan\theta} \right)} \quad (3.58)$$

where θ is assumed to be 65° in the derivation of the drift capacity model (Elwood 2002).

The drift of the member can be obtained by summing the contributions from the beam-column element shear and flexural deformations,

$$\Delta_{drift} = \theta_{n1}l_1 + \theta_{n2}l_2 + \Delta_{sh} \quad (3.59)$$

where θ_{n1} and θ_{n2} are the natural flexural deformations for each end of the element, and l_1 and l_2 are the lengths from each end to the inflection point ($l_1 + l_2 = L_{col}$, column height). This relation holds true for columns in double curvature and for cantilever columns, which is a special case of single curvature with inflection point at one end. For elements in single curvature, with moments at each end different from zero, Equation

(3.59) cannot be used. However, loading conditions of such cases are not expected to occur in structural members considered relevant for shear-critical analysis.

The direction of evolution in the non-uniform contraction model points inwards the shear failure surface, as shown in Figure 3-23. A target point can be determined based on $\{dF_s^*\}$ to which the surface shrinks. The softening component, $\{dF_s^*\}$, can be calculated according to the procedure outlined in Section 3.3.5.

By using a non-uniform contraction rule, biaxial interaction effects on the evolution of the post-shear failure surface can be accounted for based on damage models. For example, damage due to excessive inelastic deformations and repeated cycles of loading in direction of y – axis will affect the capacities of the member in direction of z – axis, and vice versa. For this purpose, separate damage indices are calculated for the positive and negative directions of y and z axes, and interaction rules are defined, as explained in Section 3.4.3. If the same damage indices are applied to the section capacities in each direction, the evolution will result in isotropic contraction of the surface.

3.3.2.2.1 Updating the State of Evolution

The formulation of the evolution model with non-uniform contraction rule is based on maintaining two states – the initial state of the shear failure surface and the current deformed state of the subsequent post-shear failure surface. Similarly to the yield surface evolution model, the updating of the state of evolution of the shear failure surface is achieved by using mapping between the state of the initial surface, represented by

superscript 0, and the current state, represented by superscript 1, as shown in Figure 3-24. Since translation is not used in this evolution model, mapping is governed only by a contraction factor matrix, $[DI_s]$, which is of size 3x3 and represents the contraction of the shear failure surface along each force axis. The matrix $[DI_s]$, is equal to the identity matrix for the initial state of the shear failure surface.

At any trial step i , a force state on the subsequent post-shear failure surface, $\{F_{s,i}^1\}$, can be mapped to a corresponding force state on the initial shear failure surface, $\{F_{s,i}^0\}$, by using the following relationship:

$$\{F_{s,i}^1\} = [DI_{s,i}]\{F_{s,i}^0\} \quad (3.60)$$

Thus, the iterations can be performed using the equations and parameters of the original shear failure surface function.

3.3.2.3 Force Recovery

For an element with shear failure surfaces describing the shear failure, the assumption is that shear failure occurs when the shear force point reaches the surface and that the force point cannot exist outside the surface. Depending on the size of the load increment, there may be situations when this requirement is violated. When shear failure occurs at a shear subhinge within a load increment, force recovery procedure is needed to return the force point on the shear failure surface.

The force recovery procedure is similar to that used for the yield surface except that in the case of shear failure, softening behaviour is considered. Under the non-uniform

contraction rule, the shear failure surface shrinks due to the degradation stiffness component, $[K_{deg}]$, as described in Section 3.3.2.2. The presence of the degradation stiffness component implies that the force increment, $\{dF_s^*\}$, will be directed inwards.

To illustrate the force recovery procedure, an element is considered for which both end 1 and 2 are elastic at load step i . In the load increment from step i to step $i + 1$, under the trial force increment $\{dF_{trial}\}$ end 1 continues to load elastically, while the force point at end 2 shoots through the shear failure surface initiating shear failure and softening, as shown in Figure 3-25. To compute the final forces at end 2, the load step needs to be divided internally into elastic and inelastic portion. The inelastic portion of the force increment is

$$\{F_{s,i+1}^{1-2}\} = (1 - \tau_s)\{dF_{trial}\} \quad (3.61)$$

The resultant force increment from step i to step $i + 1$ is based on dividing into two internal steps, elastic from $f_{s,i}$ to $f_{s,i+1}^2$ and inelastic from $f_{s,i+1}^2$ to $f_{s,i+1}^3$, as shown in Figure 3-25. The beginning of the inelastic portion of the step marks the softening of the shear subhinge. The force increment $\{dF_s^*\}$ is negative or directed inwards and gives the location of point $f_{s,i+1}^3$, to which the shear failure surface is contracted.

The resulting imbalance in axial load between ends 1 and 2 can be averaged and updated for each end. The force point for end 2 is moved back onto the surface using constant – P return.

During continued inelastic action, a softening shear subhinge exists at the beginning of the increment. The force increment $\{dF_s^*\}$ is first calculated using the procedure in Section 3.3.5, and then the post-shear failure surface is further contracted so that the new force point is located on the surface.

In the post-shear failure response, the moments are assumed to unload while the shear strength is degrading. The conditions for satisfying equilibrium at the element level considering different scenarios of failure are described in Section 3.3.5. As discussed by Elwood (2002), additional lateral demand after shear failure results in shear strength degradation and an increase in the shear deformations but a slight reduction in flexural deformation may be assumed, still achieving an increase in the total deformation of the beam-column response. Experimental results by Sezen (2002) suggest that the shear deformations increase significantly after shear failure but do not conclusively show whether the flexural deformations increase or decrease.

In addition to reaching the shear failure surface or moving inwards to the contracted state of the surface, change in subsequent loading may cause the softening shear subhinge to unload elastically. In this event, the entire load increment is repeated using the elastic properties.

In cyclic response, an unloaded softened shear subhinge may be formed again during subsequent loading. If such event occurs within one load increment and the force point

shoots though the current post-shear failure surface, force recovery procedures as described above have to be applied to return the force point on the current contracted surface.

3.3.3 Post-Yield Flexure-Shear Interaction

3.3.3.1 Shear Failure Modes and Criteria for Shear Failure

Reinforced concrete columns are conventionally analyzed for shear failure based on the ratio of shear capacity to shear demand. In this approach, primarily, the failure mode governed by brittle shear failure is captured. Experimental works (Ghee et al. 1989, Wong et al. 1993, Priestley et al. 1994, Sezen 2002) have shown that reinforced concrete columns may be vulnerable to shear failure after flexural yielding due to the weakening of the concrete shear mechanism in the flexural plastic hinge region. As summarized by Yang (1994), a classification of column responses has been suggested by Ghee et al. (1989) based on experimental work involving the seismic shear strength of 25 cantilever squat circular reinforced concrete columns. The responses of columns were classified into four categories, (1) brittle shear failure, (2) limited ductile with shear failure, (3) moderately ductile with shear failure and (4) ductile flexural. Therefore, in the models for seismic response analysis of reinforced concrete structures the different types of shear failure modes should be considered, as illustrated in Figure 3-26.

In the first case, the element is loading elastically when the shear force demand exceeds the shear capacity. Thus, the behaviour is governed by brittle shear failure. In the second case, the element has already yielded under the combined action of axial force and

bending moments and is hardening when the shear force demand exceeds the shear capacity. The element exhibits limited ductile behaviour with shear failure. In these two conditions, a force based criterion can be used to determine shear failure in the element. In the third condition, shear failure occurs after the element has yielded and undergone some level of inelastic deformations when the element response crosses the shear limit surface. The element exhibits moderately ductile behaviour with shear failure resulting from degradation of the shear strength due to inelastic flexure-shear interaction. In this case, in addition to the force based criterion, a displacement ductility based criterion has to be used to detect shear failure as a function of the drift, as described in the following section.

To illustrate the concepts of the model being developed, an example of a cantilever column subjected to lateral load is considered, as shown in Figure 3-27. If the shear demand exceeds the initial shear capacity of the member prior to yielding, the force points at end 1 and end 2 of the element will reach the shear failure surfaces simultaneously. The force points will remain inside the yield surfaces. This implies that in reality brittle shear failure may occur at any section along the member. In another case when flexural plastic hinge forms at end 1 and the shear capacity is sufficiently greater than the shear demand at yielding, the force point at end 1 is on the yield surface but inside the initial shear failure surface. As the flexural displacement ductility demand increases, the initial shear capacity of the plastified end 1 degrades. Eventually, the force point at end 1 reaches the degraded shear failure surface. Since the moment at end 2 is zero and the initial shear capacity is sufficient, end 2 remains elastic and undamaged.

This response can be interpreted as moderate ductile with shear failure in the plastic hinge zone.

3.3.3.2 Shear Limit Surface Formulation

To model the degradation of shear strength in the flexural plastic hinge zone (case 3 in Figure 3-26), the initial shear failure surface is contracted under pronounced flexural displacement ductility demand. The shrinkage of the shear failure surface under such conditions is controlled by monitoring the element's flexural displacement ductility demand imposed about each axis, and updating the shear failure surface as governed by a shear limit surface. The post-yield shear strength degradation in this research is based on the ductility-related shear limit surface developed by Kaul (2004), described next.

Based on the drift capacity models proposed by Elwood (2002), Kaul (2004) developed an equation to describe the shear limit surface as follows:

$$\frac{V}{V_n} = \frac{1}{\alpha} \ln \left(a_0 \frac{\Delta}{L} + b_0 \right) + c_0 \quad (3.62)$$

where α is a constant that controls the curvature of the curve; α and c_0 are calculated such that $V/V_n = 0.5$ at $\Delta/L = 0.1$, which implies that as the shear in the member decreases, the drift ratio at shear failure exponentially increases. The parameters a_0 and b_0 are drift ratios at shear failure corresponding to $V/V_n = 1.0$ and $V/V_n = 0.7$, respectively, and are derived from the empirical equation proposed by Elwood (2002) to estimate the drift ratio at shear failure as follows:

$$\frac{\Delta_s}{L} = \frac{3}{100} + 4\rho'' - \frac{1}{40} \frac{v}{\sqrt{f'_c}} - \frac{1}{40} \frac{P}{A_g f'_c} \geq \frac{1}{100} \text{ (MPa units)} \quad (3.63)$$

where Δ_s is the drift at shear failure, ρ'' is the transverse reinforcement ratio, $\rho'' = A_{st,trans}/bs$ and v is the nominal shear stress, $v = V_n/bd$.

In this research, shear limit surfaces given by Equation (3.62) are defined for y – and z – axes to govern the shear capacity in the corresponding direction. Since accumulated damage in inelastic excursions in one direction affects the shear strength and behaviour in other out-of-plane directions, biaxial interaction effects on the shear limit surfaces are considered in modeling 3D behaviour of reinforced concrete members, as explained in the section that follows.

3.3.3.3 Shear Failure Surface Degradation

To describe the mechanism of degradation of the shear failure surface due to inelastic flexure-shear interaction, an example of a cantilever column subjected to lateral load is considered, as shown in Figure 3-28. The lateral load acts in direction of y –axis only and increases monotonically; the axial load is zero. The response of the studied column is moderately ductile. End 1 of the element is fixed and the inelastic action is expected to occur at that end.

The initial shear failure surface defined for the shear subhinge at end 1 of the element corresponds to the initial shear capacity of the member prior to yielding. In Figure 3-28, the shear failure surface for end 1 is shown in terms of V_y and V_z , and the P –axis is

omitted for the purpose of clarity. As the moment at the fixed end 1 increases, end 1 yields in flexure and undergoes some level of inelastic deformations in the post-yield hardening response. At the end of each step, the shear demand is checked versus the shear capacity. This is done by first calculating shear demand using Equation (3.43), then substituting the current level of shear force in the shear failure surface function, given by Equation (3.49). If the shear failure surface function is less than 1.0, then the initial shear capacity is sufficiently greater than the shear demand.

After reaching a critical level of inelastic displacement, $\Delta_{y,cr}$, the shear strength, V_{yn} , begins to degrade. The degradation of shear strength in the plastic hinge region is governed by the shear limit surface, as described in the previous section. At step i , the displacement is $\Delta_{y,i}$, and the corresponding degraded shear strength, $V_{y,i}$, is obtained using the shear limit surface. The shear failure surface is updated by reducing the shear capacity in direction of positive y –axis from V_{yn} to $V_{y,i}$. The shear failure surface is also contracted along the other force axes to consider the effects of damage from the inelastic actions in direction of positive y –axis on the degradation of shear strength in all other directions, namely V_{yn}^- , V_{zn}^+ and V_{zn}^- . The biaxial interaction effects are accounted for by using contraction factor matrix, $[DI_{sf}]$, which represents the contraction of the shear failure surface along each force axis based on damage indices.

In this example, the shear demand at step i is lower than the degraded shear capacity, $V_{y,i}$, corresponding to the displacement $\Delta_{y,i}$. At the end of the next step $i + 1$, the degraded shear capacity is updated to $V_{y,i+1}$ by using the shear limit surface and the shear failure

surface is further contracted. Substituting the current level of shear force in the shear failure surface function gives a result greater than 1.0, which means that the shear demand is greater than the current degraded shear capacity. Shear failure is detected to occur within this step. The shear force point actually shoots through the current degraded shear failure surface and force recovery techniques are used to return the force point to the surface, similar to those described in Section 3.3.2.3. In Figure 3-28, the event of shear failure is illustrated as the shear force-deformation response crossing the shear limit surface.

3.3.4 Element Tangent Stiffness

In order to derive the element tangent stiffness for the hardening/softening macro-model developed herein, first the element tangent stiffness formulation for a simple plastic hinge model is reviewed.

3.3.4.1 Element Tangent Stiffness for Plastic Hinge Model without Hardening

The formulation of a concentrated plasticity element with rigid-perfectly plastic hinges can be based on a stress resultant yield surface with no evolution and a corresponding flow rule. The flow rule is the criteria governing the plastic deformations (Bathe 1996). The elastic element stiffness matrix is modified to include a plastic reduction matrix, K_r . The formulation of K_r depends on the yield function and the corresponding flow rule. The use of a plastic reduction matrix causes the force increment to move tangent to the yield surface (McGuire et al. 2000).

At a plastified end, the resultant incremental displacement can be represented as a sum of the elastic and plastic components.

$$\{d\Delta\} = \{d\Delta_e\} + \{d\Delta_p\} \quad (3.64)$$

The normality criterion states that if plastic deformations occur, the resultant is normal to the surface at that force point. Then,

$$\{d\Delta_p\}_i = \lambda_i \{g\}_i \quad (3.65)$$

where λ_i is the magnitude of plastic deformation in the hinge at end i , and $\{g\}_i$ is the gradient at the point on the surface.

$$\{g\} = \begin{pmatrix} \frac{\partial \Phi}{\partial P} \\ \frac{\partial \Phi}{\partial M_y} \\ \frac{\partial \Phi}{\partial M_z} \end{pmatrix} \quad (3.66)$$

Previous work by El-Tawil (1996) has demonstrated the applicability of the normality criterion to reinforced concrete sections.

The orthogonality of plastic deformation and incremental force vector implies that

$$\{dF\} \{d\Delta_p\}^T = 0 \quad (3.67)$$

For the entire element with ends i and j , the plastic deformation can be expressed as follows:

$$\{d\Delta_p\} = \begin{Bmatrix} d\Delta_{pi} \\ d\Delta_{pj} \end{Bmatrix} = \begin{bmatrix} \{g\}_i & 0 \\ 0 & \{g\}_j \end{bmatrix} \begin{Bmatrix} \lambda_i \\ \lambda_j \end{Bmatrix} = [G]\{\lambda\} \quad (3.68)$$

The incremental element forces can be expressed as:

$$\{dF\} = [K_e]\{d\Delta_e\} = [K_e]\{\{d\Delta\} - \{d\Delta_p\}\} \quad (3.69)$$

Premultiplying the above equation by $[G]^T$ gives:

$$[G]^T\{dF\} = [G]^T[K_e]\{d\Delta\} - [G]^T[K_e]\{d\Delta_p\} \quad (3.70)$$

Due to the normality rule $[G]^T\{dF\} = 0$ and $\{d\Delta_p\} = [G]\{\lambda\}$,

$$[G]^T[K_e]\{d\Delta\} = [G]^T[K_e][G]\{\lambda\} \quad (3.71)$$

By rearranging this equation, the magnitude of plastic deformation $\{\lambda\}$ can be related to the total deformation $\{d\Delta\}$ as follows:

$$\{\lambda\} = [[G]^T[K_e][G]]^{-1}[G]^T[K_e]\{d\Delta\} \quad (3.72)$$

From equations (3.65) and (3.69):

$$\{dF\} = \left[[K_e] - [K_e][G][[G]^T[K_e][G]]^{-1}[G]^T[K_e] \right] \{d\Delta\} \quad (3.73)$$

Therefore the incremental force:

$$\{dF\} = [K_t]\{d\Delta\} \quad (3.74)$$

where $[K_t]$ is the tangent stiffness matrix, $[K_t] = [K_e] - [K_r]$, and $[K_r]$ is the plastic reduction matrix,

$$[K_r] = [K_e][G][G]^T[K_e][G]^{-1}[G]^T[K_e] \quad (3.75)$$

3.3.4.2 Element Tangent Stiffness for Hardening Model

Post-yield hardening response in flexure can be accomplished by using an element plastic stiffness, $[K_p]$, such that the incremental force includes a component for inelastic hardening, $\{dF^*\}$, due to $[K_p]$, and a component that is tangential to the surface, $\{dF_t\}$.

The plastic stiffness, $[K_p]$, is a diagonal matrix consisting of terms for the moment and axial components. The incremental force can be written as,

$$\{dF\} = \{dF_t\} + \{dF^*\} = \{dF_t\} + [K_p]\{d\Delta_p\} \quad (3.76)$$

From Equation (3.69), the incremental force can alternatively be expressed as:

$$\{dF\} = [K_e]\{d\Delta\} - [K_e]\{d\Delta_p\} \quad (3.77)$$

Premultiplying both sides of the above equation by $[G]^T$ gives,

$$[G]^T\{dF\} = [G]^T[K_e]\{d\Delta\} - [G]^T[K_e]\{d\Delta_p\} \quad (3.78)$$

or,

$$[G]^T\{\{dF_t\} + \{dF^*\}\} = [G]^T[K_e]\{d\Delta\} - [G]^T[K_e]\{d\Delta_p\} \quad (3.79)$$

From the normality rule governing the direction of plastic flow, $\{dF_t\}\{d\Delta_p\}^T = 0$, or

$\{dF_t\}[G]^T = 0$. Equation (3.79) can be written as,

$$[G]^T \{dF^*\} = [G]^T [K_e] \{d\Delta\} - [G]^T [K_e] \{d\Delta_p\} \quad (3.80)$$

Also, since $\{dF^*\} = [K_p] \{d\Delta_p\}$ and $\{d\Delta_p\} = \{\lambda\}[G]$,

$$[G]^T [K_p] \{\lambda\}[G] = [G]^T [K_e] \{d\Delta\} - [G]^T [K_e] \{\lambda\}[G] \quad (3.81)$$

Rearranging, the magnitude of the plastic deformation, $\{\lambda\}$, is obtained as:

$$\{\lambda\} = \left[[G]^T [K_e + K_p] [G] \right]^{-1} [G]^T [K_e] \{d\Delta\} \quad (3.82)$$

where $\{d\Delta\}$ is the total deformation including the contribution from the hardening term, $[K_p]$. The plastic reduction matrix, $[K_r]$, can be determined by substituting the value of $\{\lambda\}$ in the following equation,

$$\{dF\} = [K_e] \{d\Delta\} - [K_e] [G] \{\lambda\}$$

or,

$$\{dF\} = \left[[K_e] - [K_e] [G] \left[[G]^T [K_e + K_p] [G] \right]^{-1} [G]^T [K_e] \right] \{d\Delta\} \quad (3.83)$$

The plastic reduction matrix is thus obtained as,

$$[K_r] = [K_e] [G] \left[[G]^T [K_e + K_p] [G] \right]^{-1} [G]^T [K_e] \quad (3.84)$$

Thus, the incremental force is $\{dF\} = [K_t] \{d\Delta\}$, where $[K_t]$ is the total tangent stiffness matrix expressed as $[K_t] = [K_e] - [K_r]$.

Also, using Equations (3.68) and (3.82) the incremental force component due to hardening, $\{dF^*\} = [K_p]\{d\Delta_p\}$, can be found as:

$$\{dF^*\} = [K_p][G] \left[[G]^T [K_e + K_p] [G] \right]^{-1} [G]^T [K_e] \{d\Delta\} \quad (3.85)$$

The hardening component $\{dF^*\}$ is required to determine the amount of yield surface translation in the evolution model described in Section 3.3.1.2.

3.3.4.3 Element Tangent Stiffness for Shear-Critical Column Model

3.3.4.3.1 Element Stiffness Including the Effects of Shear Deformations

To include the effects of shear deformations in the element stiffness, the formulation is developed using the flexibility approach (McGuire et al. 2000). The flexibility approach for developing the element stiffness is used in Kaul (2004) for 2D cases. The formulations here are extended to 3D cases. As discussed in McGuire et al. (2000), formulation of the element flexibility equations for combined transverse shear and flexural deformations is straightforward, while the direct formulation of the corresponding element stiffness is extremely difficult. The element flexibility equations can then be transformed into element stiffness equations by inversion and by supplemental matrix operations, as described in this section. Using this approach also allows modeling the post-shear failure softening behaviour by modifying the shear components in the element stiffness, as described in the following section.

In dealing with transverse shear deformation, a simplified approach based on “equivalent shear area,” A_s , can be adopted. This area multiplied by the shearing stress, τ_{na} , at the neutral axis of the beam element gives the total shear force on the cross-section. The actual shear stress and strain vary over the cross-section. The assumption is that the area A_s corresponds to equivalent constant shear strain $\gamma = V/A_s G$, and stress, $\tau_{na} = V/A_s$. (Bathe 1996)

To formulate the flexibility matrix using the principle of virtual forces, a cantilever with end 1 fixed and a lateral force F_{y2} at end 2 is considered. The deformations at end 2, including the effects of shear, are:

$$\begin{aligned} v_2 &= F_{y2} \left(\frac{L^3}{3EI_z} + \frac{L}{A_s G} \right) + M_{z2} \left(\frac{L^2}{2EI_z} \right) \\ \theta_{z2} &= F_{y2} \left(\frac{L^2}{2EI_z} \right) + M_{z2} \left(\frac{L}{EI_z} \right) \end{aligned} \quad (3.86)$$

where G is the shear modulus ($G = E/2(1 + \nu)$) and ν is the Poisson’s ratio. The effective shear area, A_s , is usually assumed to be $5/6 A_g$.

Assembling the equations in (3.86) in matrix form, $\{\Delta\} = [d]\{F\}$

$$\begin{Bmatrix} v_2 \\ \theta_{z2} \end{Bmatrix} = \begin{bmatrix} \frac{L^3}{3EI_z} + \frac{L}{A_s G} & \frac{L^2}{2EI_z} \\ \frac{L^2}{2EI_z} & \frac{L}{EI_z} \end{bmatrix} \begin{Bmatrix} F_{y2} \\ M_{z2} \end{Bmatrix} \quad (3.87)$$

Thus the flexibility matrix is:

$$[d_z] = \begin{bmatrix} \frac{L^3}{3EI_z} + \frac{1}{K_s} & \frac{L^2}{2EI_z} \\ \frac{L^2}{2EI_z} & \frac{L}{EI_z} \end{bmatrix} \quad (3.88)$$

where K_s is the shear stiffness ($K_s = A_s G/L$)

From the equilibrium equation,

$$\begin{Bmatrix} F_{y1} \\ M_{z1} \end{Bmatrix} = \begin{bmatrix} -1 & 0 \\ -L & -1 \end{bmatrix} \begin{Bmatrix} F_{y2} \\ M_{z2} \end{Bmatrix} \quad (3.89)$$

Thus, the equilibrium matrix is

$$[\Phi] = - \begin{bmatrix} 1 & 0 \\ L & 1 \end{bmatrix} \quad (3.90)$$

The element stiffness matrix in terms of $\{v_2 \ \theta_{z2} \ v_1 \ \theta_{z1}\}$ can be constructed as follows:

$$[K] = \begin{bmatrix} [d]^{-1} & [d]^{-1}[\Phi]^T \\ [\Phi][d]^{-1} & [\Phi][d]^{-1}[\Phi]^T \end{bmatrix} = \begin{bmatrix} k_{22} & K_{21} \\ k_{12} & k_{11} \end{bmatrix} \quad (3.91)$$

After solving for the respective terms:

$$[k_{22,z}] = \begin{bmatrix} \frac{12EI_z}{(L^3K_s + 12EI_z)}K_s & -\frac{6LEI_z}{(L^3K_s + 12EI_z)}K_s \\ -\frac{6LEI_z}{(L^3K_s + 12EI_z)}K_s & K_{dz} \end{bmatrix} \quad (3.92)$$

$$[k_{21,z}] = \begin{bmatrix} -\frac{12EI_z}{(L^3K_s + 12EI_z)}K_s & -\frac{6LEI_z}{(L^3K_s + 12EI_z)}K_s \\ \frac{6LEI_z}{(L^3K_s + 12EI_z)}K_s & \frac{6L^2EI_z}{(L^3K_s + 12EI_z)}K_s - K_{dz} \end{bmatrix}$$

$$[k_{12,z}] = \begin{bmatrix} -\frac{12EI_z}{(L^3K_s + 12EI_z)}K_s & \frac{6LEI_z}{(L^3K_s + 12EI_z)}K_s \\ -\frac{6LEI_z}{(L^3K_s + 12EI_z)}K_s & \frac{6L^2EI_z}{(L^3K_s + 12EI_z)}K_s - K_{dz} \end{bmatrix}$$

$$[k_{11,z}] = \begin{bmatrix} \frac{12EI_z}{(L^3K_s + 12EI_z)}K_s & \frac{6LEI_z}{(L^3K_s + 12EI_z)}K_s \\ \frac{6LEI_z}{(L^3K_s + 12EI_z)}K_s & K_{dz} \end{bmatrix}$$

where

$$K_{dz} = \frac{4(L^3K_s + 3EI_z)EI_z}{L(L^3K_s + 12EI_z)}$$

To extend the formulation to 3D cases, a cantilever with end 1 fixed and a lateral force F_{z2} at end 2 is considered. Taking into account the different orientation of the $x - z$ coordinate system, the deformations at end 2 are:

$$w_2 = F_{z2} \left(\frac{L^3}{3EI_y} + \frac{L}{A_s G} \right) - M_{y2} \left(\frac{L^2}{2EI_y} \right) \quad (3.93)$$

$$\theta_{y2} = -F_{z2} \left(\frac{L^2}{2EI_y} \right) + M_{y2} \left(\frac{L}{EI_y} \right)$$

Similarly, the flexibility matrix in this case is:

$$[d_y] = \begin{bmatrix} \frac{L^3}{3EI_y} + \frac{1}{K_s} & -\frac{L^2}{2EI_y} \\ -\frac{L^2}{2EI_y} & \frac{L}{EI_y} \end{bmatrix} \quad (3.94)$$

Following the same approach as in the case of bending about the z axis, the terms of the stiffness matrix in terms of $\{w_2 \ \theta_{y2} \ w_1 \ \theta_{y1}\}$ are:

$$[k_{22,y}] = \begin{bmatrix} \frac{12EI_y}{(L^3K_s + 12EI_y)} K_s & \frac{6LEI_y}{(L^3K_s + 12EI_y)} K_s \\ \frac{6LEI_y}{(L^3K_s + 12EI_y)} K_s & K_{dy} \end{bmatrix}$$

$$[k_{21,y}] = \begin{bmatrix} -\frac{12EI_y}{(L^3K_s + 12EI_y)} K_s & \frac{6LEI_y}{(L^3K_s + 12EI_y)} K_s \\ -\frac{6LEI_y}{(L^3K_s + 12EI_y)} K_s & \frac{6L^2EI_y}{(L^3K_s + 12EI_y)} K_s - K_{dy} \end{bmatrix} \quad (3.95)$$

$$[k_{12,y}] = \begin{bmatrix} -\frac{12EI_y}{(L^3K_s + 12EI_y)} K_s & -\frac{6LEI_y}{(L^3K_s + 12EI_y)} K_s \\ \frac{6LEI_y}{(L^3K_s + 12EI_y)} K_s & \frac{6L^2EI_y}{(L^3K_s + 12EI_y)} K_s - K_{dy} \end{bmatrix}$$

$$[k_{11,y}] = \begin{bmatrix} \frac{12EI_y}{(L^3K_s + 12EI_y)}K_s & -\frac{6LEI_y}{(L^3K_s + 12EI_y)}K_s \\ -\frac{6LEI_y}{(L^3K_s + 12EI_y)}K_s & K_{dy} \end{bmatrix}$$

where

$$K_{dy} = \frac{4(L^3K_s + 3EI_y)EI_y}{L(L^3K_s + 12EI_y)}$$

Thus, the effects of shear deformations are included in general frame analysis by replacing terms of the complete element stiffness matrix given in Equation (3.1) by the terms derived above.

3.3.4.3.2 Degradation of Element Tangent Stiffness

After shear failure is detected, the shear force-deformation response follows a descending branch governed by K_{deg} , as described in Section 3.3.2.2. To accomplish the softening behaviour, the shear components of the element stiffness matrix are updated to include degradation. This allows the shear force in the element to reduce linearly to zero, and the moments to unload, as the imposed drift reaches the drift at axial failure, as shown in Figure 3-22. Altering the shear response of the element is achieved by modifying the stiffness, K_s , corresponding to the shear deformations using a degradation coefficient as described next.

The total deformations are calculated as a combination of the flexural and shear components as follows:

$$\Delta_t = \Delta_f + \Delta_{sh} \quad (3.96)$$

The response expressed in terms of stiffness is:

$$\frac{1}{K_t} = \frac{1}{K_f} + \frac{1}{K_s} \quad (3.97)$$

where $K_f = 3EI/L^3$, and $K_s = GA_s/L$

From the above equation, the shear stiffness can be expressed as:

$$K_s = \frac{K_f K_t}{K_f - K_t} \quad (3.98)$$

A degradation coefficient, δ , is determined to achieve total tangent stiffness, K_t ,

corresponding to the negative degradation stiffness, K_{deg} as follows:

$$\delta = \frac{1}{K_s} \frac{K_f K_{deg}}{K_f - K_{deg}} \quad (3.99)$$

The degradation stiffness, K_{deg} , can be calculated by using Equation (3.57).

The shear stiffness K_s is replaced with δK_s in the flexibility matrix corresponding to the direction of the shear force that caused failure of the element. After modifying K_s , the flexibility matrices are updated and assembled, as given in Equations (3.88) and (3.94).

Then the degraded tangent stiffness matrix of the complete element, $[K_{t,deg}]$, is derived following the approach described in the previous section.

3.3.5 State Determination – Inelastic Response to Monotonic Loading

State determination for an element with yield surfaces, shear failure surfaces and inelastic flexure-shear interaction involves a certain number of steps, which are summarized in Table 3-1. Figure 3-29 shows the state diagram of the element inelastic response to monotonic loading. The possible loading states are elastic, yielding and hardening, shear failure and post-shear failure degradation, and residual shear strength. The conditions for each state are summarized in Table 3-2. The different paths illustrated in Figure 3-29 represent the state transitions depending on the member behaviour, as discussed in this section. Details of the state determination procedure for Path 1, representing ductile flexural behaviour, are given in Table 3-3, and for Path 2, representing behaviour governed by brittle shear failure, are given in Table 3-4.

The conditions for satisfying equilibrium at element level in different possible scenarios of failure are summarized in Table 3-5. The following assumptions are made:

- When shear failure occurs at an element end, and shear strength starts degrading at that end, shear force at the other end starts unloading. Moments at both ends start unloading, too.
- When one end is yielding and hardening, and the displacement ductility exceeds the critical value, the shear capacities at both ends are governed by the shear limit surfaces.

The conditions presented in Table 3-5 hold true for elements with linear moment distribution in double curvature, which are representative for column members under seismic loading. Maximum moments occur at the element ends. The corresponding shear distribution along the element length is constant. Cantilever columns are a subset of the general case described above, thus the same conditions apply.

Path 1 represents ductile flexural behaviour, as shown in Figure 3-30. The element is initially elastic (state 1), and then yielding and hardening in flexure (state 2). The shear capacity is sufficiently higher than the shear demand even after the element has undergone significant inelastic deformations. Following the procedure outlined in Table 3-1,

Step 1: Predict tangent stiffness

In the elastic state, the predicted tangent stiffness is the element elastic stiffness, $[K_e]$.

Step 2: Compute trial force

The trial force is computed using the predicted tangent stiffness, in this state, $\{dF_{\text{trial}}\} = [K_e]\{d\Delta\}$. This force is trial force 1 shown in Figure 3-30(b).

Step 3: Check for yielding

The force points corresponding to the trial force are substituted in the yield surface functions. If the force point at an end shoots through the yield surface, $\Phi(p, m_y, m_z) >$

1.0, this indicates that the element end has yielded and is hardening. Within this step, a transition is made from state 1 to state 2.

Step 4: Recalculate trial force consistent with yield surface

Trial force 2 is computed based on the yield surface formulation. Force recovery technique is used to return the force point on the yield surface. Details are given in Table 3-3.

Step 5: Calculate shear forces from equilibrium

Shear forces consistent with the state of yielding and hardening are calculated from equilibrium (Equation 3.43). Details are also given in Table 3-5.

Step 6: Update shear failure surface based on ductility-dependent shear limit surface

The displacement ductility for the yielding element is calculated. If the current displacement ductility exceeds the critical displacement ductility, the corresponding degraded shear capacity is obtained from the shear limit surface. The shear failure surface is then updated.

Step 7: Check for shear failure

The shear force point corresponding to the force consistent with the yield surface is substituted in the shear failure surface function. In this case, $\Phi_s(p, v_y, v_z) < 1.0$, which indicates that the element has sufficient shear capacity.

Step 8: Calculate corrected force consistent with shear failure surface

Not required because the element did not fail in shear.

Step 9: Update element tangent stiffness

The element tangent stiffness, $[K_t] = [K_e] - [K_r]$, is returned to the global solver.

Path 2 represents behaviour governed by brittle shear failure, as shown in Figure 3-31.

The element is loading elastically (state 1) when shear demand exceeds the shear capacity (state 3). Following the procedure outlined in Table 3-1,

Step 1: Predict tangent stiffness

The predicted tangent stiffness is the element elastic stiffness, $[K_e]$, in state 1.

Step 2: Compute trial force

The trial force, shown in Figure 3-31a, is computed as, $\{dF_{\text{trial}}\} = [K_e]\{d\Delta\}$.

Step 3: Check for yielding

In this case, $\Phi(p, m_y, m_z) < 1.0$, which indicates that the element has not yet yielded.

Steps 4, 5 and 6: Not required because the element did not yield.

Step 7: Check for shear failure

The shear force points corresponding to the trial force are substituted in the shear failure functions. The force point shoots through the surface, $\Phi_s(p, v_y, v_z) > 1.0$, which indicates the element has failed in shear and the shear strength is degrading. Within this step, a transition is made from state 1 to state 3.

Step 8: Calculate corrected force consistent with shear failure surface

Corrected force is computed based on the shear failure surface formulation. Force recovery technique is used to return the shear force point on the degrading shear failure surface. Details are given in Table 3-4. As the element is softening in shear, the moments unload. The conditions for satisfying equilibrium are presented in Table 3-5, cases 3.1, 3.3 and 3.4.

Step 9: Update element tangent stiffness

The element tangent stiffness is updated to include degradation in the shear stiffness components. The degraded stiffness, $[K_t] = [K_{t,deg}]$, is returned to the solver.

Path 3 represents limited ductility behaviour with shear failure, as shown in Figure 3-32.

The element is initially elastic (state 1), then yields and starts hardening in flexure (state 2). For columns with comparable shear and moment capacity, the shear demand exceeds the shear capacity after yielding and hardening in moment at a relatively low ductility level (state 3). Following the procedure outlined in Table 3-1,

Steps 1 to 5: The same as for Path 1

The element is in State 2. Trial force 2 shown in Figure 3-32a is consistent with the yield surface.

Step 6: Update shear failure surface based on ductility-dependent shear limit surface

The displacement ductility for the yielding element is calculated. In this case, the current displacement ductility is lower than the critical displacement ductility. Therefore, contraction of the shear failure surface is not required.

Step 7: Check for shear failure

The shear force point corresponding to trial force 2 shown in Figure 3-32a is substituted in the shear failure surface function. The force point shoots through the surface, $\Phi_s(p, v_y, v_z) > 1.0$, which indicates the element has failed in shear and the shear strength is degrading. Within this step, a transition is made from state 2 to state 3.

Step 8 to 9: Similar to the corresponding steps in Path 2

The procedure for unloading of moments consistent with the degradation in shear is given in Table 3-5, cases 4.1, 4.3 and 4.4.

Path 4 represents moderate ductility behaviour with shear failure, as shown in Figure 3-33. The element is initially elastic (state 1), then yields and starts hardening in flexure (state 2) undergoing some level of inelastic deformations. For columns with significantly higher initial shear capacity than shear demand, shear failure may occur after the element

has reached the ductility limit as shear strength degrades in the plastic hinge zone. Following the procedure outlined in Table 3-1,

Steps 1 to 5: The same as for Path 1

The element is in State 2. The trial force shown in Figure 3-33 is consistent with the yield surface.

Step 6: Update shear failure surface based on ductility-dependent shear limit surface

The displacement ductility for the yielding element is calculated. In this case, the current displacement ductility exceeds the critical displacement ductility. The corresponding degraded shear capacity is obtained from the shear limit surface. The shear failure surface is then updated using the non-uniform contraction rule.

Step 7: Check for shear failure

The shear force point corresponding to the trial force shown in Figure 3-33 is substituted in the updated shear failure surface function using mapping techniques. The force point shoots through the contracted surface, $\Phi_s(p, v_y, v_z) > 1.0$, which indicates the element has failed in shear and the shear strength is degrading. Within this step, a transition is made from state 2 to state 3.

The updating of the shear failure surface based on the limit surface is performed only after the force consistent with the yield surface has been determined. This is to avoid switching between pre- and post-shear failure states within a single load (or time) step.

Consequently, small steps are required to adequately determine when the shear limit is exceeded. Similar procedure for capturing shear failure is also adopted in Elwood (2002).

Step 8 to 9: Similar to the corresponding steps in Path 2

The procedure for calculating corrected forces and moments consistent with the degradation in shear is given in Table 3-5, cases 5.1, 5.2 and 5.5.

Paths 5 and 6 represent the transition from degradation to total loss of shear strength, as shown in Figure 3-34. The element has suffered failure and its shear strength is degrading governed by the contracting shear failure surface (state 3 or 4) until the residual shear surface is reached (state 5), which represents the total loss in the analysis. Following the steps in Table 3-1,

Step 1: Predict tangent stiffness

The element is in state 3 (4). Deformations are increasing and shear strength is degrading, i.e. the shear force point is on the contracted shear failure surface. Moments are unloading, thus the force point is inside the yield surface. The element tangent stiffness is assumed to be the degraded tangent stiffness, $[K_{t,deg}]$.

Step 2: Compute trial force

The trial force, computed as, $\{dF_{trial}\} = [K_{t,deg}]\{d\Delta\}$, is obtained to be below the residual shear capacity, as shown in Figure 3-34.

Step 3: Check for yielding

In this case, $\Phi(p, m_y, m_z) < 1.0$. The element continues to unload in moment.

Step 4: Recalculate trial force consistent with yield surface

Not required since the trial force point is inside the yield surface

Step 5: Calculate shear forces from equilibrium

Since the element is not yielding, no correction is necessary in the shear force state.

Step 6: Update shear failure surface based on ductility-dependent shear limit surface

Not required since the element is not yielding.

Step 7: Check for shear failure

In the state of post-shear failure degradation, this check is modified to test for the residual shear capacity. The trial force point is inside the residual shear surface, $\Phi_{s,res}(p, v_y, v_z) < 1.0$ and $\Delta > \Delta_{res}$. Within this step, a transition is made from state 3(4) to state 5.

Step 8: Calculate corrected force consistent with shear failure surface

Corrected force is computed based on the shear failure surface formulation. Force recovery technique is used to return the shear force point on the residual shear surface, $\Phi_{s,res}(p, v_y, v_z) = 1.0$. The procedure is similar to that described in Table 3-4 but the

trial force is recalculated using the residual stiffness, $[K_{t,res}]$ with $K_s = 0$, as tangent stiffness.

Step 9: Update element tangent stiffness

The element tangent stiffness is updated with the residual shear capacity indicating total loss of shear strength. The residual stiffness, $[K_t] = [K_{t,res}]$, is returned to the solver.

3.4 Quasi-Elastic Cyclic Formulation

During inelastic excursions, the member accumulates damage which leads to degradation in unloading and reloading stiffness as well as reduction in strength in the cyclic response. The approach used in the cyclic behaviour modeling is based on the incorporation of damage models in the beam-column element formulation to track the evolution of damage and its effects on the gradual deterioration in stiffness and loss of strength. Upon unloading after yielding in flexure and/or failing in shear, the force state is inside the yield surface and the shear failure surface. The element response is no longer controlled by the surface evolution models. During the state of unloading and subsequent reloading prior to reaching either of the surfaces, the quasi-elastic degraded cyclic response is controlled by cyclic models, as discussed in this section. First, the cyclic stiffness model, which controls the element hysteretic response dominated by flexure, is presented.

3.4.1 Cyclic Stiffness Model

3.4.1.1 Event Based Formulation and State Determination

Peak-oriented models, such as those proposed by Clough and Penzien (1993), have been shown to describe well the cyclic flexural behaviour of reinforced concrete members. The cyclic stiffness model developed in this research is based on the peak-oriented model concepts.

The cyclic stiffness model is formulated separately from the generalized plastic hinge model to control the degrading stiffness upon unloading after yielding and subsequent reloading. The cyclic stiffness model requires force, deformation and damage index from the element response in order to provide degradation factors to vary the element stiffness components. Similarly to Kaul (2004) model, the cyclic stiffness model is formulated in normalized force-deformation space. The governing force quantity is the element shear normalized by the shear force corresponding to first yield. The governing deformation is the maximum natural rotation of the two ends of the element normalized by the rotation at first yield.

The formulation of cyclic models is based on an event-to-event strategy, where an “event” occurs when the loading state of the element changes. The cyclic flexural response of an element in a full loading cycle is shown in Figure 3-35. From the initial state of zero force and zero deformations up to event 1, the state of the element is loading. The inelastic portion of the loading state is controlled by the yield surface and the evolution models, as explained in the previous section. The deformations at event 1

are the peak deformations for this loading state. Event 1 marks the beginning of the unloading state which continues to zero force level at event 2. Event 2 represents the cross-over state, i.e. transition from unloading to reloading. In the analysis, event 2 may occur within one step, thus splitting of the step at zero force level and changing of the tangent stiffness will be required, as illustrated in Figure 3-35. Event 2 also marks the beginning of the reloading state. The direction of the quasi-elastic degraded reloading has to be assumed since no previous history parameters exist for the negative excursions. A target peak corresponding to event 3 can be determined based on the point of yielding and amount of hardening in the previous positive excursions to account for the Bauschinger effect. The element response from event 1 to event 3 is controlled by the cyclic stiffness model.

At the point of yielding in the negative direction (event 3), the control of the element response is passed to the yield surface and evolution models until unloading occurs (event 4). The direction of the quasi-elastic degraded reloading initiated at event 5 is determined based on the previous peak at event 1. Thus, the loading cycle is completed.

To characterize the cyclic excursions, the concept of full and “half” cycles is used in the cyclic model by Kaul (2004). Full cycle is defined when the cyclic excursion exceeds the peak from previous cycles, otherwise the cycle is defined as “half” (incomplete or follower). In the cyclic stiffness model developed herein, the concept of primary and follower half cycles is applied to facilitate the separation of positive and negative excursions. As summarized by Altoontash (2004), the concept of primary and follower

half cycles has previously been used in Kratzig (1989) in the development of cumulative damage index based on dissipated energy. In this cyclic stiffness model, positive and negative excursions are distinguished entirely based on deformations and a consistent generalized approach for state determination is developed that captures the member response to general repeated cyclic load reversals. Half cycles are identified separately for positive and negative deformations. Primary half cycle is defined as a half cycle with maximum deformation amplitude that exceeds the peak deformation from previous half cycles in the corresponding direction (positive or negative). Half cycles with smaller deformation amplitudes in the given direction are treated as follower half cycles. Figure 3-36 shows an example of primary and follower half cycles in a general cyclic loading.

Applying the above concept, the cyclic response shown in Figure 3-35 consists of two primary half cycles, with event 1 being the peak of the positive and event 4 being the peak of the negative primary half cycle.

In the event based formulation, the forces and deformations at each event are used as history parameters during the analysis. Events are stored separately for positive and negative excursions. Two types of events can be identified in the cyclic stiffness model, namely peaks and cross-overs. Peak events represent the maximum inelastic deformation and corresponding capacity for a loading state. Peak events are also used as target points for reloading in subsequent cycles. It should be noted that peaks that occur only in primary half cycles are treated as events. Cross-over events mark the transition from unloading to reloading in the quasi-elastic degraded response, which occurs at zero force

level ($F_i = 0$). Since a cross-over event may not always occur at the end of a load (time) step, it can be captured by checking the sign of the quantity ($F_i \Delta_i$). If there is a change in the sign, then a cross-over event has occurred within the current step, and the trial force is updated as explained later in this section. A positive or negative sign is assigned to the cross-over event depending on the sign of the quantity ($F_i \Delta_i$) at the end of the load (time) step, which is used to determine the type of the half cycle as explained later.

The conditions defining the loading states in the cyclic stiffness model are given in Table 3-6 for positive excursions and in Table 3-7 for negative excursions. It can be noticed that the conditions describing a loading state in positive excursions are the same as those describing its counterpart in negative excursions. Thus, the conditions can be generalized for the state determination process for positive and negative excursions. The unique conditions for each state are given in Table 3-8. It can also be noticed that the deformation condition in Table 3-8 has been modified for the states of reloading in the opposite direction, state 4, 4a, 8 and 8a. If the deformations are measured from the zero point, then the deformations decrease in state 4 and 8, which can cause confusion with the state of unloading. Furthermore, when the response crosses the force axis, i.e. state 4a and 8a, the deformation condition cannot be defined unambiguously. For consistency, deformations in these cases can be measured relative to the deformation at the preceding cross-over event, Δ^c , so that they increase in the state of reloading in the opposite direction and decrease in the state of unloading.

Furthermore, to distinguish between complete and incomplete half cycles, the cross-over events are divided into negative cross-overs for which $(F_i\Delta_i) < 0$, and positive cross-overs for which $(F_i\Delta_i) > 0$, as explained earlier. A half cycle is considered incomplete when unloading occurs prior to reaching zero point for the deformations. For loading histories that consist entirely of complete primary half cycles, for example the one shown in Figure 3-37, only negative cross-over events occur. In such cases, deformations relative to the cross-over, $|\Delta^c - \Delta_i|$, are calculated for state determination purposes, as explained above. However, for loading histories that contain incomplete half cycles, which may be primary as well as follower half cycles, such as that shown in Figure 3-38, both negative and positive cross-over events occur. In Figure 3-38, event 2 is a negative cross-over and event 4 is a positive one. When a positive cross-over event is detected, deformations measured from the zero point are used in the conditions for state determination as in the case of reloading in the initial direction, given in Table 3-8.

Typically, cross-over event occurs within a load (time) step and the sign of the event is determined at the end of the step by checking the condition $(F_i\Delta_i) \leq 0$. Then the step is split, the appropriate tangent stiffness is determined and the portion after the cross-over event is redone. When the force at the end of a step is at zero level, however, the cross-over occurs between two steps and the sign of the event is undetermined ($(F_i\Delta_i) = 0$). In such cases, first the condition $(F_i\Delta_i) \leq 0$ is checked in the step that follows, and then the proper set of conditions is selected to determine the state of the future excursion. Details are given in Table 3-9.

The state transition diagram shown in Figure 3-39 summarizes the concepts of the event-based strategy used in the formulation of the cyclic stiffness model. It can be noticed that the diagrams for positive and negative excursions follow the same logic, thus the same sets of conditions are used for state determination regardless of the sign of the excursion. Examples to demonstrate the application of the proposed approach for state determination and the viability of the cyclic models are provided in Section 4.5.

3.4.1.2 Stiffness Degradation

A bilinear peak-oriented model is considered in the implementations of the cyclic stiffness model. The unloading stiffness is different from the reloading stiffness but they remain constant throughout a loading cycle, as shown in Figure 3-35.

In general, element stiffness in models that capture flexure and shear effects and flexure-shear interactions has two components, flexural (EI) and shear ($K_s = GA_s/L$), as described in previous sections. Degradation in stiffness can be achieved by applying degradation factors to the flexural and shear stiffness components so that $K_{deg} = K(\alpha EI, \beta K_s)$. In the developed model, the degradation factors, α and β , are based on a combination of damage indices. For 2D case, these are as follows.

$$\begin{aligned}\alpha &= w_{\alpha 1} DI_+ + w_{\alpha 2} DI_- \\ \beta &= w_{\beta 1} DI_+ + w_{\beta 2} DI_-\end{aligned}\tag{3.100}$$

where $w_{\alpha 1}$, $w_{\alpha 2}$, $w_{\beta 1}$ and $w_{\beta 2}$ are weighting factors; DI_+ and DI_- are damage indices for positive and negative excursions, respectively. The damage indices are calculated by

damage models that interact with the element during inelastic excursions and keep track of the accumulated damage during the loading history, as described in details in Section 3.5.

In the developed cyclic stiffness model, the unloading stiffness, $K_{e,deg}^{unload}$, is degraded using damage indices based on flexural deformations and dissipated hysteretic energy. The degradation factor α accounts for the effects of damage in the negative direction on the flexural response in positive excursions and vice versa. Applying the event-based strategy, when a peak event occurs in the positive direction, the weighting factor $w_{\alpha 1}$ becomes equal to 1.0 and continues to be equal to 1.0 until a peak event occurs in the negative direction. The degradation factor β here accounts for the flexural damage effects on the shear stiffness. In this model, the effects of damage on the flexural stiffness components are the primary effects, whereas the effects on the shear stiffness components are secondary.

The element tangent stiffness changes from the unloading stiffness to the reloading stiffness when a cross-over event occurs. The reloading stiffness, $K_{e,deg}^{reload}$, is determined based on force and deformation quantities from previous events so that peak oriented response is obtained. Degraded elastic stiffness for unloading and reloading are updated for each loading cycle. Figure 3-37 shows an example of degrading cyclic response to a loading history that consists only of primary half cycles in both positive and negative excursions. Figure 3-38 shows cyclic response to a loading history which begins with a primary half cycle and continues with follower half cycles in positive excursions only.

3.4.1.3 Biaxial Interaction Effects on Stiffness Degradation

The formulations of the cyclic stiffness model presented in the previous section describe 2D cyclic flexural response of an element. To extend the formulations to 3D behaviour, biaxial interaction effects on stiffness degradation should be considered. As discussed in Chen and Powell (1982), ignoring the coupling in stiffness degradation between the two transverse directions, i.e. y – and z –axis, could result in discrepancies with the actual response.

Therefore, it is assumed that the degrading stiffness is based not only on the accumulated damage during positive and negative excursions in the direction of loading but also on the accumulated damage in the direction at right angles when biaxial cyclic loading is considered.

For 3D case, the degraded stiffness is $K_{\text{deg}} = K(\alpha_y EI_y, \beta_y K_s; \alpha_z EI_z, \beta_z K_s)$ and the degradation factors are as follows.

$$\begin{aligned}
 \alpha_y &= w_{\alpha y 1} DI_{y+} + w_{\alpha y 2} DI_{y-} + w_{\alpha y 3} DI_{z+} + w_{\alpha y 4} DI_{z-} \\
 \alpha_z &= w_{\alpha z 1} DI_{y+} + w_{\alpha z 2} DI_{y-} + w_{\alpha z 3} DI_{z+} + w_{\alpha z 4} DI_{z-} \\
 \beta_y &= w_{\beta y 1} DI_{y+} + w_{\beta y 2} DI_{y-} + w_{\beta y 3} DI_{z+} + w_{\beta y 4} DI_{z-} \\
 \beta_z &= w_{\beta z 1} DI_{y+} + w_{\beta z 2} DI_{y-} + w_{\beta z 3} DI_{z+} + w_{\beta z 4} DI_{z-}
 \end{aligned} \tag{3.101}$$

Extending the concept to 3D case, the degradation factor α_y accounts for the effects of accumulated damage from previous excursion in direction of z –axis on the flexural

response to loading in y –axis. Correspondingly, the degradation factor α_z accounts for the effects of damage in the y –axis on the flexural response to loading in z –axis. Positive and negative excursions are also treated separately, as in the 2D case.

3.4.2 Cyclic Pinching Model

3.4.2.1 Event Based Formulation and State Determination

After failing in shear and softening, the cyclic pinching model controls the degrading stiffness upon unloading and during subsequent reloading, which is characterized by pinching. Similarly to the cyclic stiffness model described in the previous section, the cyclic pinching model is formulated separately from the generalized plastic hinge model and uses force, deformation and damage index quantities from the element response to provide degradation factors for the stiffness components. The event-to-event strategy used in the cyclic pinching model is similar to that described in the previous section except that another type of event is added to describe the pinching behaviour, as explained next.

The cyclic response of an element failing in shear is shown in Figure 3-40. The state of loading spans from the point of zero force-zero deformation to event 1. The inelastic portion of the loading state up to the peak force at shear failure is controlled by the yield surface evolution models. The ensuing post-shear failure softening response is controlled by the shear failure surface evolution models. Event 1 marks the beginning of the

unloading state and corresponds to the peak deformations attained during the previous loading state. Event 2 is the cross-over from unloading to reloading in the opposite direction, which is marked by pinching. A target pinching point corresponding to event 3 has to be assumed since no previous history parameters exist for the negative excursions. At event 3, the reloading elastic stiffness is regained. Upon yielding in the negative direction, the control of the element response is passed to the plastic hinge models until unloading occurs (event 4). The direction of the quasi-elastic degraded reloading initiated at event 5 is determined based on a target pinching point for positive excursions. In Kaul's (2004) cyclic shear model, pinching is assumed to continue until the imposed deformation equals the peak deformation after shear failure. Here, event 6 is determined in a similar way. At event 6, the reloading stiffness is regained and directed towards the previous peak at event 1.

The roles of peak and cross-over events in the cyclic pinching model are the same as in the cyclic stiffness model. In addition to these types of events, a pinching event is defined to be used as a target point for reloading in subsequent cycles after shear failure.

The conditions defining the loading states in the cyclic pinching model are based on the concepts used in the cyclic stiffness model. These are summarized in Tables 3-10 and 3-11 for positive and negative excursions. Figure 3-44 shows the state transition diagrams for the cyclic pinching model.

3.4.2.2 Stiffness Degradation and Pinching

In the developed cyclic pinching model, the unloading stiffness, $K_{e,deg}^{unload}$, is degraded using damage indices based on shear deformations and dissipated hysteretic energy. For 2D case, the degradation factors α and β , given in Equation (3.100), are used to vary the flexural and shear stiffness components, respectively. As in the cyclic stiffness model, positive and negative deformations are treated separately. The degradation factor α here accounts for the shear damage effects on the flexural stiffness. The degradation factor β accounts for the effects of damage in the negative direction on the shear response in positive excursions and vice versa. Similarly to the event-based formulation of the cyclic stiffness model, when a peak event occurs in the positive direction, the weighting factor $w_{\beta 1}$ becomes equal to 1.0 and continues to be equal to 1.0 until a peak event occurs in the negative direction.

The element tangent stiffness changes from the unloading stiffness to the pinching stiffness when a cross-over event occurs. The pinching stiffness, K_{pinch} , is determined based on force and deformation quantities from previous cross-over events and target pinching events. When the target pinching event is reached, the stiffness is changed to the degraded reloading stiffness, $K_{e,deg}^{reload}$, determined to obtain peak oriented response.

Degraded elastic stiffness for unloading, pinching and reloading are updated for each loading cycle. Examples of degrading post-shear failure cyclic response to different loading histories are shown in Figures 3-41, 3-42 and 3-43. It can be noticed in the

response in Figure 3-42 that when the target pinching event is the negative direction is not reached, there is no pinching in reloading in positive excursions.

3.4.2.3 Biaxial Interaction Effects on Stiffness Degradation

The cyclic pinching model is extended to 3D by considering the biaxial interaction effects on stiffness degradation based on the same concept used in the cyclic stiffness model. The degradation factors $\alpha_y, \alpha_z, \beta_y$ and β_z , given in Equation (3.101), are used to vary the flexural and shear stiffness components to achieve degradation in the tangent stiffness, $K_{deg} = K(\alpha_y EI_y, \beta_y K_s; \alpha_z EI_z, \beta_z K_s)$. The degradation factor β_y accounts for the effects of accumulated damage from previous excursions in direction of z –axis on the shear response to loading in y –axis. Correspondingly, the degradation factor β_z accounts for the effects of damage in the y –axis on the shear response to loading in z –axis. The degradation factors α_y and α_z here account for the shear damage effects on the flexural stiffness in y – and z –axis, respectively. Positive and negative excursions are also treated separately in each axis.

3.4.3 Cyclic Strength Degradation Model

To model the loss of strength under repeated load reversals, cyclic strength degradation model is developed that performs the interaction between the cyclic stiffness and pinching models and the surface evolution models. During reloading in the quasi-elastic degraded range of response, this model controls the contraction of the yield surface and the shear failure surface using cumulative damage models based on hysteretic energy.

The effects of accumulated damage on the strength degradation of a reinforced concrete component in this model are considered based on the same concept used in the cyclic stiffness and pinching models. For example, damage accumulated during positive excursions in direction of $y -$ axis, is considered to affect not only the moment and shear resistance in this direction but also in the negative direction of $y -$ axis as well as in the direction at right angles ($z -$ axis).

Degradation factors corresponding to each of the components of the force interaction surfaces, e.g. axial load, moment or shear capacity, are calculated based on a combination of damage indices, as follows:

$$\begin{aligned}
DI_{pc} &= w_{pc1}DI_{y+} + w_{pc2}DI_{y-} + w_{pc3}DI_{z+} + w_{pc4}DI_{z-} \\
DI_{pt} &= w_{pt1}DI_{y+} + w_{pt2}DI_{y-} + w_{pt3}DI_{z+} + w_{pt4}DI_{z-} \\
DI_{m_y^+} &= w_{myp1}DI_{y+} + w_{myp2}DI_{y-} + w_{myp3}DI_{z+} + w_{myp4}DI_{z-} \\
DI_{m_y^-} &= w_{myn1}DI_{y+} + w_{myn2}DI_{y-} + w_{myn3}DI_{z+} + w_{myn4}DI_{z-} \\
DI_{m_z^+} &= w_{mzp1}DI_{y+} + w_{mzp2}DI_{y-} + w_{mzp3}DI_{z+} + w_{mzp4}DI_{z-} \\
DI_{m_z^-} &= w_{mzn1}DI_{y+} + w_{mzn2}DI_{y-} + w_{mzn3}DI_{z+} + w_{mzn4}DI_{z-} \\
DI_{v_y^+} &= w_{vyp1}DI_{y+} + w_{vyp2}DI_{y-} + w_{vyp3}DI_{z+} + w_{vyp4}DI_{z-} \\
DI_{v_y^-} &= w_{vyn1}DI_{y+} + w_{vyn2}DI_{y-} + w_{vyn3}DI_{z+} + w_{vyn4}DI_{z-} \\
DI_{v_z^+} &= w_{vzp1}DI_{y+} + w_{vzp2}DI_{y-} + w_{vzp3}DI_{z+} + w_{vzp4}DI_{z-} \\
DI_{v_z^-} &= w_{vzn1}DI_{y+} + w_{vzn2}DI_{y-} + w_{vzn3}DI_{z+} + w_{vzn4}DI_{z-}
\end{aligned} \tag{3.102}$$

The degradation factors, $DI_{pc}, DI_{pt}, DI_{m_y^+}, DI_{m_y^-}, DI_{m_z^+}, DI_{m_z^-}, DI_{v_y^+}, DI_{v_y^-}, DI_{v_z^+}, DI_{v_z^-}$, are the terms of the contraction factor matrices $[DI]$ and $[DI_s]$ used in Equation (3.36) and (3.60), respectively. As explained in Sections 3.3.1.2 and 3.3.2.2, the contraction factor matrices are applied to the yield surface and the shear failure surface to model the reduction of moment and shear capacity. Using different weighting factors, w_i , to account for the interaction effects on strength degradation, non-uniform contraction of the surfaces is achieved.

In the framework of the event-based strategy presented in the previous sections, the yield surface and the shear failure surface are updated when a cross-over event occurs to mark the end of a half cycle. The degraded elastic reloading stiffness used for a peak-oriented response is determined in accordance with updated yield surface or shear failure surface.

Examples of cyclic response using the developed cyclic degradation model are shown in Figures 3-45 and 3-46. The response shown in Figure 3-45 is dominated by flexural yielding whereas that shown in Figure 3-46 is governed by flexure-shear failure and softening. It can be noticed that the attained strength reduces in each subsequent loading cycle when the same level of inelastic displacement is maintained.

3.5 Damage Models

Damage in reinforced concrete structures subjected to seismic loading can be caused by large inelastic deformations as well as by repeated load reversals. Damage in reinforced concrete components is commonly associated with concrete cracking, rebar yielding,

fracture or buckling, and loss of bond between rebars and concrete. Damage for individual components can be evaluated through the structural analysis based on data such as element deformations, forces and dissipated energy. Global damage assessment of the entire structural system can be achieved based on aggregating local damage indices representing damage of individual components into a global damage index. Damage evaluation on a global basis is particularly appropriate for assessment of collapse vulnerability and remaining safety margin of structural systems. Individual component damages are appropriate for evaluating losses prior to collapse. Brief overview of local and global damage models developed for quantifying seismic damage in reinforced concrete components and structures, respectively, is presented in the following section.

3.5.1 Overview of Damage Models for Reinforced Concrete Components and Structures

In a state-of-the-art review by Williams and Sexsmith (1995), seismic damage indices for reinforced concrete components are categorized as non-cumulative, cumulative and combined indices. Non-cumulative damage indices are generally based on normalized peak deformation values and do not account for damage due to repeated cycling. Cumulative damage indices consider damage due to cyclic loading based on accumulated plastic deformations or based on dissipated energy. The low-cycle fatigue concept is commonly used in the development of deformation-based cumulative damage indices. As summarized in Williams and Sexsmith (1995) and Altoontash (2004), among the deformation-based indices are those proposed by Banon et al. (1981), Wang and Shah (1987), Chung et al. (1987, 1989), Mehanny and Deierlein (2000), Hindi and Sexsmith

(2001). Among the energy-based indices are those proposed by Gosain et al. (1977), Elms et al. (1989), Kratzig et al. (1989). Combined damage indices consider damage based on a combination of excessive deformations and energy absorption. One of the most widely used is the combined damage model proposed by Park and Ang (1985). Park and Ang damage model is relatively simple and has been calibrated against a significant amount of observed seismic damage. Most damage indices are dimensionless parameters ranging from 0.0 to 1.0, where 0.0 corresponds to undamaged state and 1.0 represents state of total damage.

In a study on damage models for performance assessment of reinforced concrete beam-column joints, Altoontash (2004) implemented in OpenSees the damage models proposed by Kratzig et al. (1989), Mehanny and Deierlein (2000), Park and Ang (1985), normalized peak damage model, and hysteretic energy damage model. The normalized peak damage model is a non-cumulative damage model based on the maximum value of a response parameter, which can be force, deformation, or plastic deformation. The Kratzig index is a cumulative damage index based on dissipated energy and applies the concept of primary and follower half cycles to account for the excursions with maximum amplitude and the cumulative effects of smaller excursions. The damage model by Mehanny and Deierlein (2000) is based on cumulative member ductility in the form of total plastic deformations. This model follows the concept for cyclic damage accumulation used in the energy-based damage model by Kratzig et al. (1989) and the model by Otes (1985). The hysteretic energy damage model is a modification of the deterioration formulation proposed by Rahnema and Krawinkler (1993). This model is

based on the dissipated energy of the last excursion and the total cumulative dissipated energy.

Phung and Lau (2008) and Phung et al. (2010) developed stiffness degradation model which takes into account cumulative damage due to flexure and shear effects. Modified Park and Ang damage model (Kunnath et al. 1992) is adopted to quantify flexural damage as follows:

$$DI_{flexure} = \frac{\theta_{max} - \theta_y}{\theta_u - \theta_y} + \frac{\beta}{M_y \theta_u} \int dE_h \quad (3.103)$$

where θ_{max} is the maximum rotation angle sustained during the loading history, θ_y is the rotation angle at yield, and θ_u is the ultimate rotation capacity of the section, M_y is the yield moment, dE_h is the incremental dissipated hysteretic energy, and β is a non-negative parameter to account for cyclic load effect on strength degradation in the hysteretic behaviour of the member.

A shear damage index is proposed as follows:

$$DI_{shear} = \begin{cases} 0 & \text{if } \mu_{max} < \mu_i \\ \frac{\mu_{max} - \mu_i}{\mu_u - \mu_i} & \text{if } \mu_i \leq \mu_{max} \leq \mu_u \\ 1 & \text{if } \mu_{max} > \mu_u \end{cases} \quad (3.104)$$

where μ_{\max} , μ_i and μ_u are the maximum curvature ductility experienced during previous cycles, the curvature ductility where shear strength begins to degrade, and the ultimate curvature ductility, respectively.

Phung et al. (2010) use global damage indices based on hysteretic energy and local flexural and shear damage indices to evaluate the overall performance of the structure. The global normalized hysteretic energy is defined as the average of the normalized hysteretic energy absorbed by all members that experience inelastic action as follows:

$$DI_{hysteretic\ energy}^{Global} = \frac{1}{N} \sum_{i=1}^N E_{nh,i} \quad (3.105)$$

where N is the number of plastic hinges formed in the structure, and the normalized hysteretic energy, $E_{nh,i}$, is defined as the ratio of the hysteretic energy dissipated through cyclic response of the member and twice the yield strain energy, $\left(E_{nh} = \frac{\int dE_h}{M_y \theta_y}\right)$.

The global flexural damage index is defined as the weighted sum of the local flexural damage indices, $DI_{flexure,i}$, of all structural members in the system as follows:

$$DI_{flexure}^{Global} = \sum_{i=1}^N w_i DI_{flexure,i} \quad (3.106)$$

where w_i is the weighting factor defined as:

$$w_i = \frac{E_{nh,i}}{\sum_{i=1}^N E_{nh,i}} \quad (3.107)$$

The global shear damage index is also defined as the weighted sum of the local shear damage indices of all structural members in the system as follows:

$$DI_{shear}^{Global} = \frac{\sum_{i=1}^N DI_{shear,i}^2}{\sum_{i=1}^N DI_{shear,i}} \quad (3.108)$$

3.5.2 Controlling Degrading Behaviour with Damage Models

In this research, the approach used in the cyclic behaviour modeling is based on the direct interaction of the beam-column element with damage models in the analysis to track the evolution of damage and its effects on the gradual deterioration in stiffness and loss of strength. At each step of the analysis, the element provides data for the forces and deformations to the damage model. The damage model uses this data to calculate the required damage indices and returns updated information for the damage indices to the element. The provided damage indices are used to degrade stiffness and strength parameters of the element. This interaction process is schematically shown in Figure 3-47.

The damage model is capable of calculating and returning damage indices for positive and negative loading excursions in the directions of $y -$ and $z -$ axes separately. Thus, four groups of damage indices are updated and stored, DI_{y+} , DI_{y-} , DI_{z+} , DI_{z-} . The separation of damage indices depending on the sign and direction of the loading excursion is essential for the model to capture the effects of hysteretic damage on strength and stiffness parameters in multi-directions.

As described in the previous section, the quasi-elastic degraded cyclic behaviour of reinforced concrete components is modeled by using cyclic stiffness model, cyclic pinching model and cyclic strength degradation model incorporated in the beam-column formulation. Each of these cyclic models interacts with the damage model during the analysis, as shown in Figure 3-48. It is possible that different damage indices, e.g. non-cumulative, cumulative or combined damage indices, are specified to be used by each of the cyclic models to account for different characteristics of the degrading behaviour.

The cyclic stiffness model uses damage indices provided by the damage model to calculate multi-component degradation factors according to Equation (3.101) to degrade the unloading stiffness. Since the cyclic stiffness model is used to model cyclic flexural behaviour of reinforced concrete members, the damage indices should be based on flexural deformations. To account for cyclic damage accumulation, cumulative damage indices based on plastic deformations such as the damage index proposed by Mehanny and Deierlein (2000) or combined damage indices such as Park and Ang damage index (Park and Ang, 1985) can be used.

Following the same concept, the cyclic pinching model calculates multi-component degradation factors based on damage indices provided by the damage model. Since the cyclic pinching model is used to model the post-shear failure cyclic response of reinforced concrete components, the damage indices should be based on shear deformations. To consider the effects of accumulated damage, the contribution of dissipated hysteretic energy can be included in the selected damage indices.

Similarly, the cyclic strength degradation model interacts with the damage model to obtain damage indices used to calculate multi-component degradation factors according to Equation (3.102). To account for damage effects due to repeated load reversals, the damage indices used by this cyclic model should be energy-based cumulative damage indices such as those proposed by Kratzig et al. (1989), Rahnama and Krawinkler (1993), or combined damage indices such as Park and Ang damage index.

Thus, the element components for modeling degrading hysteretic behaviour have access to different damage indices in the analysis to update the deterioration in stiffness and strength. By using the concept of direct interaction between the beam-column element and the damage model, a flexible and extensible framework for considering the effects of progression and accumulation of damage on the element response can be achieved.

3.6 Summary

The key aspects of the formulation of the new beam-column element are summarized as follows:

- Interaction between axial force and biaxial bending moments is implemented through yield surface models
- Post-yield force interaction and inelastic hardening behaviour in flexure is achieved by kinematic evolution of the yield surface

- Interaction between axial force and biaxial shear forces and shear failure is captured by shear failure surface models
- Post-shear failure softening behaviour is modeled by non-uniform contraction of the shear-failure surface. In-cycle strength degradation is achieved by degradation of the element tangent stiffness.
- Post-yield flexure-shear interaction is considered in the model to capture degradation of shear strength in the plastic hinge zone with increasing flexural displacement ductility demand. The effects of damage accumulated in inelastic excursions in the direction of loading on shear strength and behaviour in other out-of-plane directions are also considered.
- Shear-critical behaviour, including behaviour governed by brittle shear failure and behaviour governed by flexure-shear failure, is captured using force-based and displacement ductility-based criteria.
- Consistent state determination of the element inelastic response is developed
- Cyclic models are based on a comprehensive event-based formulation
- Degradation in elastic unloading and reloading stiffness and pinching behaviour are captured by the cyclic models.
- Strength degradation under repeated cyclic load reversals is achieved by contraction of the yield surface and/or shear failure surface using cumulative damage indices based on the total hysteretic energy dissipated by the structural member
- Cyclic behaviour modeling approach is based on the incorporation of damage models in the beam-column element formulation to capture the evolution of damage and its effects on the gradual deterioration in stiffness and loss of strength

- Biaxial interaction effects on stiffness and strength degradation are considered in modeling full 3D behaviour of reinforced concrete members based on multi-component damage models capturing hysteretic damage in multi-directions.

Table 3-1 General state determination process for elements with yield surfaces and shear failure surfaces – Monotonic response

Step No.	Description
1	Predict element tangent stiffness
2	Compute trial force using predicted tangent stiffness
3	Check for yielding ($\Phi(p, m_y, m_z) \leq 1.0$)
4	Recalculate trial force consistent with yield surface (force return to yield surface)
5	Calculate shear forces from equilibrium
6	Update shear failure surface based on ductility-dependent shear limit surface
7	Check for shear failure ($\Phi_s(p, v_y, v_z) \leq 1.0$)
8	Calculate corrected force consistent with shear failure surface (force return to shear surface)
9	Update element tangent stiffness

Table 3-2 Conditions for state determination – Monotonic response

No.	State	Tangent Stiffness	Loading Criteria	Yield Surface Condition	Shear Failure Surface Condition
1	Elastic	$K_t = K_e$	$F_{i+1} > F_i$ $\Delta_{i+1} > \Delta_i$	$\Phi(p, m_y, m_z) < 1.0$	$\Phi_s(p, v_y, v_z) < 1.0$
2	Yielding and hardening in flexure	$K_t = K_e - K_r$	$F_{i+1} > F_i$ $\Delta_{i+1} > \Delta_i$	$\Phi(p, m_y, m_z) = 1.0$	$\Phi_s(p, v_y, v_z) < 1.0$
3	Shear failure at initial shear capacity and post-shear failure degradation	$K_t = K_{t,deg}$	$F_{i+1} < F_i$ $\Delta_{i+1} > \Delta_i$	$\Phi(p, m_y, m_z) < 1.0$	$\Phi_s(p, v_y, v_z) = 1.0$
4	Shear failure at degraded shear capacity and post-shear failure degradation	$K_t = K_{t,deg}$	$F_{i+1} < F_i$ $\Delta_{i+1} > \Delta_i$	$\Phi(p, m_y, m_z) < 1.0$	$\Phi_s(p, v_y, v_z) = 1.0$
5	Residual shear limit	$K_t = K_{t,res}$	$F_{i+1} \approx F_i$ $\Delta_{i+1} > \Delta_i$	$\Phi(p, m_y, m_z) < 1.0$	$\Phi_s(p, v_y, v_z) = 1.0$

Table 3-3 Path 1: from elastic (state 1) to flexural yielding (state 2). Conditions for state determination and transition between states

Step No.	Description	State
1	Compute trial forces, $\{dF_{trial}\} = [K_e]\{d\Delta\}$.	State 1
2	Check for yielding. If the force point is within the elastic region, $\Phi(p, m_y, m_z) < 1.0$, the trial forces are the final forces for the current state.	State 1
3	<p>If the force point shoots through the yield surface, $\Phi(p, m_y, m_z) > 1.0$, the element has yielded within this increment and is hardening.</p> <p>Force recovery is used so that the force point is on the yield surface, $\Phi(p, m_y, m_z) = 1.0$.</p> <p>The step is split into elastic and inelastic portion.</p> <p>The elastic portion of the trial force is, $\tau\{dF_{trial}\} = \tau[K_e]\{d\Delta\}$.</p> <p>The inelastic portion of the trial force is, $(1 - \tau)\{dF_{trial}\} = (1 - \tau)[K_e]\{d\Delta\}$.</p> <p>The magnitude of plastic deformation based on the inelastic portion of the trial force can be calculated as,</p> $\{\lambda_{(\tau)}\} = [G]^T [K_e + K_p] [G]^{-1} [G]^T (1 - \tau) [K_e] \{d\Delta\}.$ <p>The trial force is recalculated, $\{dF\} = \{dF_{trial}\} - [K_e]\{d\Delta_p\} = [K_e]\{d\Delta\} - [K_e][G]\{\lambda_{(\tau)}\}$.</p> <p>The final force at the end of the step is, $\{F_i\} = \{F_{i-1}\} + \{dF\}$.</p> <p>In the inelastic hardening response, the evolution rules govern the state of the yield surface. The amount of yield surface translation is determined based on the hardening component, $[dF^*] = [K_p]\{d\Delta_p\} = [K_p][G]\{\lambda_{(\tau)}\}$.</p> <p>Due to the convexity of the yield surface, the force point corresponding to $\{F_i\}$ may be outside the translated surface. Centroidal return is used to return the force point to the surface. The force points at the two ends of the element may be out of balance. Axial loads are averaged at the two ends. The force recovery is finalized at the current state using constant-P return.</p> <p>The element tangent stiffness is updated for the current state,</p>	Transition from State 1 to State 2

	<p>$[K_t] = [K_e] - [K_r]$ and returned to the solver. The plastic reduction stiffness is, $[K_r] = [K_e][G] \left[[G]^T [K_e + K_p][G] \right]^{-1} [G]^T [K_e]$</p>	
4	<p>The force point is on the yield surface at the beginning of the increment, $\Phi(p, m_y, m_z) = 1.0$ The element is plastically hardening. Compute the trial force using the element tangent stiffness from the previous state, $\{dF_{trial}\} = [K_t]\{d\Delta\}$.</p> <p>The magnitude of plastic deformations can be calculated as, $\{\lambda\} = \left[[G]^T [K_e + K_p][G] \right]^{-1} [G]^T \{dF_{trial}\}$ The final force at the end of the step is, $\{F_{i+1}\} = \{F_i\} + \{\{dF_{trial}\} - [K_e][G]\{\lambda\}\}$.</p> <p>The new position of the yield surface is determined based on the hardening component, $\{dF^*\} = [K_p]\{d\Delta_p\} = [K_p][G]\{\lambda\}$.</p> <p>Due to the use of plastic reduction matrix and the convexity of the yield surface, the incremental force drifts away from the surface. The force point corresponding to $\{F_{i+1}\}$ is returned to the translated surface using centroidal return. After balancing the axial load at the two ends of the element, the force recovery is finalized using constant-P return.</p> <p>Finally, the element tangent stiffness is updated for the current state, $[K_t] = [K_e] - [K_r]$.</p>	State 2
5	<p>Check for continued plastic loading.</p> <p>If there is an increase in the load and the deformations, $F_{i+1} > F_i$ and $\Delta_{i+1} > \Delta_i$, the element continues to load plastically. The steps in item 4 are followed.</p>	State 2
6	<p>If there is a decrease in the load and the deformations, $F_{i+1} < F_i$ and $\Delta_{i+1} < \Delta_i$, the element is unloading elastically, as shown in Figure 3-30(c).</p>	Unloading from State 2

Table 3-4 Path 2: from elastic (state 1) to shear failure and post-shear failure degradation (state 3).

Conditions for state determination and transition between states

Step No.	Description	State
1	Compute trial forces, $\{dF_{trial}\} = [K_e]\{d\Delta\}$.	State 1
2	Check for shear failure. If the shear force point is within the elastic region, $\Phi_s(p, v_y, v_z) < 1.0$, the trial forces are the final forces for the current state.	State 1
3	<p>If the shear force point shoots through the shear failure surface, $\Phi_s(p, v_y, v_z) > 1.0$, the element has failed in shear within this increment and is softening.</p> <p>Force recovery is used so that the force point is on the shear failure surface, $\Phi_s(p, v_y, v_z) = 1.0$</p> <p>The step is split into elastic and inelastic softening portion.</p> <p>The elastic portion of the trial force is, $\tau_s\{dF_{trial}\} = \tau_s[K_e]\{d\Delta\}$.</p> <p>The inelastic portion of the trial force is, $(1 - \tau_s)\{dF_{trial}\} = (1 - \tau_s)[K_e]\{d\Delta\}$.</p> <p>The slope of degradation is determined as, $K_{deg} = V_u/(\Delta_a - \Delta_s)$</p> <p>The shear force at shear failure, V_u, is the initial shear capacity, V_n.</p> <p>The deformation at shear failure can be calculated as, $\{\Delta_s\} = \{\Delta_{i-1}\} + \tau_s\{d\Delta\}$.</p> <p>The predicted drift at axial failure, Δ_a, is calculated for the current level of axial load.</p> <p>Degradation coefficient is determined, $\delta = \frac{1}{K_s} \frac{K_f K_{deg}}{K_f - K_{deg}}$</p> <p>The flexural and shear stiffness components are $K_f = 3EI/L^3$ and $K_s = GA_s/L$.</p> <p>The tangent stiffness is updated to include degradation in the shear stiffness components, $[K_{t,deg}] = [K(EI, \delta K_s)]$, using a flexibility approach.</p> <p>The trial force is recalculated, $\{dF\} = \tau_s[K_e]\{d\Delta\} + (1 - \tau_s)[K_{t,deg}]\{d\Delta\}$ The final force at the end of the step is, $\{F_i\} = \{F_{i-1}\} + \{dF\}$.</p>	Transition from State 1 to State 3

	<p>In the post-shear failure degrading/softening response, the evolution rules govern the state of the shear failure surface. The amount of surface contraction in the direction of the shear force axis where failure occurred is determined based on the softening component, $dF_s^* = K_{deg}(1 - \tau_s)d\Delta$. The shear failure surface is updated based on the non-uniform contraction rule.</p> <p>As the element is softening in shear, moments are assumed to unload. The moments are calculated by satisfying equilibrium (Table 3.5, cases 3.1, 3.3, and 3.4).</p> <p>The increase in the total deformations is due only to the contribution of the shear components.</p> <p>The updated element tangent stiffness, $[K_{t,deg}] = [K(EI, \delta K_s)]$, is returned to the solver.</p>	
4	<p>The shear force point is on the degrading shear failure surface at the beginning of the increment, $\Phi_s(p, v_y, v_z) = 1.0$. The element is softening in shear. The force increment is computed using the element degraded tangent stiffness from the previous state, $\{dF\} = [K_{t,deg}]\{d\Delta\}$. The shear failure surface is updated to include the additional degradation experienced in this increment. The moments are updated to continue unloading.</p> <p>The element tangent stiffness is the same degraded tangent stiffness, $[K_{t,deg}]$, as in the previous converged step.</p>	State 3
5	<p>Check for continued failing in shear.</p> <p>If there is an increase in the deformations, $\Delta_{i+1} > \Delta_i$, the element continues to fail in shear. The steps in item 4 are followed.</p>	State 3
6	<p>If there is a decrease in the load and the deformations, $F_{i+1} < F_i$ and $\Delta_{i+1} < \Delta_i$, the element is unloading elastically, as shown in Figure 3-31(b).</p>	Unloading from State 3

Table 3-5 Conditions for maintaining / satisfying equilibrium - Case 1.1 to 1.5

End 1 / End 2	Elastic	Ductile yielding in flexure	Brittle shear failure	Limited ductile with shear failure	Moderate ductile with shear failure
Elastic	<p><u>Case 1.1</u> End 1 is elastic. End 2 is elastic.</p> $M_1 = M_{1el} < M_{1yield}$ $M_2 = M_{2el} < M_{2yield}$ $V_{demand} = \frac{(M_{1el} + M_{2el})}{L}$ $V_1 = V_2 = V_{demand}$ $V_{demand} < V_{1n}, V_{2n}$	<p><u>Case 1.2</u> End 1 starts to yield when end 2 is elastic. Next, end 1 is hardening while end 2 continues to load elastically. Shear failure does not occur.</p> $M_1 = M_{1yield} \rightarrow \text{yield}$ $M_1 = M_{1p} \rightarrow \text{hardening}$ $M_{1yield} \leq M_{1p} \leq M_{1ult}$ $M_2 = M_{2el} < M_{2yield}$ $V_{demand} = \frac{(M_{1p} + M_{2el})}{L}$ $V_1 = V_2 = V_{demand}$ $V_{demand} < V_{1n}, V_{2n}$ $\Delta > \Delta_{cr}$ $V_{1n} \text{ reduces to } V_{1lim}$ $V_{2n} \text{ reduces to } V_{2lim}$ $V_{demand} < V_{1lim}, V_{2lim}$ <p>Yielding at end 1, and the related increasing displacement ductility demand, affects the shear capacity at both end 1 and end 2. (Shear limit surface is defined as shear capacity vs. total displ./drift.)</p>	<p><u>Case 1.3</u> End 1 fails in shear prior to yielding and end 2 is still elastic. Next, shear strength at end 1 is degrading while shear force at end 2 is unloading. Moments at both end 1 and 2 are unloading.</p> $M_1 = M_{1el} < M_{1yield}$ $M_2 = M_{2el} < M_{2yield}$ $V_{demand} = \frac{(M_{1el} + M_{2el})}{L}$ $V_1 = V_2 = V_{demand}$ $V_{demand} > V_{1n}$ $V_1 = V_{1n} \rightarrow \text{fail}$ $V_2 < V_{2n} \rightarrow \text{elastic}$ $V_1 = V_{1deg} \rightarrow \text{degrade}$ $V_2 = V_1 \rightarrow \text{unload}$ $M_1 = \alpha M_{1el} \rightarrow \text{unload}$ $M_2 = \alpha M_{2el} \rightarrow \text{unload}$ $\alpha = V_{demand} / V_{1deg}$	<p><u>Case 1.4</u> End 1 yields and starts hardening when end 2 is elastic. End 1 fails in shear after yielding and hardening while end 2 is still elastic. Next, shear strength at end 1 is degrading while shear force at end 2 is unloading. Moments at both end 1 and 2 are unloading.</p> $M_1 = M_{1yield} \rightarrow \text{yield}$ $M_1 = M_{1p} \rightarrow \text{hardening}$ $M_2 = M_{2el} < M_{2yield}$ $V_{demand} = \frac{(M_{1p} + M_{2el})}{L}$ $V_1 = V_2 = V_{demand}$ $V_{demand} > V_{1n}$ $V_1 = V_{1n} \rightarrow \text{fail}$ $V_2 < V_{2n} \rightarrow \text{elastic}$ $V_1 = V_{1deg} \rightarrow \text{degrade}$ $V_2 = V_1 \rightarrow \text{unload}$ $M_1 = \alpha M_{1p} \rightarrow \text{unload}$ $M_2 = \alpha M_{2el} \rightarrow \text{unload}$ $\alpha = V_{demand} / V_{1deg}$	<p><u>Case 1.5</u> End 1 is hardening while end 2 is still elastic. Due to increasing displacement ductility demand, shear capacity at end 1 is reduced by the limit surface. End 1 fails when shear at that end exceeds the limit capacity. Next, shear strength at end 1 is degrading while shear force at end 2 is unloading. Moments at both end 1 and 2 are unloading.</p> $M_1 = M_{1p} \rightarrow \text{hardening}$ $M_2 = M_{2el} < M_{2yield}$ $\Delta > \Delta_{cr}$ $V_{1n} \text{ reduces to } V_{1lim}$ $V_{demand} = \frac{(M_{1p} + M_{2el})}{L}$ $V_1 = V_2 = V_{demand}$ $V_{demand} > V_{1lim}$ $V_1 = V_{1lim} \rightarrow \text{fail}$ $V_2 < V_{2n} (V_{2lim}) \rightarrow \text{elastic}$ $V_1 = V_{1deg} \rightarrow \text{degrade}$ $V_2 = V_1 \rightarrow \text{unload}$ $M_1 = \alpha M_{1p} \rightarrow \text{unload}$ $M_2 = \alpha M_{2el} \rightarrow \text{unload}$ $\alpha = V_{demand} / V_{1deg}$

Table 3-5 (Continued) Case 2.1 to 2.5

End 1 End 2	Elastic	Ductile yielding in flexure	Brittle shear failure	Limited ductile with shear failure	Moderate ductile with shear failure
Ductile yielding in flexure	<p><u>Case 2.1</u></p> <p>Similar to case 1.2</p> $M_1 = M_{1el} < M_{1yield}$ $M_2 = M_{2yield} \rightarrow \text{yield}$ $M_2 = M_{2p} \rightarrow \text{hardening}$ $M_{2yield} \leq M_{2p} \leq M_{2ult}$ $V_{demand} = \frac{(M_{1el} + M_{2p})}{L}$ $V_1 = V_2 = V_{demand}$ $V_{demand} < V_{1n}, V_{2n}$ $\Delta > \Delta_{cr}$ $V_{1n} \text{ reduces to } V_{1lim}$ $V_{2n} \text{ reduces to } V_{2lim}$ $V_{demand} < V_{1lim}, V_{2lim}$	<p><u>Case 2.2</u></p> <p>End 1 and 2 start to yield simultaneously or End 1 is hardening when end 2 starts to yield (vice versa).</p> $M_1 = M_{1yield} \rightarrow \text{yield}$ $M_1 = M_{1p} \rightarrow \text{hardening}$ $M_{1yield} \leq M_{1p} \leq M_{1ult}$ $M_2 = M_{2yield} \rightarrow \text{yield}$ $M_2 = M_{2p} \rightarrow \text{hardening}$ $M_{2yield} \leq M_{2p} \leq M_{2ult}$ $V_{demand} = \frac{(M_{1p} + M_{2p})}{L}$ $V_1 = V_2 = V_{demand}$ $V_{demand} < V_{1n}, V_{2n}$ $\Delta > \Delta_{cr}$ $V_{1n} \text{ reduces to } V_{1lim}$ $V_{2n} \text{ reduces to } V_{2lim}$ $V_{demand} < V_{1lim}, V_{2lim}$	<p><u>Case 2.3</u></p> <p>Not possible in practice</p>	<p><u>Case 2.4</u></p> <p>Not possible in practice</p>	<p><u>Case 2.5</u></p> <p>End 1 and 2 are hardening. Due to increasing displ. ductility demand, shear capacity at end 1 and 2 are reduced by the limit surface. End 1 fails when shear exceeds the limit capacity while end 2 still has sufficient capacity. Next, shear strength at end 1 is degrading while shear force at end 2 is unloading. Moments at both end 1 and 2 are unloading.</p> $M_1 = M_{1p} \rightarrow \text{hardening}$ $M_2 = M_{2p} \rightarrow \text{hardening}$ $V_{demand} = \frac{(M_{1p} + M_{2p})}{L}$ $V_1 = V_2 = V_{demand}$ $V_{demand} < V_{1n}, V_{2n}$ $\Delta > \Delta_{cr}$ $V_{1n} \text{ reduces to } V_{1lim}$ $V_{2n} \text{ reduces to } V_{2lim}$ $V_{demand} > V_{1lim}$ $V_1 = V_{1lim} \rightarrow \text{fail}$ $V_{demand} < V_{2lim}$ $V_1 = V_{1deg} \rightarrow \text{degrade}$ $V_2 = V_1 \rightarrow \text{unload}$ $M_1 = \alpha M_{1p} \rightarrow \text{unload}$ $M_2 = \alpha M_{2el} \rightarrow \text{unload}$ $\alpha = V_{demand} / V_{1deg}$

Table 3-5 (Continued) Case 3.1 to 3.5

End 1 End 2	Elastic	Ductile yielding in flexure	Brittle shear failure	Limited ductile with shear failure	Moderate ductile with shear failure
Brittle shear failure	<p><u>Case 3.1</u></p> <p>Similar to case 1.3</p> $M_1 = M_{1el} < M_{1yield}$ $M_2 = M_{2el} < M_{2yield}$ $V_{demand} = \frac{(M_{1el} + M_{2el})}{L}$ $V_1 = V_2 = V_{demand}$ $V_{demand} > V_{2n}$ $V_1 < V_{1n} \rightarrow \text{elastic}$ $V_2 = V_{2n} \rightarrow \text{fail}$ $V_2 = V_{2deg} \rightarrow \text{degrade}$ $V_1 = V_2 \rightarrow \text{unload}$ $M_1 = \alpha M_{1el} \rightarrow \text{unload}$ $M_2 = \alpha M_{2el} \rightarrow \text{unload}$ $\alpha = V_{demand} / V_{2deg}$	<p><u>Case 3.2</u></p> <p>Similar to case 2.3</p> <p>Not possible in practice.</p>	<p><u>Case 3.3</u></p> <p>End 1 and 2 fail in shear simultaneously prior to yielding.</p> <p>Based on the assumption that if one end fails in shear, the other end has to unload in shear to satisfy equilibrium, shear failure must occur at the two ends simultaneously.</p> <p>Next, shear strength at end 1 and 2 is degrading while moments are unloading.</p> $M_1 = M_{1el} < M_{1yield}$ $M_2 = M_{2el} < M_{2yield}$ $V_{demand} = \frac{(M_{1el} + M_{2el})}{L}$ $V_1 = V_2 = V_{demand}$ $V_{1n} = V_{2n} = V_n$ $V_{demand} > V_n$ $V_1 = V_n \rightarrow \text{fail}$ $V_2 = V_n \rightarrow \text{fail}$ $V_1 = V_2 = V_{deg}$ $M_1 = \alpha M_{1el} \rightarrow \text{unload}$ $M_2 = \alpha M_{2el} \rightarrow \text{unload}$ $\alpha = V_{demand} / V_{deg}$	<p><u>Case 3.4</u></p> <p>End 1 yields and starts hardening when end 2 is elastic.</p> <p>End 1 fails in shear after yielding and hardening while end 2 fails in shear prior to yielding. Shear failure occurs at the two ends simultaneously.</p> <p>Next, shear strength at end 1 and 2 is degrading while moments are unloading.</p> $M_1 = M_{1yield} \rightarrow \text{yield}$ $M_1 = M_{1p} \rightarrow \text{hardening}$ $M_2 = M_{2el} < M_{2yield}$ $V_{demand} = \frac{(M_{1p} + M_{2el})}{L}$ $V_1 = V_2 = V_{demand}$ $V_{1n} = V_{2n} = V_n$ $V_{demand} > V_n$ $V_1 = V_n \rightarrow \text{fail}$ $V_2 = V_n \rightarrow \text{fail}$ $V_1 = V_2 = V_{deg}$ $M_1 = \alpha M_{1el} \rightarrow \text{unload}$ $M_2 = \alpha M_{2el} \rightarrow \text{unload}$ $\alpha = V_{demand} / V_{deg}$	<p><u>Case 3.5</u></p> <p>Not possible in practice.</p>

Table 3-5 (Continued) Case 4.1 to 4.5

End 1 End 2	Elastic	Ductile yielding in flexure	Brittle shear failure	Limited ductile with shear failure	Moderate ductile with shear failure
Limited ductile with shear failure	<p><u>Case 4.1</u></p> <p>Similar to case 1.4</p> $M_1 = M_{1el} < M_{1yield}$ $M_2 = M_{yield} \rightarrow \text{yield}$ $M_2 = M_{2p} \rightarrow \text{hardening}$ $V_{demand} = \frac{(M_{1el} + M_{2p})}{L}$ $V_1 = V_2 = V_{demand}$ $V_{demand} > V_{2n}$ $V_1 < V_{1n} \rightarrow \text{elastic}$ $V_2 = V_{2n} \rightarrow \text{fail}$ $V_2 = V_{2deg} \rightarrow \text{degrade}$ $V_1 = V_2 \rightarrow \text{unload}$ $M_1 = \alpha M_{1p} \rightarrow \text{unload}$ $M_2 = \alpha M_{2el} \rightarrow \text{unload}$ $\alpha = V_{demand} / V_{2deg}$	<p><u>Case 4.2</u></p> <p>Not possible in practice.</p>	<p><u>Case 4.3</u></p> <p>Similar to case 3.4</p> $M_1 = M_{1el} < M_{1yield}$ $M_2 = M_{yield} \rightarrow \text{yield}$ $M_2 = M_{2p} \rightarrow \text{hardening}$ $V_{demand} = \frac{(M_{1el} + M_{2p})}{L}$ $V_1 = V_2 = V_{demand}$ $V_{1n} = V_{2n} = V_n$ $V_{demand} > V_n$ $V_1 = V_n \rightarrow \text{fail}$ $V_2 = V_n \rightarrow \text{fail}$ $V_1 = V_2 = V_{deg}$ $M_1 = \alpha M_{1el} \rightarrow \text{unload}$ $M_2 = \alpha M_{2el} \rightarrow \text{unload}$ $\alpha = V_{demand} / V_{deg}$	<p><u>Case 4.4</u></p> <p>End 1 and 2 yield and start hardening. End 1 and 2 fail in shear after yielding and hardening. Shear failure occurs at the two ends simultaneously.</p> $M_1 = M_{1yield} \rightarrow \text{yield}$ $M_1 = M_{1p} \rightarrow \text{hardening}$ $M_{1yield} \leq M_{1p} \leq M_{1ult}$ $M_2 = M_{2yield} \rightarrow \text{yield}$ $M_2 = M_{2p} \rightarrow \text{hardening}$ $M_{2yield} \leq M_{2p} \leq M_{2ult}$ $V_{demand} = \frac{(M_{1p} + M_{2p})}{L}$ $V_1 = V_2 = V_{demand}$ $V_{1n} = V_{2n} = V_n$ $V_{demand} > V_n$ $V_1 = V_n \rightarrow \text{fail}$ $V_2 = V_n \rightarrow \text{fail}$ $V_1 = V_2 = V_{deg}$ $M_1 = \alpha M_{1el} \rightarrow \text{unload}$ $M_2 = \alpha M_{2el} \rightarrow \text{unload}$ $\alpha = V_{demand} / V_{deg}$	<p><u>Case 4.5</u></p> <p>Not possible in practice.</p>

Table 3-5 (Continued) Case 5.1 to 5.5

End 1 End 2	Elastic	Ductile yielding in flexure	Brittle shear failure	Limited ductile with shear failure	Moderate ductile with shear failure
Moderate ductile with shear failure	<p><u>Case 5.1</u></p> <p>Similar to case 1.5</p> <p>$M_1 = M_{1el} < M_{1yield}$ $M_2 = M_{2p} \rightarrow$ hardening $\Delta > \Delta_{cr}$ V_{2n} reduces to V_{2lim} V_{1n} reduces to V_{1lim} $V_{demand} = \frac{(M_{1p} + M_{2el})}{L}$ $V_1 = V_2 = V_{demand}$ $V_{demand} > V_{2lim}$ $V_2 = V_{2lim} \rightarrow$ fail $V_1 < V_{1lim} \rightarrow$ elastic</p> <p>$V_2 = V_{2deg} \rightarrow$ degrade $V_1 = V_2 \rightarrow$ unload $M_1 = \alpha M_{1p} \rightarrow$ unload $M_2 = \alpha M_{2el} \rightarrow$ unload $\alpha = V_{demand}/V_{2deg}$</p>	<p><u>Case 5.2</u></p> <p>Similar to case 2.5</p> <p>$M_1 = M_{1p} \rightarrow$ hardening $M_2 = M_{2p} \rightarrow$ hardening $V_{demand} = \frac{(M_{1p} + M_{2p})}{L}$ $V_1 = V_2 = V_{demand}$ $V_{demand} < V_{1n}, V_{2n}$ $\Delta > \Delta_{cr}$ V_{1n} reduces to V_{1lim} V_{2n} reduces to V_{2lim} $V_{demand} < V_{1lim}$ $V_{demand} > V_{2lim}$ $V_2 = V_{2lim} \rightarrow$ fail</p> <p>$V_2 = V_{2deg} \rightarrow$ degrade $V_1 = V_2 \rightarrow$ unload $M_1 = \alpha M_{1p} \rightarrow$ unload $M_2 = \alpha M_{2el} \rightarrow$ unload $\alpha = V_{demand}/V_{2deg}$</p>	<p><u>Case 5.3</u></p> <p>Similar to case 3.5</p> <p>Not possible in practice.</p>	<p><u>Case 5.4</u></p> <p>Similar to case 4.5</p> <p>Not possible in practice.</p>	<p><u>Case 5.5</u></p> <p>End 1 and 2 are hardening. Due to increasing displacement ductility demand, shear capacity at end 1 and 2 are reduced by the limit surface. End 1 and 2 fail simultaneously when shear exceeds the limit capacity.</p> <p>Next, shear strength at end 1 and 2 is degrading while moments are unloading.</p> <p>$M_1 = M_{1p} \rightarrow$ hardening $M_2 = M_{2p} \rightarrow$ hardening $V_{demand} = \frac{(M_{1p} + M_{2p})}{L}$ $V_1 = V_2 = V_{demand}$ $V_{1n} = V_{2n} = V_n$ $V_{demand} < V_n$ $\Delta > \Delta_{cr}$ V_n reduces to V_{lim} $V_{demand} > V_{lim}$ $V_1 = V_{lim} \rightarrow$ fail $V_2 = V_{lim} \rightarrow$ fail</p> <p>$V_1 = V_2 = V_{deg}$ $M_1 = \alpha M_{1el} \rightarrow$ unload $M_2 = \alpha M_{2el} \rightarrow$ unload $\alpha = V_{demand}/V_{deg}$</p>

Table 3-6 Conditions defining states in the cyclic stiffness model - positive excursions (deformations)

State No	State Description					
1	Loading, initial elastic response followed by inelastic response	F_i^+, F_{i-1}^+ $ F_i > F_{i-1} $	$\Delta_i^+, \Delta_{i-1}^+$ $ \Delta_i > \Delta_{i-1} $	$F_i \Delta_i > 0$	$F_i F_{i-1} > 0$	$\Delta_i \Delta_{i-1} > 0$
2	Unloading after yielding, quasi-elastic degraded response	F_i^+, F_{i-1}^+ $ F_i < F_{i-1} $	$\Delta_i^+, \Delta_{i-1}^+$ $ \Delta_i < \Delta_{i-1} $	$F_i \Delta_i > 0$	$F_i F_{i-1} > 0$	$\Delta_i \Delta_{i-1} > 0$
3	Cross-over Transition from unloading to reloading	F_i^-, F_{i-1}^+ $ F_i \leq F_{i-1} $	$\Delta_i^+, \Delta_{i-1}^+$ $ \Delta_i < \Delta_{i-1} $	$F_i \Delta_i < 0$	$F_i F_{i-1} < 0$	$\Delta_i \Delta_{i-1} > 0$
4	Reloading in the opposite direction after yielding and unloading, quasi-elastic degraded response	F_i^-, F_{i-1}^- $ F_i > F_{i-1} $	$\Delta_i^+, \Delta_{i-1}^+$ $ \Delta_i < \Delta_{i-1} $	$F_i \Delta_i < 0$	$F_i F_{i-1} > 0$	$\Delta_i \Delta_{i-1} > 0$
4a	Reloading cross-over Transition from positive to negative excursions	F_i^-, F_{i-1}^- $ F_i > F_{i-1} $	$\Delta_i^-, \Delta_{i-1}^+$ $ \Delta_i \leq \Delta_{i-1} $	$F_i \Delta_i > 0$	$F_i F_{i-1} > 0$	$\Delta_i \Delta_{i-1} < 0$

Table 3-7 Conditions defining states in cyclic stiffness model - negative excursions (deformations)

State No	State Description					
5	Reloading inelastic response	F_i^-, F_{i-1}^- $ F_i > F_{i-1} $	$\Delta_i^-, \Delta_{i-1}^-$ $ \Delta_i > \Delta_{i-1} $	$F_i \Delta_i > 0$	$F_i F_{i-1} > 0$	$\Delta_i \Delta_{i-1} > 0$
6	Unloading after yielding, quasi-elastic degraded response	F_i^-, F_{i-1}^- $ F_i < F_{i-1} $	$\Delta_i^-, \Delta_{i-1}^-$ $ \Delta_i < \Delta_{i-1} $	$F_i \Delta_i > 0$	$F_i F_{i-1} > 0$	$\Delta_i \Delta_{i-1} > 0$
7	Cross-over Transition from unloading to reloading	F_i^+, F_{i-1}^- $ F_i \leq F_{i-1} $	$\Delta_i^-, \Delta_{i-1}^-$ $ \Delta_i < \Delta_{i-1} $	$F_i \Delta_i < 0$	$F_i F_{i-1} < 0$	$\Delta_i \Delta_{i-1} > 0$
8	Reloading in the opposite direction after yielding and unloading, quasi-elastic degraded response	F_i^+, F_{i-1}^+ $ F_i > F_{i-1} $	$\Delta_i^-, \Delta_{i-1}^-$ $ \Delta_i < \Delta_{i-1} $	$F_i \Delta_i < 0$	$F_i F_{i-1} > 0$	$\Delta_i \Delta_{i-1} > 0$
8a	Reloading cross-over	F_i^+, F_{i-1}^+ $ F_i > F_{i-1} $	$\Delta_i^+, \Delta_{i-1}^-$ $ \Delta_i \leq \Delta_{i-1} $	$F_i \Delta_i > 0$	$F_i F_{i-1} > 0$	$\Delta_i \Delta_{i-1} < 0$

Table 3-8 State determination in cyclic stiffness model

Previous state	Check condition	Possible current state	Positive excursions	Negative excursions
Loading	$ \Delta_i \leq \Delta_{i-1} $	$ \Delta_i > \Delta_{i-1} $ $ \Delta_i < \Delta_{i-1} $	Continued loading Unloading	
Unloading	$ \Delta_i \leq \Delta_{i-1} , F_i F_{i-1} \leq 0$	$ \Delta_i < \Delta_{i-1} , F_i F_{i-1} > 0$ $ \Delta_i < \Delta_{i-1} , F_i F_{i-1} < 0$ $ \Delta_i > \Delta_{i-1} , F_i F_{i-1} > 0$	Continued unloading Cross-over (-ve) Reloading	
Reloading in the opposite direction (preceded by a negative cross-over event)	$ \Delta^c - \Delta_i \leq \Delta^c - \Delta_{i-1} $	$ \Delta^c - \Delta_i > \Delta^c - \Delta_{i-1} $ $ \Delta^c - \Delta_i < \Delta^c - \Delta_{i-1} $	Continued reloading Unloading in the opposite direction	

Table 3-8 (Continued)

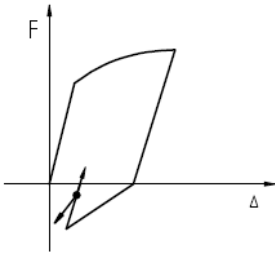
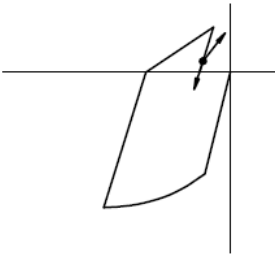
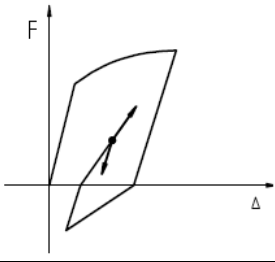
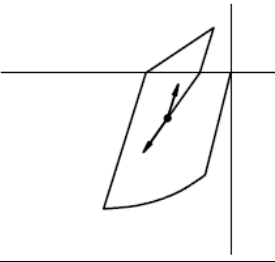
Previous state	Check condition	Possible current state	Positive excursions	Negative excursions
Unloading in the opposite direction before reaching peak / yielding	$ \Delta^c - \Delta_i \leq \Delta^c - \Delta_{i-1} $ $F_i F_{i-1} \leq 0$	$ \Delta^c - \Delta_i < \Delta^c - \Delta_{i-1} $ $F_i F_{i-1} > 0$ $ \Delta^c - \Delta_i < \Delta^c - \Delta_{i-1} $ $F_i F_{i-1} < 0$ $ \Delta^c - \Delta_i > \Delta^c - \Delta_{i-1} $ $F_i F_{i-1} > 0$		
Reloading in the initial direction (preceded by a positive cross-over event)	$ \Delta_i \leq \Delta_{i-1} $	$ \Delta_i > \Delta_{i-1} $ $ \Delta_i < \Delta_{i-1} $		

Table 3-9 Cross-over event determination in cyclic stiffness model

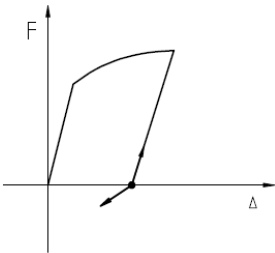
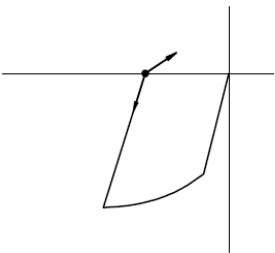
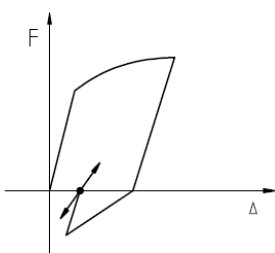
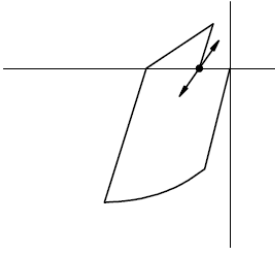
Previous state	Check condition	Possible current state		Positive excursions	Negative excursions
Unloading in primary half cycle ending at cross-over	$(F_i \Delta_i) \leq 0$	$(F_i \Delta_i) > 0 \rightarrow$ $ \Delta_i > \Delta_{i-1} $	Reloading to previous peak		
Unloading in follower half cycle ending at cross-over	$(F_i \Delta_i) \leq 0$	$(F_i \Delta_i) > 0 \rightarrow$ $ \Delta_i > \Delta_{i-1} $	Reloading to previous peak		

Table 3-10 State determination in cyclic pinching model

Previous state	Check condition	Possible current state	Positive excursions	Negative excursions
Loading (post-shear failure in-cycle degradation)	$ \Delta_i \leq \Delta_{i-1} $	$ \Delta_i > \Delta_{i-1} $ $ \Delta_i < \Delta_{i-1} $	Continued loading Unloading	
Unloading	$ \Delta_i \leq \Delta_{i-1} , F_i F_{i-1} \leq 0$	$ \Delta_i < \Delta_{i-1} , F_i F_{i-1} > 0$ $ \Delta_i < \Delta_{i-1} , F_i F_{i-1} < 0$ $ \Delta_i > \Delta_{i-1} , F_i F_{i-1} > 0$	Continued unloading Cross-over (-ve) Pinching / Reloading	
Pinching / Reloading in the opposite direction	$ \Delta^c - \Delta_i \leq \Delta^c - \Delta_{i-1} $	$ \Delta^c - \Delta_i > \Delta^c - \Delta_{i-1} $ $ \Delta^c - \Delta_i < \Delta^c - \Delta_{i-1} $	Continued reloading Unloading in the opposite direction	

Table 3-10 (Continued)

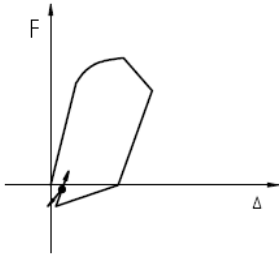
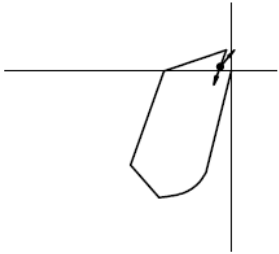
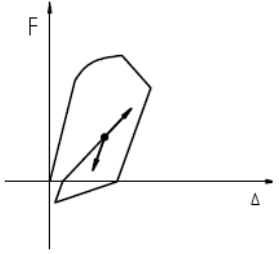
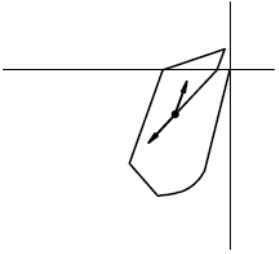
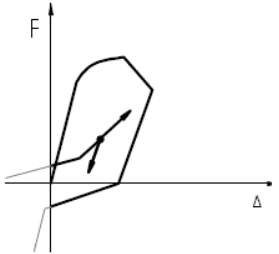
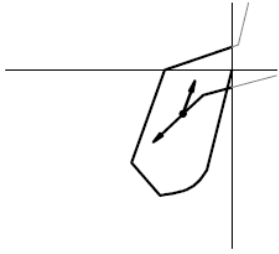
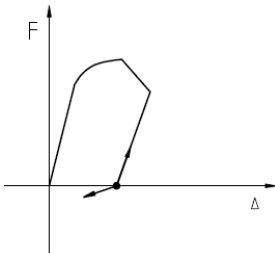
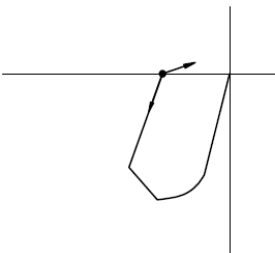
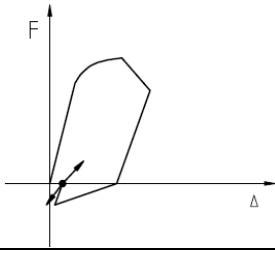
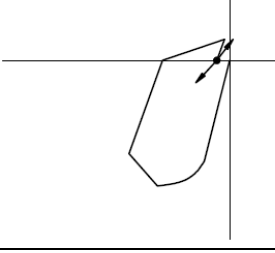
Previous state	Check condition	Possible current state	Positive excursions	Negative excursions
Unloading in the opposite direction before reaching end of pinching	$ \Delta^c - \Delta_i \leq \Delta^c - \Delta_{i-1} $ $F_i F_{i-1} \leq 0$	$ \Delta^c - \Delta_i < \Delta^c - \Delta_{i-1} $ $F_i F_{i-1} > 0$ $ \Delta^c - \Delta_i < \Delta^c - \Delta_{i-1} $ $F_i F_{i-1} < 0$ $ \Delta^c - \Delta_i > \Delta^c - \Delta_{i-1} $ $F_i F_{i-1} > 0$	<p>Continued unloading</p> <p>Cross-over (+ve)</p> <p>Reloading</p> 	
Reloading in the initial direction (post-shear failure in-cycle degradation)	$ \Delta_i \leq \Delta_{i-1} $	$ \Delta_i > \Delta_{i-1} $ $ \Delta_i < \Delta_{i-1} $	<p>Continued reloading</p> <p>Unloading</p> 	
Reloading after pinching	$ \Delta_i \leq \Delta_{i-1} $	$ \Delta_i > \Delta_{i-1} $ $ \Delta_i < \Delta_{i-1} $	<p>Continued reloading</p> <p>Unloading</p> 	

Table 3-11 Cross-over event determination in cyclic pinching model

Previous state	Check condition	Possible current state	Positive excursions	Negative excursions
Unloading in primary half cycle ending at cross-over	$(F_i \Delta_i) \leq 0$	$(F_i \Delta_i) > 0 \rightarrow \Delta_i > \Delta_{i-1} $ $(F_i \Delta_i) < 0 \rightarrow \Delta^c - \Delta_i > \Delta^c - \Delta_{i-1} $		
Unloading in follower half cycle ending at cross-over	$(F_i \Delta_i) \leq 0$	$(F_i \Delta_i) > 0 \rightarrow \Delta_i > \Delta_{i-1} $ $(F_i \Delta_i) < 0 \rightarrow \Delta^c - \Delta_i > \Delta^c - \Delta_{i-1} $		

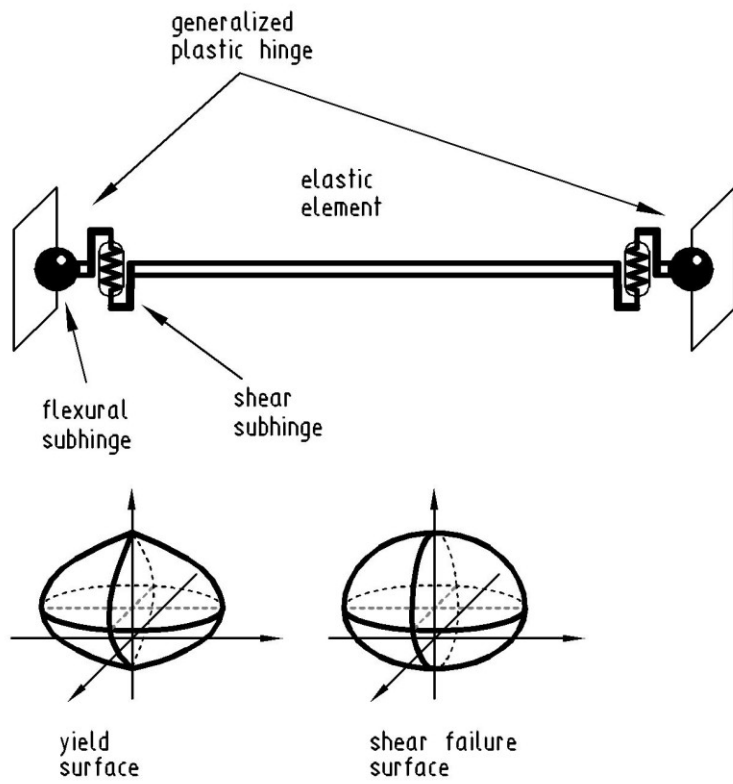


Figure 3-1 Schematics of the element

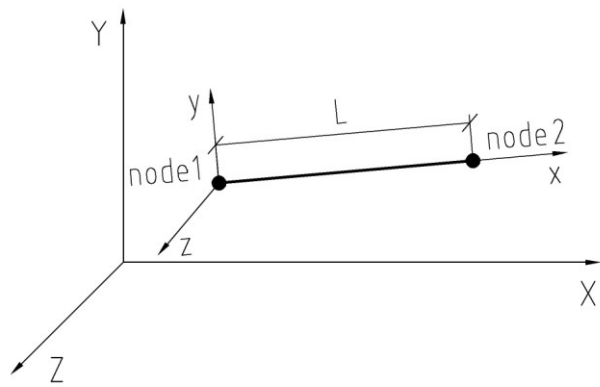


Figure 3-2 Orientation of the element

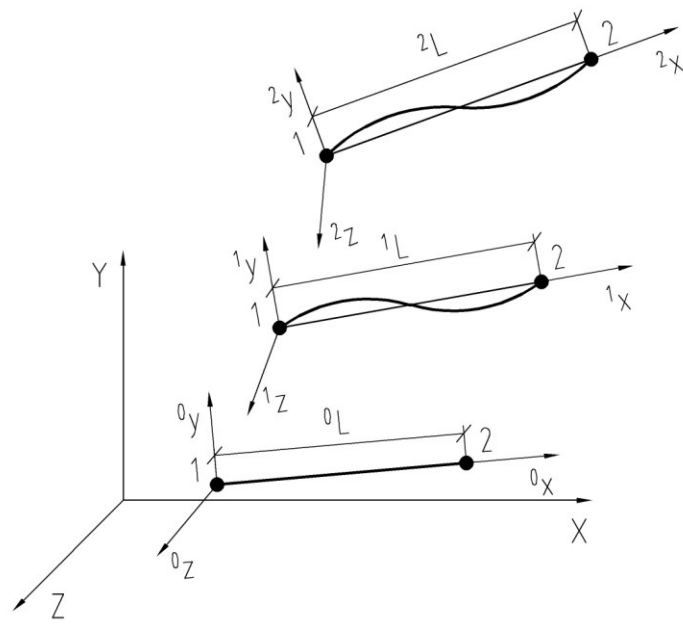


Figure 3-3 Motion of a three-dimensional beam-column element

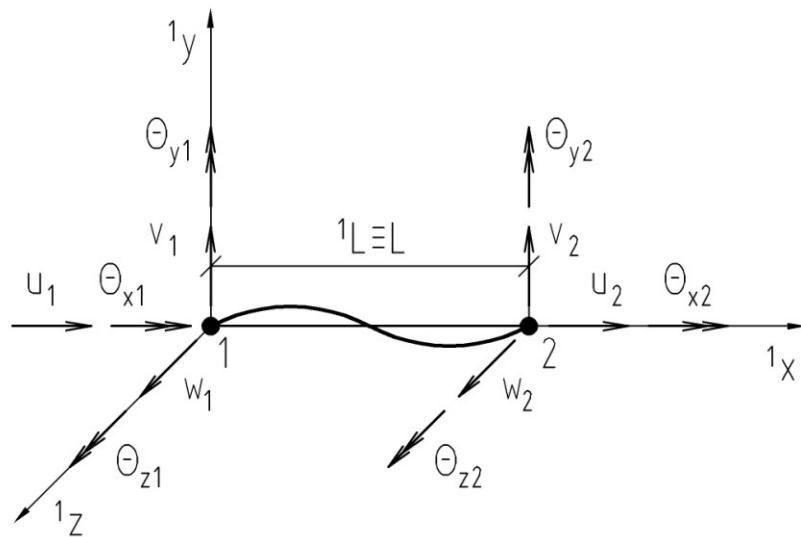


Figure 3-4 Cartesian degrees of freedom of the element in Deformed Configuration (1)

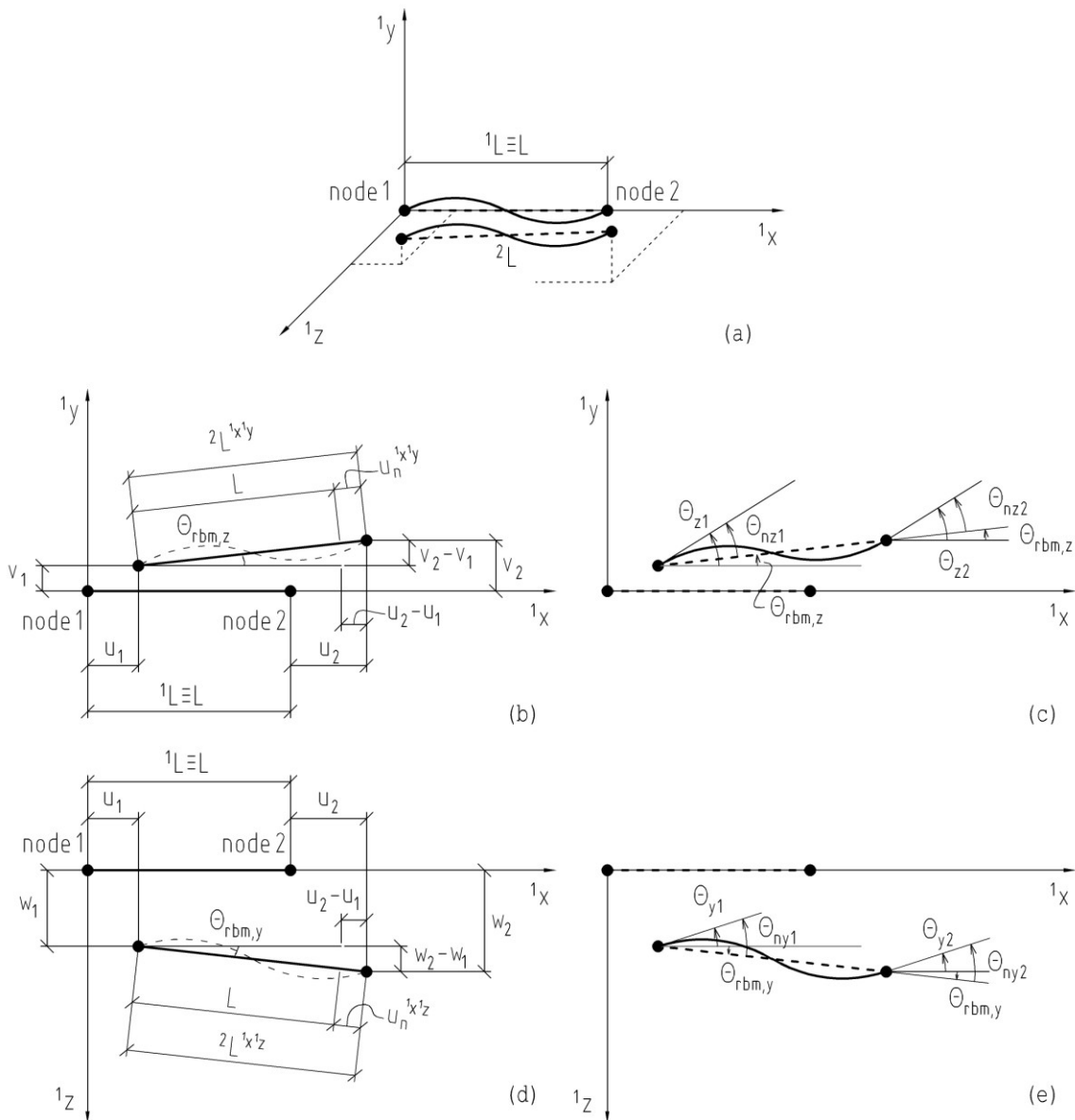


Figure 3-5 Force recovery – natural deformation approach: (a) Deformed Configuration (2); (b) Nodal displacements, projection in $^1x - ^1y$ plane; (c) Rotations, projection in $^1x - ^1y$ plane; (d) Nodal displacements, projection in $^1x - ^1z$ plane; (e) Rotations, projection in $^1x - ^1z$ plane

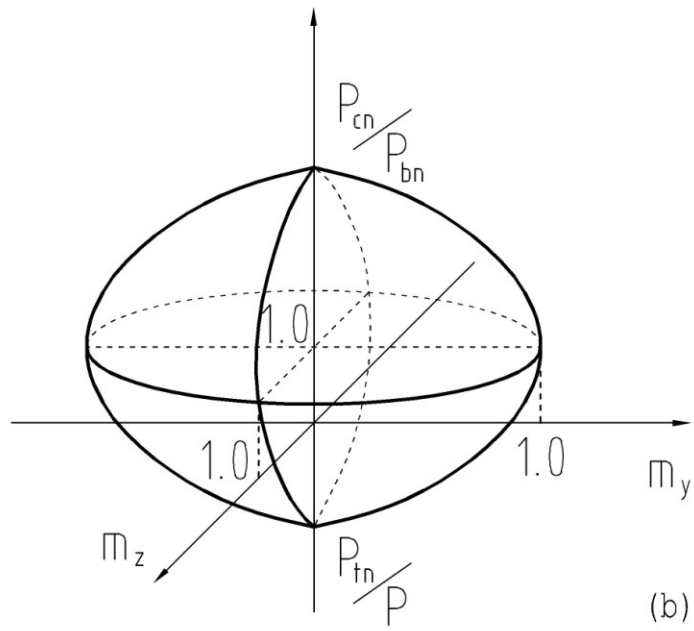
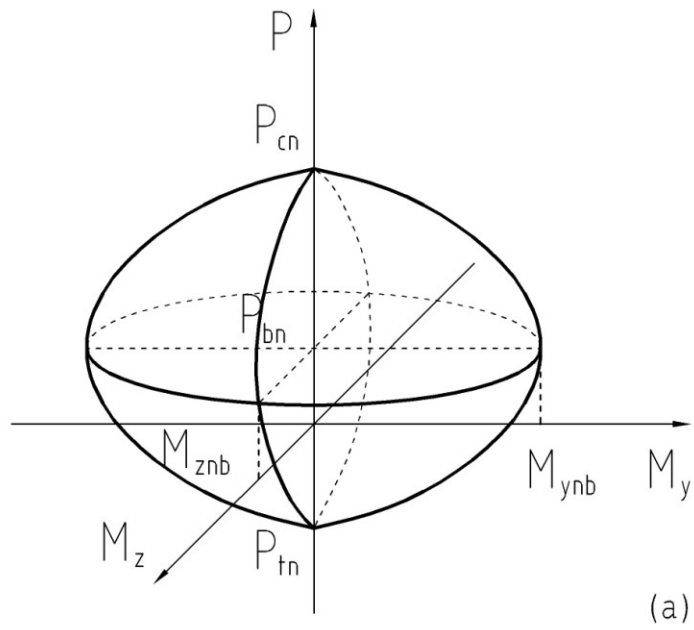


Figure 3-6 Yield surface model: (a) Force space; (b) Normalized force space

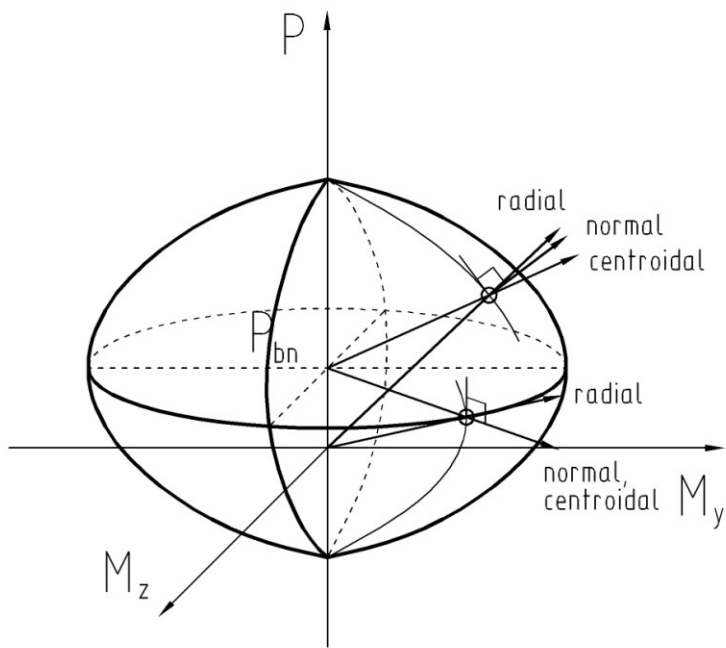


Figure 3-7 Examples of yield surface direction of evolution

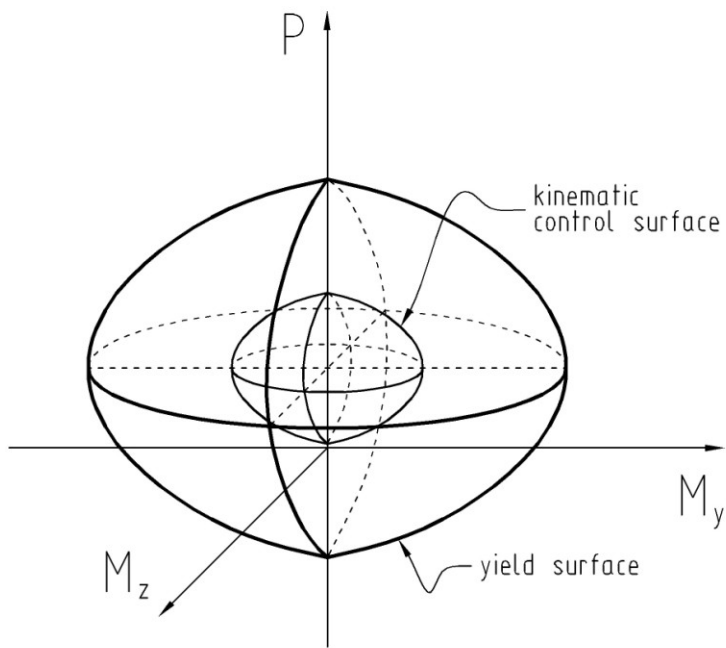


Figure 3-8 Kinematic control surface

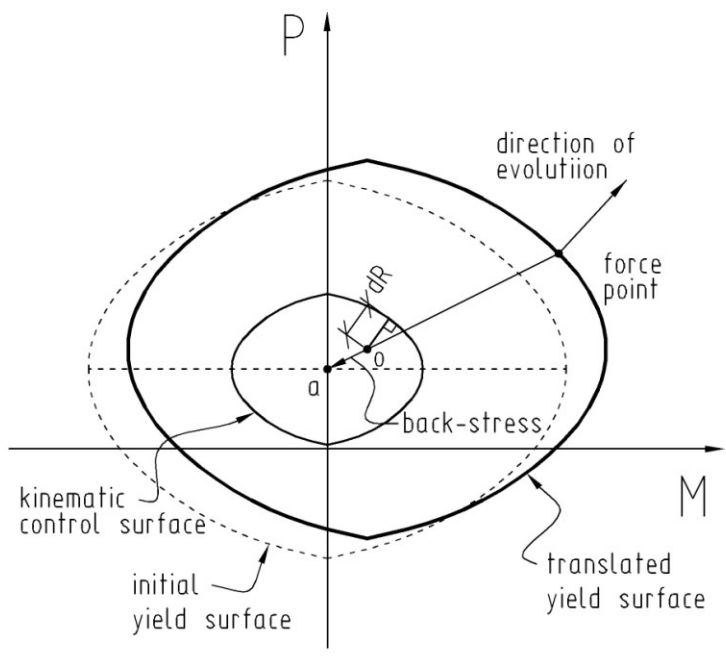
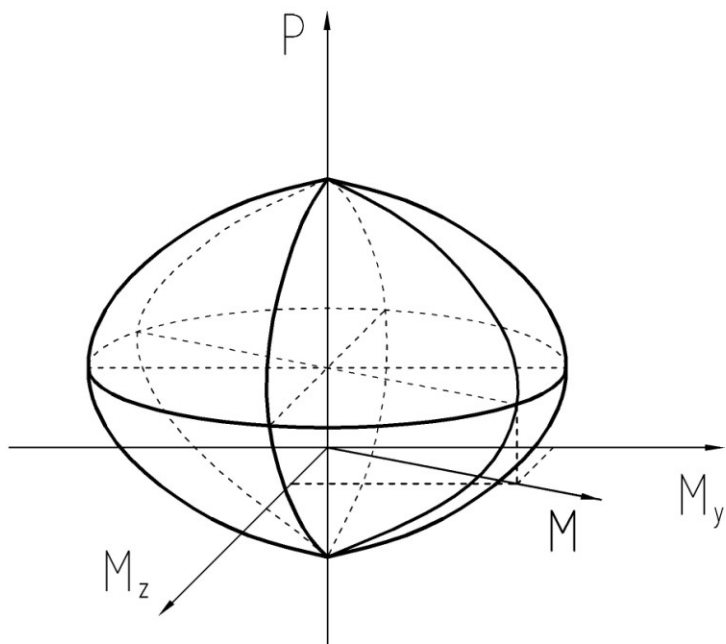


Figure 3-9 Translation in the kinematic control surface evolution model

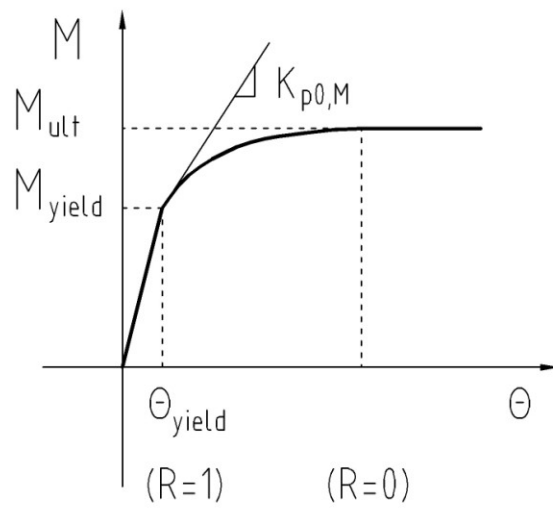


Figure 3-10 Force-deformation response with kinematic hardening model

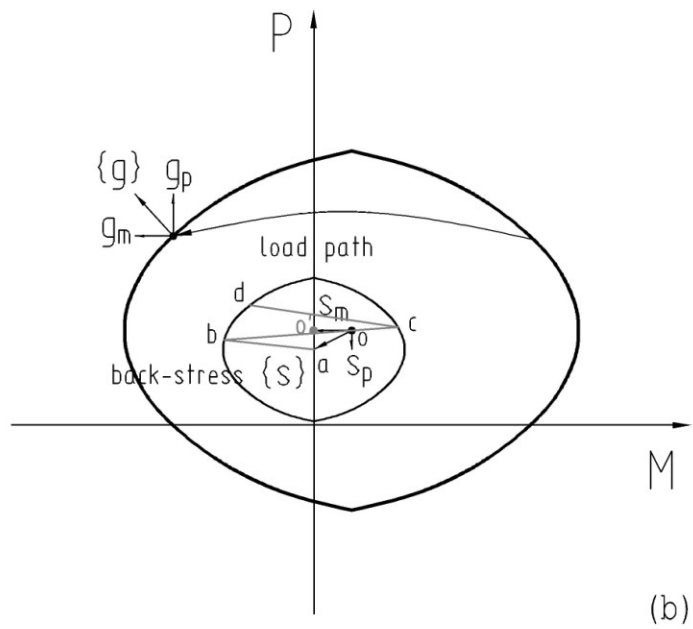
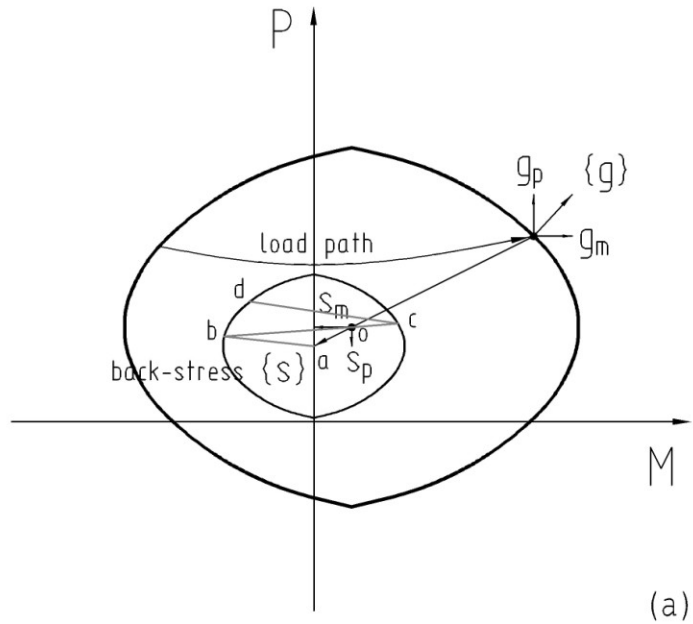


Figure 3-11 Kinematic control surface evolution model for cyclic loading: (a) $s_m g_m < 0$; (b) $s_m g_m > 0$

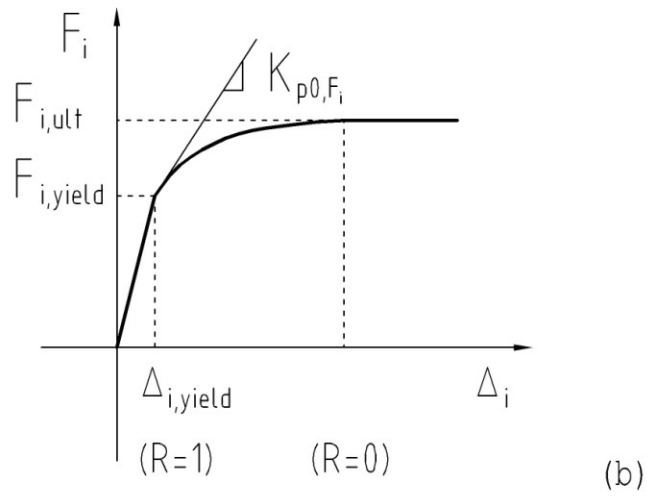
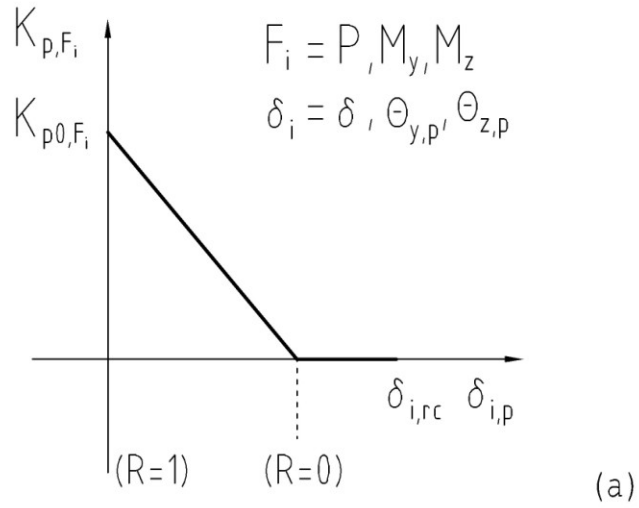


Figure 3-12 Relation of inelastic element response to plastic stiffness in kinematic control evolution model: (a) Relation between plastic stiffness and plastic deformations; (b) Force-deformation response

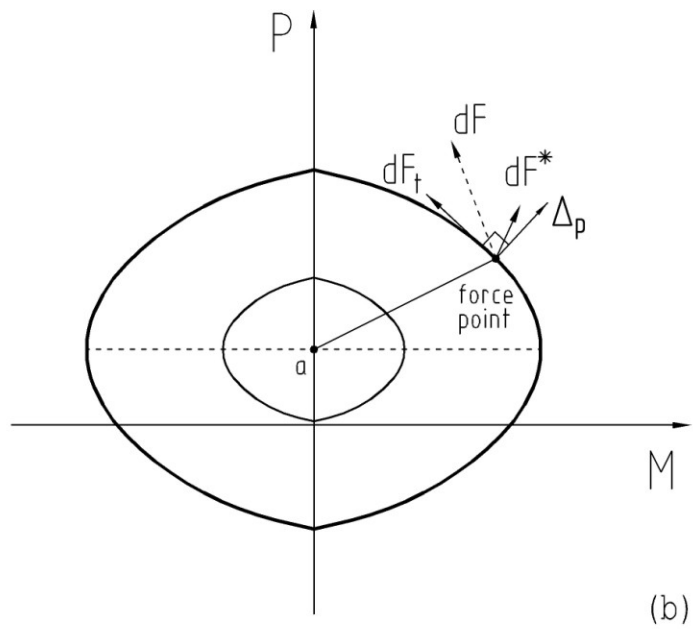
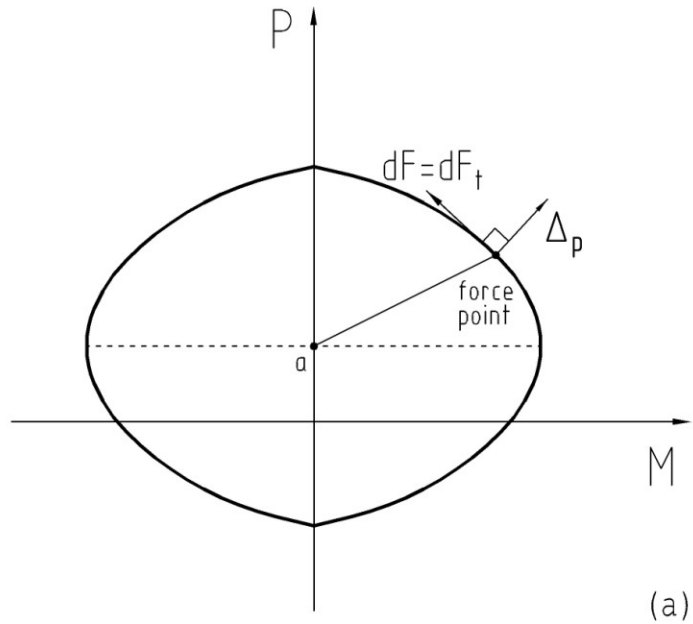


Figure 3-13 Incremental force: (a) Elastic-perfectly plastic material; (b) Elasto-plastic-strain hardening material

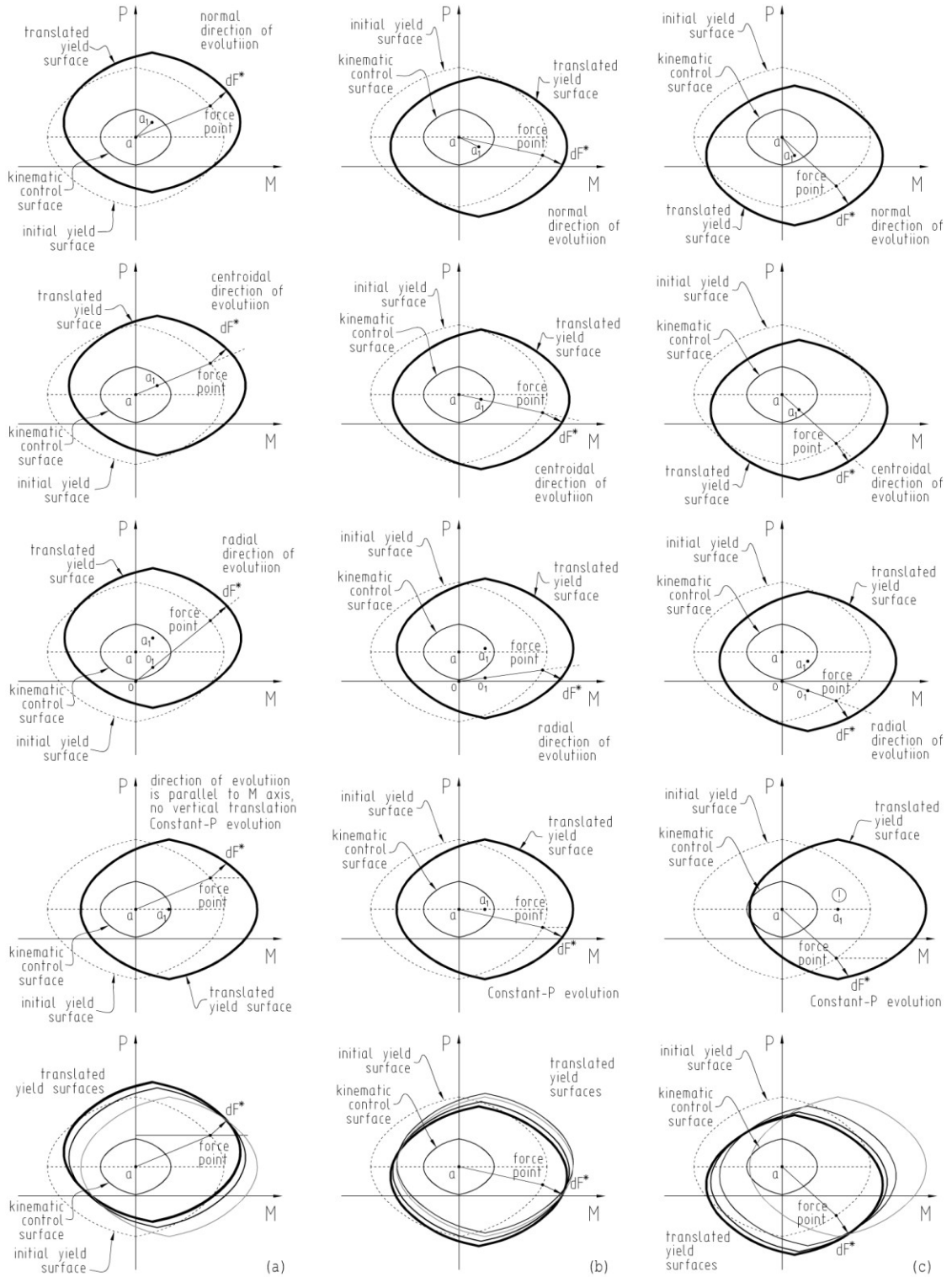


Figure 3-14 Directions of evolution: (a) Axial load is above the balanced failure point level (compression); (b) Axial load is below the balanced failure point level but above zero level (compression); (c) Axial load is below zero level (tension)

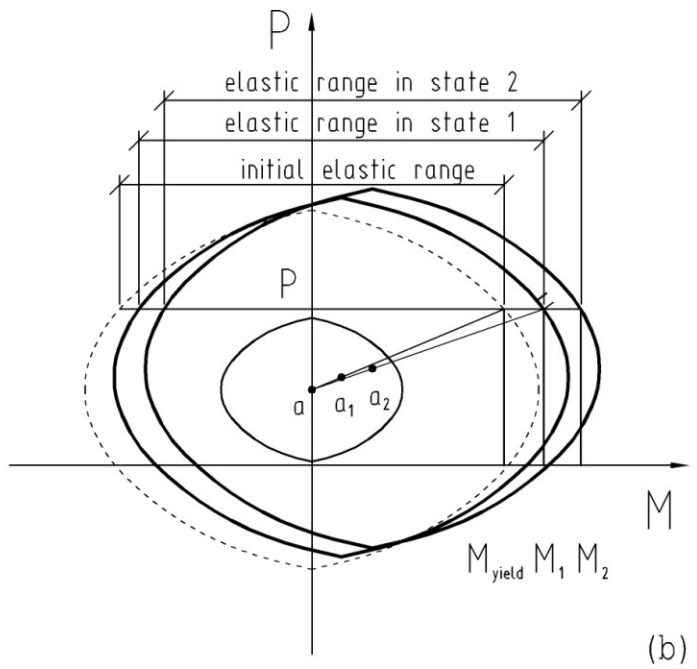
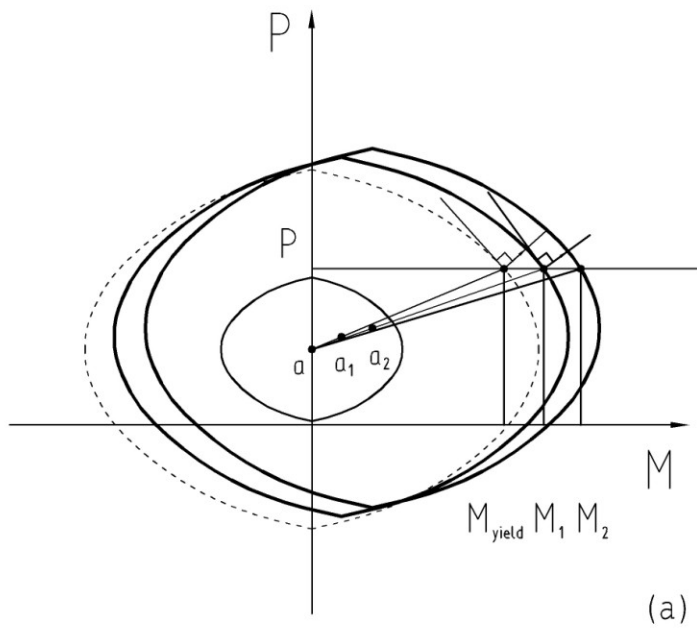


Figure 3-15 Centroidal direction of evolution with constant axial force: (a) Motion of the yield surface; (b) Change in elastic range during evolution

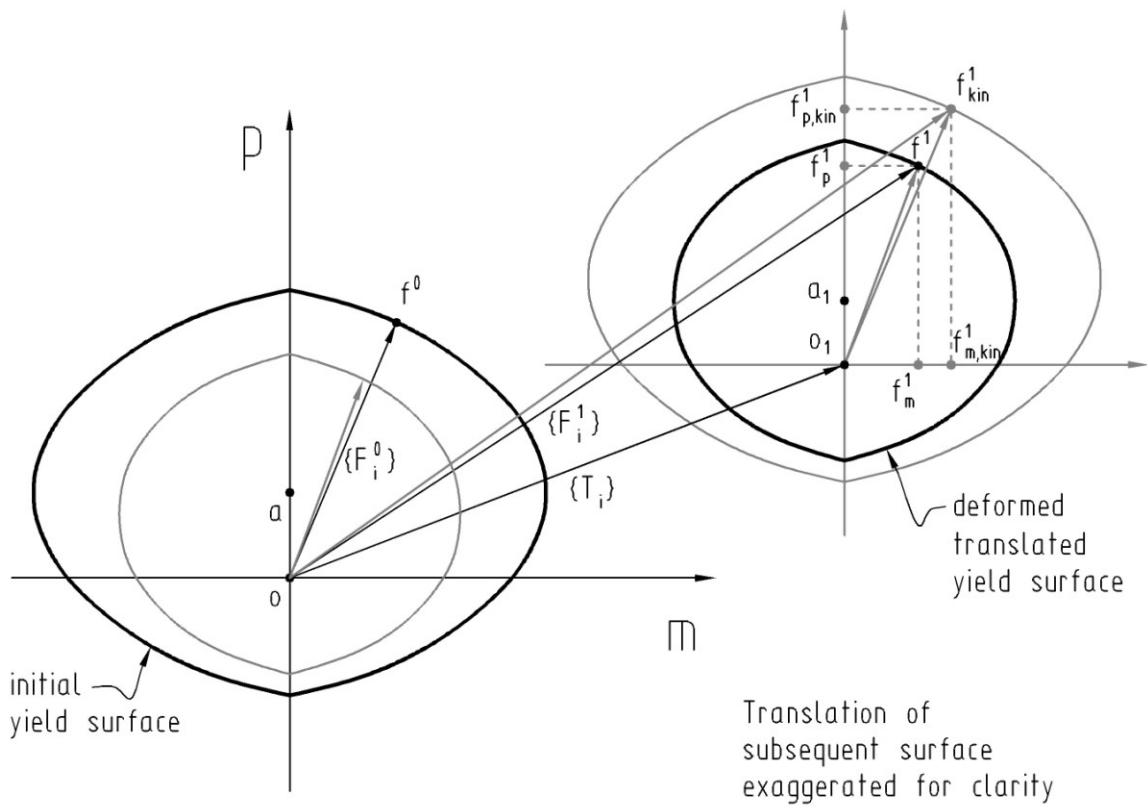


Figure 3-16 Mapping between subsequent surface (translated deformed) and initial yield surface

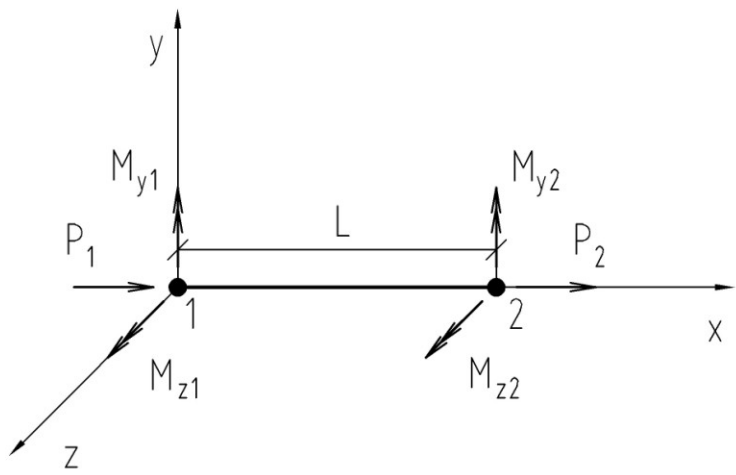


Figure 3-17 Inelastic force recovery example

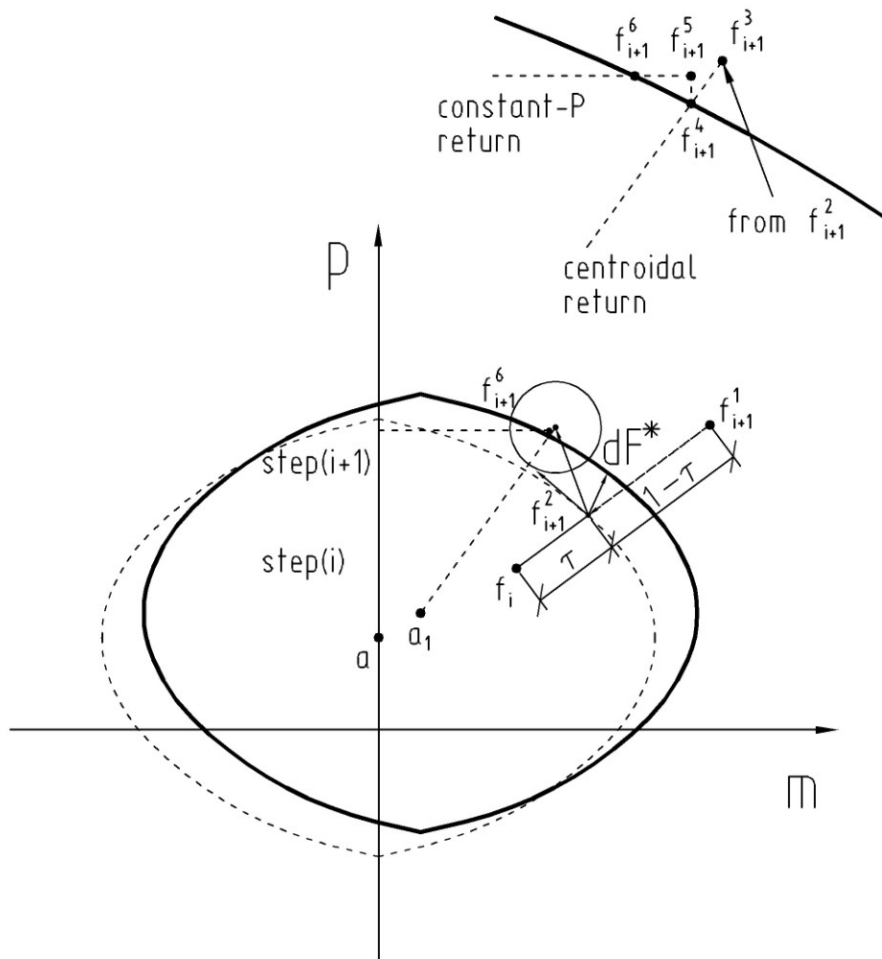


Figure 3-19 Force recovery for the case of hardening materials

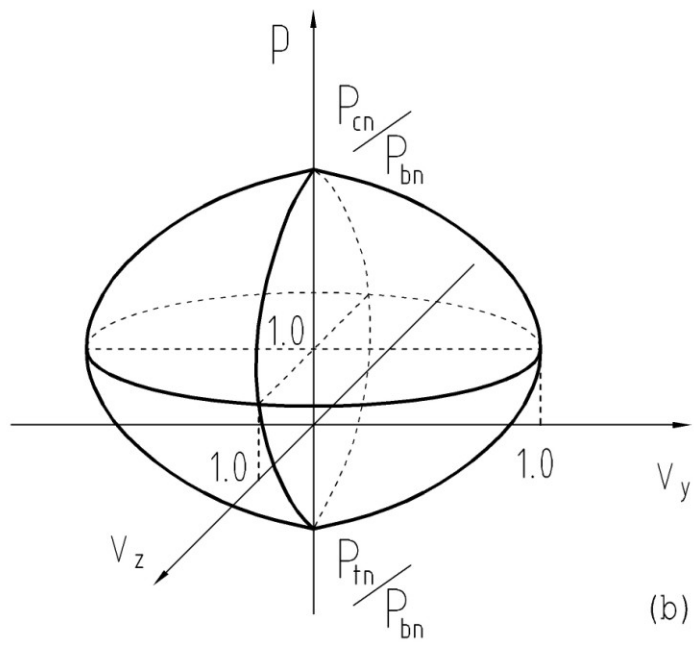
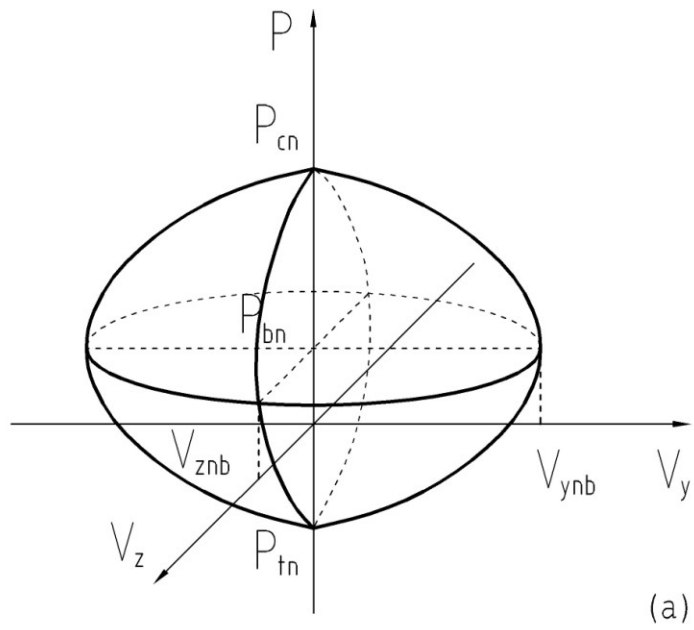


Figure 3-20 Shear failure surface model: (a) Force space; (b) Normalized force space

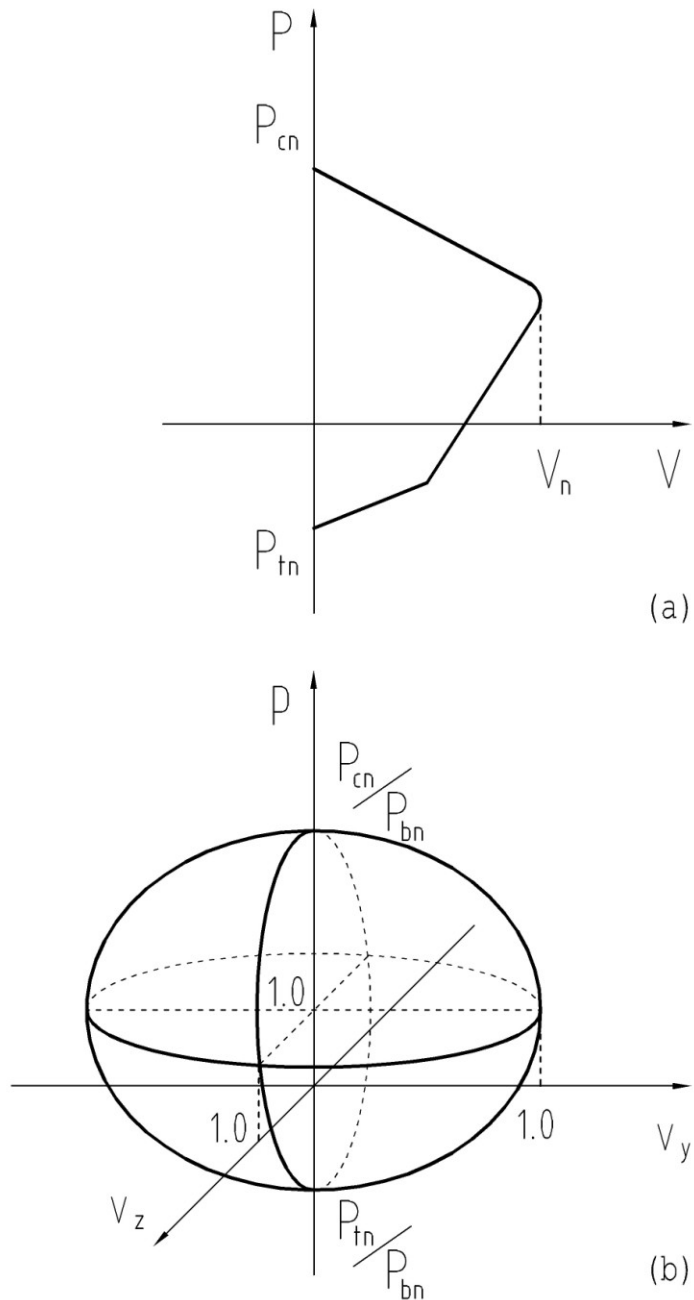


Figure 3-21 Axial force-shear force interaction diagram: (a) Experimental (Vecchio and Collins 1986); (b) Model proposed by ElMandooh Galal and Ghojarah (2003)

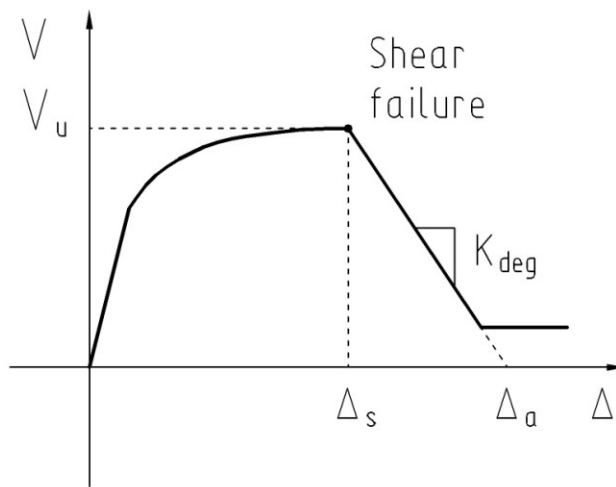


Figure 3-22 Degradation stiffness in post-shear failure force-deformation response

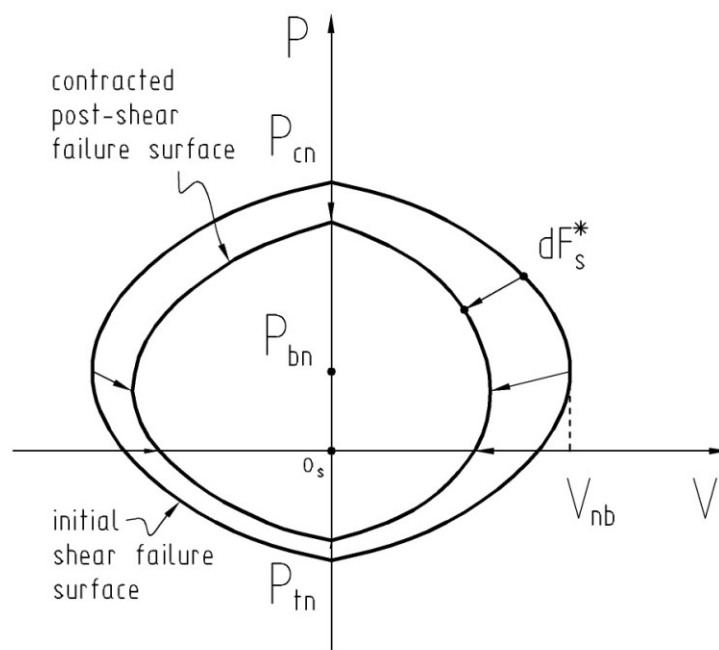


Figure 3-23 Non-uniform contraction evolution model

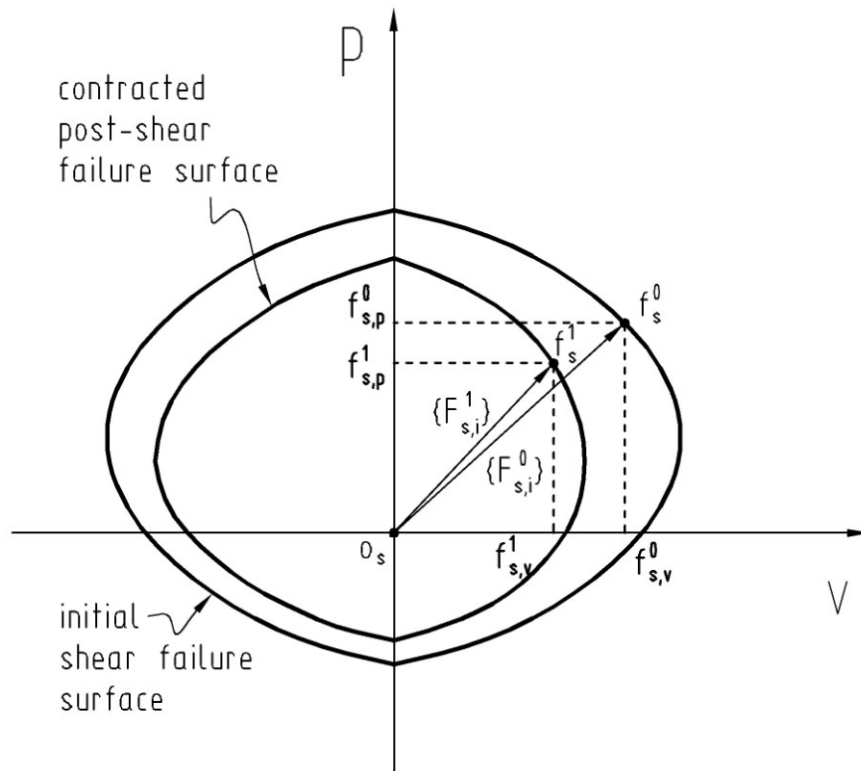


Figure 3-24 Mapping between subsequent surface (deformed) and initial shear failure surface

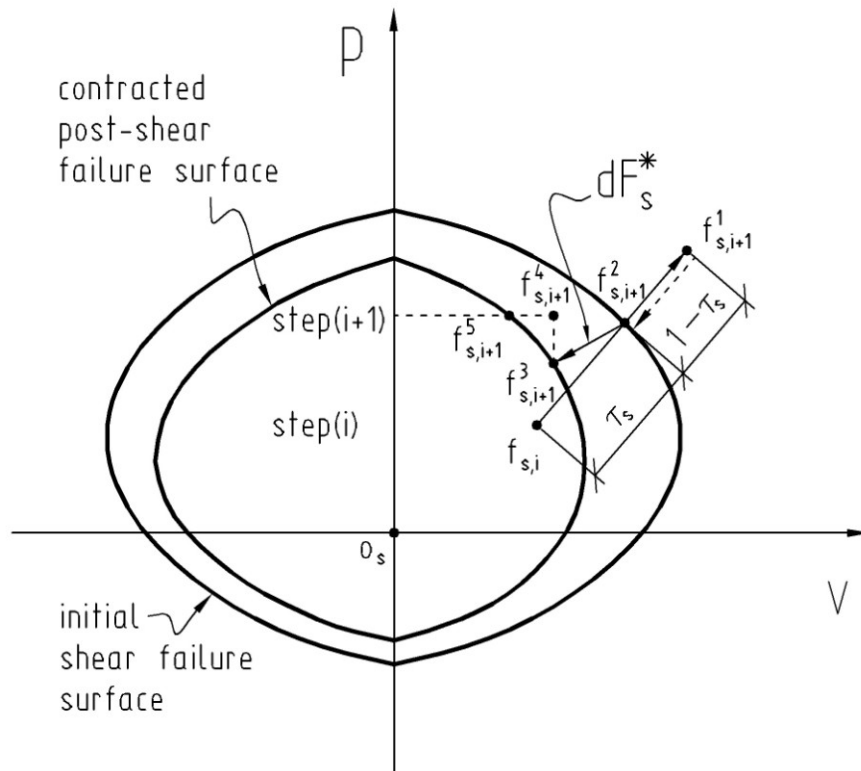


Figure 3-25 Force recovery to the shear failure surface

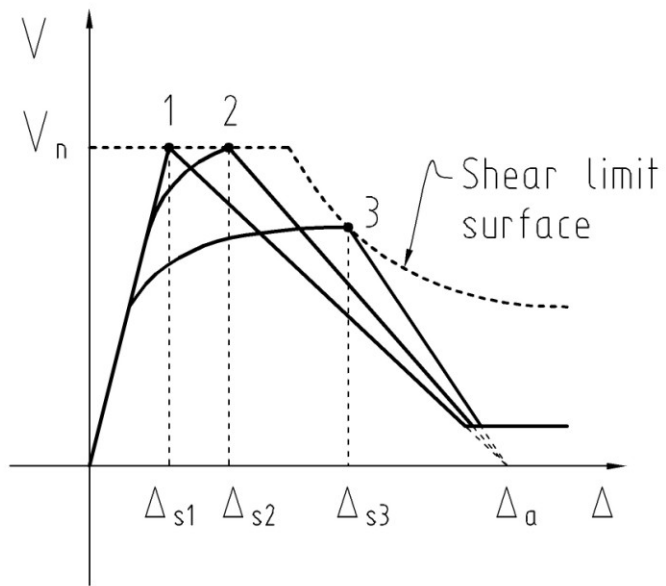


Figure 3-26 Shear failure modes

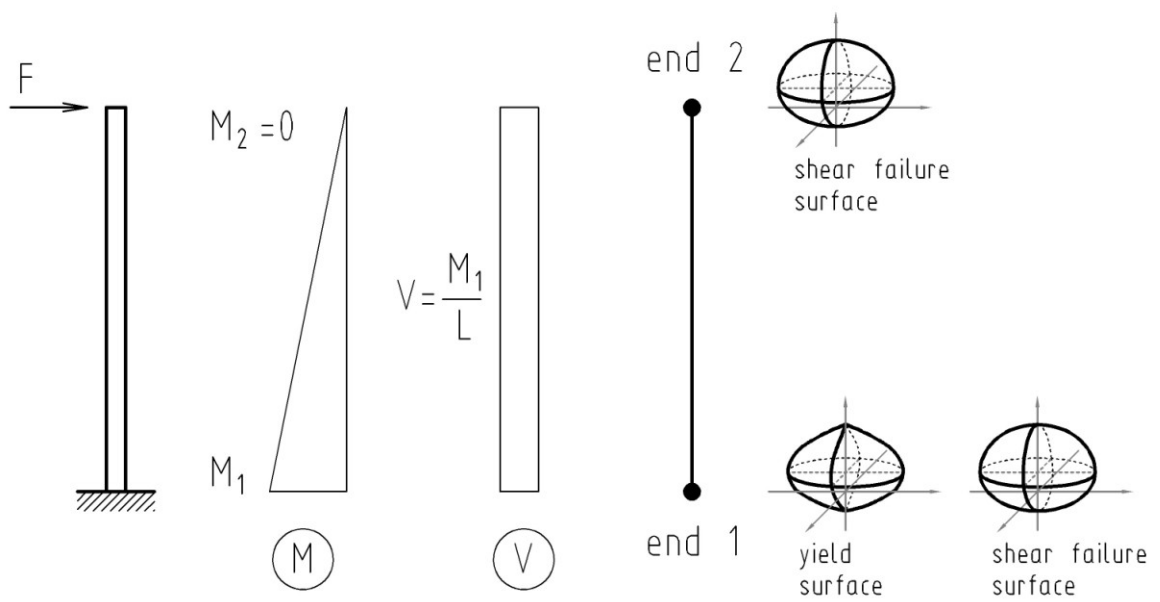


Figure 3-27 Model of a cantilever column

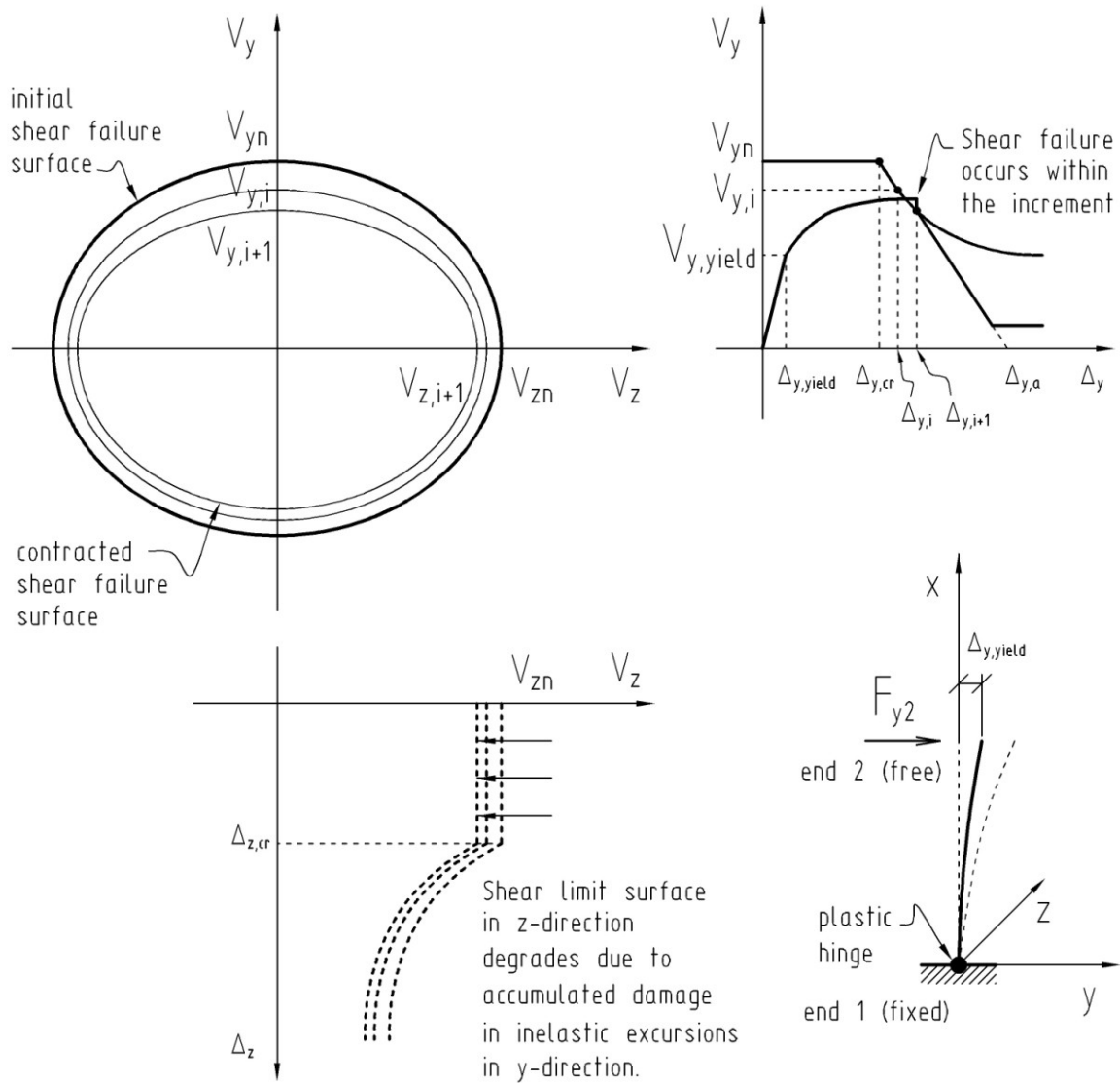


Figure 3-28 Post-yield degradation of the shear failure surface

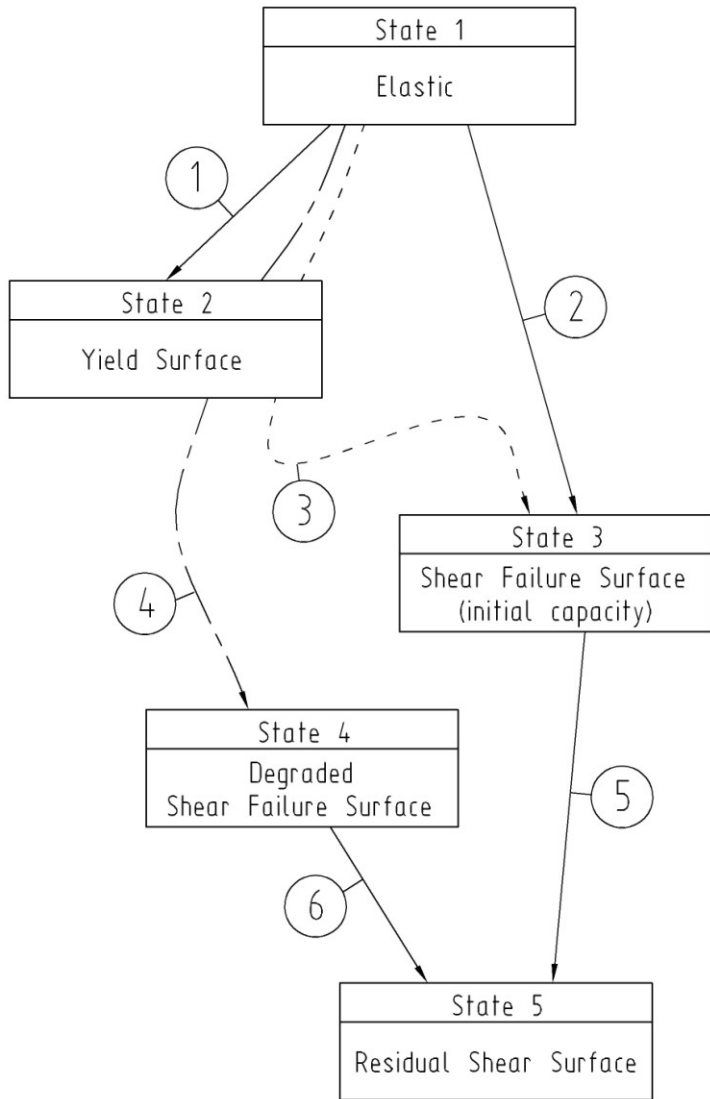


Figure 3-29 State diagram for monotonic loading

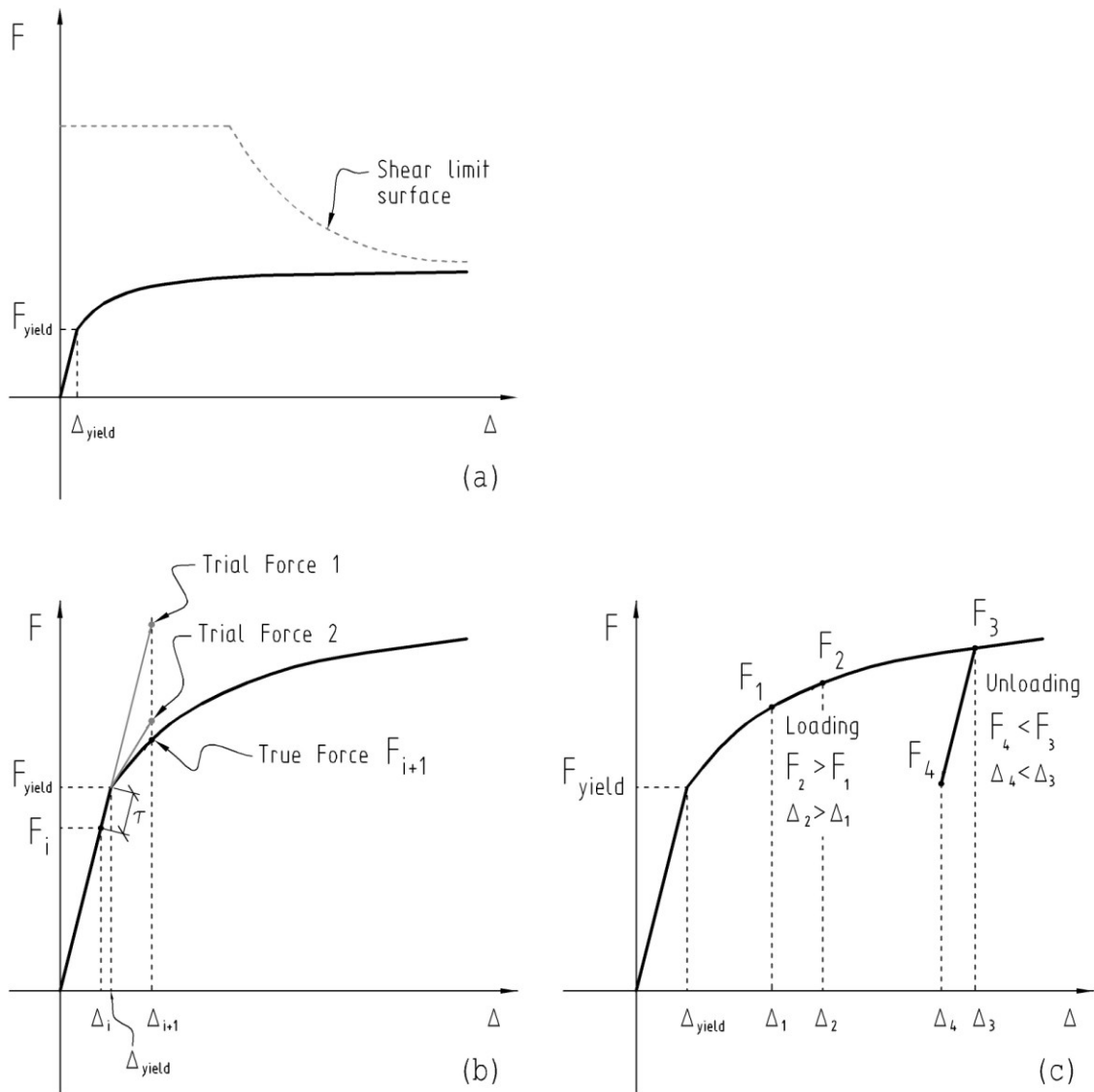


Figure 3-30 Path 1: from elastic (state 1) to flexural yielding (state 2): (a) Force-deformation response for ductile behaviour; (b) Transition from state 1 to state 2; (c) Loading/Unloading criteria for state 2

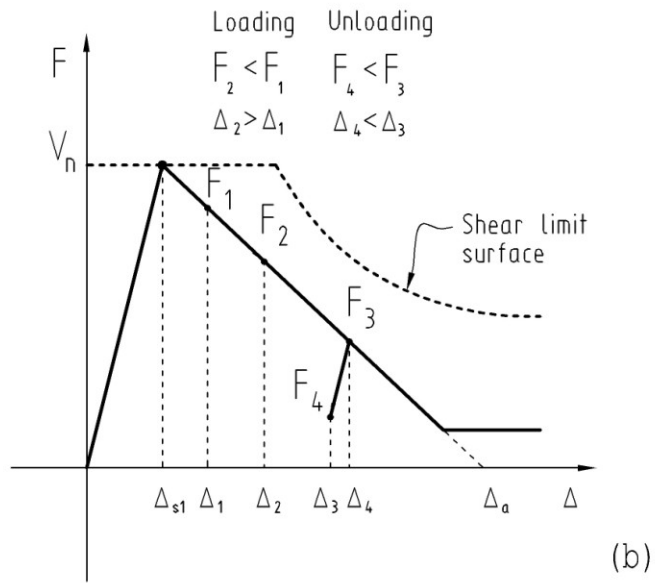
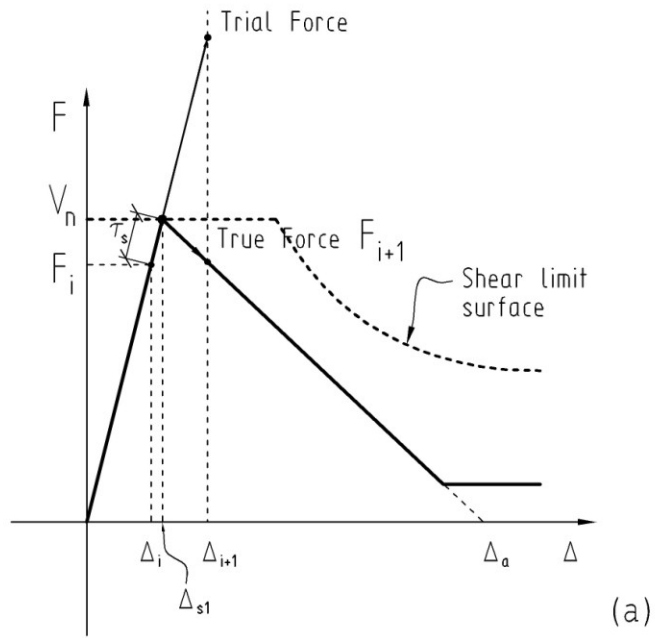


Figure 3-31 Path 2: from elastic (state 1) to shear failure and post-shear failure degradation (state 3):

(a) Transition from state 1 to state 3; (b) Loading / Unloading criteria for state 3

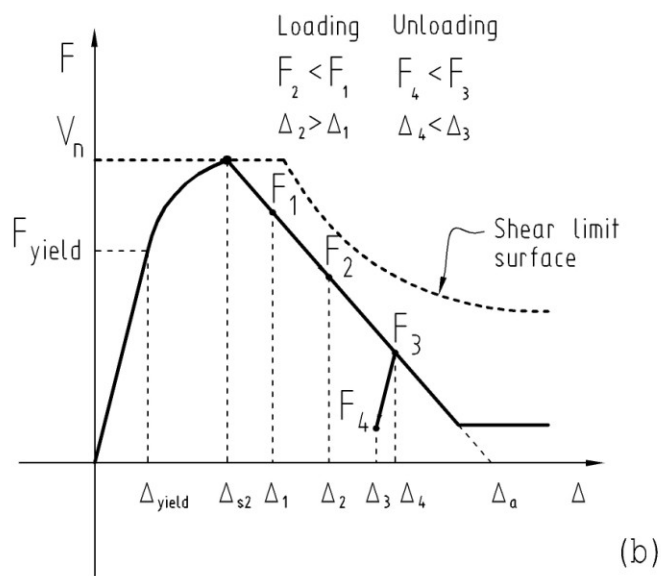
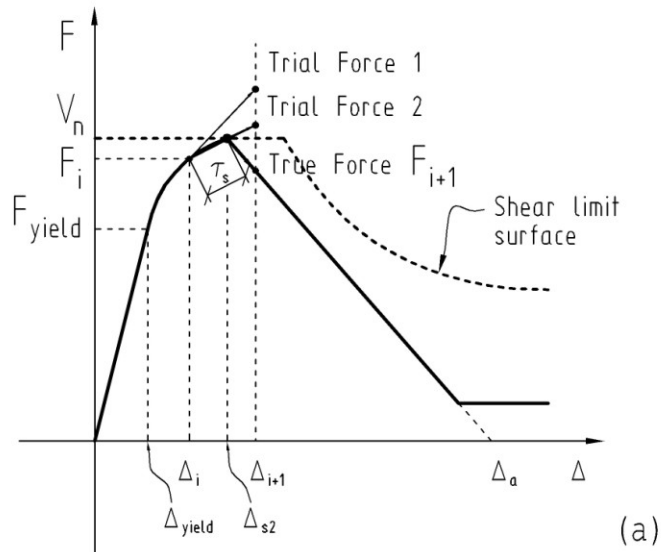


Figure 3-32 Path 3: from elastic (state 1) to flexural yielding (state 2) to shear failure and post-shear failure degradation (state 3); (a) Transition from state 2 to state 3; (b) Loading / Unloading criteria for state 3

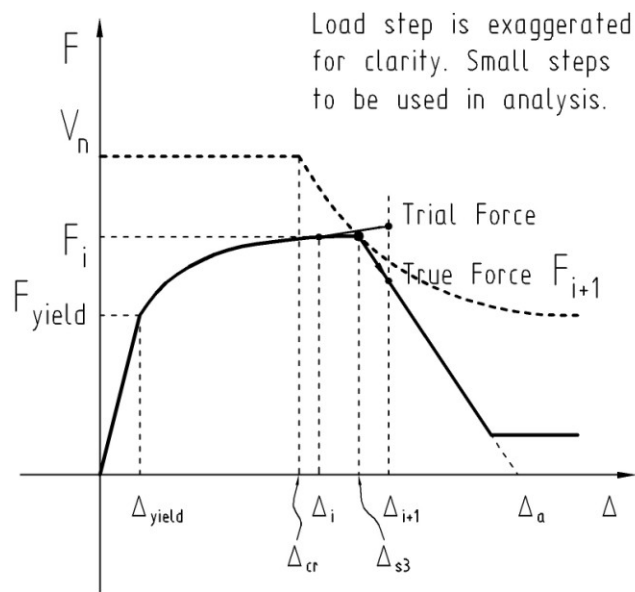


Figure 3-33 Path 4: from elastic (state 1) to flexural yielding (state 2) to shear failure at degraded capacity and post-shear failure degradation (state 4)

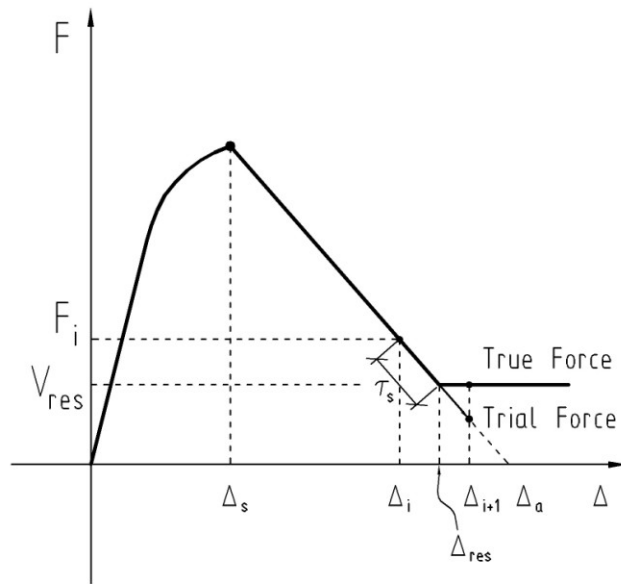


Figure 3-34 Path 5 (6): from shear failure and post-shear failure degradation (state 3 or 4) to residual shear capacity (state 5)

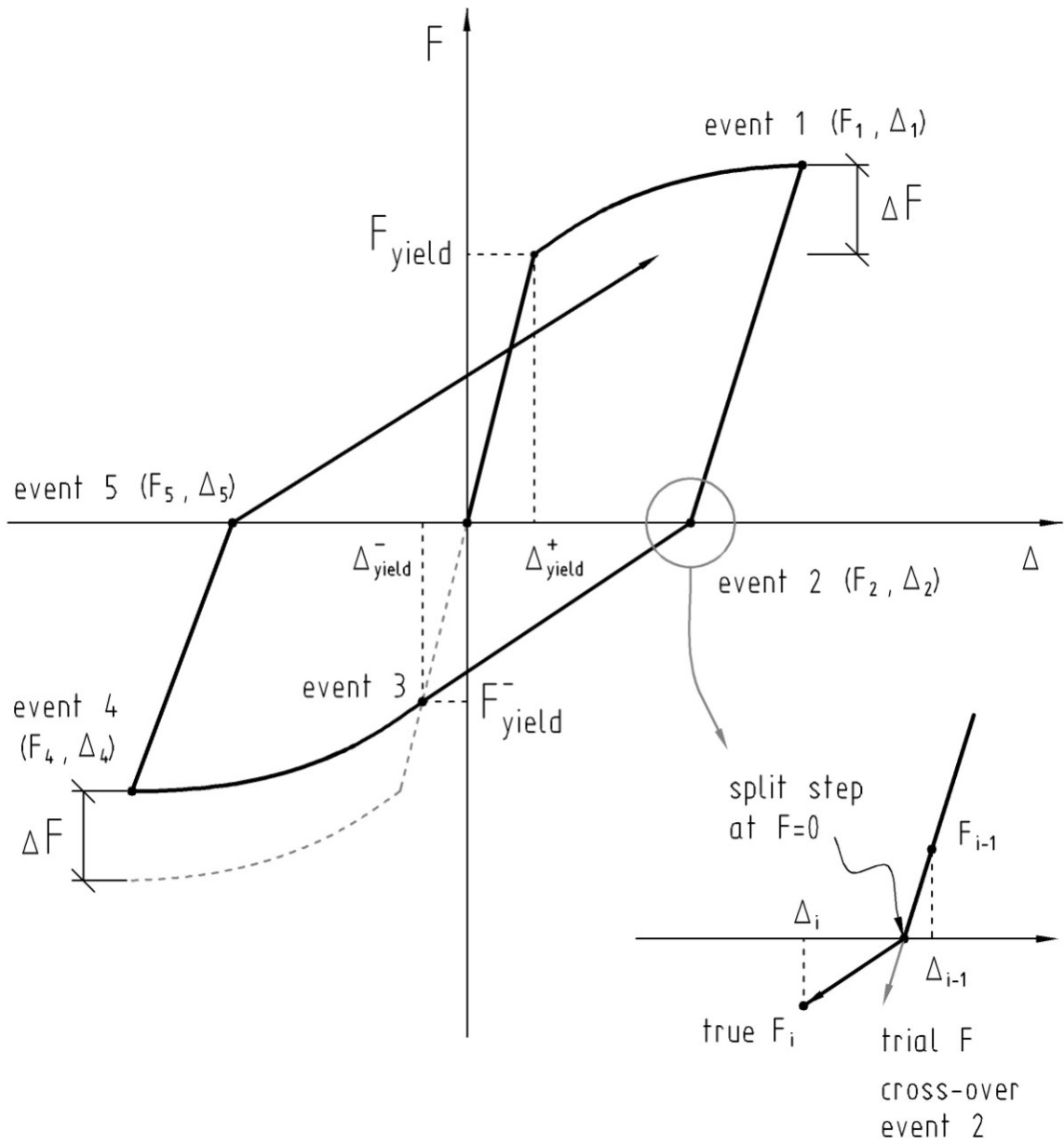


Figure 3-35 Cyclic stiffness model – full cycle

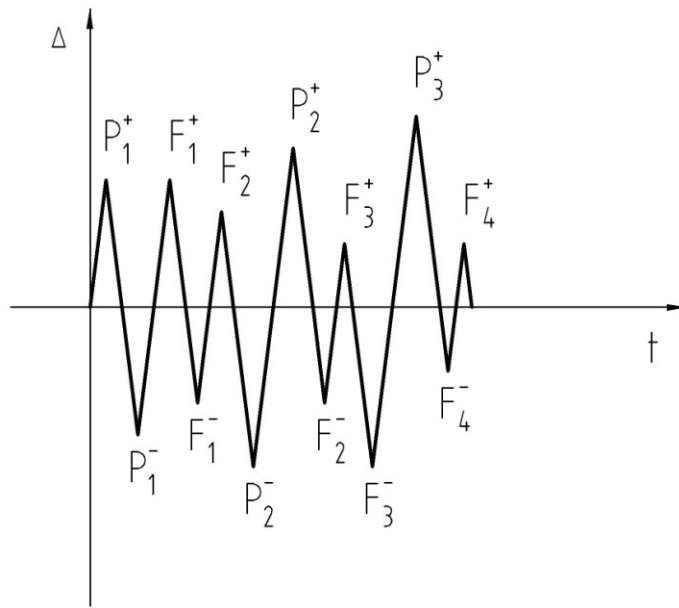


Figure 3-36 Example of primary and follower half cycles

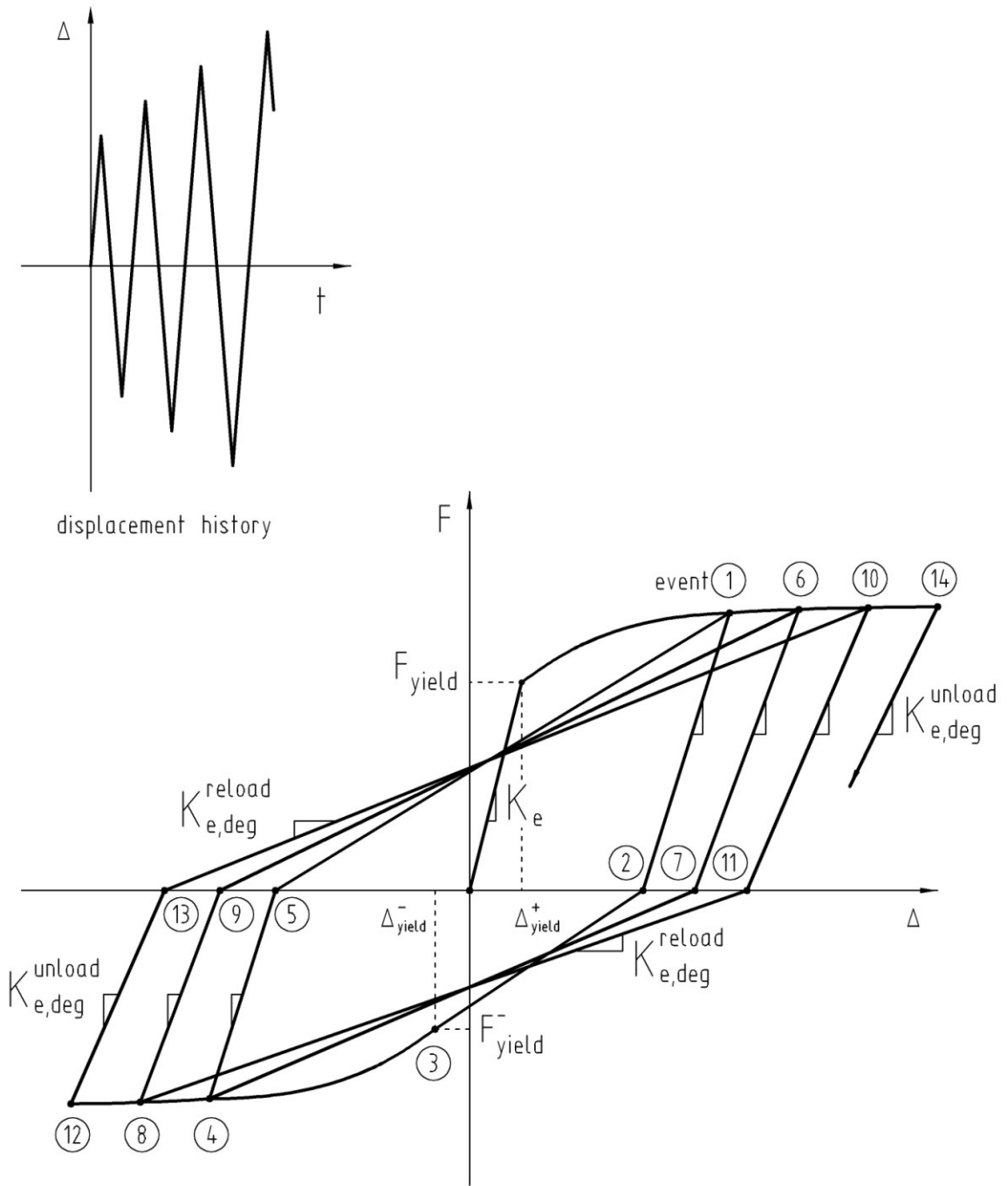


Figure 3-37 Cyclic stiffness model – response to primary half cycles in positive and negative excursions

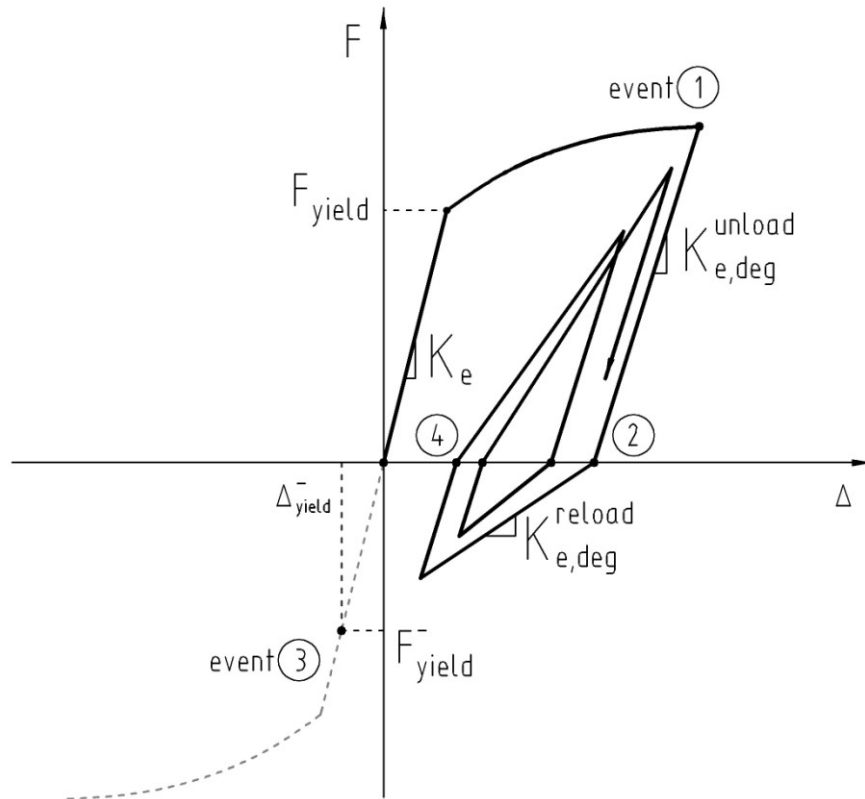
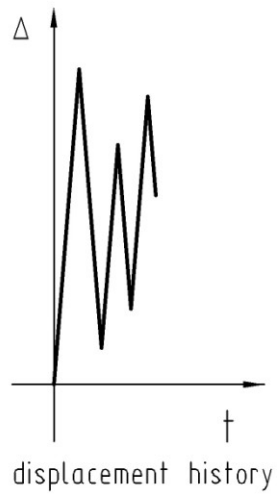


Figure 3-38 Cyclic stiffness model – response to a primary half cycle and follower half cycles in positive excursions

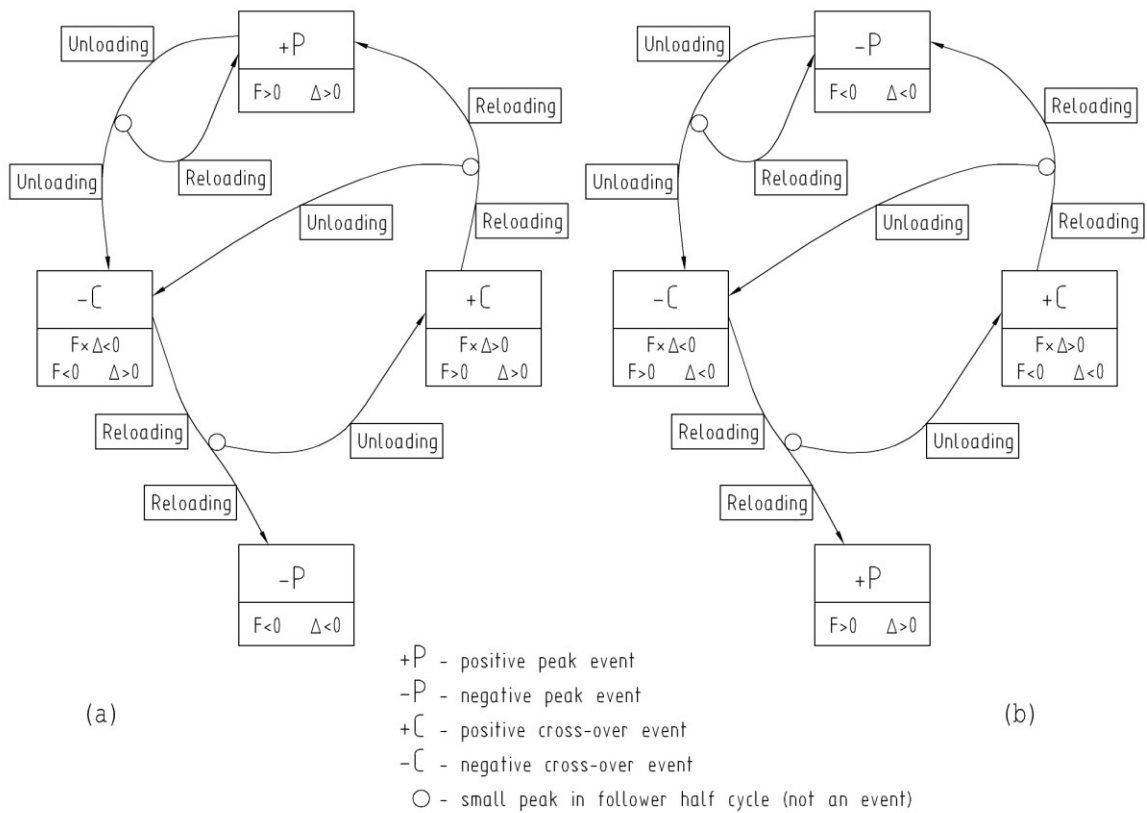


Figure 3-39 State transition diagram in cyclic stiffness model: (a) positive excursions; (b) negative excursions

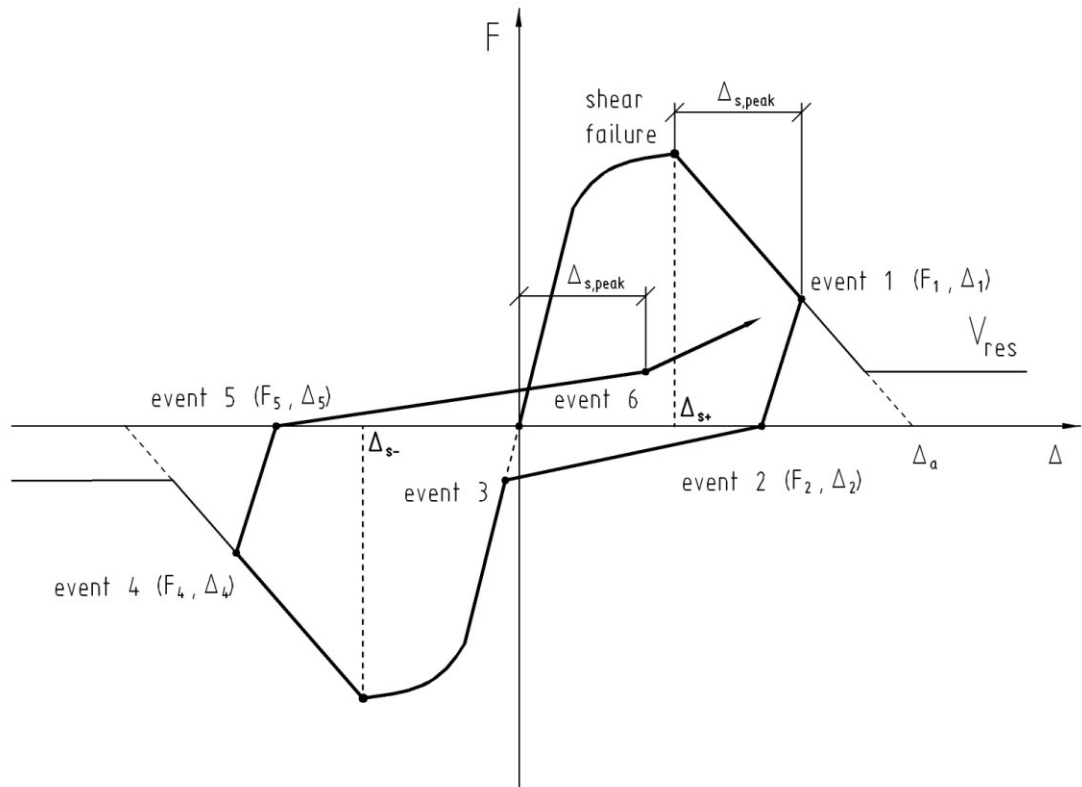


Figure 3-40 Cyclic pinching model – full cycle

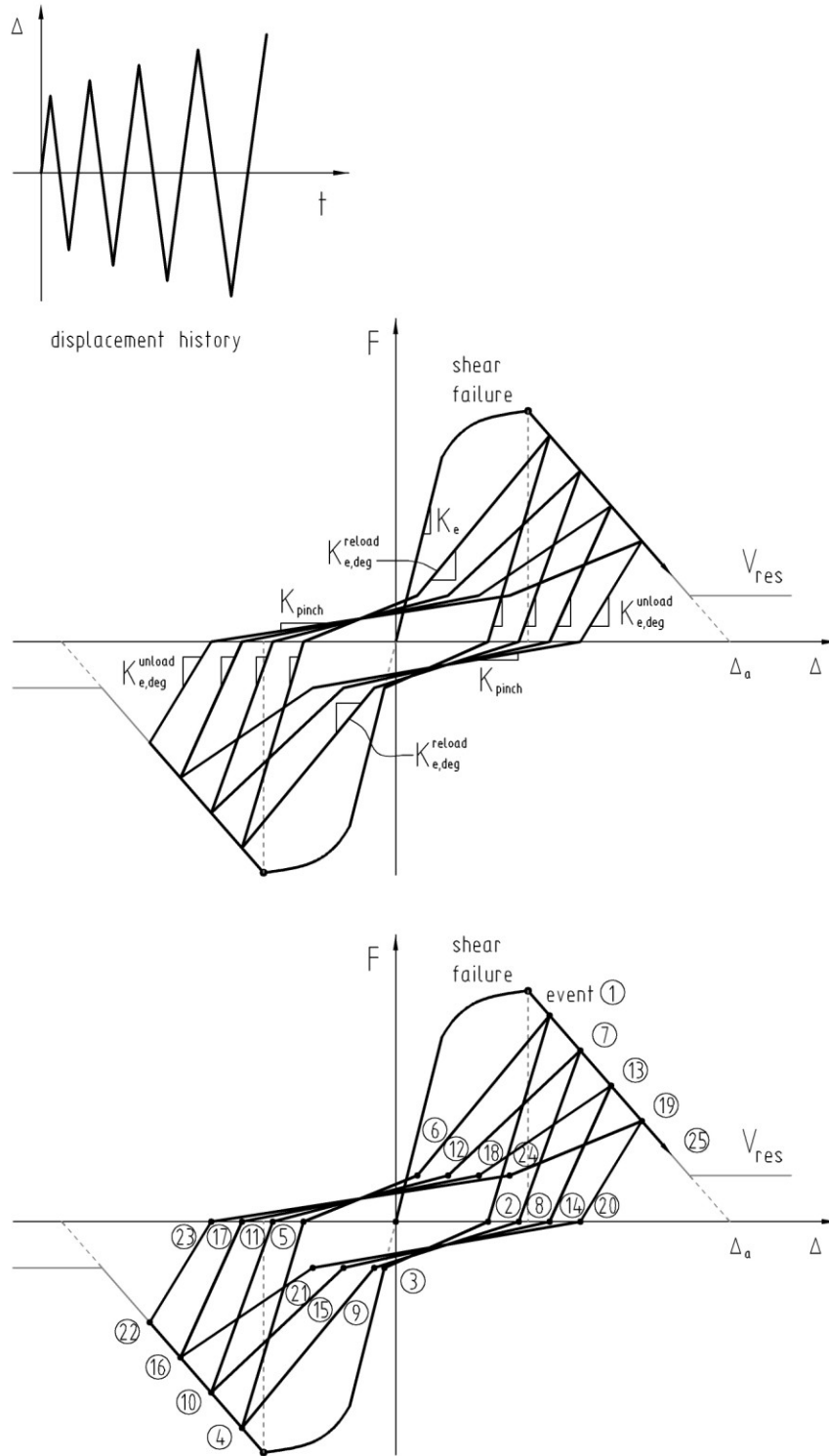


Figure 3-41 Cyclic pinching model – response to primary half cycles in positive and negative excursions

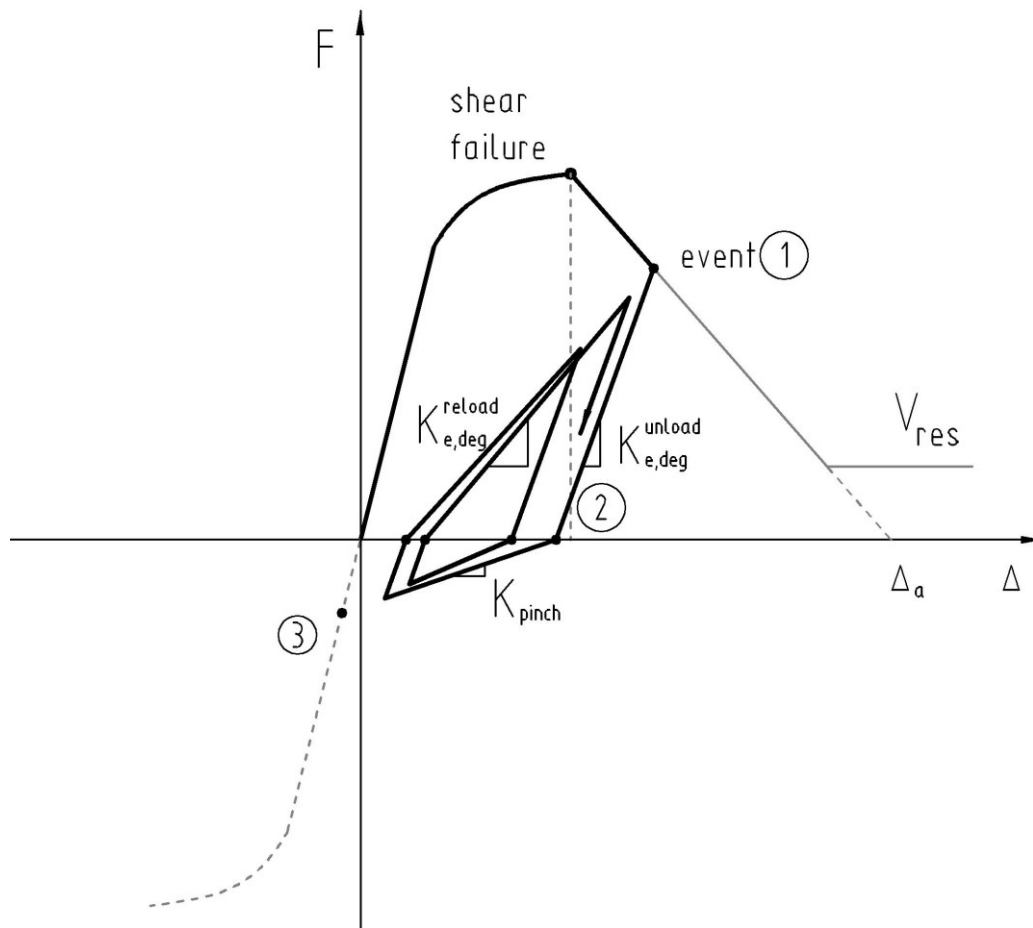
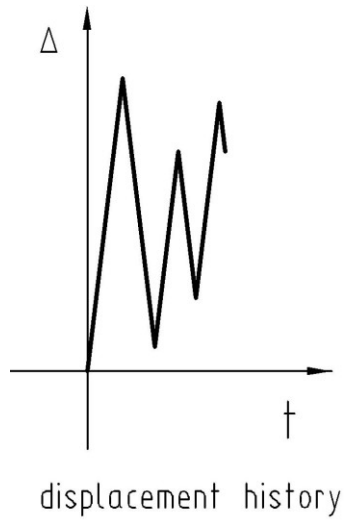


Figure 3-42 Cyclic pinching model – response to a primary half cycle and follower half cycles in positive excursions

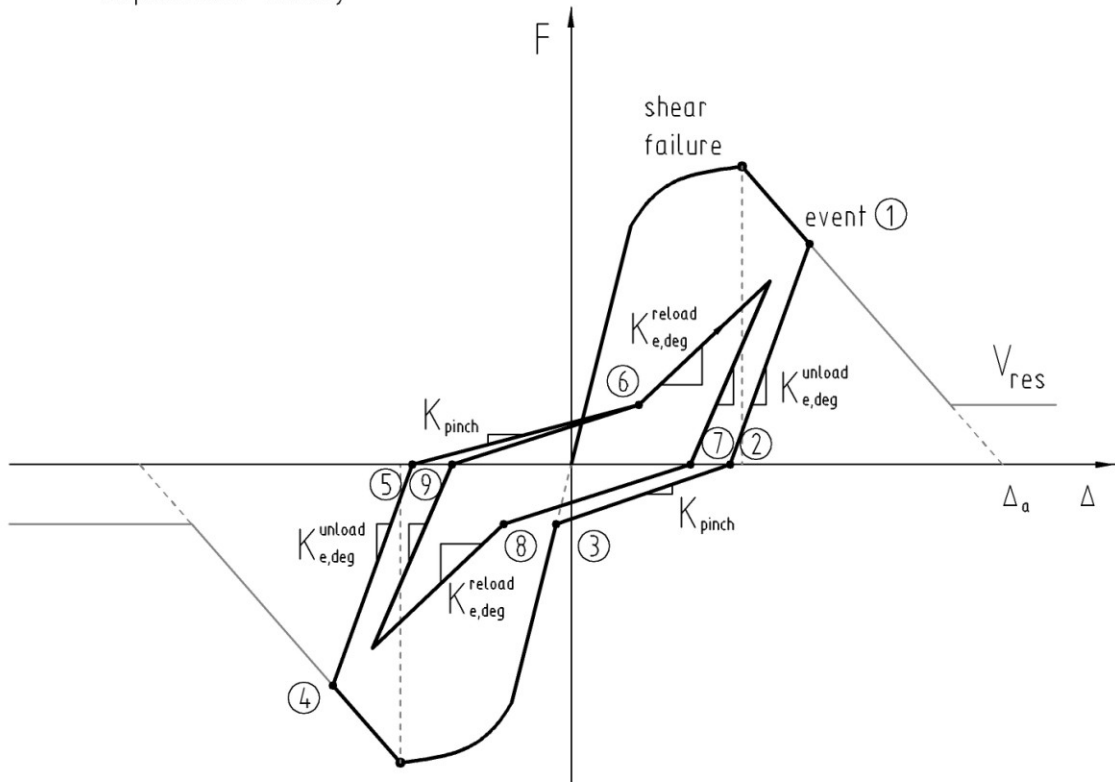
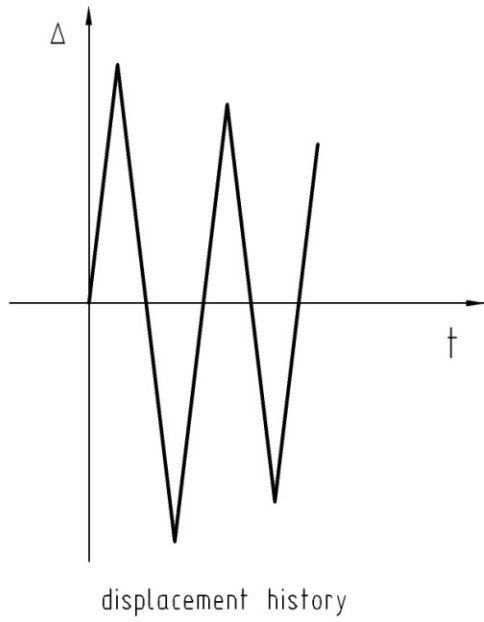


Figure 3-43 Cyclic pinching model – response to a primary half cycle and follower half cycles in positive and negative excursions

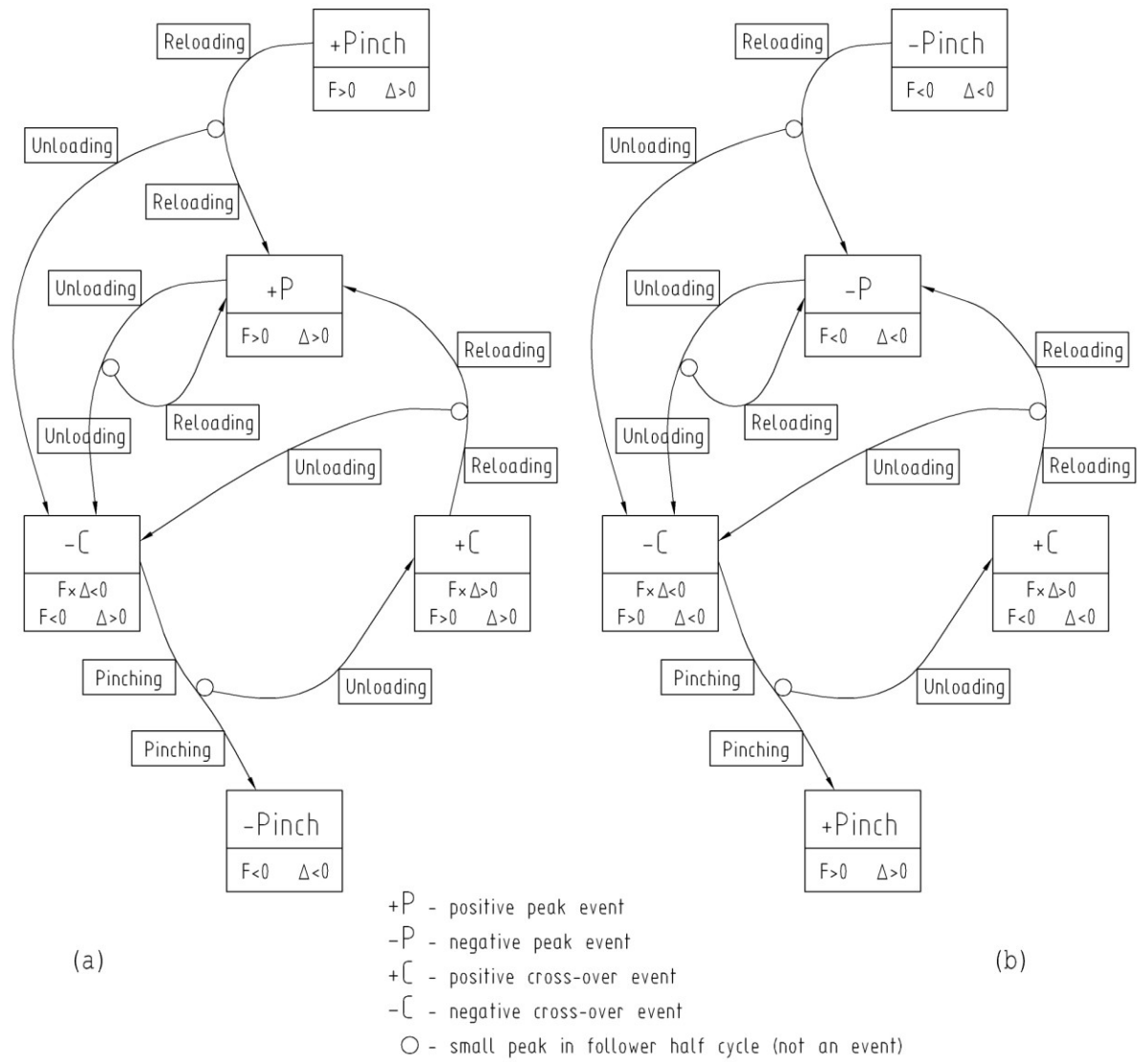


Figure 3-44 State transition diagram in cyclic pinching model: (a) positive excursions; (b) negative excursions

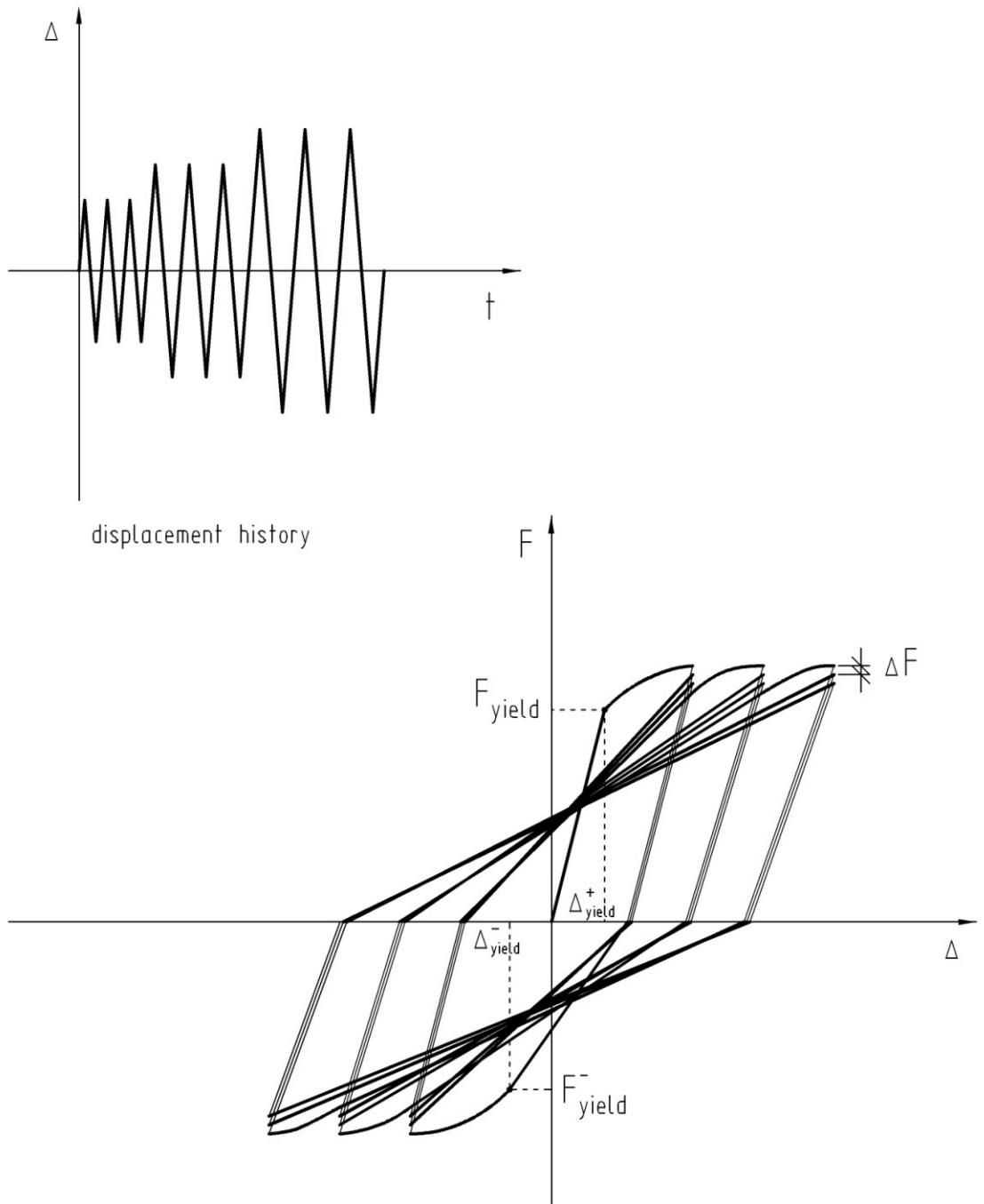


Figure 3-45 Cyclic strength degradation model – flexural response

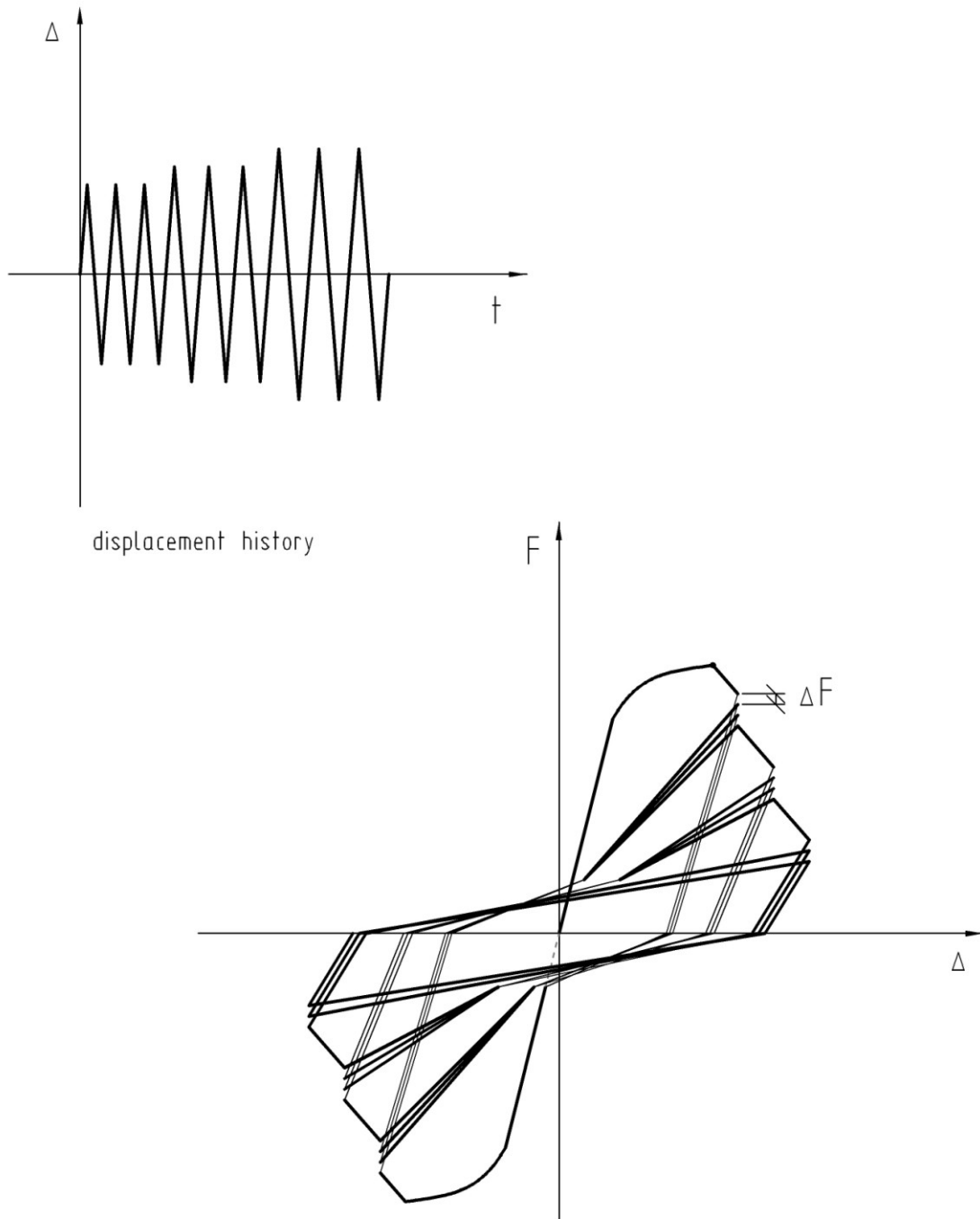


Figure 3-46 Cyclic strength degradation model – shear response



Figure 3-47 Schematics of element – damage model interaction

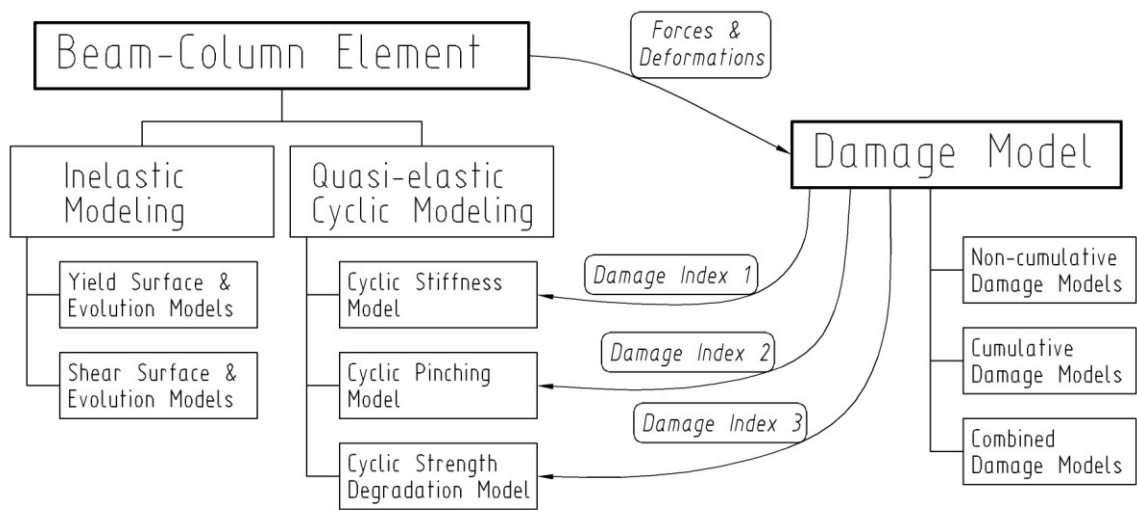


Figure 3-48 Interaction with damage model at element component level

4 Chapter: Implementation of Models in OpenSees Software

Framework

4.1 Introduction

In the past most finite element analysis programs were developed using Fortran programming language and were procedural in nature. In more recent years, object oriented programming concepts have been introduced and tried for developing and maintaining finite element analysis software. OpenSees (Open System for Earthquake Engineering and Simulation) is a large-scale software framework for finite element analysis based on object oriented programming concepts. The key advantage of using object oriented methodologies is that programming languages with object oriented capabilities, such as C++, provide attributes to the program components that offer flexibility and code extensibility. Abstractions, encapsulation, inheritance and polymorphism are among the attributes that contribute to creating program structures with potential to be expanded and extended.

In this chapter, background to object oriented programming concepts is first provided, followed by an overview of the finite element classes for structural systems in OpenSees and a detailed discussion of the implementation of new models proposed in this research.

4.1.1 Object Oriented Programming Concepts

Object oriented programming languages, such as C++, provide structures which encapsulate the data and the operations performed on that data. These structures are

known as classes. The encapsulated data are the attributes and the operations are the member functions of the class. The behaviour of the class is characterized by the member functions, also referred to as methods. Classes that invoke the methods of another class are referred to as clients of the latter. The methods for communication with other classes are declared through interfaces, thus allowing the class to have its attributes and method implementations hidden from the clients. This feature has important implications: the hiding of information enables modifications to a member function without affecting the code of the clients.

An instance of a class is known as an object. All objects of a class share the same copy of member functions but each object owns a separate copy of the data unless the data is declared static in the class declarations. The interaction between objects is performed according to the declarations in the class interface. An object invokes its methods in response to messages or function calls sent to it by objects of the client class.

The key features of object oriented design include abstractions, inheritance and polymorphism. Abstractions describe the behaviour characteristics of a class; inheritance is a property that allows the derivation of new classes from existing base classes; and polymorphism is a feature that allows run-time implementation of derived classes through virtual methods and dynamic binding. The process of designing object oriented software involves developing abstractions to characterize the behaviour of new classes, establishing the inheritance mechanisms within the class structure, specifying the attributes of the classes and defining the interactions between the classes.

In this approach, a system is represented by a set of base classes which enclose the characteristics of generalized concepts. The base classes are usually abstract and as such they need not necessarily provide the implementation of all the member functions. The special cases of an abstract class are derived through the inheritance property. The new derived classes, also referred to as subclasses, can inherit and extend the behaviour of the parent base class. In a class structure, there may be several levels of subclasses depending on the levels of abstractions. The final classes, which are at the bottom of the class structure hierarchy, must contain all the implementations of the member functions. Instances (objects) can be created only from final classes, also referred to as concrete classes. The attributes and methods in a class can be declared as private, protected or public. Private attributes and methods are property only of the current class, which means that they cannot be inherited by subclasses and cannot be accessed by clients of the class. Protected status extends the scope of attributes and methods to subclasses, whereas public status extends the scope to the entire system. There are two types of inheritance, interface inheritance and implementation inheritance. In the interface inheritance, the base class is focused entirely on describing the behaviour and the implementation of member functions is to be provided by the derived classes. In the implementation inheritance, most of the implementations are provided at the first few levels of the class structure hierarchy, and are inherited by the subclasses.

Methods in abstract classes can also be declared as virtual, which means that the subclasses are able to override these methods and thus modify the behaviour inherited

from the abstract base class. The ability to process objects differently depending on their data type and class, and more specifically to redefine methods for derived classes, is a characteristic of the polymorphism property of object-oriented programming languages. Derived classes have "is-a" relation with the parent class. For example, the class BeamColumn3D is derived from the abstract base class Element. The abstract class Element can contain a virtual method for obtaining tangent stiffness in its class declaration without actually providing the implementation. In that case this method is a pure-virtual method and the derived class BeamColumn3D can override the Element's method by providing the implementation and return a suitable value for the tangent stiffness. The virtual method which is invoked during the program execution depends on what the base class pointer is pointing at that time. If the Element pointer is set to a BeamColumn3D object, then the method for obtaining tangent stiffness of BeamColumn3D object will be invoked. This process is known as dynamic binding.

Object oriented programming languages, such as C++, also provide the ability to have multiple methods with the same name but with different parameters. This property is known as method overloading. Abstract base classes can declare several virtual methods with different parameters. Derived classes can choose which method to override depending on what parameters are used in their class declarations.

Inheritance, polymorphism and method overloading enable the extensibility of object-oriented programs by allowing system design decisions to be developed at the abstract level without prior knowledge of all possible object types. The behaviour of abstract base

classes can be modified and extended in the derived classes by overriding methods and providing method implementations for new object types without affecting the base class code.

The key difference between procedural and object oriented programming is that the former is organized based on function calls (verbs), whereas the latter is structured around data (nouns). A program that is procedural in nature contains a set of sub-routines which represent different functions and the entire program is designed using function calls. Programs based on object oriented concepts are designed around objects which interact with each other through messages depending on what functionality is provided by each of the involved objects. For example, in a procedural program that contains a sub-routine for storing the element tangent stiffness in a matrix, a function call will be used to invoke this sub-routine. The sub-routine would use a logical statement "switch" to determine the correct tangent stiffness based on the element type provided in the function call parameters. If a new element type has to be added to the procedural program, modifications will be required both to the sub-routine's "switch" statement and to the main program declarations to register the new element type. Such modifications require detailed knowledge of the entire procedural program functionalities. In the case of a program created using object based design, the method for storing the tangent stiffness will be declared as a virtual method in the abstract base class Element and can be invoked by a solver object. By using the inheritance property, a new element type can be added as a subclass derived from the parent class Element. This new subclass will provide the implementation of the method for tangent stiffness based on its characteristics, e.g.

linear-elastic element or nonlinear element. If the new element class is instantiated, i.e. an object is created, the method for tangent stiffness of this new class will be dynamically invoked using the polymorphism property. In the object based design, the extension of a program only requires knowledge of the base class functionality, more specifically the virtual methods declared in the base class that have to be overridden in the new derived classes.

4.2 OpenSees Overview: Finite Element Classes for Structural Systems

This section provides a brief overview of generic main classes used to model structural systems in the OpenSees software framework (McKenna 1997). OpenSees is a framework of components which includes the domain of objects for modeling elements, materials, constraints, etc. created by model-builders and the solution procedures represented by analysis, algorithm and equation solver modules. The interaction of these objects with storage and visualization tools provide the basis for user interface and post-processing. The conceptual module layout of these high-level objects are schematically shown in Figure 4-1. The four main classes at high-level abstractions in the OpenSees framework, ModelBuilder, Domain, Analysis and Recorder, and the interaction between them are shown in Figure 4-2.

The main function of the ModelBuilder class is to manage the creation, storage and deletion of all objects that are part of the Domain and the Analysis classes. TclModelBuilder is a sub-class of ModelBuilder that provides user interface through TCL scripting language and accommodates adding of commands to the TCL library for

managing new classes.

The Domain class is responsible for storing all the components of a finite element model of a structural system. These components include the classes Node, Element, Load, Constraint, etc. which are described in more detail in the following section. Domain stores the last converged state and the current trial state of the model. It provides methods for the Analysis object to access domain components and update the state at each trial or converged step. Domain also allows access for the Recorder object to obtain and store parameters of domain components defined by the user at each converged step.

The Analysis class is an abstract class that provides an interface for formulation and solving the system of governing equations for a finite element model of a structural system. Analysis object is an aggregation of different types of objects such as Algorithm and Integrator that control the solutions algorithm and virtual time increment for a linear or nonlinear structural system. Analysis object updates the model contained in the Domain from the current state to another state at each load step. Analysis object also provides the capability to reset the virtual time of the Domain in case of errors such as lack of convergence to its previous converged state and use different analysis parameters for the next trial step. Subclasses derived from Analysis abstract class include StaticAnalysis, EigenAnalysis and TransientAnalysis for performing static, modal and dynamic analysis, respectively.

The Recorder class is an abstract class that provides an interface for obtaining information from the model in the Domain during the analysis. Recorders can be used to monitor response quantities such as element forces, nodal displacements, drift, or damage, by exporting the saved information to an output file or a visualization tool like OpenGLRenderer.

4.2.1 Node, Element, Load and Constraint Classes

The main components of the Domain used to model structural systems are the classes Node, Element, Load and Constraint. Figure 4-3 identifies these main classes in a one-bay, three-story frame structure.

The Node class is used to represent discrete points in space which are interconnected by elements in the model of a global system. In frame structures, nodes typically define the end points of beams and columns. Thus each frame element has two nodes, one at each node. Physical beams or columns may be discretized into several elements. A node is shared by multiple elements in joints where more than two elements interconnect. In finite element models, Node objects are associated with degrees of freedom (DOF), the number of which determines the dimension of the global system and the associated matrix size. A Node object keeps track of nodal displacements, velocities and accelerations along its degrees of freedom. In nonlinear systems where for each time increment or load step the analysis may go through a number of trial steps before reaching convergence, the node objects also keep record of both the current trial state and the previous converged state. In finite element models, the element objects have pointers

to node objects, which provide them with the end coordinates, connectivity conditions and boundary conditions.

In finite element models of frame structures, elements are used to model structural components such as beams, columns, joints, etc. Frame elements such as beam-columns or truss members are typically associated with only two nodes, one node at each end of the element. Modeling capabilities of frame elements can vary widely, from a simple formulation for a linear elastic beam-column element to sophisticated formulations that capture complex inelastic behaviour and geometric nonlinearities, including second order effects. In a finite element model, the Element class provides information on the element state to the global solver, including linearized tangent stiffness, mass and damping matrices as well as resisting member force vectors. The element object computes these quantities after obtaining the boundary conditions through the associated nodes at the element ends. In general for inelastic modeling, elements use external material classes which provide constitutive relations for forces and deformations. In nonlinear analysis, the element class also performs state determination, including force recovery, computation of tangent stiffness, etc. at every trial step and also keeps record of the current trial state and the previous converged state.

The Load class represents the physical loads on a structure in the model of the structural system. Loads may be static or dynamic. For example, loads due to earthquake excitation or wind may be defined as dynamic. Loads can act on a node, in which case they are nodal point loads, or on an element. The element loads may be either point loads or

distributed loads over the entire element length or a part of it. The Load class provides an interface for defining and applying loads. The sub-classes derived from the abstract Load class are NodalLoad and ElementalLoad, and they are associated with a Node or an Element class, respectively.

The Constraint class represents the boundary conditions of the structure. To model the boundary conditions a node object is associated with a constraint object which specifies if rotations and translations are allowed or not along a given degree of freedom of the node. Constraints can also be used to assign a specific displacement path to a degree of freedom, or to define relationship between degrees of freedom of two nodes. In a finite element model of a structure, constraints are necessary to render the system of governing equations solvable. Constraints that act on only one degree of freedom and are associated with one node are known as single-point constraints, whereas constraints associated with two or more nodes, and a vector of degrees of freedom are known as multi-point constraints. Single- and multi-point constraints are usually implemented under separate classes due to the fundamental differences in their underlying concepts.

4.3 Object Oriented Design of New Models

As summarized in Section 1.3, the objectives of this research is to develop simulation models for seismic response analysis of reinforced concrete structures that capture the behaviour of members in new structures designed as ductile as well as non-ductile members in existing older deficient structures. The element formulation in the proposed models is based on concentrated plasticity approach using force interaction surfaces and

evolution models for the generalized plastic hinges at the element ends, as discussed in Chapter 3. Object oriented design is considered for the implementations of the proposed models since it allows extensibility and code reusability. This section presents the methodology for designing the class hierarchy and the strategies to accomplish object oriented design of the new models developed in this research.

4.3.1 Interface Design

The interface design is a very important consideration in the process of creating or extending object-oriented programs. Properly designed interfaces contribute to having a functional core that allows programs to be easily extended by adding multiple classes that implement the interface. Having a common interface also provides a basic common functionality of all the objects. There should be a root interface from which all other interfaces are derived and the type of new derived classes is refined for their specific interface. In the OpenSees framework, for example, the root interfaces for most classes are the TaggedObject and MovableObject. All new types of classes in OpenSees should be derived from the TaggedObject and MovableObject classes. Deriving from TaggedObject allows the model builder (TclModelBuilder) to manage the creation, storage and deletion of various objects by using an array of tagged objects. MovableObject provides the interface necessary for shipping objects over a Channel to a database for storing the state at discrete steps during the analysis.

4.3.2 Hierarchy Structure and Functionalities of New Classes

The conceptual development of an object based design for a problem commences with

identifying the individual components and defining the functionality of each component. In this process the base classes are established by determining the abstractions that describe the behaviour of individual components. The interface and the interactions between the abstract base classes is then established. In this research, the formulation of the proposed models for seismic response analysis of reinforced concrete structures consists of a beam-column element with zero-length generalized plastic hinges associated with force interaction surfaces and evolution models concentrated at the element ends. From the modeling perspective, an inelastic concentrated-plasticity element suitable for capturing the behaviour of ductile as well as non-ductile reinforced concrete members should have the following capabilities:

- Capture large deformations.
- Provide axial force-bending moment interaction through yield surface models.
- Simulate hardening in the post-yield response by translating the yield surface in the force space.
- Detect brittle or limited ductility type of failure in shear through axial force-shear force interaction surface models.
- Implement degradation of shear strength in the plastic hinge zone through shear limit surface dependent on displacement ductility in order to detect failure in shear for members with moderate ductility.
- Simulate softening in the post-shear failure response by shrinking the axial force-shear force interaction surface in the force space.
- Capture hysteretic characteristics including stiffness degradation and cyclic strength deterioration through cyclic models.

- Control cyclic behaviour by keeping track of maximum inelastic deformations, and number and types of cycles with inelastic excursions based on event-to-event strategy.
- Provide relations between accumulated damage and degradations in strength and stiffness through the interaction of cyclic models and evolution models with damage models.
- Follow the progression and accumulation of damage throughout the analysis.

Considering the required functionalities, the following base classes are established: beam-column element class, yield surface class, yield surface evolution class, shear failure surface class, shear failure surface evolution class, shear limit surface class, cyclic model class, cyclic control class, damage model class, damage progression class.

The new beam-column element class has to be developed for 3D elements and to provide functionalities for capturing large deformations and inelastic modeling. At the abstract base level, the new element class has to provide the size of the stiffness, mass and damping matrices and the resisting force vector as well as the large deformation effects so these properties can be inherited by the derived classes. A final class can be derived directly from the base class to provide elastic stiffness matrix that can be used for simulating elastic large deformation effects. The inelastic modeling capabilities can be developed at the next level of abstractions by associating a derived class with force interaction surface classes and evolution model classes. In one branch of derived classes, the inelastic modeling capabilities can be reduced to monotonic response for this final

class so that the user has the option to use a simpler model when this suffices. The other branch of derived classes can provide the inelastic modeling capabilities for cyclic response by being associated with cyclic control and cyclic model classes.

The modeling of inelastic behaviour governed by flexural yielding is separated from the element implementations by creating new yield surface class and evolution model class to deal with this part of the problem. This class structure ensures the independence of the yield surface implementation, which is important considering that the force state is defined in a normalized non-dimensional coordinate system in the yield surface model whereas it is described in a vector format with the respective units for forces and moments in the element formulation. The element class developed for inelastic modeling is associated with yield surface class to provide the functionality for capturing yielding and hardening in the post-yield response. At the abstract base level, the new yield surface class provides the interface for interactions with the element class. The abstract base class of the yield surface is also associated with evolution model class to enable the translation of the surface in the force space. The derived classes inherit these basic functionalities and have to provide specific functions describing different yield surface types.

The modeling of non-ductile behaviour governed by failure in shear and in-cycle strength degradation in the post-shear failure state is handled by the new shear failure surface and evolution model classes. This functionality is also separated from the element implementation because the force state is defined as a point in a normalized non-dimensional space similarly to the yield surface model. The element class is associated

with shear failure surface classes in addition to the yield surface classes. The hierarchy structure of the shear failure surface class is similar to that of the yield surface class: the abstract base class provides the interface for interactions with the element class and the shear failure surface evolution class; and the derived classes implement specific functions for individual shear failure surface models. The evolution model class that is associated with the shear failure surface class enables the contraction of the shear failure surface to simulate the softening in the post-shear failure response.

The new class provided for the shear limit surface model expands the functionalities of the element with the capability to capture the behaviour of members with moderate ductility where shear failure occurs after yielding and undergoing some level of inelastic excursions. The main purpose of this class is to provide displacement-ductility based rule for reducing the initial shear strength with increasing ductility. To achieve this, the shear limit surface class interacts with the element to obtain the current ductility level and communicates the required reduction of shear strength to the shear evolution model class. The interface for these interactions as well as any transformations of the force state from one coordinate system to another, e.g. vector format in the element system to normalized non-dimensional space in the shear failure surface system, have to be performed at the abstract base class level and inherited by the derived classes. The subclasses have to provide specific functions for determining the reduction in shear strength based on ductility. The shear limit surface class is introduced as a new class independent from the element implementation and the shear failure surface implementation for the following main reason. The shear failure surface and evolution classes provide the functionality to

capture behaviour governed by brittle or limited ductility failure in shear. Capturing the degradation of shear strength in the plastic hinge zone requires additional implementations and introducing a new class specifically for this purpose provides a better structure and a possibility to modify and expand the shear limit surface implementations without affecting the surface and evolution model implementations.

As previously mentioned, to extend the inelastic modeling capabilities of the element for capturing cyclic response, new classes for cyclic control and cyclic models are required. Cyclic models are used to define the constitutive relationships for the quasi-elastic part of the response that is characterized by degradation of stiffness and deterioration of strength. Considering the various hysteretic characteristics that a concrete member may exhibit, such as unloading stiffness degradation, peak-oriented reloading stiffness, pinching and cyclic strength deterioration, new individual classes can be developed to capture each of these characteristics and provide the appropriate tangent stiffness. As described in Chapter 3, the prediction of the tangent stiffness in the trial steps is determined using event-based strategy. The abstract base class of the cyclic control has to define the basis for the event-to-event strategy and manage the information on previous cycles with inelastic excursions. It also has to provide the interface for interactions with the element for obtaining current force state and deformations and returning the current tangent stiffness to the element by invoking the appropriate cyclic model class. The final cyclic control class has to implement specific rules for the event-based strategy. The hierarchy structure of the cyclic control class and its collaborative relation with the cyclic model classes and the element classes ensures the independence of the cyclic modeling from the

element implementation and provides the possibility to expand the modeling capabilities by adding new cyclic models.

As described in Chapter 3, damage models are used in the formulations to capture the progression of damage during inelastic excursions and its effect on the gradual deterioration of stiffness and loss of strength. For this purpose, new damage model classes and damage progression classes can be introduced in the class structure. At the abstract base level, the new damage model class provides the interface for interactions with the cyclic control class to obtain current element forces and deformations, and return computed damage indices. The derived classes have to provide specific relationships for calculating damage indices based on maximum plastic deformations, hysteretic energy or a combination of the two. As mentioned above, the cyclic control class invokes the appropriate cyclic model classes depending on the previous history of events. Having obtained current damage indices from the damage model class, the cyclic control class passes the information on the damage to the respective cyclic models so that degradation in stiffness and strength can be calculated based on the accumulated damage. The progression of damage can be monitored by a separate new class which interacts with the cyclic control class to obtain current damage indices, stores the information during the analysis and is capable to provide an output.

By creating base classes and independent implementations for each of the main components of the formulations as described above, the proposed class hierarchy and

interface for collaboration among the classes provides a comprehensive and flexible design that allows extensibility.

4.4 Implementation of New Models in OpenSees

This section describes the object oriented methodology and design issues for implementing the new models in the OpenSees framework. Class details of element classes (public, protected and private member function details) are provided in Appendix A. The models described in this section may be extended by overriding or implementing specific methods/functions, as explained in Section 4.1.1. The terminologies related to the formulations are presented in Chapter 3.

4.4.1 Beam-Column Element Classes

The main characteristics of the Element class hierarchy developed as part of this research are as follows:

- the base class Element is provided by OpenSees from which all subclasses are derived.

- the second level of abstractions in the hierarchy is based on the degrees of freedom in the element type. In this research, the proposed models are 3D beam-column elements with total of 12 degrees of freedom for the end nodes. As shown in Figure 4-4, the second level abstract class is called UpdatedLagrangianBeamColumn3D. In this abstract class most of the pure-virtual functions defined by the Element class are implemented and the sizes of

the vectors for resisting forces and end displacements as well as the sizes of stiffness and mass matrices are defined. Thus, the subclasses derived from this class share the same vector/matrix sizes. For 3D elements, the matrices are [12x12] and the vectors are {12x1}. In this class, pointers to the end nodes can be stored to provide updates in displacements at each analysis step. The transformation between global and local displacements and natural deformations is implemented at this level to provide the basis for the large deformation formulation (geometric nonlinearity).

- the third level of abstractions adds the inelastic modeling capabilities using yield surfaces and shear failure surfaces at each end of the beam-column elements. The class developed at this level, InelasticGNL3D, inherits the capability for nonlinear geometric analysis from the parent class UpdatedLagrangianBeamColumn3D.

4.4.1.1 Geometrically Nonlinear Elastic Element (ElasticGNL3D)

As mentioned in the previous section, the abstract class UpdatedLagrangianBeamColumn3D is derived from the base class Element and implements large deformation effects based on the updated Lagrangian formulation described in Chapter 3. The UpdatedLagrangianBeamColumn3D class has pointers to the two end nodes which provide access to global nodal displacements and accelerations. In this class, two new pure-virtual methods are declared that the subclasses are required to provide, one is for obtaining the tangent stiffness matrix and the other for the mass matrix. This class also provides methods for obtaining converged, trial and incremental

local and natural deformations. Most of the virtual methods defined in the Element class are implemented in the UpdatedLagrangianBeamColumn3D class, including those required by Recorder.

One final (or concrete) class that is derived directly from UpdatedLagrangianBeamColumn3D class is the ElasticGNL3D class. Figure 4-5 shows the collaboration diagram for ElasticGNL3D class. The black arrows in Figure 4-5 indicate an "is a" relation while the dashed gray arrows show a "has a" relation. For instance, ElasticGNL3D class is a subclass of UpdatedLagrangianBeamColumn3D and its parent class has pointers which belong to the Node class. ElasticGNL3D class provides an elastic local stiffness matrix and a lumped mass matrix for 3D beam-column elements when its methods for tangent stiffness and mass matrix are invoked. This final class can be used for simulating elastic large deformation effects. It can also be used for inelastic analysis when combined with plastic hinges at each of the element ends. The plastic hinges can be defined as Zero-Length Elements with a constitutive relation to describe the flexural/shear behaviour.

4.4.1.2 Inelastic Elements (InelasticGNL3D)

In the class design, the inelastic element, InelasticGNL3D, is derived from UpdatedLagrangianBeamColumn3D class, as shown on Figure 4-4. Similarly to the ElementGNL3D class, InelasticGNL3D inherits the geometric nonlinear modeling capabilities from the parent class. As described in Chapter 3, the inelastic response can be simulated by employing generalized hinge concepts for elements with yield/shear surfaces at their ends, and InelasticGNL3D element is designed based on this concept.

The post-yield P-M interaction and the post-shear failure P-V interaction are implemented in separate classes - YieldSurfaceMD and ShearFailureSurfaceMD, respectively. The flexure-shear interaction is implemented in a different class - ShearLimitSurface. The functionalities of these classes are described in details in the subsequent sections.

The InelasticGNL3D class has pointers to two yield surfaces and two shear failure surfaces, one of each type for each end. It also has pointers to two shear limit surfaces that are associated with both the yield surfaces and the shear failure surfaces. InelasticGNL3D is still an abstract class. At this level, the post-yield behaviour, shear-flexure interaction and post-shear failure behaviour are fully incorporated through the yield surface, shear limit surface and shear failure surface classes, respectively. The collaboration diagram of a final class derived from InelasticGNL3D class shown on Figure 4-6 depicts the relations between InelasticGNL3D element and the failure surface models. In the following paragraphs, the interaction among the element class and the abovementioned surface classes is explained.

In the post-yield behaviour, the incremental force and the element tangent stiffness can be obtained as:

$$\{dF\} = [K_t]\{d\Delta\} \quad (4.1)$$

and

$$[K_t] = [K_e] - [K_e][G] \left[[G]^T [K_e + K_p][G] \right]^{-1} [G]^T [K_e] \quad (4.2)$$

where $[K_e]$ is the quasi-elastic stiffness matrix, $[K_p]$ is the plastic stiffness, $[G]$ is the yield surface gradient, and $\{d\Delta\}$ is the vector of incremental displacement. As described in detail in the formulations in Chapter 3, if the incremental force causes the trial force to drift away from the yield surface, the trial force is returned to the yield surface using force-recovery techniques. Hardening response is implemented by kinematic evolution of the yield surface based on $\{dF^*\}$,

$$\{dF^*\} = [K_p]\{d\Delta_p\} = [K_p]\{\lambda\}[G] \quad (4.3)$$

where $\{d\Delta_p\}$ is the vector of incremental plastic deformations and $\{\lambda\}$ is the magnitude of plastic deformations given by:

$$\{\lambda\} = \left[[G]^T [K_e + K_p] [G] \right]^{-1} [G]^T [K_e] \{d\Delta\} \quad (4.4)$$

The trial displacements are obtained from the element end nodes. The quasi-elastic stiffness is the property of the element and the plastic stiffness is obtained through the yield surface. The element requires the magnitude $\{\lambda\}$ to calculate the inelastic portion of deformations and the yield surface requires $\{\lambda\}$ to determine $\{dF^*\}$. The gradient is the property of the yield surface formulation. Upon obtaining the plastic stiffness and the gradient, $\{\lambda\}$ can be calculated by the element and provided to the yield surface.

In the post-shear failure behaviour, the shear force-deformation relation is governed by degradation in stiffness that results in a softening response. The incremental force is calculated using the degraded tangent stiffness matrix, as described in Section 3.3.4.3.2.

The negative degradation stiffness K_{deg} used in the determination of the total degraded

tangent stiffness is the property of the shear failure surface. It is calculated based on the shear force in the element at shear failure and the drifts at shear failure and axial failure, as given in Equation (3.57). The total deformations which are a combination of the flexural and shear components given by:

$$\Delta_t = \Delta_f + \Delta_{sh} \quad (4.5)$$

are calculated by the element. The degradation coefficient δ given in Equation (3.99) is determined within the shear failure surface class and is used by the element to obtain the total degraded tangent stiffness based on a flexibility approach as described in Section 3.3.4.3.2.

Upon computing the trial force, the element calls the yield surface class to conduct a check for yielding. The yield surface class returns the status of the trial force to the element. If yielding has been detected, the above mentioned interactions between the element class and the yield surface class take place to determine the inelastic portion of the deformation, recalculate the trial force and update the element tangent stiffness. Next, the element calculates the shear forces from equilibrium.

The flexure-shear interaction in the post-yield behaviour is governed by the shear limit surface model, as described in Section 3.3.3.2. To reduce the initial shear strength after developing flexural plastic hinges at the element ends, the initial shear failure surface is contracted under pronounced flexural displacement ductility demand. The shrinkage of the shear failure surface under such conditions is controlled by monitoring the element's

flexural displacement ductility demand imposed about each axis, and updating the shear failure surface as governed by a shear limit surface.

The element provides the current flexural displacement ductility to the shear limit surface class. The latter calculates the reduction factor for the shear capacity and passes it onto the shear failure surface class. Next, the element calls the updated shear failure surface to conduct a check for shear failure. If shear failure has been detected, the interactions between the element class and the shear failure surface class described above take place to calculate corrected force consistent with the updated shear capacity and obtain the element tangent stiffness.

In the case where yielding has not been detected by the yield surface class, the element calls the shear failure surface using the elastic trial force. If shear failure is detected by the surface class, the same process is followed as described above. This case represents behaviour governed by brittle shear failure.

The `InelasticGNL3D` class is designed to fully implement the general state determination process for monotonic response, and the classes derived from it inherit these capabilities. Two final classes are derived from this class, as explained in the following sections.

4.4.1.2.1 Inelastic Element for Monotonic Response (`InelasticMON3D`)

`InelasticMON3D` is a final class derived from `InelasticGNL3D`, as shown on Figure 4-4. The collaboration diagram of `InelasticMON3D` class is shown on Figure 4-6. It provides

the same constant elastic local tangent stiffness matrix as ElementGNL3D. The capabilities of this class include large deformation effects, axial force-flexure interactions, post-yield hardening, post-yield flexure-shear interactions, axial force-shear force interactions and post shear failure softening. Since its elastic stiffness does not include cyclic degradations, i.e. remains constant upon unloading/reloading, this element class is suitable only for monotonic response analysis such as "push over" analysis.

4.4.1.2.2 Inelastic Element for Cyclic Response (InelasticCYC3D)

InelasticCYC3D is the other final class derived from InelasticGNL3D, as shown on Figure 4-4. It inherits the same capabilities from the parent class as InelasticMON3D. In this class, the cyclic degradation capabilities are included as described next.

The InelasticCYC3D class has pointers to cyclic control models, one for each end of the element. The collaboration diagram for this class is shown on Figure 4-7. This class provides the elastic local tangent stiffness matrix as the base matrix at the start of the analysis, which is used until detecting inelastic behavior. During inelastic excursions, the member accumulates damage which leads to degradation in unloading and reloading stiffness as well as reduction in strength in the cyclic response, as described in Section 1.2. During the state of unloading after yielding in flexure and/or failing in shear and the state of reloading prior to reaching either of the failure surfaces, the InelasticCYC3D element class interacts with the cyclic control models to update the elastic stiffness matrix using the appropriate cyclic degradation model. At each step of the analysis, the element provides the current element forces and deformations for each end to the cyclic

control models. Depending on the current state and the response history of the element, e.g. prior flexural yielding or failure in shear, the cyclic control class engages the appropriate cyclic degradation model to calculate the required damage indices. The damage indices are then returned to the element which uses this data to degrade the stiffness and strength parameters, thus achieving quasi-elastic degraded cyclic response.

The interactions between the element and the cyclic control models enable the process of tracking the evolution of damage and its effects on the gradual deterioration in stiffness and loss of strength. This process is captured by the event-based formulation where an “event” occurs when the loading state of the element changes, as described in Section 3.4. The cyclic control class implements the event-based formulation as explained in the subsequent sections on cyclic degradation models.

The InelasticCYC3D class is designed to incorporate the most sophisticated modeling capabilities and is suitable for capturing cyclic behaviour of reinforced concrete beam-columns. It also requires the most parameters for the constructor, compared to the other elements described above.

4.4.2 Yield Surface Classes

The part of inelastic modeling that involves the axial force-bending moment interaction is based on yield surface plasticity theories as described in Section 3.3.1. The yield surface is assumed to be a continuous, convex, rate dependent limit state function of axial force and bending moments on a cross-section of the member. With respect to the

implementation of the formulations, the interactions between the element class and the yield surface class occur at three occasions. First, the element requires the location of the current state of element end forces relative to the yield surface to determine whether the current state is elastic or inelastic. The element class provides the current force state to the yield surface class, and the yield surface class performs the required checks and returns the current status to the element. Second, if the force state is on the yield surface, the element requires the yield surface gradient and an associated plastic stiffness for computing the element tangent stiffness. The calculation of the gradient for the current force state is performed within the yield surface class and provided to the element. The yield surface class also obtains the plastic stiffness from a plastic stiffness material model and passes it to the element. Thirdly, during the force recovery process, the force state that shoots through the yield surface needs to be retrieved onto the surface. The yield surface class performs the required force recovery operations, balances the end forces and provides these updates to the element.

An abstract base class for the yield surface is created that declares public virtual methods to provide the required functionality for interactions with the inelastic element. The inelastic beam-column element is associated with two yield surface objects, one for each end as mentioned in the previous section. By creating a separate class for the yield surface, the independence of the yield surface implementation from the element implementation is ensured. In the element formulation, the force state is described in a vector format which contains forces as well as moments with their respective units. In the yield surface formulation, the force state is described by a point defined by three

normalized coordinates on a 3D non-dimensional surface. To facilitate the interactions with the element, the yield surface class implements protected methods for transforming the data types (vectors, matrices) from the client system (the element) to the appropriate yield surface system and vice-versa. These methods will be referred to as transformation functions.

The hierarchy of the proposed yield surface implementation consists of three levels, as shown on Figure 4-8. The abstract base class `YieldSurfaceMD`, as mentioned above, provides the interface for interactions with the element which is the client for the yield surface class. The second level is based on the yield surface dimensions. At this level, the class `YieldSurfacePMM3D` is derived from the base class and provides the functionality for 3D surfaces, suitable for use by 3D elements. New pure virtual methods are declared at the second level to obtain surface specific information and implement numerical issues pertinent to 3D space. The final classes provide specific formulas for different yield surface models. At the final level, only two methods need to be implemented, one for computing the drift of the force state from the surface, and the second for computing the gradient of the surface at a point. In this research, the yield surface model proposed by El-Tawil (1996) is considered for final class implementation, class `ElTawil3D`, but other models can be added.

This class hierarchy structure provides an optimal class design with focus on extensibility and flexibility. The main advantage is that the higher level classes deal with client interactions and numerical computations. At the final level, different yield surface models

can be added without complications by implementing two methods for drift and gradient which are specific to the yield-surface shape.

4.4.3 Shear Failure Surface Classes

The shear failure modeling is based on shear failure surface which defines the axial force-shear force interaction as described in Section 3.3.2. Similarly to the yield surface, the shear failure surface is assumed to be a continuous, convex function of axial force and shear forces on a cross-section of the member. The inelastic beam-column element is associated with two shear failure surface objects, one for each end, in addition to the yield surface objects. In the implementation of the formulations, the element first checks for yielding and interacts with the yield surface class if yielding is detected as described in the previous section. Next, the element checks for shear failure through the following interactions. First, the element requires the location of the current state of element end forces with respect to the shear failure surface to determine whether the current state is one of shear failure or not. The element class provides the current force state to the shear failure surface class, and the surface class carries out the required checks and returns the status to the element. Second, if the force state is on the shear failure surface, the element requires the respective degradation stiffness for computing the element tangent stiffness. The shear failure surface class obtains the degradation stiffness from a degrading shear stiffness material class and passes it to the element. Lastly, the force state that shoots through the shear failure surface needs to be retrieved to the surface through the force recovery process. The shear failure surface performs the required force recovery operations, balances the end forces and provides them to the element class.

The hierarchy of the proposed shear failure surface implementations follows a similar philosophy as the yield surface class hierarchy. As shown on Figure 4-9, the hierarchy comprises three levels. The abstract base class `ShearFailureSurfaceMD` provides the interface for the interactions with the client - the element class. In the shear failure surface formulation, the force state is described by a point defined by three normalized coordinates on a 3D non-dimensional surface. The shear failure surface class implements transformation functions at the abstract base level to facilitate the interactions with the element, similarly to the yield surface class. At the second level of hierarchy, the class `ShearFailureSurfacePVV3D` defines the dimensions and provides the functionality for 3D shear failure surface. The final classes derived from `ShearFailureSurfacePVV3D` class provide specific formulas for different shear failure surface models. At the final level, only two methods need to be implemented, one for computing the drift of the force state from the surface, and the second for obtaining the stiffness degradation coefficient. Variety of shear failure surface models can be added under the final class, and the proposed hierarchy structure facilitates the extensibility and the independence of the shear failure surface implementation from the element implementation.

4.4.4 Yield Surface Evolution Classes

The part of inelastic modeling that captures hardening behaviour after yielding has occurred is based on evolution rules which determine how the yield surface evolves in space as described in Section 3.3.1. The yield surface models used with the elements provide the axial force-bending moment interaction. To enable the yield-surface

evolution implementation, a new class structure is introduced that provides the following functionalities: managing the yield surface evolution; obtaining plastic stiffness; and providing direction of evolution.

Each yield surface object, which is defined for an element end, is associated with a yield-surface evolution model to implement the abovementioned functionalities required for modeling hardening behaviour. The hierarchy structure of the proposed evolution model is shown on Figure 4-10. As a new model introduced in the OpenSees framework, it is derived from classes `TaggedObject` and `Movable Object`. The abstract base class `YS_EvolutionMD` has two main functions required for the interactions with its client, the yield surface class. First, the base class declares the public methods that the yield surface object can invoke, such as functions for obtaining plastic stiffness and evolving the surface. Second, it implements methods for storing the attributes required to manage the surface evolution. This is achieved by maintaining mapping between the initial state and the subsequent deformed state. Yield surface objects can invoke the mapping methods to translate the current state of force to the original state and use the equations describing the surface directly to compute drift or gradient, as described in details in Section 3.3.1.

At the second level of abstraction, class `YS_Evolution3D` is based on the dimensions of the yield surface. In this case, it is developed for 3D surfaces. The combined isotropic and kinematic transformations for 3D yield surfaces are implemented at this level. The final classes derived from class `YS_Evolution3D` are only required to implement methods

for providing plastic stiffness. The collaboration diagram for PlasticHardening3D final class is shown on Figure 4-11.

Besides the abstract class YS_Evolution3D, a final class Null_Evolution3D is also derived from the base class as shown on Figure 4-10. Null_Evolution3D specifies zero translation of the surface, so the surface remains at its initial position in space. When this class is associated with a yield surface object, it results in perfectly plastic response, i.e. no hardening.

The proposed hierarchy structure leads to a flexible design by providing the possibility to include new evolution models based on plastic stiffness implementation.

4.4.5 Shear Failure Surface Evolution Classes

The modeling of post-shear failure response to continued loading, which is characterized by softening, is based on evolution rules that govern the evolution of the shear failure surface in space. As described in Section 3.3.2 a non-uniform contraction rule determines the change of the surface in both size and shape by allowing the surface to contract differently in each direction. The shear failure surface models associated with the element ends provide the axial force-shear force interaction. Similarly to the yield surface evolution implementation, a new class structure is introduced to deal with the shear failure surface evolution by providing the following functionalities: managing the surface evolution by mapping, obtaining degradation stiffness, and providing direction of evolution.

Each shear failure surface object defined for an element end is associated with a surface evolution model to implement the abovementioned functionalities required for modeling post-shear failure softening behaviour. Figure 4-12 shows the hierarchy of the proposed shear surface evolution model. The abstract base class `SFS_EvolutionMD` has two main functions required for the interactions with its client, the shear failure surface class. First, the base class declares the public methods that the shear failure surface object can invoke, such as functions for obtaining degradation stiffness and evolving the surface. Second, it implements methods for storing the attributes required to manage the surface evolution by maintaining mapping between the initial state and the subsequent deformed state. This implementation follows a similar philosophy to that of the yield surface evolution model. Shear failure surface objects can invoke the mapping methods to expand the current state of force, which is on the contracted surface, to the original undeformed state. This mapping allows using the equations that describe the surface directly in computing the softening component, $\{dF_s^*\}$, and performing the iterative analysis procedures, as described in details in Section 3.3.2.

Class `SFS_Evolution3D` which represents the second level of abstraction in the proposed implementations is based on the dimensions of the shear failure surface. The contraction transformations for 3D shear failure surfaces are implemented at this level. The final classes derived from class `SFS_Evolution3D` are only required to implement methods for providing degradation stiffness. The `SFS_NonUniform3D` final class is provided for implementing the non-uniform contraction rule that allows using a different degradation

stiffness quantity for each direction, whereas the SFS_Isotropic3D final class is used to provide the same degradation stiffness which results in uniform shrinking of the surface. The collaboration diagram for SFS_NonUniform3D final class is shown on Figure 4-13.

4.4.6 Plastic Stiffness Classes

As described in the previous sections, surface evolution models are required to obtain current stiffness relationships for each force component of the surface. To implement this functionality, yield surface evolution models have pointers to plastic flexural stiffness models and shear failure surface evolution models have pointers to degrading shear stiffness models. These stiffness models are implemented as separate classes derived from Material class. The hierarchy structures of the proposed PlasticFlexuralStiffness class and DegradingShearStiffness class are shown in Figures 4-14 and 4-15, respectively.

The PlasticFlexuralStiffness class provides a relationship between the plastic flexural stiffness K_p and either plastic deformations or a normalized force component depending on the evolution type. The base class provides the interface for the interactions with the yield surface evolution model and the final classes are required to implement the methods for getting plastic stiffness. The final classes derived from PlasticFlexuralStiffness class are NullPlasticStiffness, MultiLinPlasticStiffness and DamagePlasticStiffness classes. NullPlasticStiffness class returns a zero plastic stiffness and can be used for elastic-perfectly plastic response. MultiLinPlasticStiffness class is intended for providing a multilinear relationship between K_p and the plastic deformations which results in

reduction of the amount of hardening in the response with increasing plastic deformations. DamagePlasticStiffness class is intended for providing plastic flexural stiffness as a function of a damage index which reduces the amount of hardening in the response with the accumulation of damage.

Similarly, the DegradingShearStiffness class provides a relations between the degradation stiffness K_{deg} and either plastic shear deformations or a normalized force component. The base class interacts with its client, the shear failure surface evolution model, and the final classes are required to implement the methods for obtaining degradation stiffness. The final classes derived from DegradingShearStiffness class are DriftAxialFailure, MultiLinDegradStiffness and DamageDegradingStiffness classes. DriftAxialFailure class is required to provide degradation stiffness as a function of the shear force and the drift at shear failure. MultiLinDegradStiffness class is intended for proving a multilinear relationship between K_{deg} and the shear deformations which results in increased softening with increasing deformations. DamageDegradingStiffness class is intended for providing degradation stiffness which decreases based on a damage index and results in further softening with damage accrual.

4.4.7 Shear Limit Surface Classes

To capture the degradation of shear strength in the plastic hinge region, the shear failure surface is contracted with increasing flexural displacement ductility demand by using a shear limit surface, as described in Section 3.3.3. A new class called ShearLimitSurface class is created to provide this functionality in the implementations.

The shear limit surface models obtain the current displacement ductility from the element and provide a relationship for reducing the initial shear strength based on ductility demand. The shear limit surface models have pointers to the shear failure surface evolution models and pass the computed reduction in shear strength to the evolution models which control the contraction of the shear failure surface.

The hierarchy structure of the ShearLimitSurface class is shown on Figure 4-16. The base class implements the interface for interaction with the element and the evolution model. The final classes are only required to provide specific relationships between shear strength and displacement ductility demand.

4.4.8 Cyclic Control and Cyclic Model Classes

Cyclic models are used to control the response of the element during the state of unloading that follows after yielding in flexure and/or failure in shear and through the state of reloading prior to reaching either of the surfaces, as described in Section 3.4. Cyclic models define the constitutive relationship to model the quasi-elastic part of the response that is characterized by degradation of stiffness and deterioration of strength. Formulation of the cyclic models is based on an event-based strategy as explained in Chapter 3, where an event occurs when the loading state of an element changes. Cyclic models are required to predict the variation of the element tangent stiffness along a future excursion. This task can be accomplished by assuming the nature of the future excursions, whether it is a full cycle or a half cycle, based on previous cyclic history and creating an appropriate trial path for that excursion.

From a modeling perspective, a separate class structure for cyclic control can be developed that manages the event-based strategy and is independent of the inelastic behaviour modeling handled by the surface class models and the evolution class models. An element can then be associated with cyclic control model which deals with the quasi-elastic degraded hysteretic response. New cyclic model classes can be developed to capture the various characteristics of hysteretic response, e.g. stiffness degradation, peak-oriented reloading stiffness, pinching, cyclic strength degradation. Following a systematic approach, the individual cyclic model classes defined for each type of cyclic response perform the interactions with the element entirely through the cyclic control class which invokes the appropriate class based on the previous cyclic history.

In this research, the element class `InelasticCyc3D` is associated with a cyclic control model as shown on the element collaboration diagram on Figure 4-7. The hierarchy structure of the proposed cyclic control class is shown in Figure 4-17. As a new model introduced in the OpenSees framework, it is derived from classes `TaggedObject` and `Movable Object`. The abstract base class `CyclicControl` has four main functions required for the interactions with its client, the element class. First, the base class declares the public methods that the element object can invoke, such as functions for obtaining trial element tangent stiffness. Second, it implements methods for storing the attributes required to manage the event-based strategy, such as history of previous peak and cross-over events. Third, it invokes the appropriate cyclic model for predicting the variation of tangent stiffness. Fourth, it interacts with damage models to obtain current damage

indices and passes this information to cyclic models for calculating damage-based stiffness and strength degradations. These relationships are schematically shown on the collaboration diagram on Figure 4-18.

As mentioned in previous sections, the force state is described in a vector format with respective units for forces and moments in the element formulation. The cyclic models operate in a normalized 2D space such that the initial tangent is equal to unity and the factor for element stiffness is simply the tangent of the hysteretic model corresponding to the current load step. To facilitate the interactions between the element and the cyclic model classes, the cyclic control class also implements methods for performing the required transformations of the data types (vectors, matrices) from the element system to the appropriate cyclic model system and vice-versa. The final class `CyclicControl3D` provides transformation functions for 3D elements.

The cyclic control class acts as a hub by gathering information on the current state of force, the history of previous excursions and damage progression, and connecting the element object with the appropriate cyclic model object. In accordance with object oriented design, the base class `CyclicControl` evaluates the current status, implements the state transition and keeps account of the events at the start and end of the current path.

The cyclic model classes are required to provide the specific functions for the path followed between the events marking the start and the end of the path. The following

cyclic model classes are proposed in this research: CyclicStiffness, CyclicPinching and CyclicStrengthDegradation.

The CyclicStiffness class handles the quasi-elastic response of elements that have undergone yielding in flexure but have not experienced failure in shear. This class provides the effective stiffness factor for the unloading stiffness after yielding and for the reloading stiffness prior to reaching the yield surface. The hierarchy structure of CyclicStiffness class is shown on Figure 4-19. The derived subclasses are LinCyclicStiffness and BiLinCyclicStiffness. The final class LinCyclicStiffness is provided for obtaining a constant tangent stiffness factor that is the same for unloading and reloading, whereas BiLinCyclicStiffness is provided for obtaining different tangent stiffness factors for unloading and reloading. The reloading stiffness factor can be peak-oriented.

The CyclicPinching class deals with the quasi-elastic response of elements that have suffered failure in shear. It provides the effective stiffness factor for the unloading stiffness and for the reloading stiffness which incorporates the pronounced effects of pinching common for element response governed by failure in shear. The hierarchy structure of Cyclicpinching class is shown on Figure 4-20. The final class MultiLinPinching derived from the base class provides the specific functions for the stiffness factors for unloading, pinching and peak-oriented reloading.

The `CyclicStrengthDegradation` class has a different function from the cyclic models described above which are used to provide tangent stiffness factors for the quasi-elastic states. `CyclicStrengthDegradation` class is used in modeling the loss of strength under repeated load reversals by using cumulative damage indices based on hysteretic energy. During reloading in the quasi-elastic degraded range of response `CyclicControl` class obtains cumulative damage indices from the damage model classes and provides this information to `CyclicStrengthDegradation` class. The latter has to calculate effective degradation indices for contracting the surface models based on the accumulated damage and provide the indices back to the `CyclicControl` class. Since the `CyclicControl` class keeps account of the previous events, it contacts the appropriate surface evolution model object to contract either the yield surface if yielding in flexure has previously occurred or the shear failure surface if failure in shear has been experienced. The `CyclicControl` class also uses the information on degradation indices obtained from the `CyclicStrengthDegradation` class to control the `CyclicStiffness` class and the `CyclicPinching` class in determining the peak-oriented reloading stiffness factor based on the updated/contracted surface models. The hierarchy structure of `CyclicStrengthDegradation` class is shown on Figure 4-21. The derived final class is `DamageDegradingStrength`. It is provided for implementing specific functions for calculating the damage-based degradation indices.

Another class that is introduced for modeling the quasi-elastic response is `BiaxialEffectStiffness`. This class deals with the coupling in stiffness degradation in two transverse directions for modeling 3D behaviour. This is achieved by using degradation

factors based on the accumulated damage during positive and negative excursions in the direction of loading as well as the direction at right angles as described in Section 3.4. The BiaxialEffectStiffness class obtains current information on damage indices from the CyclicControl class similarly to the CyclicStrengthDegradation class. It then uses the damage indices to calculate degradation factors for modifying the unloading and reloading tangent stiffness for each direction. The CyclicControl class provides the degradation factors obtained by the BiaxialEffectStiffness class to either the CyclicStiffness class or the CyclicPinching class depending on the previous history of events and the projected future path. The hierarchy structure of BiaxialEffectStiffness class is shown on Figure 4-22. The derived subclasses are IsoBiaxEffect and NonUniBiaxeffect. The final class IsoBiaxEffect is provided for obtaining the same degradation factors for the tangent stiffness in every direction regardless the direction of previous loading, whereas NonUniBiaxeffect is provided for obtaining different degradation factors for the tangent stiffness in each direction. The degradation factors can be based on weighting coefficients that are functions of the amplitude of previous excursions.

The proposed class hierarchy structures of the cyclic model classes and the collaborative relationships between the cyclic model classes and the cyclic control class provide an optimal class design with focus on extensibility and flexibility. The main advantage is that the cyclic control class deals with client (element and surface evolution models) interactions at the higher level. By creating a separate group of classes to deal with the quasi-elastic response, the independence of the cyclic behaviour modeling

implementation from the inelastic behaviour modeling implementation handled by the surface and evolution models is ensured. Other cyclic model classes can be added within the cyclic control structure without complications.

4.4.9 Damage Model and Damage Progression Classes

As described in the previous section, the cyclic control class is required to obtain information on damage indices and to keep track of damage accumulation. Damage indices are used by cyclic model classes to determine damage-based stiffness and strength degradations. To implement this functionality, the cyclic control model has pointers to damage models and damage progression recorder. These damage models and damage progression recorder are implemented as separate new classes derived from classes TaggedObject and Movable Object. The hierarchy structures of the proposed DamageModel class and DamageProgression class are shown in Figures 4-23 and 4-24, respectively.

The DamageModel class provides damage indices based on plastic deformations or hysteretic energy, or a combination of the two. The base class provides the interface for the interactions with the cyclic control class and the final classes are required to implement specific functions for calculating damage indices. Current state of force and plastic deformations required for calculation of damage indices is provided by the cyclic control model. Final classes can be implemented that calculate damage indices based on models proposed by Park and Ang (1985), Kratzig et al. (1989), Mehanny and Deierlein (2000), among others.

The `DamageProgression` class is provided for storing information on damage accumulation. The base class provides the interface for the interactions with the cyclic control class and the final class provides the functionality for recording the damage indices at each converged step of the analysis for the damage models invoked by the cyclic control class. When the cyclic control model obtains current damage indices from the damage model, the former passes this information to the damage progression recorder for storing and making it available as output at the end of the analysis.

4.5 Implementation Examples

4.5.1 Example on Cyclic Stiffness Model Event-Based Strategy

The example presented here demonstrates the application of the event-based strategy developed for the state determination of the cyclic stiffness model using consistent conditions generalized for positive and negative cyclic excursions.

The cyclic response used for this example is shown on Figure 4-25. The events are indicated on the force-deformation curve with their respective values. Events 1 and 4 mark the initial yielding in the positive and negative directions, respectively. Event 4 is created using the force and deformation values of event 1 but with negative sign and it is used in the peak-oriented model in the initial reloading in the opposite direction. After the initial yielding in the positive and negative direction, events 1 and 4 are no longer stored by the cyclic control model since they are not actual peak events. The positive peak

events are events 2, 7, 8, 12, 13 and 17. The negative peak events are events 5, 10 and 15. It can be noticed that event 7 duplicates event 2 but it is given an individual designation to distinguish from the peak in the previous cycle. The actual peak event to be stored by the cyclic control model during the course of analysis is only event 2 and its force-deformation values are assigned to the fictitious peak event 7 which is used in the subsequent cycle of positive excursions in the peak-oriented model. The same relationship is valid for the couples of peak events 8 and 12, and 13 and 17. The negative peak events 10 and 15 are marked with an asterisk to note that these are not actual events since they are not reached in the cyclic response. The force-deformation values of event 5 are assigned to events 10 and 15 as these are used in the peak-oriented model for the negative excursions.

The conditions used to check and determine the loading state of the member subjected to cyclic load reversals are presented in Table 4-1. Events mark the beginning and the end of a loading path as indicated in Table 4-1 and depending on the condition status, the event type is identified as peak or cross-over. The details of the member cyclic response are provided in Table 4-2. It can be noted that when a peak event is identified, the current half cycle is determined as a primary half cycle. In the case where a peak event is not reached, the half cycle is determined as a follower half cycle. Half cycle No. 5 in this example is a follower half cycle. The half cycles in this example are also identified on the displacement history shown on Figure 4-25. The positive peak event 8 is greater than the previous peak in the positive excursions (peak event 2), thus the half cycle is determined as primary and the new peak event (event 8) is recorded and stored by the cyclic control

model. Positive cross-over events occur after negative cross-over events in the case of unloading prior to reaching zero point in terms of deformations and the peak in the opposite direction. The positive cross-over events mark an incomplete half cycle. It can be noticed from this example that complete half cycles have only negative cross-over events (half cycles No. 1, 2 and 4), whereas incomplete half cycles contain both negative and positive cross-over events (half cycle No. 3). Based on their attributes, the following half cycle types are distinguished: primary complete; primary incomplete; follower complete; and follower incomplete.

Since the events in the future excursions are unknown at the current step, it is assumed that the current half cycle is a primary complete half cycle. When the condition checks yield a different result, the half cycle type is redefined as a follower or incomplete, and the corresponding steps in the flow of the condition checks are undertaken. For instance, the fictitious peak event 10 is created in the beginning of half cycle No. 3 using the force-deformation values of the previous peak in the negative excursions (event 5) and it is assumed that the new peak (event 10) will be reached in the reloading state. The identification of a positive cross-over event (event 11) determines half cycle No. 3 as incomplete and triggers the start of a new cycle and the creation of a new fictitious positive peak event (event 12) which is to be followed in the new reloading state.

4.5.2 Examples with Cyclic Models

The examples presented here demonstrate the viability of the proposed cyclic degradation models. Figure 4-26 shows the column dimensions and details of reinforcement as well as

the deflection history. In the first example, the details of the column and the deflection history are similar to the ones of test specimen U1 in Saatcioglu and Ozcebe (1989). As reported by Saatcioglu and Ozcebe (1989), the specimen developed its full flexural yield strengths prior to shear failure. Figure 4-27 shows the lateral load - top displacement cyclic response of the model, capturing stiffness degradation and cyclic strength deterioration. In the second example, the same column is used but with increased spacing between the transverse reinforcement such that the shear strength is around 200 kN and is less than the shear strength required to develop the full flexural yield strength. Figure 4-28 shows the lateral load - top displacement cyclic response of the model, which undergoes brittle shear failure prior to yielding and exhibits softening under increased displacement and pronounced stiffness degradation and pinching.

Table 4-1 Condition checks for loading state

Path ID	Event ID	Event Type	Excursion Type	Condition Check	Condition Status	Loading State
0 - 1	-	-	Positive	$ \Delta_i \leq \Delta_{i-1} $	$ \Delta_i > \Delta_{i-1} $	Loading
-	1	YS	Positive	$ \Delta_i \leq \Delta_{i-1} $	$ \Delta_i > \Delta_{i-1} $	Loading
1 - 2	-	-	Positive	$ \Delta_i \leq \Delta_{i-1} $	$ \Delta_i > \Delta_{i-1} $	Loading
-	2	+ P	Positive			Transition, Peak, Positive
2 - 3	-	-	Positive	$ \Delta_i \leq \Delta_{i-1} ; F_i F_{i-1} \leq 0$	$ \Delta_i < \Delta_{i-1} ; F_i F_{i-1} > 0$	Unloading
-	3	- C	Positive	$ \Delta_i \leq \Delta_{i-1} ; F_i F_{i-1} \leq 0; (F_i \Delta_i) \leq 0$	$ \Delta_i < \Delta_{i-1} ; F_i F_{i-1} < 0; (F_i \Delta_i) < 0$	Transition, Cross-over, Negative
3 - 4	-	-	Positive	$ \Delta^c - \Delta_i \leq \Delta^c - \Delta_{i-1} $	$ \Delta^c - \Delta_i > \Delta^c - \Delta_{i-1} $	Reloading in the opposite direction
			Negative	$ \Delta_i \leq \Delta_{i-1} $	$ \Delta_i > \Delta_{i-1} $	Reloading in the opposite direction
-	4	YS	Negative	$ \Delta_i \leq \Delta_{i-1} $	$ \Delta_i > \Delta_{i-1} $	Reloading in the opposite direction
4 - 5	-	-	Negative	$ \Delta_i \leq \Delta_{i-1} $	$ \Delta_i > \Delta_{i-1} $	Reloading in the opposite direction
	5	- P	Negative			Transition, Peak, Negative
5 - 6	-	-	Negative	$ \Delta_i \leq \Delta_{i-1} ; F_i F_{i-1} \leq 0$	$ \Delta_i < \Delta_{i-1} ; F_i F_{i-1} > 0$	Unloading
	6	- C	Negative	$ \Delta_i \leq \Delta_{i-1} ; F_i F_{i-1} \leq 0; (F_i \Delta_i) \leq 0$	$ \Delta_i < \Delta_{i-1} ; F_i F_{i-1} < 0; (F_i \Delta_i) < 0$	Transition, Cross-over, Negative
6 - 7	-	-	Negative	$ \Delta^c - \Delta_i \leq \Delta^c - \Delta_{i-1} $	$ \Delta^c - \Delta_i > \Delta^c - \Delta_{i-1} $	Reloading in the initial direction
			Positive	$ \Delta_i \leq \Delta_{i-1} $	$ \Delta_i > \Delta_{i-1} $	Reloading in the initial direction
-	7	YS	Positive	$ \Delta_i \leq \Delta_{i-1} $	$ \Delta_i > \Delta_{i-1} $	Reloading in the initial direction
7 - 8	-	-	Positive	$ \Delta_i \leq \Delta_{i-1} $	$ \Delta_i > \Delta_{i-1} $	Reloading in the initial direction
-	8	+ P	Positive			Transition, Peak, Positive
8 - 9	-	-	Positive	$ \Delta_i \leq \Delta_{i-1} ; F_i F_{i-1} \leq 0$	$ \Delta_i < \Delta_{i-1} ; F_i F_{i-1} > 0$	Unloading
-	9	- C	Positive	$ \Delta_i \leq \Delta_{i-1} ; F_i F_{i-1} \leq 0; (F_i \Delta_i) \leq 0$	$ \Delta_i < \Delta_{i-1} ; F_i F_{i-1} < 0; (F_i \Delta_i) < 0$	Transition, Cross-over, Negative

Table 4-1 (Continued)

Path ID	Event ID	Event Type	Excursion Type	Condition Check	Condition Status	Loading State
9 - 10	-	-	Positive	$ \Delta^c - \Delta_i \leq \Delta^c - \Delta_{i-1} $	$ \Delta^c - \Delta_i > \Delta^c - \Delta_{i-1} $	Reloading in the opposite direction
-	10*	- P	Positive			Negative peak not reached
10 -11	-	-	Positive	$ \Delta^c - \Delta_i \leq \Delta^c - \Delta_{i-1} $	$ \Delta^c - \Delta_i < \Delta^c - \Delta_{i-1} $	Unloading in the opposite direction
-	11	+ C	Positive	$ \Delta^c - \Delta_i \leq \Delta^c - \Delta_{i-1} $ $F_i F_{i-1} \leq 0; (F_i \Delta_i) \leq 0$	$ \Delta^c - \Delta_i < \Delta^c - \Delta_{i-1} $ $F_i F_{i-1} < 0; (F_i \Delta_i) > 0$	Transition Cross-over, Positive
11 -12	-	-	Positive	$ \Delta_i \leq \Delta_{i-1} $	$ \Delta_i > \Delta_{i-1} $	Reloading in the initial direction
-	12	YS	Positive	$ \Delta_i \leq \Delta_{i-1} $	$ \Delta_i > \Delta_{i-1} $	Reloading in the initial direction
12 -13	-	-	Positive	$ \Delta_i \leq \Delta_{i-1} $	$ \Delta_i > \Delta_{i-1} $	Reloading in the initial direction
-	13	+ P	Positive			Transition, Peak, Positive
13 -14				$ \Delta_i \leq \Delta_{i-1} ; F_i F_{i-1} \leq 0$	$ \Delta_i < \Delta_{i-1} ; F_i F_{i-1} > 0$	Unloading
-	14	- C	Positive	$ \Delta_i \leq \Delta_{i-1} ; F_i F_{i-1} \leq 0; (F_i \Delta_i) \leq 0$	$ \Delta_i < \Delta_{i-1} ; F_i F_{i-1} < 0; (F_i \Delta_i) < 0$	Transition, Cross-over, Negative
14 -15	-	-	Positive	$ \Delta^c - \Delta_i \leq \Delta^c - \Delta_{i-1} $	$ \Delta^c - \Delta_i > \Delta^c - \Delta_{i-1} $	Reloading in the opposite direction
	-	-	Negative	$ \Delta_i \leq \Delta_{i-1} $	$ \Delta_i > \Delta_{i-1} $	Reloading in the opposite direction
-	15*	- P	Negative			Negative peak not reached
15 -16	-	-	Negative	$ \Delta_i \leq \Delta_{i-1} ; F_i F_{i-1} \leq 0$	$ \Delta_i < \Delta_{i-1} ; F_i F_{i-1} > 0$	Unloading
-	16	- C	Negative	$ \Delta_i \leq \Delta_{i-1} ; F_i F_{i-1} \leq 0; (F_i \Delta_i) \leq 0$	$ \Delta_i < \Delta_{i-1} ; F_i F_{i-1} < 0; (F_i \Delta_i) < 0$	Transition, Cross-over, Negative
16 -17	-	-	Negative	$ \Delta^c - \Delta_i \leq \Delta^c - \Delta_{i-1} $	$ \Delta^c - \Delta_i > \Delta^c - \Delta_{i-1} $	Reloading in the initial direction

Table 4-2 Cyclic response details

Path	Event	Event	Excursion	Response	Force	Displ.	Half Cycle Details	
ID	ID	Type	Type	Type	kN	mm	ID	Type
0 - 1	-	-	Positive	Elastic			1	Primary Complete
-	1	YS	Positive	Yielding	400	3	1	Primary Complete
1 - 2	-	-	Positive	Inelastic			1	Primary Complete
-	2	+ P	Positive		533	15	1	Primary Complete
2 - 3	-	-	Positive	Quasi elastic degraded			1	Primary Complete
-	3	- C	Positive		0	10	1	Primary Complete
3 - 4	-	-	Positive	Quasi elastic degraded			1	Primary Complete
	-	-	Negative				2	Primary Complete
-	4	YS	Negative	Yielding	-400	-3	2	Primary Complete
4 - 5	-	-	Negative	Inelastic			2	Primary Complete
	5	- P	Negative		-533	-15	2	Primary Complete
5 - 6	-	-	Negative	Quasi elastic degraded			2	Primary Complete
	6	- C	Negative		0	-10	2	Primary Complete
6 - 7	-	-	Negative	Quasi elastic degraded, peak-oriented			2	Primary Complete
	-	-	Positive				3	Primary Incomplete
-	7	YS	Positive	Yielding	533	15	3	Primary Incomplete
7 - 8	-	-	Positive	Inelastic			3	Primary Incomplete
-	8	+ P	Positive		540	19	3	Primary Incomplete
8 - 9	-	-	Positive	Quasi elastic degraded			3	Primary Incomplete

Table 4-2 (Continued)

Path	Event	Event	Excursion	Response	Force	Displ.	Half Cycle Details	
ID	ID	Type	Type	Type	kN	mm	ID	Type
-	9	- C	Positive		0	13	3	Primary Incomplete
9 - 10	-	-	Positive	Quasi elastic degraded, peak-oriented			3	Primary Incomplete
-	10*	- P	Positive		-533	-15	3	Primary Incomplete
10 -11	-	-	Positive	Quasi elastic degraded			3	Primary Incomplete
-	11	+ C	Positive		0	4.5	3	Primary Incomplete
11 -12	-	-	Positive	Quasi elastic degraded, peak-oriented			4	Primary Complete
-	12	YS	Positive	Yielding	540	19	4	Primary Complete
12 -13	-	-	Positive	Inelastic			4	Primary Complete
-	13	+ P	Positive		543	23	4	Primary Complete
13 -14	-	-	Positive	Quasi elastic degraded			4	Primary Complete
	14	- C	Positive		0	16	4	Primary Complete
14 -15	-	-	Positive	Quasi elastic degraded, peak-oriented			4	Primary Complete
	-	-	Negative	Quasi elastic degraded, peak-oriented			5	Follower Incomplete
-	15*	- P	Negative		-533	-15	5	Follower Incomplete
15 -16	-	-	Negative	Quasi elastic degraded			5	Follower Incomplete
	16	- C	Negative		0	-6	5	Follower Incomplete
16 -17	-	-	Negative	Quasi elastic degraded, peak-oriented			5	Follower Incomplete
-	17*	+ P	Positive		543	23	5	Follower Incomplete

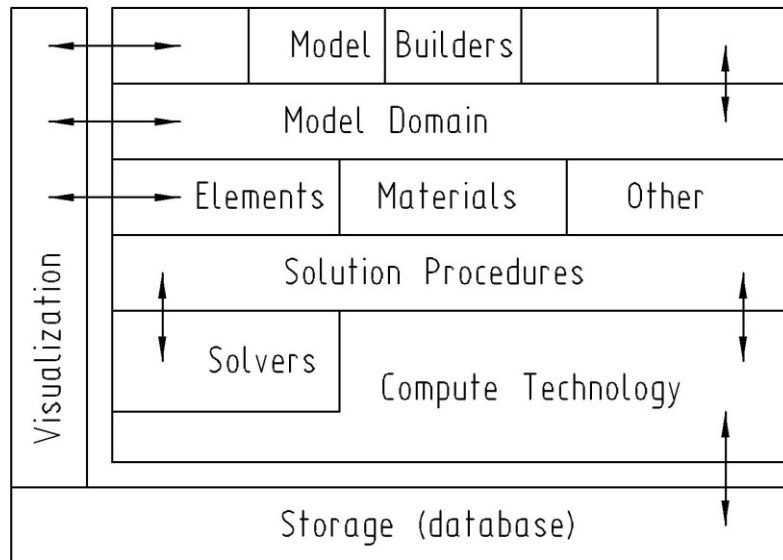


Figure 4-1 Conceptual module layout of OpenSees software framework. Reproduced from Fenves et al. (2004)

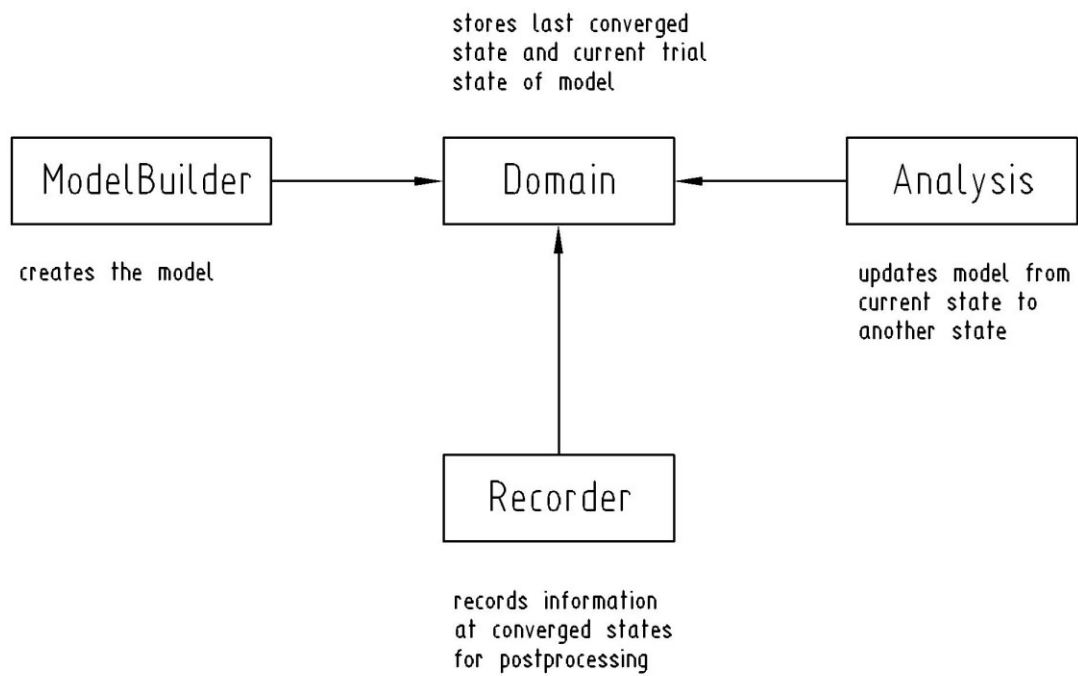


Figure 4-2 Main high-level abstractions in OpenSees software framework. Reproduced from Fenves et al. (2004)

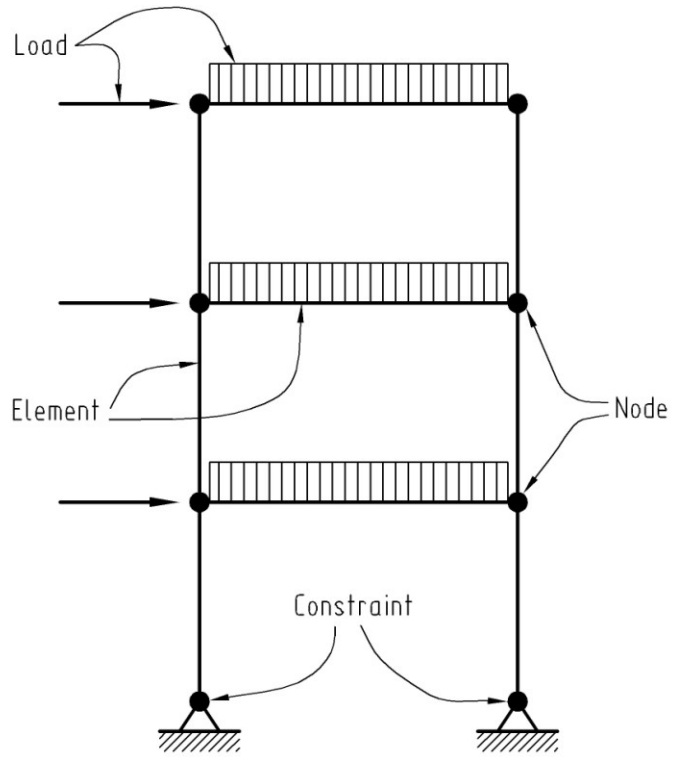


Figure 4-3 Main classes of a finite element model

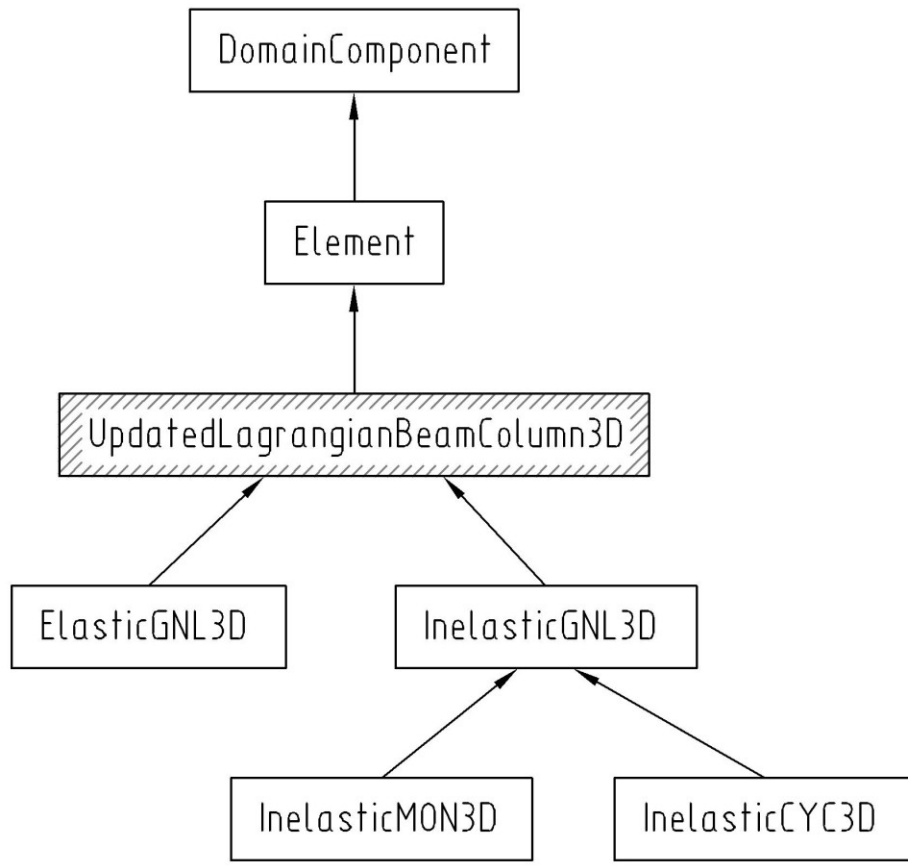


Figure 4-4 Beam-column element class hierarchy

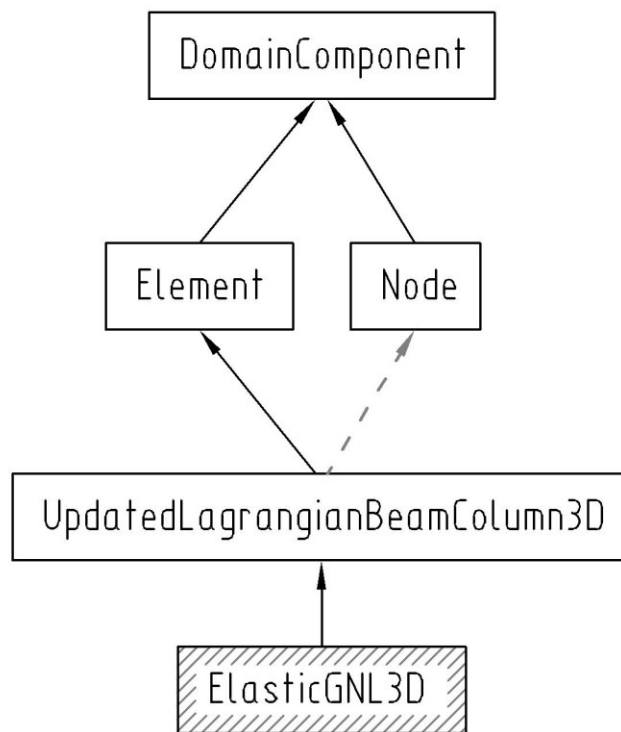


Figure 4-5 Element ElasticGNL3D collaboration diagram

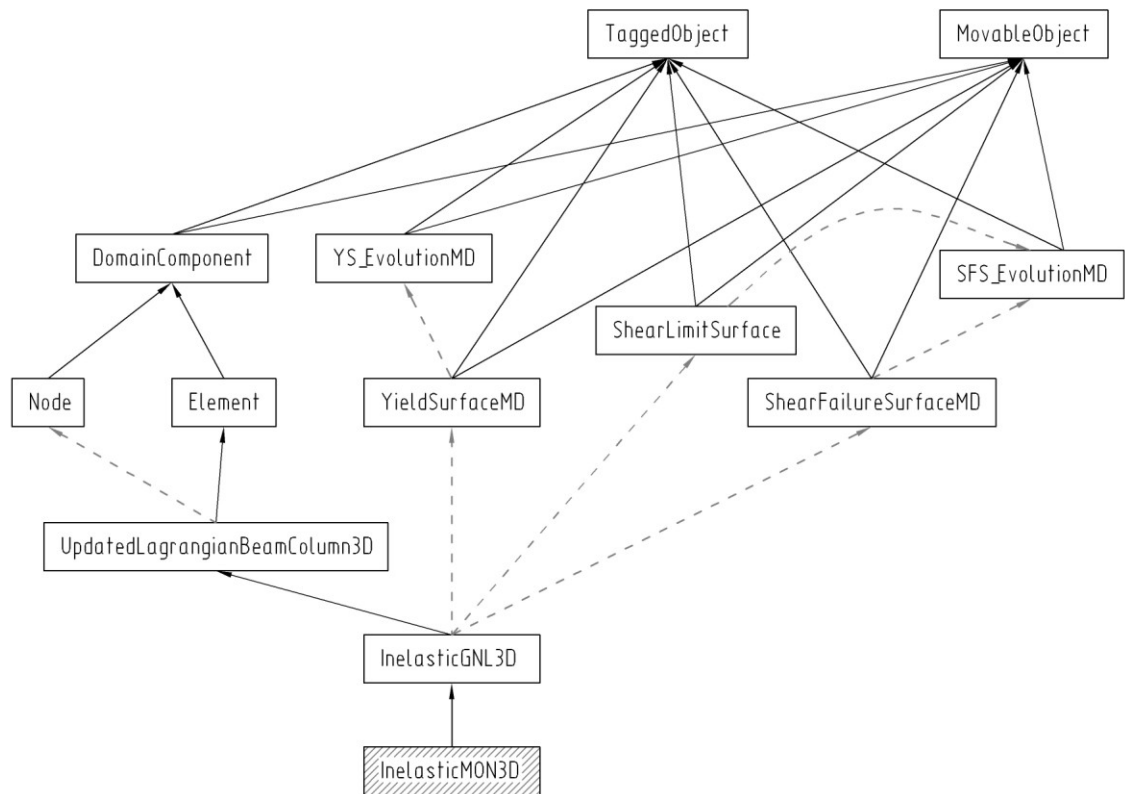


Figure 4-6 Element InelasticMON3D collaboration diagram

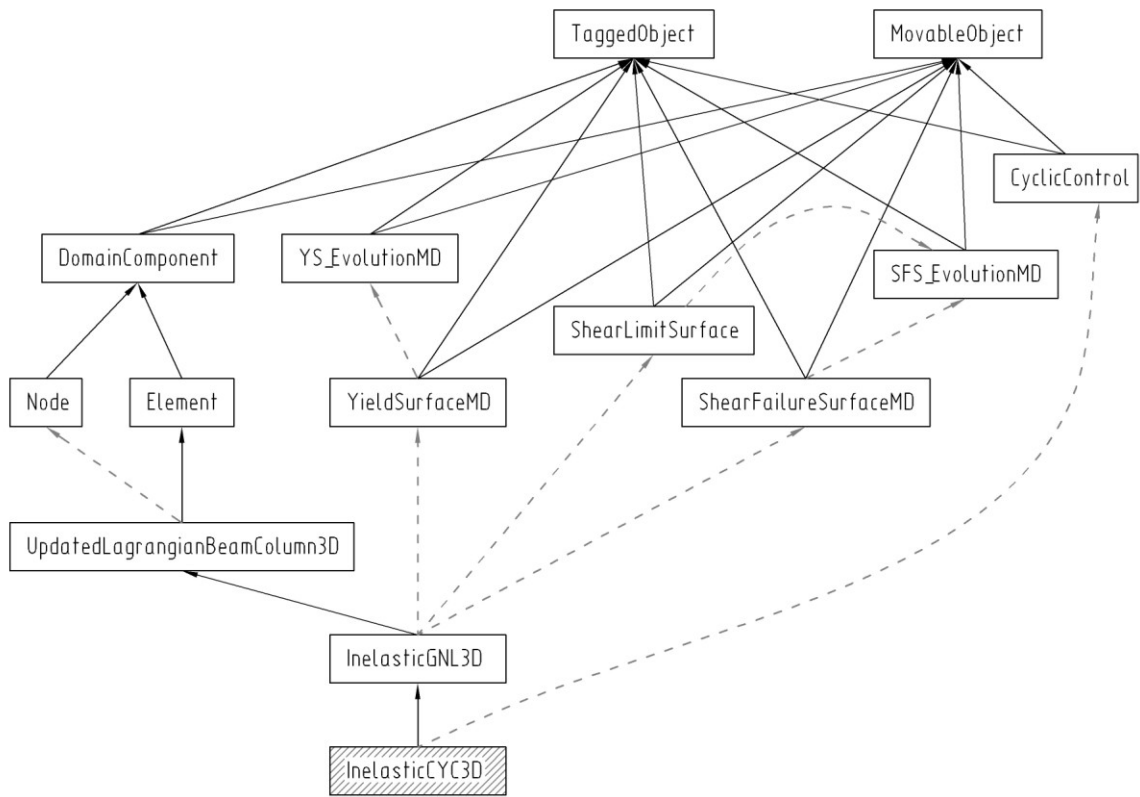


Figure 4-7 Element InelasticCYC3D collaboration diagram

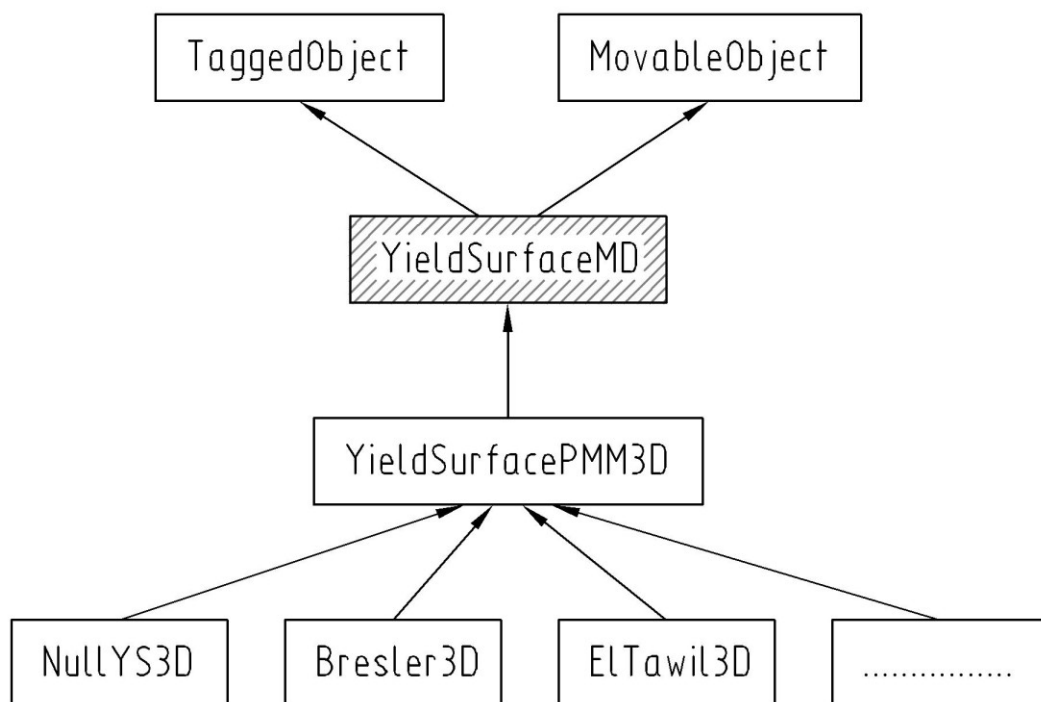


Figure 4-8 Yield surface class hierarchy

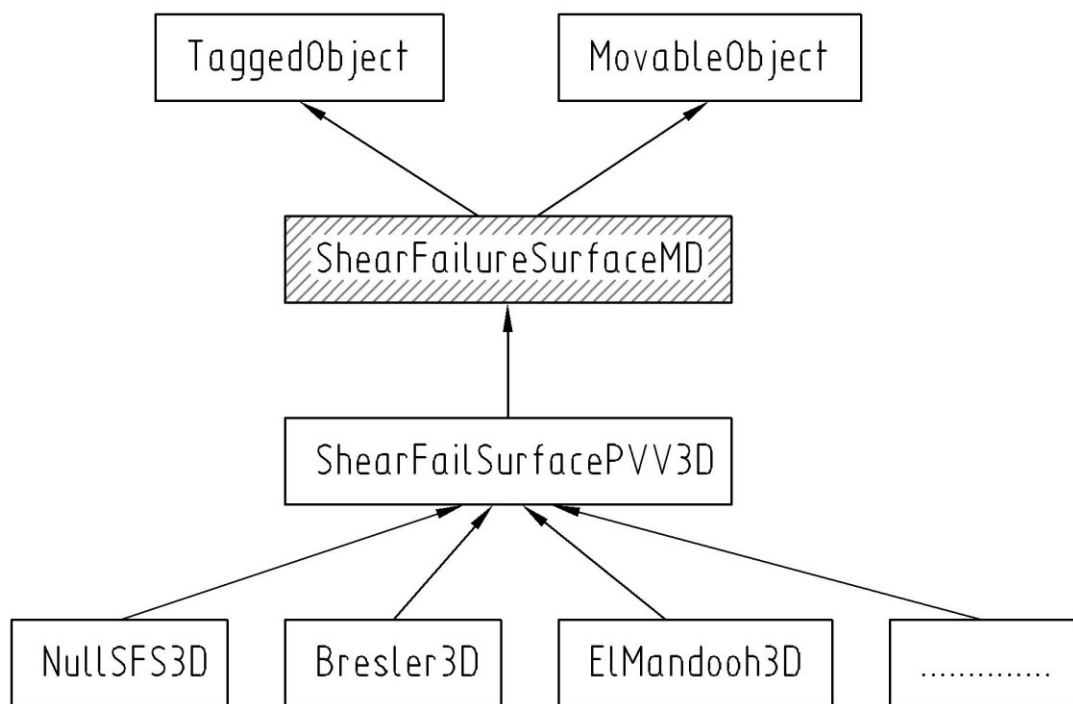


Figure 4-9 Shear failure surface class hierarchy

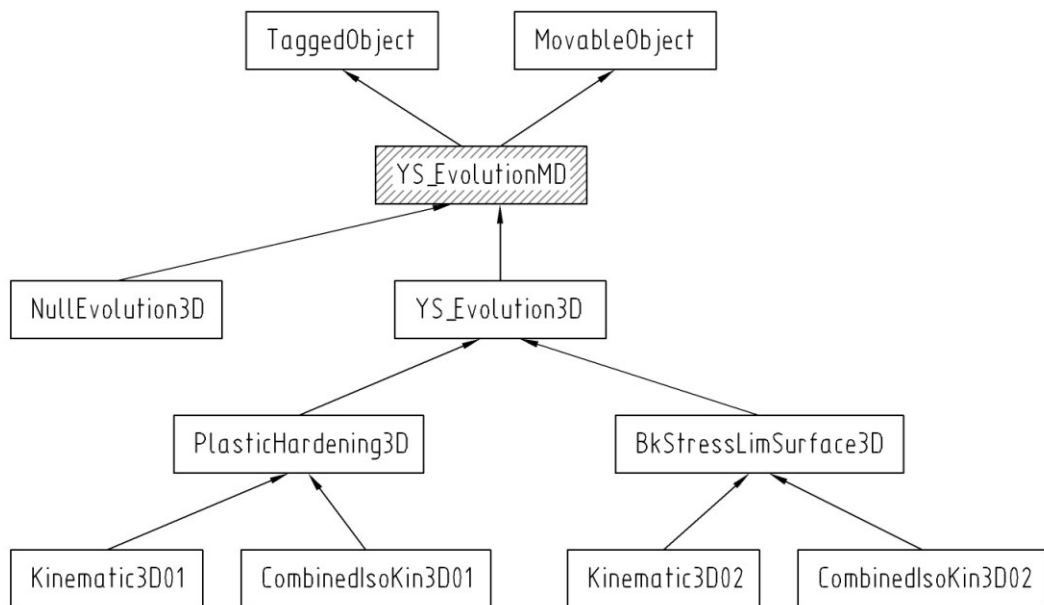


Figure 4-10 Yield surface evolution class hierarchy

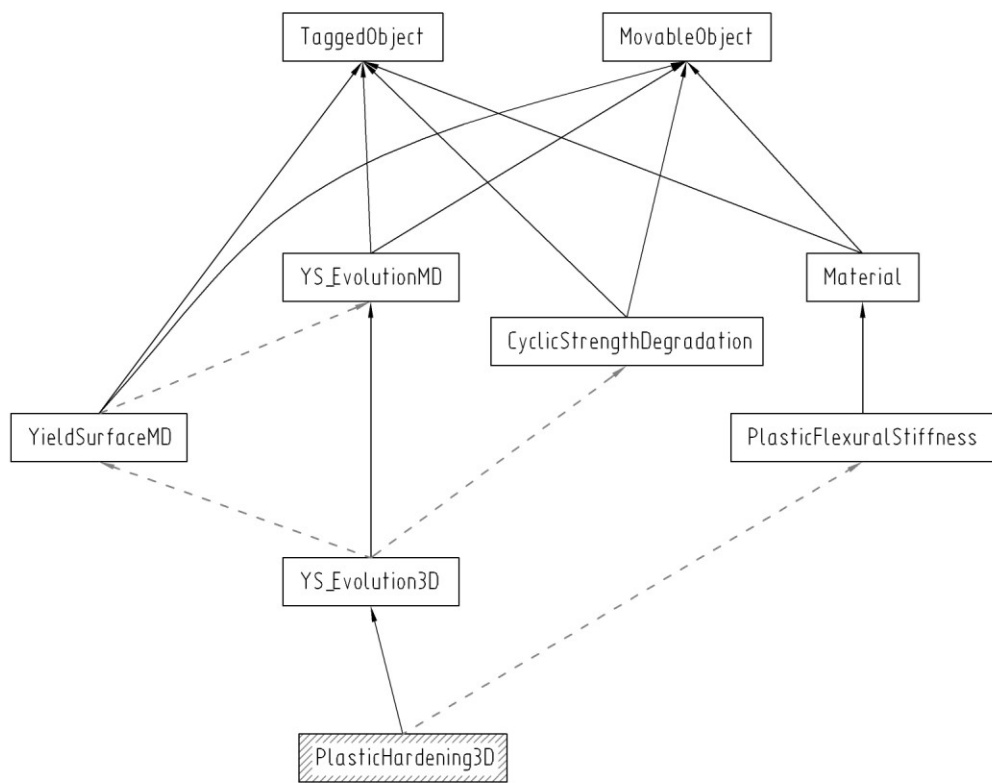


Figure 4-11 PlasticHardening3D collaboration diagram

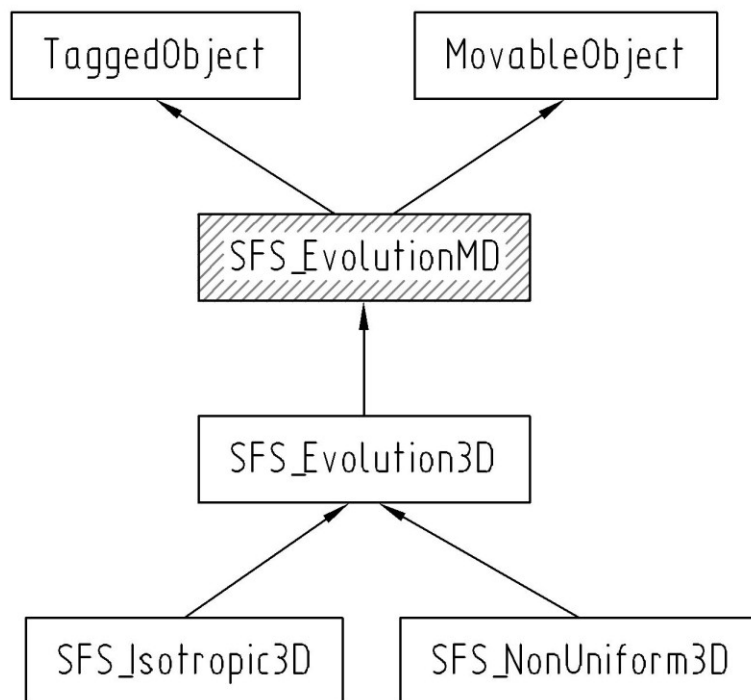


Figure 4-12 Shear failure surface evolution class hierarchy

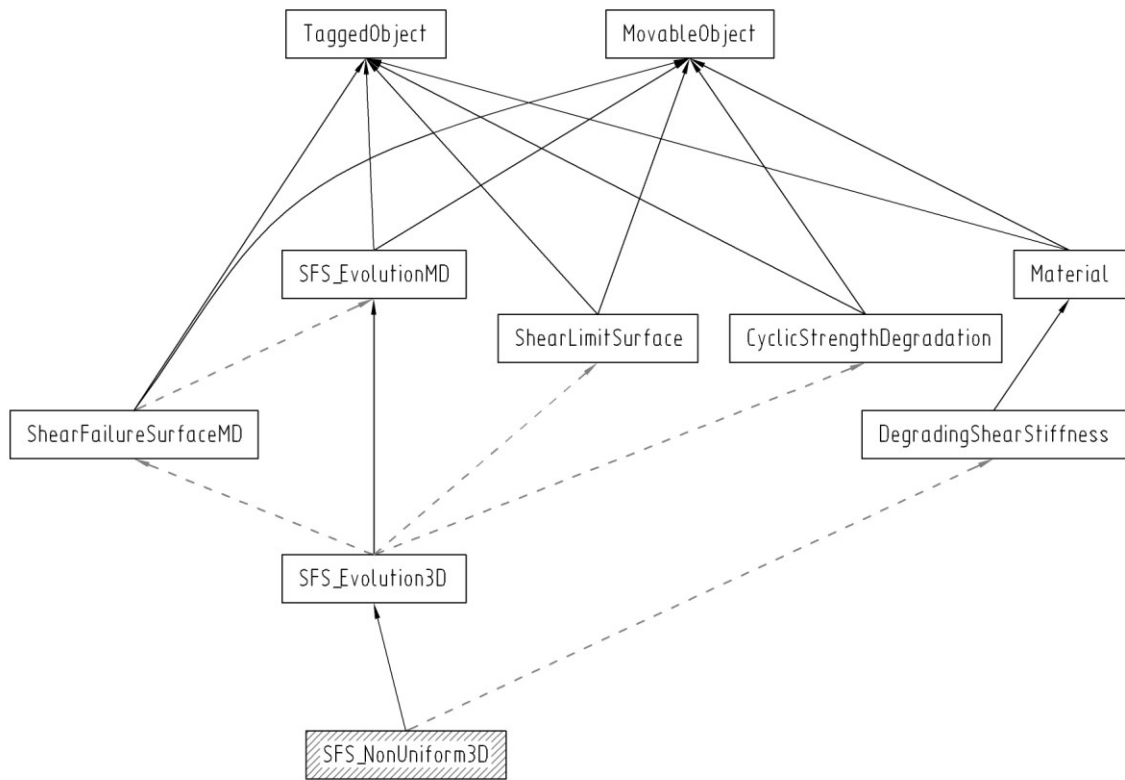


Figure 4-13 SFS_NonUniform3D collaboration diagram

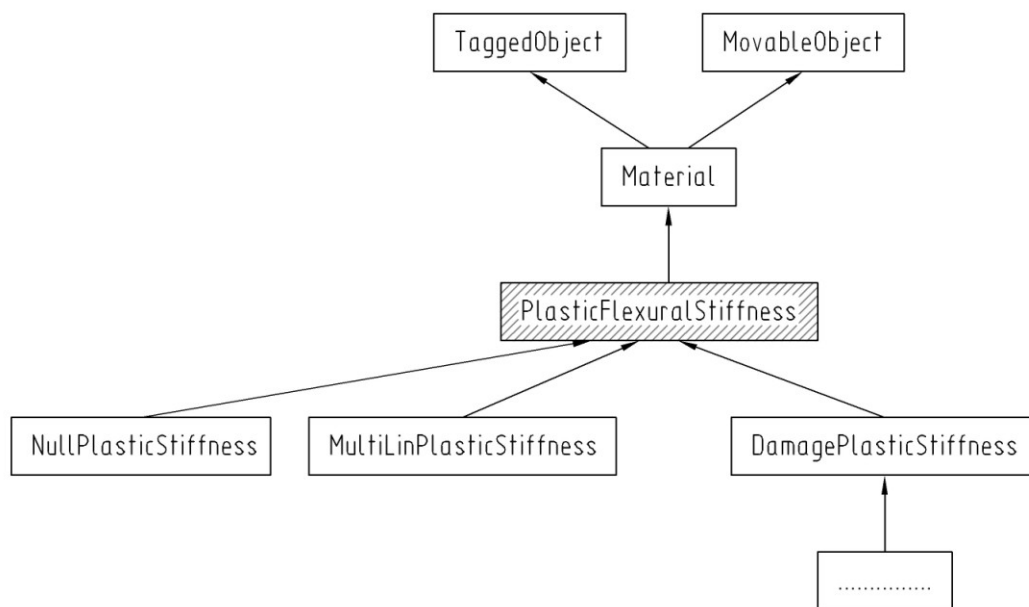


Figure 4-14 Plastic flexural stiffness class hierarchy

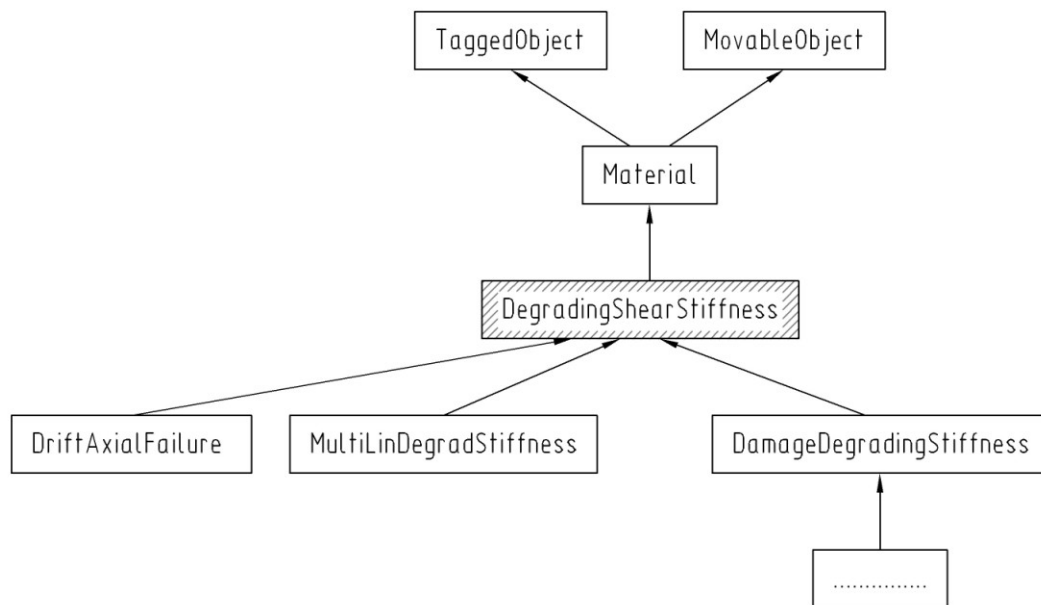


Figure 4-15 Degrading shear stiffness class hierarchy

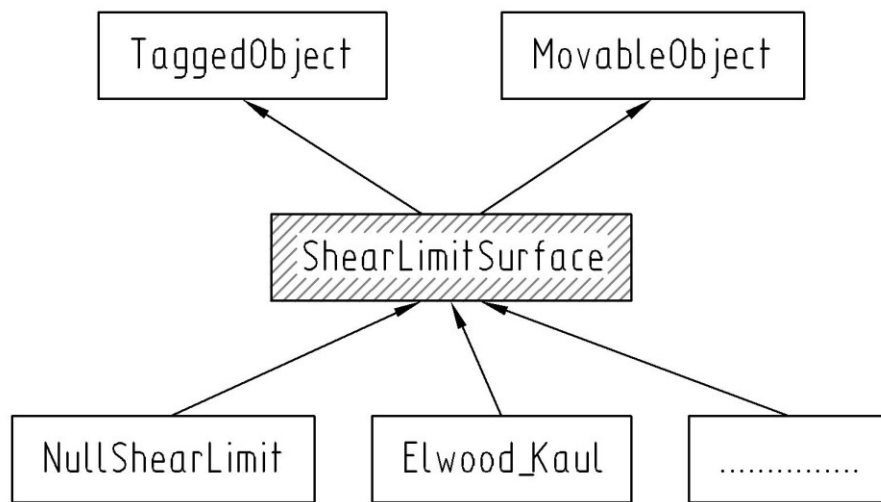


Figure 4-16 Shear limit surface class hierarchy

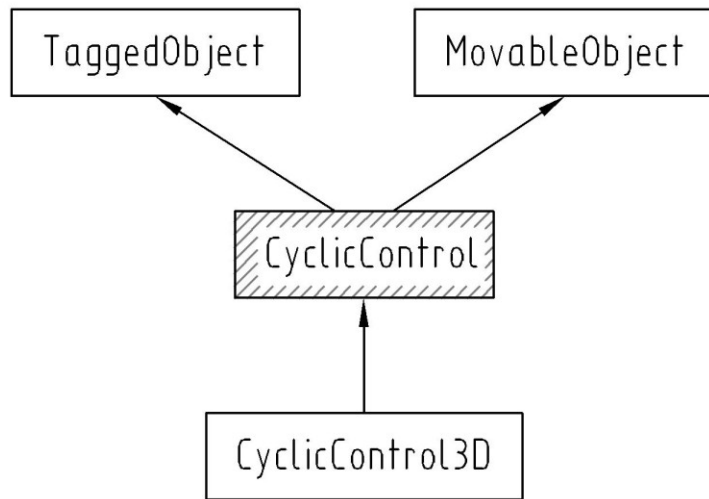


Figure 4-17 Cyclic control class hierarchy

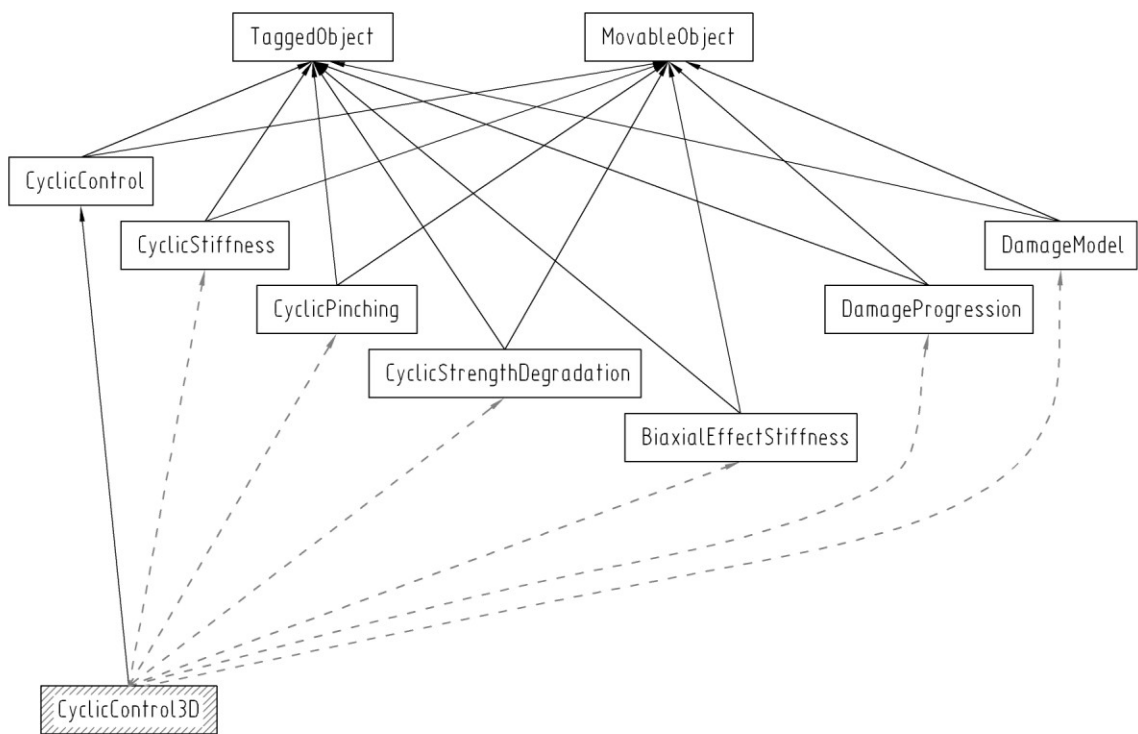


Figure 4-18 CyclicControl3D collaboration diagram

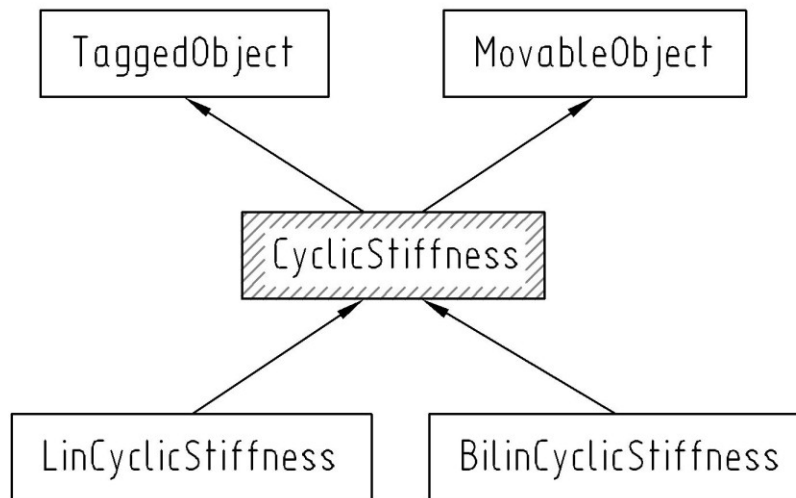


Figure 4-19 Cyclic stiffness class hierarchy

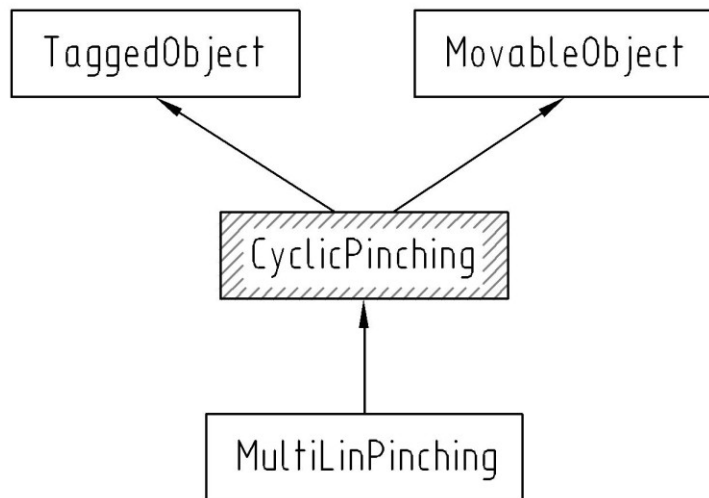


Figure 4-20 Cyclic pinching class hierarchy

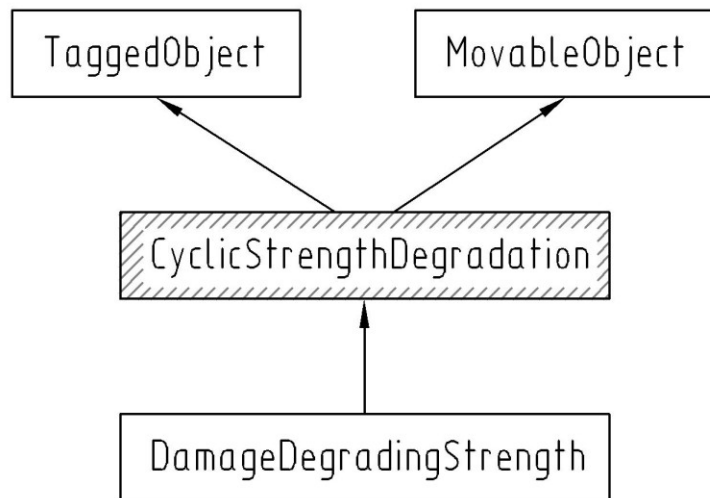


Figure 4-21 Cyclic strength degradation class hierarchy

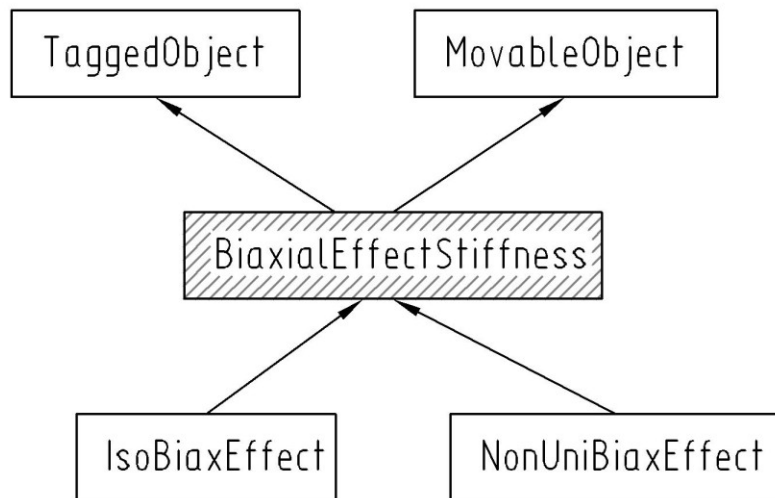


Figure 4-22 Biaxial effects on stiffness class hierarchy

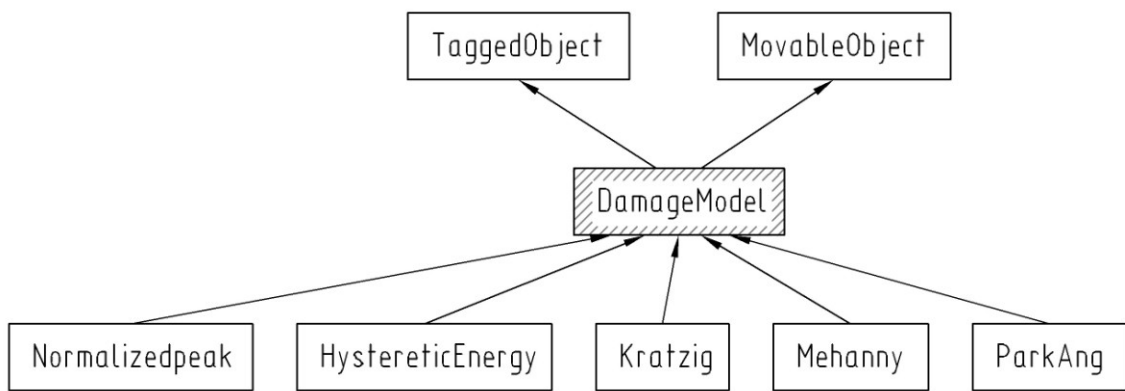


Figure 4-23 Damage model class hierarchy. Reproduced from Altoontash (2004)

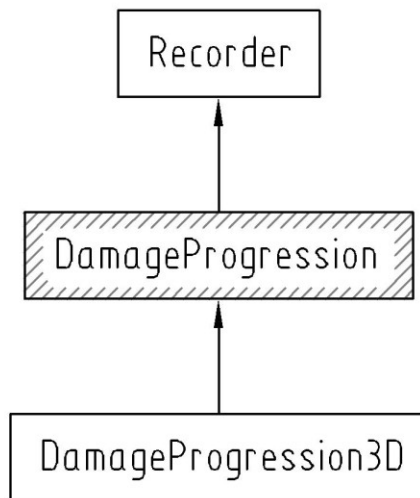


Figure 4-24 Damage progression class hierarchy

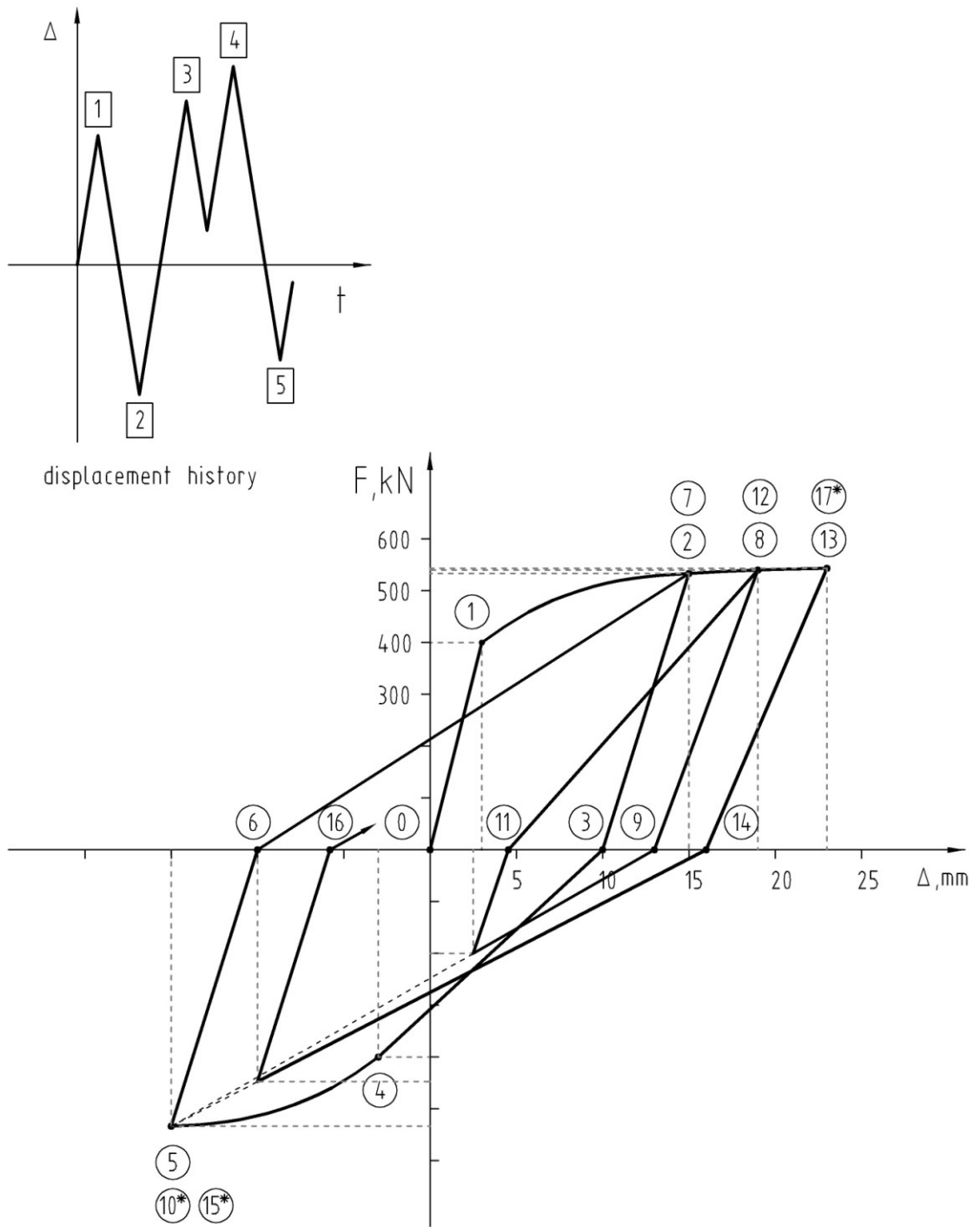


Figure 4-25 Cyclic response example

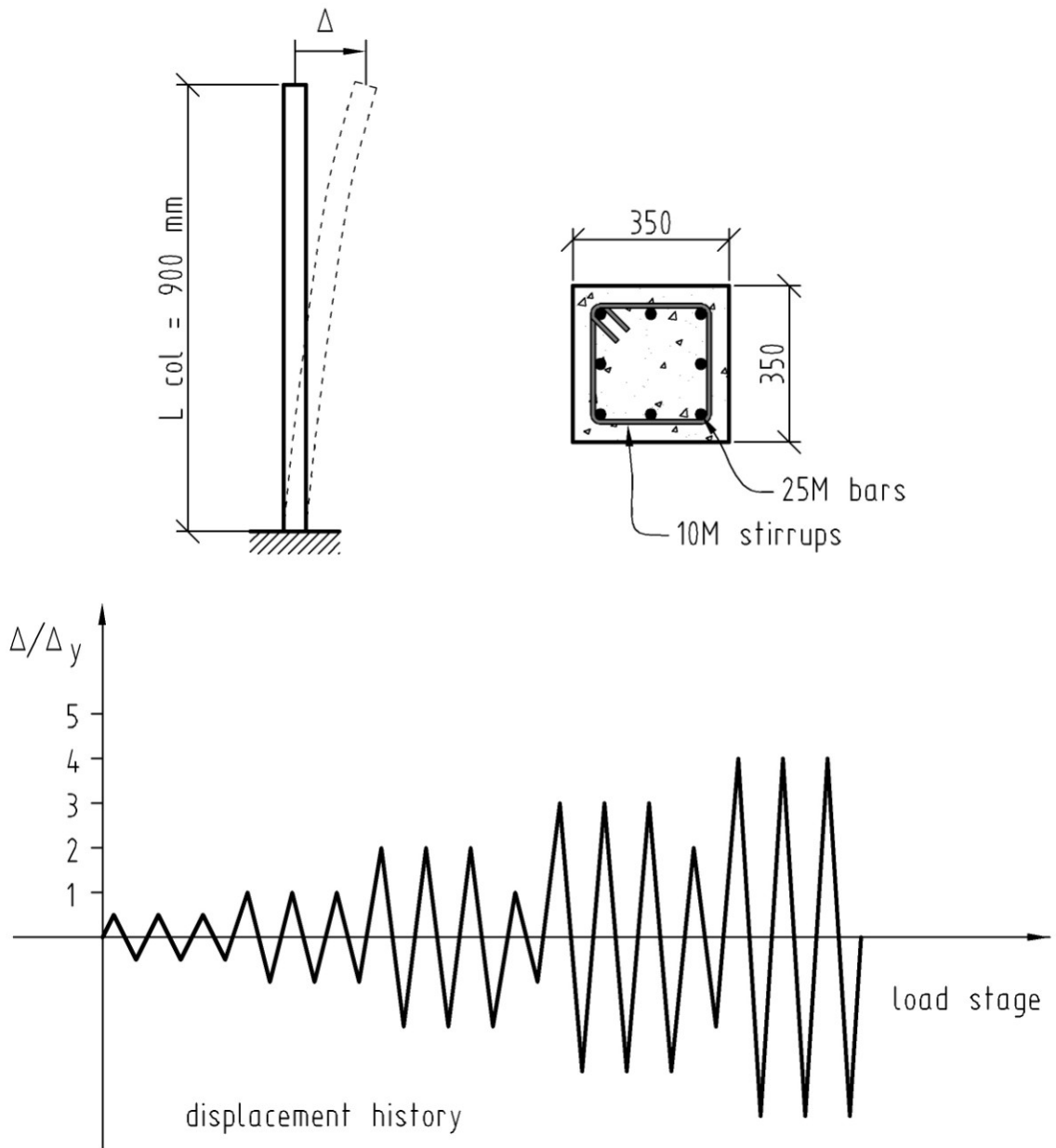
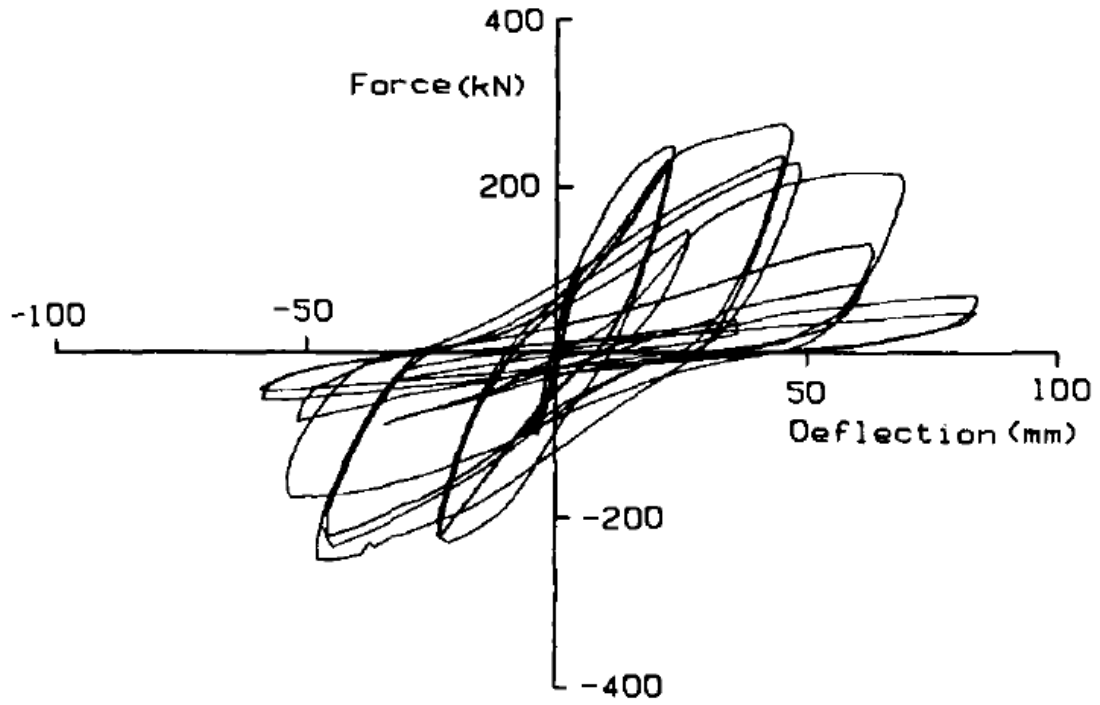
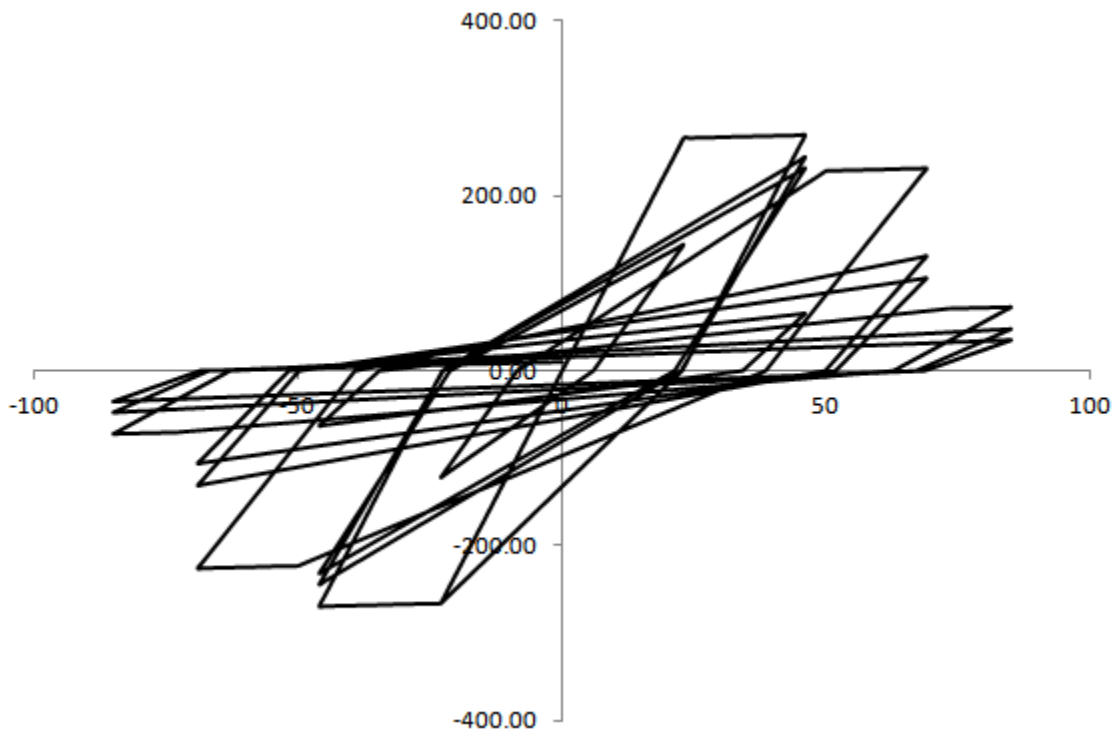


Figure 4-26 Example of reinforced concrete column subjected to cyclic loading



experimental



analytical

Figure 4-27 Example 1 cyclic response: lateral load - displacement at top of column

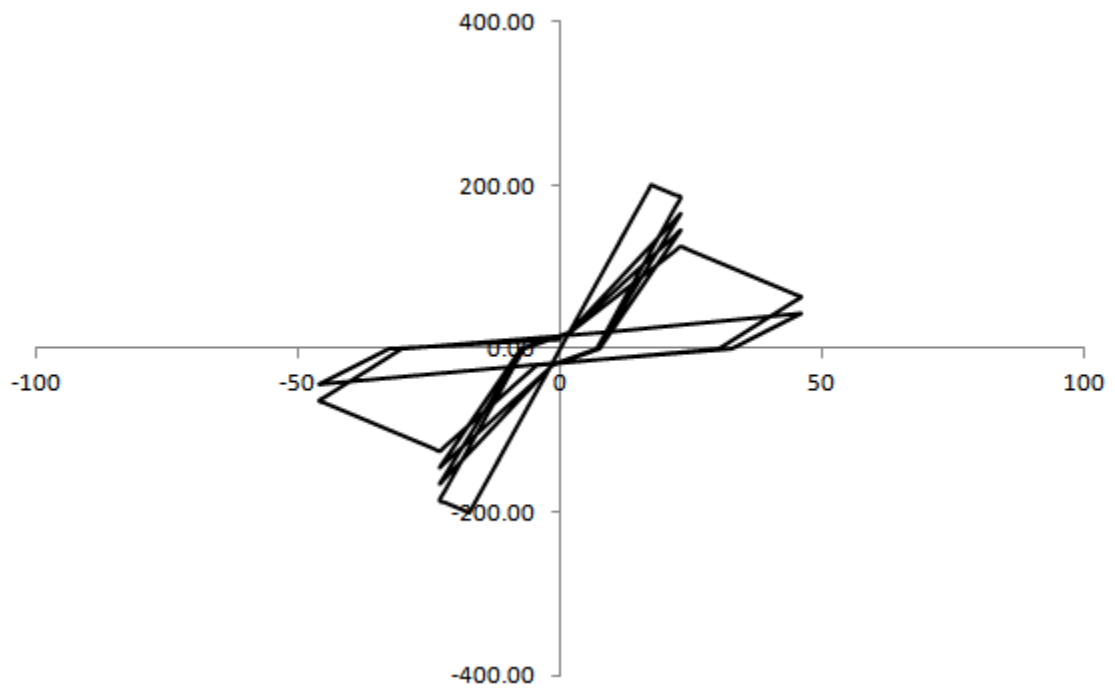


Figure 4-28 Example 2 cyclic response: lateral load-displacement at top of column

5 Chapter: Conclusions and Future Work

5.1 Summary

The principal objective of this research is to develop the formulation of a comprehensive model for seismic response analysis of reinforced concrete structures that captures the behaviour of members in new structures designed as ductile as well as non-ductile members in existing older deficient structures, and propose a framework for the implementations of the new model using object oriented design concepts. This study focuses on beam-column element formulation based on concentrated plasticity approach employing force interaction surfaces and evolution models for the generalized plastic hinges at the element ends and damage-based cyclic degradation models. The framework for the implementations of the proposed model is conceptually developed using object oriented design to facilitate the extensibility and flexibility of the model structure recognizing the need for future developments.

The main aspects of the behaviour of reinforced concrete members, broadly divided into monotonic and cyclic behaviour, are summarized in Chapter 1. Common idealized models of beam-columns developed for nonlinear response analysis are presented and their underlying formulations are discussed. Within the scope of monotonic behaviour, response characteristics of reinforced concrete members, such as effective elastic stiffness, nominal yield strength and post-yield hardening were reviewed, and their dependency on parameters, such as reinforcement steel ratio, concrete confinement and axial load level was discussed. The cyclic behaviour characteristics were related to the

damage accrued during inelastic excursions of repeated reversed cycles. The pronounced effects of damage on the gradual degradation of stiffness and loss of strength and the approach to quantify the rate of degradation based on damage indices were discussed. The specifics of shear critical behaviour observed in reinforced concrete columns in older structures with inadequate seismic detailing were discussed. The major types of failure were summarized as follows: brittle failure in shear prior to yielding, shear failure at relatively low ductility level and post-yield shear failure under large lateral drifts due to shear strength reduction in the plastic hinge zone. The cyclic behaviour of non-ductile members suffering failure in shear characterized by severe strength degradation and significant pinching was also discussed.

Literature review of existing analytical models incorporating flexural and shear effects based on concentrated and distributed plasticity concepts is presented in Chapter 2. Through careful review of the capabilities and the limitations of existing models, the need for development of a comprehensive model that captures the entire range of reinforced concrete member behaviour, from ductile to brittle and in between, was identified. The full interaction of axial load, flexure and shear effects and the effects of accumulation of damage on the three-dimensional monotonic and cyclic behaviour were considered for incorporation in the proposed model.

The formulation of the analytical models developed for capturing the behaviour of reinforced concrete members designed as ductile as well as non-ductile shear-critical column members in existing older structures, which can range from brittle behaviour

governed by shear failure to moderately ductile governed by flexure-shear failure, is described in Chapter 3. The focus is on concentrated plasticity beam-column models since they are computationally more efficient than distributed plasticity fiber models and require fewer parameters to capture the degrading behaviour under cyclic loading. These features, in general, render concentrated plasticity models more practical for modeling complex phenomena like post-shear failure response.

The inelastic behaviour modeling is based on stress-resultant plasticity concepts using force interaction surfaces and evolution models. Yield surface is defined to model the interaction between axial force and biaxial bending moments. Post-yield force interaction and inelastic hardening in flexure is captured by the yield-surface evolution models. Shear failure is captured by shear failure surface defined in terms of axial force and shear forces. Post-shear failure softening behaviour is captured by shear failure surface evolution models. Each generalized plastic hinge at an element end comprises a yield surface, a shear failure surface and their associated evolution models. The degradation of shear strength in the plastic hinge region with increasing flexural displacement ductility demand is captured by using ductility-related shear limit surface associated with the shear failure surface evolution model. Force recovery procedures are described for both the yield surface and the shear failure surface. A generalized procedure for state determination is developed considering different paths in the state transitions that encompass the entire spectrum of possible member behaviour varying from ductile behaviour governed by flexural yielding through moderately ductile behaviour controlled

by shear-flexure interactions in the plastic hinge zone to non-ductile behaviour characterized by brittle failure in shear.

The cyclic behaviour modeling is based on the incorporation of damage models in the beam-column element formulation to track the evolution of damage and its effects on the gradual deterioration in stiffness and loss of strength. During the state of unloading that follows after yielding in flexure and/or failure in shear and through subsequent reloading prior to reaching either of the surfaces, the quasi-elastic degraded cyclic response is controlled by cyclic models capturing the different degradation characteristics. Cyclic stiffness model is used to control the degrading stiffness upon unloading after yielding and subsequent reloading in the element hysteretic response dominated by flexure. Cyclic pinching model is used to provide degradation factors for the stiffness components in the post-shear failure cyclic response characterized by softening and pinching. The unloading and reloading stiffness components in the cyclic models are degraded using damage indices based on plastic deformations and hysteretic energy. Biaxial interaction effects on stiffness degradation for behaviour dominated by flexure or shear are also considered based on the accumulated damage during positive and negative excursions in each direction of loading. Cyclic strength degradation model is developed to capture the loss of strength under repeated load reversals by contracting the yield surface and the shear failure surface using cumulative damage models based on hysteretic energy. The formulation of cyclic models is based on an event-to-event strategy, where an “event” occurs when the loading state of the element changes. By applying the concept of full and "half" cycles and defining positive and negative peak and cross-over events in the cycles,

the developed generalized state determination procedure is demonstrated to be valid for both positive and negative excursions.

The framework for the implementations of the proposed models using object oriented design is discussed in Chapter 4. Background to object oriented programming concepts in the context of the OpenSees software framework and a discussion of the key advantages of object based versus procedural finite element analysis programs are also presented in this chapter. The individual components of the proposed model are identified and the functionalities of each component are defined in the conceptual development of the object based design. Abstract base classes are established to describe the behaviour of individual components. The interface and the interactions between the abstract base classes are also established based on the required functionalities.

In the development process, the features of the proposed inelastic concentrated-plasticity model for capturing the behaviour of ductile as well as non-ductile reinforced concrete members, including large deformations, inelastic axial load-shear-flexure interactions, post-yield hardening, post-shear failure softening, stiffness and strength cyclic degradations, are carefully considered and the following base classes are established: beam-column element class, yield surface class, yield surface evolution class, shear failure surface class, shear failure surface evolution class, shear limit surface class, cyclic model class, cyclic control class, damage model class, damage progression class. To incorporate the full capabilities for inelastic cyclic behaviour modeling, the element class is associated with yield surface and shear failure surface classes, which in their turn are

interacting with evolution model classes, and with a cyclic control class, which handles damage-based stiffness and strength degradation cyclic models. The independent implementations for each of the main components of the formulations within a separate base class and the hierarchical structure of the proposed classes are designed to provide a comprehensive and flexible design that allows extensibility.

5.2 Conclusions

The formulation is focused on concentrated plasticity beam-column models employing yield surface and shear failure surface models to describe the section behaviour of generalized plastic hinges at the element ends. Being a macro model, the concentrated plasticity beam-column model is computationally more efficient than distributed plasticity fiber models and more suitable for modeling post-shear failure response. However, it is challenging to describe the complex behaviour of reinforced concrete sections by using only a single equation, which is the basis of yield surface and shear failure surface models. Several parameters used in the force interaction surface models need to be determined by using either fiber section analysis or empirical relations. Particularly for the shear failure surface further experimental research is needed to better describe the shear force - axial load interaction. In this study, only force interaction surfaces for symmetric sections are considered. Additional effort would be required to develop yield surface and shear failure surface models suitable for representing asymmetric sections. In the implementation framework of this study, the inelastic behaviour modeling that features force interaction surface models and surface evolution

models is therefore separated from the element class to enable adding new models describing the section behaviour as they become available.

In the cyclic behaviour modeling careful consideration is given to the development of a consistent generalized approach for state determination. The derived set of conditions capture the state transitions for cyclic response of members designed as ductile as well as non-ductile members by keeping track of positive and negative peak and cross-over events in repeated reversed cyclic excursions. In the implementation framework, the proposed event-based strategy is incorporated in the functionalities of the cyclic control class to enable consistent state determination and effective interaction between the element class and the various cyclic model classes. The independent implementation of the cyclic behaviour modeling from the element implementation enables adding new cyclic models describing the quasi-elastic degraded state of reinforced concrete members as they are developed in future research. The cyclic control class also provides the functionalities for interaction among cyclic models and damage models to degrade strength and stiffness properties using damage indices during the course of analysis. Following the accumulation of damage and its effects on the gradual stiffness deterioration and loss of strength is essential in realistic prediction of progressive collapse behaviour of structural systems.

5.3 Recommendations for Future Work

Recommendations for potential areas of future work related to this research are summarized as follows:

- Incorporation of the implementations in the object based finite element software framework OpenSees. In this study, the formulation of a nonlinear beam-column model for seismic response analysis is developed with the aim to be comprehensive to capture the behaviour of ductile as well as non-ductile reinforced concrete members and the framework for the object based implementations of the new model is established by structuring the functionalities and focusing on extensibility. The detailed implementations following the developed object based design should be completed in future research. Incorporating the full array of proposed new models in a finite element analysis software such as the OpenSees framework would bring significant benefits in conducting nonlinear seismic response analysis of global structural systems such as reinforced concrete frame buildings and bridges to obtain realistic prediction of seismic progressive collapse behaviour.

- Development of efficient and reliable numerical techniques to compute the variations of parameters with element forces, such as effective elastic stiffness, plastic rotation capacity, hardening rate, post-shear failure softening, during the course of nonlinear analysis. Currently, these parameters are commonly determined by using fiber section analysis or empirical relations prior to conducting nonlinear analysis of the global structural system. It has previously been shown that section response varies significantly with axial load levels, and thus using fiber section analysis output from a single axial load level may not be

sufficient to capture the behaviour characteristics. Conducting fiber section analysis at various axial load levels and interpolating parameters during the nonlinear analysis may be a viable option but needs further research to develop appropriate numerical techniques.

- Development of more shear failure surface models capturing realistic shear force - axial load interaction based on experimental research.
- Incorporation of yield surface and shear failure surface models for asymmetric sections to render the beam-column model applicable for more general cases.
- Development of models to simulate rigid-body deformations related to bond-slip effects and anchorage of longitudinal reinforcement at column ends and their incorporation into the class structure of the proposed beam-column model.

Appendices

Appendix A : Element Class Details

The key member functions of the element classes are listed here.

A.1 Element Class UpdatedLagrangianBeamColumn3D

Public Member Functions	Description
UpdatedLagrangianBeamColumn3D	Constructor
~UpdatedLagrangianBeamColumn3D	Destructor
getExternalNodes	Method to deal with the element nodes
getNodePointers	Method to deal with pointers to the element nodes
getNumberDOF	Method to deal with the element DOF's
setDomain	Method to set the element object in the domain
commitState	Method to deal with the committed (converged) state
revertToLastCommitState	Method to revert to the previous converged state
getTangentStiffness	Method to return and store current linearized stiffness matrix
getInitialStiffness	Method to return and store initial elastic stiffness matrix
getMass	Method to return and store mass matrix
getDamping	Method to return and store damping matrix
getLoadVector	Method to return and apply loads
addLoad	Method to deal with applied loads

getResistingForce	Method to calculate resisting force and update state
transformResistingForce	Method to transform from local to global coordinates

Protected Member Functions

Description

getLocalStiffness	Method to obtain current stiffness matrix from sub-classes
getLocalMass	Method to obtain mass matrix from sub-classes
getLocalDamping	Method to obtain damping matrix from sub-classes
getIncrementalLocalDisp	Method to calculate incremental displacements
transformIncrementalLocalDisp	Method to transform incremental displacements to local coordinates
getTrialNaturalDisp	Method to calculate trial displacements using the natural deformation approach
getIncrementalNaturalDisp	Method to calculate incremental displacements using the natural deformation approach
getConvergedLocalDisp	Method to return converged displacements in local coordinates
getTrialLocalForce	Method to compute trial local force
updateDirCosState	Update direction cosines to the new trial state
addInternalGeomStiffness	Method to implement the internal geometric stiffness matrix
transformStiffnessToGlobal	Method to transform stiffness matrix to global coordinates

A.2 Element Class ElasticGNL3D

Public Member Functions	Description
ElasticGNL3D	Constructor
~ElasticGNL3D	Destructor

Protected Member Functions	Description
getLocalStiffness	Method to implement elastic stiffness matrix
getLocalMass	Method to implement mass matrix
getLocalDamping	Method to implement damping matrix

A.3 Element Class InelasticGNL3D

Public Member Functions	Description
InelasticGNL3D	Constructor
~InelasticGNL3D	Destructor
getResistingForce	Method to be re-implemented from parent class to calculate resisting force for inelastic response and update state
getTangentStiffness	Method to be re-implemented from parent class to return and store current linearized stiffness matrix for inelastic response
commitState	Method to be re-implemented from parent class to deal with the committed (converged) state in inelastic response
updateState	Method to compute trial local force and implement framework for the force recovery procedure for elements with yield surfaces and shear failure surfaces

Protected Member Functions	Description
getLocalStiffness	Method to obtain current stiffness matrix from sub-classes
getLocalMass	Method to implement mass matrix
getLocalDamping	Method to implement damping matrix
checkStatus	Method to check if current status is elastic or inelastic, either yielding or failing in shear

Private Member Functions	Description
---------------------------------	--------------------

checkForceYieldStatus	Method to check if the force state is inside, within or shoots through the yield surface; carry out check for each end of the element
splitStepYield	Method to calculate the factor by which the current step is split and split the trial force in the case when the trial force shoots through the yield surface
yieldOneEnd	Method to obtain plastic stiffness, calculate the gradient of the yield surface, and calculate the magnitude of plastic deformation in the case of yielding at one element end
yieldBothEnds	Method to obtain plastic stiffness, calculate the gradient of the yield surface, and calculate the magnitude of plastic deformation in the case of yielding at both element ends
returnYieldForceOneEnd	Method to recover force to the yield surface and recalculate trial force in the case of yielding at one element end
returnYieldForceBothEnds	Method to recover force to the yield surface and recalculate trial force in the case of yielding at both element ends
updateLocalStiffness	Method to calculate the plastic reduction matrix and update the element tangent stiffness matrix in case of yielding
balanceForcesYield	Method to balance axial and shear forces in case of yielding upon completion of force recovery
updateShearStrength	Method to calculate displacement ductility of the yielding element, check if current ductility exceeds critical value and update shear strength based on a shear limit surface
checkForceShearStatus	Method to check if the force state is inside, within or shoots through the shear failure surface; carry out check for each end of the element
splitStepShear	Method to calculate the factor by which the current step is split and split the trial force in the case when the trial force shoots through the

	shear failure surface
failShearOneEnd	Method to obtain degraded stiffness and calculate shear deformation components in the case of shear failure at one element end
failShearBothEnds	Method to obtain degraded stiffness and calculate shear deformation components in the case of shear failure at both element ends
returnShearForceOneEnd	Method to recover force to the shear failure surface and recalculate trial force in the case of shear failure at one element end
returnShearForceBothEnds	Method to recover force to the shear failure surface and recalculate trial force in the case of shear failure at both element ends
updateDegradedLocalStiffness	Method to calculate the degraded stiffness matrix and update the element tangent stiffness matrix in case of shear failure
balanceForcesShearFail	Method to balance axial forces and bending moments in case of shear failure upon completion of force recovery

A.4 Element Class InelasticMON3D

Public Member Functions

InelasticMON3D

~ InelasticMON3D

Description

Constructor

Destructor

Protected Member Functions

getLocalStiffness

Description

Method to implement elastic stiffness matrix to be used as the base matrix at the start of analysis until detecting inelastic behaviour

A.5 Element Class InelasticCYC3D

Public Member Functions	Description
InelasticCYC3D	Constructor
~ InelasticCYC3D	Destructor
commitState	Method to be re-implemented from parent class to deal with the committed (converged) state in inelastic cyclic response
updateState	Method to be re-implemented from parent class to extend the framework to degraded cyclic response
Protected Member Functions	Description
getLocalStiffness	Method to implement elastic stiffness matrix to be used as the base matrix at the start of analysis until detecting inelastic behaviour
getDegradedElastLocalStiffness	Method to update degraded stiffness during quasi-elastic degraded response by interacting with cyclic control class
updateDegradingState	Method to compute trial local force during quasi-elastic degraded response

References

- Abou-Elfath, H., Ghojarah, A. and Aziz, T. S. (1998). Seismic Analysis of Non-Ductile Frames. *Proceedings, Sixth U.S. National Conference on Earthquake Engineering*, Earthquake Engineering Research Institute, EERI, Oakland, CA, 12 pp. (CD-ROM)
- Alsawat, J. M. and Saatcioglu, M. (1992). Reinforcement Anchorage Slip under Monotonic Loading. *Journal of Structural Engineering*, 118 (9), pp. 2421-2438.
- Ayoub, A. S. and Filippou, F. C. (2000). Mixed Formulation of Nonlinear Steel-Concrete Composite Beam Element. *ASCE Journal of Structural Engineering*, 126 (3), pp. 371-381.
- Aschheim, M. and Moehle, J. P. (1992). Shear Strength and Deformability of RC Bridge Columns Subjected to Inelastic Displacements. *UCB/EERC-92/04, Earthquake Engineering Research Center*, University of California, Berkeley, CA.
- Bairan, J. M. (2005). A Nonlinear Coupled Model for the Analysis of Reinforced Concrete Sections under Bending, Shear, Torsion and Axial Forces. *Ph.D. Dissertation*, Technical University of Catalonia, Barcelona, Spain.
- Banon, H., Biggs, J. and Irvine, M. (1981). Seismic Damage in Reinforced Concrete Frames. *ASCE Journal of the Structural Division*, 100 (ST9), pp. 1713-1729.
- Bathe, K. J. (1996). Finite Element Procedures. *Prentice Hall*, Englewood Cliffs, New Jersey 07632.
- Bazant, Z. P. and Oh, B. H. (1985). Microplane Model for Progressive Fracture of Concrete and Rock. *ASCE Journal of Engineering Mechanics*, 111 (4), pp. 559-582.
- Bazant, Z. P. and Ozbolt, J. (1990). Nonlocal Microplane Model for Fracture, Damage, and Size Effect in Concrete Structures. *ASCE Journal of Engineering Mechanics*, 116 (11), pp. 2484-2504.
- Bazant, Z. P. and Prat, P. C. (1988). Microplane Model for Brittle-Plastic Material. Parts I and II. *ASCE Journal of Engineering Mechanics*, 114 (10), pp. 1672-1702.
- Belarbi, A. and Hsu, T. T. C. (1995). Constitutive Laws of Softened Concrete in Biaxial Tension-Compression. *ACI Structural Journal*, 92 (5), pp. 562-573.
- Belarbi, A. and Hsu, T. T. C. (1995). Constitutive Laws of Concrete in Tension and Reinforcing Bars Stiffened by Concrete. *ACI Structural Journal*, 91, pp. 465-474.

- Bentz, E. C. (2000). Sectional Analysis of Reinforced Concrete Members. *Ph.D. Dissertation*, University of Toronto, Toronto, Canada.
- Brancaleoni, F., Ciampi, V. and Di Antonio, R. (1983). Rate-type Models for Non Linear Hysteretic Structural Behavior. *EUROMECH colloquium*, Palermo, Italy.
- Celebi, M. and Penzien, J. (1973). Experimental Investigation into the Seismic Behaviour of the Critical Regions of Reinforced Concrete Components as Influenced by Moment and Shear. *UCB/EERC-73/04, Earthquake Engineering Research Center*, University of California, Berkeley, CA.
- Ceresa, P., Petrini, L. and Pinho, R. (2007). Flexure-Shear Fiber Beam-Column Elements for Modeling Frame Structures under Seismic Loading – State of the Art. *Journal of Earthquake Engineering*, 11, pp. 46-88.
- Ceresa, P., Petrini, L., Pinho, R. and Sousa, R. (2009). A Fibre Flexure-Shear Model for Seismic Analysis of RC Framed Structures. *Earthquake Engineering and Structural Dynamics*, 38, pp. 565-586.
- Chen, P. F. S. and Powell, G. H. (1982). Generalized Plastic Hinge Concepts for 3D Beam-Column Elements. *UCB/EERC-82/20, Earthquake Engineering Research Center*, University of California, Berkeley, CA.
- Chen, W. F. and Han, D. J. (2007). *Plasticity for Structural Engineers*. J. Ross Publishing.
- Ciampi, V. and Carlesimo, L. (1986). A Nonlinear Beam Element for Seismic Analysis of Structures. *8th European Conference on Earthquake Engineering*, Lisbon.
- Clough, R. W., Benuska, K. L., and Wilson, E. L. (1965). Inelastic Earthquake Response of Tall Buildings. *Proceedings of the 3rd World Conference on Earthquake Engineering*, Wellington, New Zealand.
- Clough, R. W., and Johnston, S. (1966). Effect of Stiffness Degradation on Earthquake Ductility Requirements. *Transactions of Japan Earthquake Engineering Symposium*. Tokyo, pp. 195-198.
- Coleman, J. and Spacone, E. (2001). Localization Issues in Nonlinear Force-Based Frame Elements. *ASCE Journal of Structural Engineering*, 127 (11), pp. 1257-1265.
- Conci, A. and Gattass, M. (1990). Natural Approach for Geometric Non-Linear Analysis of Thin-Walled Frames. *International Journal for Numerical Methods in Engineering*, 30, pp. 207-231.
- Corley, G. W. (1966). Rotation Capacity of Reinforced Concrete Beams. *ASCE Journal of the Structural Division*, 92 (10), pp. 121-146.
- Dafalias, Y. H. and Popov, E. P. (1977). Cyclic Loading for Materials with Vanishing Elastic Region. *Nuclear Engineering and Design*, 41, pp. 293-302.

- D'Ambrissi, A. and Filippou, F. C. (1999). Modeling of Cyclic Shear Behavior in RC Members. *ASCE Journal of Structural Engineering*, 125 (10), pp. 1143-1150.
- Darvall, L. P. and Mendis, P. (1985). Elastic-Plastic-Softening Analysis of Plane Frames. *ASCE Journal of Structural Engineering*, 11 (ST4), pp. 871-888.
- Dotiwala, F. S., (1996). A Nonlinear Flexural-Shear Model for RC Columns Subjected to Earthquake Loads. *MS Advanced Independent Study Report*, Department of Civil and Environmental Engineering, University of Wisconsin, Madison.
- ElMandooh Galal, K. (2002). Modeling and Rehabilitation of Non-Ductile Spatial RC Columns. *Ph.D. Dissertation*, Department of Civil Engineering, Earthquake Engineering Research Group, McMaster University, Hamilton, Ontario, Canada.
- ElMandooh Galal, K. and Ghobarah, A. (2003). Flexural and Shear Hysteretic Behaviour of Reinforced Concrete Columns with Variable Axial Load. *Engineering Structures*, 25, pp. 1353-1367.
- Elwood, K. J. (2002). Shake Table Tests and Analytical Studies on the Gravity Load Collapse of Reinforced Concrete Frames. *Ph.D. Dissertation*, Department of Civil and Environmental Engineering, University of California, Berkeley, CA.
- Elwood, K. J. and Moehle, J. P. (2003). Shake Table Tests and Analytical Studies on the Gravity Load Collapse of Reinforced Concrete Frames. *PEER Report 2003/01, Pacific Earthquake Engineering Research Center*, University of California, Berkeley, CA.
- Elwood, K. J. (2004). Modeling failures in existing reinforced concrete columns. *Canadian Journal of Civil Engineering*, 31, pp. 846-859.
- El-Tawil, S. (1996). Inelastic Dynamic Analysis of Mixed Steel-Concrete Space Frames. *Ph.D. Dissertation*, School of Civil and Environmental Engineering, Cornell University, Ithaca, NY 14853.
- El-Tawil, S. and Deierlein, G. G. (1996). Inelastic Dynamic Analysis of Mixed Steel-Concrete Space Frames. *Report No. 96-5, School of Civil and Environmental Engineering*, Cornell University, May 1996.
- El-Tawil, S. and Deierlein, G. G. (1998). Stress-resultant Plasticity for Frame Structures. *ASCE Journal of Engineering Mechanics*, 124 (12), pp. 1360-1370.
- Emori, K. and Schnobrich, W. C. (1981). Inelastic Behaviour of Concrete Frame-Wall Structures. *ASCE Journal of the Structural Division*, 107 (ST1), January 1981.
- FEMA P-440A. 2009. Effects of Strength and Stiffness Degradation on Seismic Response. *Federal Emergency Management Agency*. Washington, D.C.

- Filippou, F. C., D'Ambrissi, A. and Issa, A. (1992). Nonlinear Static and Dynamic Analysis of Reinforced Concrete Subassemblies. *UCB/EERC-92/08, Earthquake Engineering Research Center*, University of California, Berkeley, CA.
- Filippou, F. C. and Issa, A. (1988). Nonlinear Analysis of Reinforced Concrete Frames under Cyclic Load Reversals. *UCB/EERC-88/12, Earthquake Engineering Research Center*, University of California, Berkeley, CA.
- Filippou, F. C. and Spacone E. (1996). FEDEAS: Nonlinear Analysis for Structural Evaluation. *Proceedings of the Eleventh World Conference on Earthquake Engineering*, Pergamon, Elsevier Science Ltd., Oxford, England, Disc 3, Paper No. 1664.
- Gartska, B., Kratzig, W. B. and Stangenberg, F. (1993). Damage Assessment in Cyclically Loaded Reinforced Concrete Members . *Structural Dynamics*, EURO DYN 93, Moan, Ed. Balkema, Rotterdam 1, pp. 121-128.
- Gerin, M. and Adebar, P. (2004). Accounting for Shear in Seismic Analysis of Concrete Structures. *Proceedings, 13th World Conference on Earthquake Engineering*, Vancouver, Canada. 13 pp. (CD-ROM)
- Ghee, A. B., Priestley, M. J. N. and Paulay, T. (1989). Seismic Shear Strength of Circular Reinforced Concrete Columns. *ACI Structural Journal*, 86 (1), pp. 45-59.
- Giberson, M. F. (1967). The Response of Nonlinear Multistory Structures Subjected to Earthquake Excitation. *Ph.D. Dissertation*, California Institute of Technology, Pasadena, CA.
- Giberson, M. F. (1969). Two Nonlinear Beams with Definitions of Ductility. *ASCE Journal of Structural Engineering*, 95 (ST2), pp. 137-157.
- Guedes, J., Pegon, P. and Pinto, A. V. (1994). A Fibre/Timoshenko Beam Element in CASTEM 2000. *Special Publication No. I.94.31, Applied Mechanics Unit*, Safety Technology Institute, Commission of the European Communities, Joint Research Centre, Ispra Establishment, Italy.
- Hellesland, J. and Scordelis, A. (1981). Analysis of RC Bridge Columns Under Imposed Deformations. *IABSE Colloquium*, Delft, Netherlands, pp. 545-559.
- Hilmy, S. I. (1984). Adaptive Nonlinear Dynamic Analysis of 3-D Steel Framed Structures with Interactive Computer Graphics. *Ph.D. Dissertation*, School of Civil and Environmental Engineering, Cornell University, Ithaca, NY 14853.
- Hsu, T. T. C. and Zhang, L. X. (1996). Nonlinear Analysis of Membrane Elements by Fixed-Angle Softened-Truss Model. *ACI Structural Journal*, 94 (5), pp. 483-492.
- Jiang, Y. and Saiidi, M. (1990). Four-Spring Element for Cyclic Response of R/C Columns. *ASCE Journal of Structural Engineering*, 116 (4).

- Jordan, R. M. (1990). Evaluation of Strengthening Schemes for Reinforced Concrete Moment-Resisting Frame Structures Subjected to Seismic Loads. *Ph.D. Dissertation*, Department of Civil Engineering, University of Texas at Austin, TX.
- Kaba, S. and Mahin, S. A. (1984). Refined Modeling of Reinforced Concrete Columns for Seismic Analysis. *UCB/EERC-84/03, Earthquake Engineering Research Center*, University of California, Berkeley, CA.
- Kanaan, A. E. and Powell, G. H. (1973). General Purpose Computer Program for Inelastic Dynamic Response of Plane Structures. *UCB/EERC-73/06, Earthquake Engineering Research Center*, University of California, Berkeley, CA.
- Kaul, R. (2004). Object Oriented Development of Strength and Stiffness Degrading Models for Reinforced Concrete Structures. *Ph.D. Dissertation*, Department of Civil and Environmental Engineering, Stanford University, Stanford, CA.
- Kent, D. C. and Park, R. (1971). Flexural Members with Confined Concrete. *ASCE Journal of the Structural Division*, 97 (ST7), pp. 1969-1989.
- Keshavarzian, M., and Schnobrich, W. (1985). Inelastic Analysis of RC Coupled Shear Walls. *Earthquake Engineering and Structural Dynamics*, 13, pp. 427-448.
- Kotronis, P. and Mazars, J. (2005). Simplified Modeling Strategies to Simulate the Dynamic Behaviour of R/C Walls. *Journal of Earthquake Engineering*, 9(2), pp. 285-306.
- Kratzig, W. B., Meyer, I. F. and Meskouris, K. (1989). Damage Evolution in Reinforced Concrete Members under Cyclic Loading. *Proceedings of the 5th International Conference on Structural Safety and Reliability (ICOSSAR 89)*, San Francisco, CA, Vol. II, pp. 795-802.
- Kunnath, S. K., Reinhorn, A. M., and Lobo, R. F. (1992). IDARC version 3.0: A Program for Inelastic Damage Analysis of RC Structures. *Technical Report NCEER-92-0022, National Center for Earthquake Engineering Research*, State University of New York, Buffalo, NY.
- Kurama, Y., Sause, R. Pessiki, S., Wu, S. and Snyder, S., (1996). Seismic Behaviour, Performance, and Retrofit of Non-Ductile Reinforced Concrete Frame Structures. *Report No. EQ-96-01*, Department of Civil Engineering and Environmental Engineering, Lehigh University, Bethlehem, PA.
- La Borderie, C. L. (1991). Phenomenes Unilateraux dans un Materiau Endommageable: Modelisation et Application a L'Analyse des Structures en Beton. *Ph.D. Dissertation*, University of Paris, France.
- Lai, S. S., Will, G. and Otani, S. (1984). Model for Inelastic Biaxial Bending of Concrete Members. *ASCE Journal of Structural Engineering*, 110 (ST11), pp. 2563-2584.

- Lee, D. H., and Elnashai, A. S. (2001). Seismic Analysis of RC Bridge Columns with Flexure-Shear Interaction. *ASCE Journal of Structural Engineering*, 127 (5), pp. 546-553.
- Lee, D. H., and Elnashai, A. S. (2002). Inelastic Seismic Analysis of RC Bridge Piers Including Flexure-Shear-Axial Interaction. *Structural Engineering and Mechanics*, 13 (3), pp. 241-260.
- Lynn, A. C. (2001). Seismic Evaluation of Existing Reinforced Concrete Building Columns. *Ph.D. Dissertation*, Department of Civil and Environmental Engineering, University of California, Berkeley, CA.
- Mahasuverachai, M. and Powell, G. H. (1982). Inelastic Analysis of Piping and Tubular Structures. *UCB/EERC-82/27, Earthquake Engineering Research Center*, University of California, Berkeley, CA.
- Mander, J. B., Priestley, M. J. N. and Park, R. (1988). Theoretical Stress-Strain Model for Confined Concrete. *ASCE Journal of Structural Engineering*, 114 (8), pp. 1804-1826.
- Mari, A. and Scordelis, A. (1984). Nonlinear Geometric Material and Time Dependent Analysis of Three Dimensional Reinforced and Prestressed Concrete Frames. *UC SESM-84/12, Department of Civil Engineering*, University of California, Berkeley, CA.
- Marini, A. and Spacone, E. (2006). Analysis of Reinforced Concrete Elements Including Shear Effects. *ACI Structural Journal*, 103 (5), pp. 645-655.
- Martinelli, L. (2008). Modeling Shear-Flexure Interaction in Reinforced Concrete Elements Subjected to Cyclic Lateral Loading. *ACI Structural Journal*, 105 (6), pp. 675-684.
- Martino, R., Spacone, E. and Kingsley, G. (2000). Nonlinear Pushover Analysis of R/C Structures. *Structures Congress, Advanced Technology in Structural Engineering*, M. Elgaaly, ed., ASCE, 8 pp. (CD-ROM)
- Mattock, A. H. (1964). Rotation Capacity of Hinging Regions in Reinforced Concrete Beams. *Flexural Mechanics of Reinforced Concrete. ACI Structural Journal*, SP-12, pp. 143-181.
- Mazars, J., Kotronis, P., Ragueneau, F. And Casaux, G. (2006). Using Multifibre Beams to Account for Shear and Torsion. Applications to Concrete Structural Elements. *Computer Methods in Applied Mechanics and Engineering*, 195(52), pp. 7264-7281.
- McGuire, W., Gallagher, R. H. and Ziemian, R. D. (2000). Matrix Structural Analysis. *Second Edition, John Wiley and Sons*, New York.

- McKenna, F. T. (1997). Object-Oriented Finite Element Programming: Frameworks for Analysis, Algorithms and Parallel Computing. *Ph.D. Dissertation*, Department of Civil and Environmental Engineering, University of California, Berkeley, CA.
- McKenna, F. T., Fenves, G. L., and Scott, M. H. (2004). OpenSees: Open System for Earthquake Engineering Simulation. Pacific Earthquake Engineering Research Center, University of California, Berkeley, CA.
- Mehanny, S. S. F. (1999). Modeling and Assessment of Seismic Performance of Composite Frames with Reinforced Concrete Columns and Steel Beams. *Ph.D. Dissertation*, Stanford University.
- Mehanny, S. S. F. and Deierlein, G. G. (2001). Seismic Collapse Assessment of Composite RCS Moment Frames. *ASCE Journal of Structural Engineering*, 127 (9), pp.
- Menegotto, M. and Pinto, P. E. (1977). Slender RC Compressed Members in Biaxial Bending. *ASCE Journal of Structural Engineering*, 103 (ST3), pp. 587-605.
- Meyer, C., Roufaiel, M.S. and Arzoumanidis, S. G. (1983). Analysis of Damaged Concrete Frames for Cyclic Loads. *Earthquake Engineering and Structural Dynamics*, 11, pp. 207-228.
- Mitchell, D., and Collins, M. P. (1974). Diagonal Compression Field Theory – A Rational Approach for Structural Concrete in Pure Tension. *ACI Journal, Proceedings*, 71 (8), pp. 396-408.
- Mostafaei, H. and Kabeyasawa, T. (2007). Axial-Shear-Flexure Interaction Approach for Reinforced Concrete Columns. *ACI Structural Journal*, 104 (2), pp. 218-226.
- Mroz, Z. (1969). An Attempt to Describe the Behavior of Metals under Cyclic Loads Using A More General Work Hardening Model. *Acta Mechanica*, 7, pp. 199-212.
- Mullapudi, T. R. and Ayoub, A. (2010). Modeling of the Seismic Behavior of Shear-Critical Reinforced Concrete Columns. *Engineering Structures*, 32, pp. 3601-3615.
- Nakamura, T. and Yoshimura, M. (2002). Gravity Load Collapse of Reinforced Concrete Columns with Brittle Failure Modes. *Journal of Asian Architecture and Building Engineering*, 1(1), pp. 21-27.
- Neuenhofer, A. and Filippou, F. C. (1997). Evaluation of nonlinear frame finite-element models. *ASCE Journal of Structural Engineering*, 123 (7), pp. 958-966.
- Ngo, D., and Scordelis, A. C. (1967). Finite Element Analysis of Reinforced Concrete Beam. *ACI Structural Journal*, 64 (3).

- Orbison, J. (1982). Nonlinear Static Analysis of 3-D Steel Frames. *Ph.D. Dissertation*, School of Civil and Environmental Engineering, Cornell University, Ithaca, NY 14853.
- Otani, S. (1974). Inelastic Analysis of R/C Frame Structures. *ASCE Journal of the Structural Division*, 100 (ST7), pp. 1433-1449.
- Otani, S., Kitayama, K. and Aoyama, H. (1985). Beam Bar Bond Stress and Behaviour of Reinforced Concrete Interior Beam-Column Joints. *Second US-NZ-Japan Seminar on Design of Reinforced Concrete Beam-Column Joints*, Tokyo, Japan, may 29-30 1985.
- Ozbolt, J. and Bazant, Z. P. (1992). Microplane Model for Cyclic Triaxial Behavior of Concrete. *ASCE Journal of Engineering Mechanics*, 118 (7), pp. 1365-1386.
- Ozcebe, G. and Saatcioglu, M. (1989). Hysteretic Shear Model for Reinforced Concrete Members. *Journal of Structural Engineering*, 115 (1), pp. 132-148.
- Palermo, D. and Vecchio, F. J. (2002). Behavior and Analysis of Reinforced Concrete Walls Subjected to Reversed Cyclic Loading. *Publication No. 2002-01*, Department of Civil Engineering, University of Toronto, Toronto, Canada.
- Palermo, D. and Vecchio, F. J. (2003). Compression Field Modeling of Reinforced Concrete Subjected to Reversed Loading: Formulation. *ACI Structural Journal*, 100 (5), pp. 616-625.
- Pang, X. B. and Hsu, T. T. C. (1995). Behavior of Reinforced Concrete Membrane Elements in Shear. *ACI Structural Journal*, 92 (6), pp. 665-679.
- Pang, X. B. and Hsu, T. T. C. (1996). Fixed-Angle Softened-Truss Model for Reinforced Concrete. *ACI Structural Journal*, 93 (2), pp. 197-207.
- Park, Y. J., and Ang, A. H-S. (1985). Mechanistic Seismic Damage Model for Reinforced Concrete. *ASCE Journal of Structural Engineering*, 111 (ST4), pp. 722-739.
- Park, R. and Paulay, T. (1975). Reinforced Concrete Structures. *John Wiley and Sons*, New York.
- Park, R., Priestley, M. J. N. and Wayne, D. G. (1982). Ductility of Square-Confined Concrete Columns. *ASCE Journal of the Structural Division*, 108 (ST4), pp. 929-951.
- Petrangeli, M., and Ciampi, V. (1997). Equilibrium Based Numerical Solutions for the Nonlinear Beam Problem. *International Journal of Numerical Journal in Engineering*, 40, pp. 423-437.

- Petrangeli, M., Pinto, P. E. and Ciampi, V. (1999). Fibre Element for Cyclic Bending and Shear of RC Structures. I: theory. *Journal of Engineering Mechanics*, 125 (9), pp. 994-1001.
- Phung, V. and Lau, D. T. (2008). Three-Dimensional Nonlinear Degrading Model for Earthquake Response Analyses of Concrete Bridges. *Proceedings of the 14th World Conference on Earthquake Engineering*, Beijing, China.
- Phung, V., Lau, D. T. and Reshotkina, S. S. (2010). Three-Dimensional Stiffness Degradation Model for Progressive Collapse Analysis of Bridges. *Proceedings of the 9th U.S. National and 10th Canadian Conference on Earthquake Engineering*, Toronto, Ontario, Canada.
- Pincheira, J. A., Dotiwala, F. S., and D'Souza, J. T. (1999). Seismic Analysis of Older Reinforced Concrete Columns. *Earthquake Spectra*, 15 (2), pp. 245-272.
- Pincheira, J. A. and Dotiwala, F. S., (1996). Modeling of Nonductile R/C Columns Subjected to Earthquake Loading. *Proceedings of the Eleventh World Conference on Earthquake Engineering*, Pergamon, Elsevier Science Ltd., Oxford, England, Paper No. 316.
- Pincheira, J. A. and Jirsa, J. O., (1992). Seismic Strengthening of Reinforced Concrete Frames Using Post-Tensioned Bracing Systems. *PMFSEL Report No. 92-3*, Department of Civil Engineering/Bureau of Engineering Research, University of Texas at Austin, TX.
- Priestley, M. J. N., Seible, F., Xiao, Y., and Verma, R. (1994). Steel Jacket Retrofitting of Reinforced Concrete Bridge Columns for Enhanced Shear Strength – Part 2: test results and comparison with theory. *ACI Structural Journal*, 91 (5), pp. 537-551.
- Priestley, M. J. N., Verma, R., and Xiao, Y. (1994). Seismic Shear Strength of Reinforced Concrete Columns. *ASCE Journal of Structural Engineering*, 120 (8), pp. 2310-2329.
- Priestley, M. J. N., Seible, F. and Calvi, G. (1996). Seismic Design and Retrofit of Bridges. *John Wiley and Sons*, New York.
- Ranzo, G. and Petrangeli, M. (1998). A Fibre Finite Beam Element with Section Shear Modeling for Seismic Analysis of RC Structures. *Journal of Earthquake Engineering*, 2, pp. 443-473.
- Rashid, Y. R. (1968). Analysis of Prestressed Concrete Pressure Vessels. *Nuclear Engineering and Design*, 4, pp. 334-344.
- Rose, B. W. (2001). A Constitutive Model for the Analysis of Reinforced Concrete Beam-Columns Subjected to Lateral Loads. *Ph.D. Dissertation*, CEAE Department, University of Colorado, Boulder, Colorado.

- Remino, M. (2004). Shear Modeling of Reinforced Concrete Structures. *Ph.D. Dissertation*, Dipartimento di Ingegneria Civile, Università degli Studi di Brescia, Italy.
- Ricles, J. M., Yang, Y.-S., and Priestley, M. J. N. (1998). Modeling Nonductile R/C Columns for Seismic Analysis of Bridges. *ASCE Journal of Structural Engineering*, 124 (4), pp. 415-425.
- Ricles, J. M., Priestley, M. J. N., Seible, F., Yang, Y.-S., Imbsen, R. and Liu, D. (1991). The Whittier Narrows 1987 Earthquake: Performance, Analysis, Repair and Retrofit of the I-5/I-605 separator. *Report No. SSRP-91/08*, University of California at San Diego, La Jolla, CA.
- Roufaiel, M. S. L. and Meyer, C. (1987). Analytical Modeling of Hysteretic Behaviour of R/C Frames. *ASCE Journal of Structural Engineering*, 113 (3), March 1987.
- Saatcioglu, M., Derecho, A. and Corley, W. G. (1983). Modeling of Hysteretic Behaviour of Coupled Walls for Dynamic Analysis. *Earthquake Engineering and Structural Dynamics*, 11 (5), pp. 711-726.
- Saatcioglu, M. and Ozcebe, G. (1989). Response of Reinforced Concrete Columns to Simulated Seismic Loading. *ACI Structural Journal*, 86 (1), pp. 3-12.
- Saatcioglu, M., Alsiwat, J. M. and Ozcebe, G. (1992). Hysteretic Behavior of Anchorage Slip in R/C Members. *ASCE Journal of Structural Engineering*, 118 (9), pp. 2439-2458.
- Saatcioglu, M., and Razvi, S. (1992). Strength and Ductility of Confined Concrete. *ASCE Journal of Structural Engineering*, 118 (6), pp. 1590-1607.
- Saiidi, M., Lawver, R. and Hart, J. (1986). User's Manual for ISADAB and SIBA, Computer Programs for Nonlinear Transverse Analysis of Highway Bridges Subjected to Static and Dynamic Lateral Loads. *CCEER Report-86/02*, Center for Civil Earthquake Research, University of Nevada, Reno, Nevada.
- Sawyer, H. A. (1964). Design of Concrete Frames for Two Failure States. *Proceedings of the International Symposium on the Flexural Mechanics of Reinforced Concrete*, Miami, ASCE-ACI, pp. 405-431.
- Setzler, E. J. and Sezen, H. (2008). Model for the Lateral Behavior of Reinforced Concrete Columns Including Shear Deformations. *Earthquake Spectra*, 24 (2), pp. 493-511.
- Sezen, H. (2002). Seismic Response and Modeling of Reinforced Concrete Building Columns. *Ph.D. Dissertation*, Department of Civil and Environmental Engineering, University of California, Berkeley, CA.

- Sezen, H. (2008). Shear Deformation Model for Reinforced Concrete Columns. *Structural Engineering Mechanics*, 28(1), 39-52.
- Sezen, H. and Moehle, J. P. (2003). Bond-slip Behaviour of Reinforced Concrete Members. *Proceedings of fib Symposium on Concrete Structures in Seismic Regions*, CEB-FIP, Athens, Greece.
- Sezen, H. and Moehle, J. P. (2004). Shear Strength Model for Lightly Reinforced Concrete Columns. *ASCE Journal of Structural Engineering*, 130 (11), pp. 1692-1703.
- Sezen, H. and Moehle, J. P. (2006). Seismic Tests of Concrete Columns with Light Transverse Reinforcement. *ACI Structural Journal*, 103 (6), pp. 842-849.
- Sezen, H. and Chowdhury, T. (2009). Hysteretic Model for Reinforced Concrete Columns Including the Effect of Shear and Axial Load Failure. *ASCE Journal of Structural Engineering*, 135 (2), pp. 139-146.
- Sezen, H. and Setzler, E. J. (2008). Reinforcement Slip in Reinforced Concrete Columns. *ACI Structural Journal*, 105 (3), pp. 280-289.
- Sheikh, S. A. and Uzumeri, S. M. (1982). Analytical Model for Concrete Confinement in Tied Columns. *ASCE Journal of the Structural Division*, 108 (ST12), pp. 2703-2722.
- Shirai, N., Moriizumi, K. and Terasawa, K. (2001). Cyclic Analysis of Reinforced Concrete Columns: Macro-Element Approach. *Modeling of Inelastic Behaviour of RC Structures under Seismic Load*, American Society of Civil Engineers, Reston, Virginia, pp. 435-453.
- Soleimani, D., Popov, E. P. and Bertero, V. V. (1979). Nonlinear Beam Model for R/C Frame Analysis. *Seventh Conference on Electronic Computation*, St. Louis, Missouri, ASCE, New York.
- Spacone, E., Filippou, F. C and Taucer, F. F. (1996). Fiber Beam-Column Model for Nonlinear Analysis of R/C Frames. I: Formulation. *Earthquake Engineering and Structural Dynamics*, 25 (7), pp. 711-725.
- Takayanagi, T. and Schnobrich, W. C. (1979). Non-Linear Analysis of Coupled Wall Systems. *Earthquake Engineering and Structural Dynamics*, 7, pp. 1-22.
- Takeda, T., Sozen, M. A. and Nielsen, N. N. (1970). Reinforced Concrete Response to Simulated Earthquakes. *ASCE Journal of the Structural Division*, 96 (12), pp. 2557-2573.
- Takizawa, H. (1976). Notes on Some Basic Problems in Inelastic Analysis of Planar RC Structures. *Transactions of Architecture Institute of Japan*, 240, Part I in February 1976, pp. 51-62, Part II in March 1976, p. 65-77.

- Takizawa, H. and Aoyama, H. (1976). Biaxial Effects in Modeling Earthquake Response of RC Structures. *Earthquake Engineering and Structural Dynamics*, 4, pp. 523-552.
- Taucer, F., Spacone, E. and Filippou, F. C. (1991). A Fiber Beam-Column Element for Seismic Response Analysis of Reinforced Concrete Structures. *UCB/EERC-91/17, Earthquake Engineering Research Center*, University of California, Berkeley, CA.
- Vecchio, F. J. and Collins, M. P. (1986). The Modified Compression-Field Theory for Reinforced Concrete Elements Subjected to Shear. *ACI Journal*, 83 (2), pp. 219-231.
- Vecchio, F. J. and Collins, M. P. (1988). Predicting the Response of Reinforced Concrete Beams Subjected to Shear Using the Modified Compression Field Theory. *ACI Journal*, 85, pp. 258-268.
- Vecchio, F. J. (1999). Towards Cyclic Load Modeling of Reinforced Concrete. *ACI Structural Journal*, 96(2), pp. 193-202.
- Vecchio, F. J. (2000). Disturbed Stress Field Model for Reinforced Concrete: Formulation. *Journal of Structural Engineering*, 126(9), pp. 1070-1077.
- Watanabe, F., and Ichinose, T. (1992). Strength and Ductility of RC Members Subjected to Combined Bending and Shear. *Concrete Shear in Earthquake*, Elsevier Applied Science, New York, pp. 429-438.
- Wong, Y. L., Paulay, T. and Priestley, M. J. N. (1993). Response of Circular Reinforced Concrete Columns to Multi-Directional Seismic Attack. *ACI Structural Journal*, 90 (2), pp. 180-191.
- Xu, S.-Y. and Zhang, J. (2010) Axial-Shear-Flexure Interaction Hysteretic Model for RC Bridge Columns under Combined Actions. *Proceedings of the 9th U.S. National and 10th Canadian Conference on Earthquake Engineering*, Toronto, Ontario, Canada.
- Xu, S.-Y. and Zhang, J. (2011) Hysteretic Shear-Flexure Interaction Model of Reinforced Concrete Columns for Seismic Response Assessment of Bridges. *Earthquake Engineering and Structural Dynamics*, 40 (3), pp. 315-337.
- Yang, Y. S. (1994). Aspects of Modeling Reinforced Concrete Bridge Structures for Dynamic Time History Analysis. *Ph.D. Dissertation*, Department of Applied Mechanics and Science, University of California at San Diego, La Jolla, CA.
- Zeris, C. A. and Mahin, S. A. (1988). Analysis of Reinforced Concrete Beam-Columns under Uniaxial Excitation. *ASCE Journal of Structural Engineering*, 114 (ST4), pp. 804-820.
- Zeris, C. A. and Mahin, S. A. (1991). Behaviour of Reinforced Concrete Structures Subjected to Biaxial Excitation. *ASCE Journal of Structural Engineering*, 117 (ST9), pp. 2657-2673.

- Zhang, L. X. and Hsu, T. T. C. (1998). Behavior and Analysis of 100 Mpa Concrete Membrane Elements. *ASCE Journal of Structural Engineering*, 124 (1), pp. 24-34.
- Zhao, Y. (1993). Modeling of Inelastic Cyclic Behaviour of Members, Connections and Joint Panels of Steel Frames. *Ph.D. Dissertation*, School of Civil and Environmental Engineering, Cornell University, Ithaca, NY 14853.
- Zhu, R. H. and Hsu, T. T. C. (2002). Poisson Effect of Reinforced Concrete Membrane Elements. *ACI Structural Journal*, 99 (5), pp. 631-640.
- Zhu, R. H., Hsu, T. T. C. and Lee, J. Y. (2001). Rational Shear Modulus for Smeared Crack Analysis of Reinforced Concrete. *ACI Structural Journal*, 98 (4), pp. 443-450.
- Ziegler, H. (1959). A Modification of Prager's Hardening Rule. *Quarterly of Applied Mathematics*, 17(1), pp. 55-65.